Geophysical Monitoring for Climatic Change

No. 10

Summary Report 1981

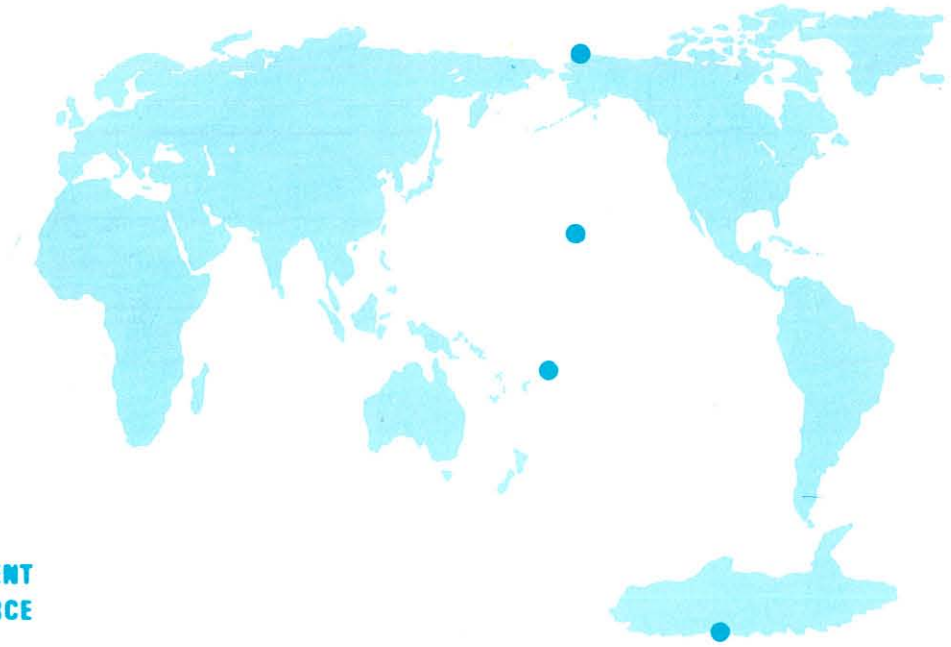

U.S. DEPARTMENT OF COMMERCE

NATIONAL OCEANIC AND ATMOSPHERIC ADMINISTRATION

ENVIRONMENTAL RESEARCH LABORATORIES

Geophysical Monitoring for Climatic Change No. 10

Summary Report 1981

Barry A. Bodhaine and Joyce M. Harris, Editors
Air Resources Laboratories
Geophysical Monitoring for Climatic Change

Boulder, Colorado

December 1982

U.S. DEPARTMENT OF COMMERCE
Malcolm Baldrige, Secretary

National Oceanic and Atmospheric Administration
John V. Byrne, Administrator

Environmental Research Laboratories
George H. Ludwig, Director

NOTICE

Mention of a commercial company or product does not constitute an endorsement by NOAA Environmental Research Laboratories. Use for publicity or advertising purposes of information from this publication concerning proprietary products or the tests of such products is not authorized.

CONTENTS

FOREWORD

It is a pleasure to introduce this 10th anniversary volume of the GMCC annual report. GMCC had its origins in early 1971 when Don Pack, ARL Deputy Director, prepared a program development plan for submission to the NOAA administration. That plan outlined certain necessary climate-related research and monitoring programs to be done within NOAA. Much of the plan was approved, and early in fiscal year 1972 GMCC was formed within ARL of NOAA. Don Pack served as the first director until his retirement in 1975, when Kirby Hanson became director.

During these first 10 years, GMCC matured as a scientific organization. Initially, much of the effort was devoted to construction of observatories at Barrow, Samoa, and the South Pole; developing new programs; purchasing and siting instruments at the observatories; and developing data processing procedures. Now, with logistical and operational aspects of many programs operating smoothly, we have more time for data analysis. Consequently, program maturity has been evidenced by significant publications on interpretation of our data.

We now have four primary areas of effort in GMCC. First, we maintain and operate our four baseline observatories. A major accomplishment of the past year was hosting the SEAREX experiment at Samoa, an intensive investigation of sea-air exchange of trace species by a consortium of university and private investigators. Second, we devote a major effort toward the CO_2-climate problem. GMCC has taken the lead, both nationally and internationally, in the monitoring of atmospheric concentrations of CO_2. Recently, we have completed expansion of our flask sampling network to 20 locations. Our third major interest involves studies related to ozone depletion. During 1981 we developed the capability to make routine and inexpensive ozone soundings to 40 km by means of a balloon-borne instrument package. Finally, we focus on atmospheric aerosols and their impact on solar radiation. Particular accomplishments were an enhanced understanding of Arctic haze at Barrow and a clear documentation of dust transport from Asia to Hawaii during spring, with its associated impact on solar radiation reaching Mauna Loa.

The year 1981 was one of transition, both within GMCC as I became Director, and also in the Federal Administration. A new NOAA Administrator, John Byrne, and a new ERL Director, George Ludwig, were appointed. The goals of the new Administration in Washington have been clearly stated to be less Federal involvement in many areas and a reduced Federal budget. Our challenge is to maintain and improve our important scientific programs within this outlook of constrained resources. I am confident that we will meet this challenge.

J. T. Peterson
Director
Geophysical Monitoring
for Climatic Change

PREFACE

This document presents a summary of the research operations and accomplishments by the Geophysical Monitoring for Climatic Change (GMCC) program and by outside investigators working cooperatively with GMCC in 1981. It includes descriptions of management and operations at GMCC's four baseline sites, scientific data from the measurement projects, conclusions from analyses of data, and recent basic research achievements.

The GMCC program, established in 1971, is one of five research programs within the Air Resources Laboratories under the directorship of Lester Machta. Its four observatories are located at Barrow, Alaska (in service since 1973); Mauna Loa, Hawaii (in service since 1956); American Samoa (in service since 1973); and South Pole (in service since 1957). Background measurements of aerosols, gases, and solar radiation that are important to the climate of the Earth are made at the observatories. The primary groups within GMCC are Monitoring Trace Gases, Aerosols and Radiation Monitoring, Acquisition and Data Management, and Analysis and Interpretation. Specific names of individuals in GMCC are not given in the main text of the report; however, the membership of each GMCC group is given in sec. 9. Publications and presentations by GMCC staff are given in sec. 7.

ACRONYMS AND ABBREVIATIONS

ACR	Active cavity radiometer
A&DM	Acquisition and Data Management (GMCC), Boulder, Colo.
ALE	Atmospheric Lifetime Experiment
ARL	Air Resources Laboratories, Rockville, Md. (ERL)
ARM	Aerosols and Radiation Monitoring (GMCC)
ASCS	Alaska Soil Conservation Service
ASRC	Atmospheric Sciences Research Center, SUNYA, Albany, N.Y.
A.U.	Astronomical Unit
BRW	Barrow Observatory, Barrow, Alaska (GMCC)
BUV	Backscattered ultraviolet
CAF	Clean Air Facility
CDC	Control Data Corporation
CMA	Chemical Manufacturers Association
CN	Condensation nuclei
CNC	Condensation nucleus counter
CSIRO	Commonwealth Scientific and Industrial Research Organization, Australia
DN	Departure from normal
DOE	Department of Energy
DOY	Day of year, Julian
dpm	Disintegrations per minute
ECC	Electrochemical concentration cell
EDXA	Energy dispersive X-ray analysis
EML	Environmental Measurements Laboratory (DOE)
EPA	Environmental Protection Agency
ERL	Environmental Research Laboratories, Boulder, Colo. (NOAA)
GAMBIT	Gridded atmospheric multilevel backward isobaric trajectories
G.E.	General Electric
GMCC	Geophysical Monitoring for Climatic Change, Boulder, Colo. (ARL)
HASL	Health and Safety Laboratory (EPA)
IAEA	International Atomic Energy Agency, Vienna, Austria
ICDAS	Instrumentation Control and Data Acquisition System
IICAMS	Interactive Instrumentation Control and Monitoring System
IR	Infrared
IS	Integrating sandwich
KUM	Cape Kumukahi, Hawaii
LBL	Lawrence Berkeley Laboratory, Berkeley, Calif.
MLO	Mauna Loa Observatory, Hawaii (GMCC)
MSL	Mean sea level
NADP	National Atmospheric Deposition Program
NARL	Naval Arctic Research Laboratory, Barrow, Alaska
NCC	National Climatic Center, Asheville, N.C.
NDIR	Nondispersive infrared
NIP	Normal incidence pyrheliometer
NMC	National Meteorological Center, Suitland, Md.
NOAA	National Oceanic and Atmospheric Administration
NRL	Naval Research Laboratory, Washington, D.C.
NSF	National Science Foundation, Washington, D.C.
NWR	Niwot Ridge, Colo.
NWS	National Weather Service
OGC	Oregon Graduate Center, Beaverton, Ore.
OPC	Optical particle counter

PIXE	Particle induced X-ray emission
PROM	Programmable read-only memory
P^3	Portable pressurizing pack
RDOS	Real-Time Disk Operating System
SBUV	Solar backscattered ultraviolet
SCM	Standard cubic meter
SEAREX	Sea-Air Exchange program
SEM	Scanning electron microscope
SIO	Scripps Institute of Oceanography, La Jolla, Calif.
SMO	Samoa Observatory, American Samoa (GMCC)
SPO	South Pole Observatory, Antarctica (GMCC)
SRL	Smithsonian Institution Radiation Biology Laboratory
SST	Sea surface temperature
SUNYA	State University of New York at Albany
URI	University of Rhode Island, Kingston, R.I.
USGS	United States Geological Survey
UPS	Universal power supply
UV	Ultraviolet
WDC-A	World Data Center-A, Asheville, N.C.
WMO	World Meteorological Organization, Geneva, Switzerland
WPL	Wave Propagation Laboratory (ERL), Boulder, Colo.
WSU	Washington State University, Pullman, Wash.

GEOPHYSICAL MONITORING FOR CLIMATIC CHANGE

NO. 10

Summary Report 1981

1. SUMMARY

At MLO, a computer system, consisting of an LSI-11/2 processor, disk, terminal, and printer, was installed and made operational in the Hilo office. A second computer system, consisting of an LSI-11/23 processor, terminal, and cassette tape unit for upgrading the lidar system, was received and made ready for installation. Plans for the construction of lava barriers upslope from MLO were completed during the year. In the event of a volcanic eruption near the summit of Mauna Loa, a lava flow approaching the observatory would be diverted for all but very large flows.

At BRW, NARL remained in a caretaker status, and BRW continued to receive power from an existing generator that has remained in operaton at NARL. A 14- × 20-ft hut was acquired from NARL and installed near the GMCC station to act as a garage for station vehicles.

At SMO, the SEAREX sampling program was completed as part of a comprehensive experiment to investigate gaseous and aerosol sea-air exchange. Three buildings located on Matatula Point and one building on the ridge remain for use by the GMCC program. A five-section tower was constructed on Matatula Point to act as the sampling platform for the GMCC CO_2 program.

At SPO, no significant additions to facilities were made, and all programs operated normally. GMCC proposed to the NSF that a Clean Air Sector be maintained upwind from the station between 330° and 110° grid directions.

The routine GMCC measurement programs at the observatories continued. These include carbon dioxide, total column and surface ozone, CFC-11 and -12, nitrous oxide, aerosol scattering coefficient, CN concentration, solar radiation, precipitation chemistry, and meteorological variables. Balloon measurements of stratospheric water vapor and ozone profiles were continued in Boulder, as were Umkehr ozone profiles. Lidar measurements of stratospheric aerosol profiles continued at MLO. Total ozone measurements continued at the four GMCC stations, one foreign cooperative station, and seven stations in the contiguous United States. Ozone observations were reinstated at the Tallahassee, Fla., station. The CO_2 flask sampling program included a total of 20 sites, with new stations established at Ocean Station M and Falkland Islands. Data for 1979-1981 show a clear seasonal cycle superimposed on a secular growth rate of about 1.4 ppm yr^{-1}. The amplitude of the seasonal cycle is maximum at the northernmost latitudes and is small in the Southern Hemisphere.

Participation continued in the WMO Global Ozone Research and Monitoring Project to upgrade Dobson spectrophotometers throughout the world. Automation of a Dobson instrument for routine Umkehr measurements was completed. That instrument may also be used in a semiautomatic mode for the measurement of total ozone.

Halocarbon and N_2O analysis capabilities were increased through the addition of a totally reconditioned gas chromatograph in the Boulder laboratory. An absolute calibration system for trace gases such as CFC-11, CFC-12, and N_2O was devised. This system involves the preparation of a mixture of the gas with CO_2, dilution to trace levels, and subsequent detection using the standard CO_2 measurement technique with highly accurate CO_2 gas standards. Sampling of CFC-11, CFC-12, and N_2O continued at five sites. CFC-11 and CFC-12 data show mean mixing ratios in the ranges 188-205 pptv and 321-345 pptv, respectively, and growth rates in the ranges 11-14 pptv yr^{-1} and 12-18 pptv yr^{-1}, respectively. N_2O data show mean mixing ratios in the range 301-304 pptv, indicating that the gas is well mixed globally. N_2O growth rates for BRW, NWR, MLO, and SPO are in the range 0.5-1.8 pptv yr^{-1}.

A modification of the ARL trajectory program was implemented on the NOAA CDC 750 computer in Boulder. The new program computes and displays isobaric trajectories at multiple pressure levels. These back trajectories can be calculated for up to 10 days for any destination in the Northern Hemisphere. A climatology of trajectories is being assembled for MLO and Bermuda.

GMCC personnel conducted numerous research projects and data analyses based on the routine measurement programs. Several studies used the CO_2 data record. A two-dimensional model of the global CO_2 distribution was developed that includes atmospheric mixing, oceanic uptake, biospheric fluxes, and fossil fuel combustion. By variation of the unknown parameters it is possible to interact with the model to facilitate the planning of sampling strategies and the estimation of oceanic and biospheric CO_2 fluxes. Analysis of the SPO CO_2 record for 1976-1980 showed that the data can be approximated by a function including a third-degree polynomial and first and second harmonics. An annual cycle and secular increase are clearly evident in the data. Correlations among CO_2 variations and sea surface temperature in the North Pacific, and the Southern Oscillation were examined. The Southern Oscillation may influence sea surface temperatures, which in turn may affect CO_2 concentrations. A study of the CO_2 vertical flux over the Arctic tundra at BRW was performed using sampling lines at 0.3- and 10-m heights. The results suggested that the BRW CO_2 cycle can be fully explained only by including the influence of mid-latitude vegetation. In a case study, air masses at BRW were classified into two types by looking at radiosonde wind, temperature, and moisture profiles as well as meteorological parameters at the station, and computed trajectories. CO_2 concentrations tended to be higher when an Arctic air mass was present, i.e., cold, dry air with a long residence time in the Arctic. When a warm, wet air mass from the North Pacific or North Atlantic regions was present, CO_2 concentrations tended to be low.

A laboratory experiment was performed to verify the calibration of CNC's. Furthermore, because confusion was found in the literature, a consistent theory of expansion ratio and supersaturation in CNC's was developed.

Work continued on development of the Umkehr method for measurement of ozone profiles in the atmosphere and development of a method for the correction of Umkehr data for the effects of stratospheric aerosols using the MLO solar radiation record. Ozone data collected using the BUV instrument and the Umkehr method were compared to study the degradation with time of satellite-borne BUV.

A summer experiment was organized at Whiteface Mountain to investigate the absorption of solar radiation in clouds and the effects of aerosol scavenging in the clouds. This was the first comprehensive attempt to measure the effects of absorbing aerosols located both within and between cloud droplets.

The GMCC standard solar infrared hygrometer was calibrated in Boulder by comparison with Denver radiosonde data and a WPL microwave water vapor meter. GMCC sponsored a comparison of 12 sunphotometers of 5 different types by means of atmospheric observations over a 2-mo period in Boulder.

Under a DOE grant, a contract was let for the construction of a photovoltaic power system at SMO. This solar power system will provide 1 kW of continuous power and will have sufficient battery backup to carry the electrical load of the observatory for two consecutive sunless days.

In 1981, GMCC again supported a substantial number of cooperative research projects. These projects are listed in sec. 2 for each station. Sixteen summary reports from these cooperative projects are included in sec. 5. They cover such topics as the global network of erythema measurements; measurement of tropospheric NO_x at MLO, with a novel method using the rising and setting sun and moon as light sources; several studies on pollution-derived aerosols and gases at BRW, MLO, SMO, and SPO; a comprehensive report on the SEAREX program at SMO; studies on the light absorptive properties of aerosols at MLO using a new technique called the integrating sandwich; sources of the Arctic aerosol using the ratio of graphitic carbon to lead as a tracer; some effects of sulfate and nonsulfate aerosol particles on light scattering and precipitation chemistry at MLO; and mathematical models of the global carbon cycle using methods derived from control and system theory.

2. OBSERVATORY REPORTS

2.1 Mauna Loa

2.1.1 Facilities

A major improvement in MLO facilities was effected in 1981 by the purchase of a powerful computer system for the Hilo office. Although there were serious problems with the system as it was delivered (damaged heads on the disk system, several features not included, and the mounting cabinet not shipped), the problems were eventually resolved and the basic system was installed and operational by October. The components in the basic system are the LSI-11/2 central processing unit, magnetic disk, video terminal, and line printer. Peripherals that were purchased, but not installed by the end of the year, are a nine-track tape drive, TU-58 cartridge system, automatic plotter, and paper-tape reader. The system operated reliably and received relatively heavy usage for various aspects of the MLO program during the last 3 months of the year.

The competitive bids for a second, but less complete, computer system were received in September, and the computer was delivered in October. This second system is to be used for upgrading the lidar operation, and for eventual automation of lidar observations. Although the LSI-11/23 central processing unit is more powerful than that in the Hilo office, the peripherals for it consist of only a video terminal and a TU-58 tape cartridge system. The system was awaiting delivery of the bootstrap, read-only memory, and parallel I/O boards at year's end.

Since the telescope dome that presently houses the lidar will be needed for a new solar tracker, the decision was made to erect a specially modified steel building for the lidar. The principal modification required was an opening in the roof for the lidar observations. Design specifications for the building and roof opening were completed in August, and a contract was let in September to Porta House, Inc., Oakland, Calif., for supply of the prefabricated building (without the roof opening). The building had not yet arrived in Hilo by the end of the year.

Because of operational problems with the four-wavelength nephelometer, the instrument was taken offline and shipped to Boulder for repair in late June. Unfortunately, repair was delayed and no nephelometer data were obtained from 1 June to 31 December.

A G.E. dewpoint hygrometer, installed at MLO in early February, operated largely trouble free during most of the year.

Operation of ICDAS was reasonably satisfactory, but the problem of spurious rewinding of the magnetic tape, with a consequent outage of the system, was experienced several times during the year. In an attempt to minimize the effects of the tape rewinds, a software routine was added in February to the operational program to reposition the tape at the end-of-file mark before writing on the tape. This was moderately successful for automatic recovery from a spurious rewind.

Since the observatory is located about 45 mi from Hilo and ICDAS failures can occur at any time, it was decided that a method of checking on system

operation by telephone would be desirable. Such a device was developed by the observatory staff and was installed in March. It has proved to be very useful, particularly on holidays and weekends, for checking system status, and on several occasions the period of outage has been decreased.

In July a replacement NOVA 1220 computer was installed in an attempt to increase the reliability of ICDAS operations. The frequency of outages was decreased, but not completely eliminated, by the replacement. System failures due to static discharges were also minimized by the installation of antistatic mats around the ICDAS rack. In spite of all measures taken, however, some failures continued throughout the year.

A supply of spare parts (Pockels cell, ruby rod, flash lamp, optical reflectors) for the lidar system was assembled in late 1981 in an effort to prevent any long interruptions of lidar operation in the future. A main contributing factor to component failures during 1981 was the vertical orientation of the laser, which permits dust particles to fall on the optical surfaces thus causing hot spots to develop in the laser beam. A logical solution to this fallout dust problem would be to mount the laser in a horizontal orientation and install a reflecting mirror for projecting the beam vertically. Such a provision should be considered in future planning for the system.

Detailed plans were completed for the construction of lava barriers upslope from the observatory for diverting possible lava flows resulting from volcanic eruptions near the summit of Mauna Loa. J. Lockwood of the Hawaiian Volcano Observatory, who was mainly responsible for the plans, made arrangements for H. Moore of USGS, Menlo Park, Calif., to analyze the behavior of lava flows approaching such diversion barriers, using numerical models. Moore's study indicated that the proposed barriers would indeed protect the observatory from all but very large volumes and speeds of lava flows and that it was unlikely that the upper reaches of Mauna Loa would generate such large flows. Thus it was decided to proceed with the project as time and budget permit, and to retain Lockwood as project leader for the task.

Howard T. Ellis, who served on the observatory staff since February 1961, retired in February 1981 after 20 years at MLO. A personal account of his experiences during the early years at MLO can be found in Ellis (1978).

2.1.2 Programs

The principal programs carried out at MLO during 1981 are listed in table 1. Brief comments on the programs follow.

Carbon Dioxide

The concentration of atmospheric CO_2 was continuously monitored by GMCC's URAS-2 NDIR gas analyzer throughout the year. The instrument performed satisfactorily without major problems. Preliminary results indicated that the rate of increase of atmospheric CO_2 was 1.5 ppm yr^{-1} for 1981.

The weekly CO_2 flask sampling programs for GMCC at MLO and KUM were carried out successfully during the year. The sampling programs involved exposing a pair of evacuated 5-ℓ flasks and exposing, by flush and fill

Table 1.--Summary of sampling programs at MLO in 1981

Program	Instrument	Sampling frequency	Remarks
Gases			
Carbon dioxide	URAS-2 infrared analyzer	Continuous	
	0.5-ℓ glass flasks, P[3]	1 pair wk^{-1}	
	0.5-ℓ glass flasks, through analyzer	1 pair wk^{-1}	Mountain and seacoast
	5-ℓ evacuated glass flasks	1 pair wk^{-1}	Mountain and seacoast
Surface ozone	Dasibi ozone meter	Continuous	
Total ozone	Dobson spectrophotometer no. 63	3 day^{-1}	
	Dobson spectrophotometer no. 83	Discrete	Special obs. during summer
Halocarbons	300-ml stainless steel flasks	1 pair wk^{-1}	
Aerosols			
Condensation nuclei	Pollak CNC	Discrete	4 meas., weekdays; 0, weekends
	G.E. CNC	Continuous	
Optical properties	Four-wavelength nephelometer	Continuous	450, 550, 700, 850 nm
Stratospheric aerosols	Lidar	Discrete	694.3 nm, 2 J
Skylight polarization	Polarizing radiometer	Discrete	8 wavelengths
Solar Radiation			
Global irradiance	Eppley pyranometers: Q, RG8	Continuous	
Direct irradiance	Eppley pyrheliometer: Q	Continuous	
	Eppley pyrheliometer: Q, OG1, RG2, RG8	Discrete	
	Eppley pyrheliometer with 13 narrowband filters	Continuous	
Turbidity	Sunphotometer with 380- and 500-nm narrowband filters	Discrete	
Meteorology			
Air temperature	Thermistor	Continuous	
	Max.-min. thermometers	1 day^{-1}	
	Hygrothermograph	Continuous	MLO and Kulani Mauka
Soil temperature	Thermistor	Continuous	
Dewpoint temperature	Dewpoint hygrometer	Continuous	
Relative humidity	Hygrothermograph	Continuous	MLO and Kulani Mauka
	Sling psychrometer	Discrete	
Pressure	Capacitance transducer	Continuous	
	Microbarograph	Continuous	
	Mercurial barometer	Discrete	
Wind (speed and direction)	Bendix Aerovane	Continuous	
Precipitation	Rain gage, 8-in	1 day^{-1}	
	Rain gage, 8-in	Twice wk^{-1}	Kulani Mauka
	Rain gage, tipping bucket	Continuous	
Total precipitable water	Foskett infrared hygrometer	Continuous	
Precipitation Chemistry			
pH	pH meter	Discrete	Rainwater collections, 6 sites
Conductivity	Conductivity bridge	Discrete	
Chemical components	Ion chromatograph	Discrete	
Cooperative Programs			
Carbon dioxide (SIO)	Infrared analyzer (Applied Physics)	Continuous	
	5-ℓ evacuated glass flasks	1 pair wk^{-1}	Mountain and seacoast
Carbon monoxide (Max Planck Inst.)	Special system	Continuous	Equipment inoperable after 26 Jan
Surface SO_2 (EPA)	Chemical bubbler system	Every 12 days	
Total surface particulates (DOE)	High-volume sampler	Continuous	Dependent on wind direction; 1 filter wk^{-1}
Total surface particulates (EPA)	High-volume sampler	Every 12 days	
Atmospheric electricity (Univ. of Minnesota)	Field mill, air conductivity meter, surface antenna	Continuous	
Ultraviolet radiation (Temple Univ.)	Ultraviolet radiometer	Continuous	Radiation responsible for sunburning of skin
Precipitation collection (DOE)	HASL wet-dry collector	Continuous	
Precipitation collection (EPA)	Misco model 93	Continuous	
Precipitation collection (Univ. of Paris)	Likens funnel collector	Twice wk^{-1}	
Precipitation collection (IAEA)	Likens funnel collector	Twice wk^{-1}	
Wet-dry deposition (Univ. of Illinois)	Exposed collection pails	Continuous	NADP
Aerosol chemistry (Florida State Univ.)	Special filters	Continuous	Equipment inoperable after 22 Jul
Aerosol chemistry (Univ. of Maryland)	Nuclepore filters	Continuous	Day-night discrimination
Aerosol chemistry (Univ. of California)	Nuclepore filters and impactors	Night only	
Aerosol chemistry (Univ. of Arizona)	Quartz filters	Continuous	Day-night discrimination
Carbon-13 (USGS)	10-ℓ stainless steel flasks	2 wk^{-1}	

Table 2.--Monthly occurrences of outgassing from the volcanic caldera on Mauna Loa

	Jan	Feb	Mar	Apr	May	Jun	Jul	Aug	Sep	Oct	Nov	Dec
No. of days	1	5	6	5	2	7	8	5	9	11	6	7
Percent of days	3	18	19	17	6	23	26	16	30	35	20	23

methods, a pair of 0.5-ℓ double-stopcock flasks at both locations. No flasks were lost or broken during shipment.

Vertical profiles of CO_2 at MLO were studied during 1981. Nine air intakes were mounted at 10-ft intervals from ground level to 80 ft. Air from each intake line was sampled for 5 minutes. Thus, air from five different intake lines could be sampled in a 30-min period. A reference gas of known concentration of CO_2 was used to compare with the air samples at ½-h intervals. A URAS-1 NDIR gas analyzer was used for the measurements, and data were recorded on a strip chart recorder. All data were analyzed by hand. The preliminary results show that the differences in CO_2 concentration at different heights along the 80-ft tower were negligibly small (within 0.5 ppm).

Outgassing from the volcanic caldera at the summit of Mauna Loa was frequently registered in the CO_2 records. It occurred mainly between midnight and 0800 LST during the southerly downslope wind flow regime. Table 2 shows the monthly occurrences of outgassing that appear in the CO_2 records.

Ozone

Surface ozone was measured continuously throughout the year with a Dasibi ozone meter.

Total ozone in the atmospheric column was measured at MLO on each of approximately 250 days during 1981. In addition, a special series of ozone measurements was taken over a 2-mo period during the summer, in response to a request from Boulder.

Surface Aerosols

Operation of the G.E. and Pollak CNC's was normal.

As mentioned in sec. 2.1.1, the four-wavelength nephelometer operated reasonably satisfactorily during the first 4 months of 1981, but was inoperable during the remainder of the year.

Stratospheric Aerosols--Lidar

The stratospheric cloud from the eruption of Mt. St. Helens in May 1980 was still observed over Hawaii throughout 1981, using lidar. The cloud became less pronounced, however, and was difficult to distinguish from the background Junge layer.

Operation of the lidar was reliable during the first and last parts of the year, and valuable data were taken on a weekly basis, weather permitting,

from 1 January to 25 March and from 14 October to 31 December. During the intervening period, occasional observations were taken, but equipment problems prevented a normal schedule. The problems are briefly outlined as follows.

(1) The Pockels cell failed on 25 March because of a window fracture due to an air bubble in the cell. The spare cell was found to be of the wrong type, being designed for "switch off" rather than "switch on" operation of the laser. In an attempt to get the old cell (Apollo) repaired, it was learned that Apollo no longer supplies or services this type of cell, so a new cell, ordered from a different supplier, was not delivered until June.

(2) This new cell was defective, and it failed during the second set of observations made with it. Since it was still under warranty, the company repaired it without cost, but observations were delayed.

(3) After the repaired cell was installed, its windows were damaged because the laser power density exceeded the damage threshold of the components. The poor condition of the ruby rod was probably the reason for the damage, but to forestall excessive energy output, a laser calorimeter was purchased for checking energy output. The Pockels cell was again returned to the company for repair, and the ruby rod was repolished. The whole system was again operational on 14 October, and it operated satisfactorily for the remainder of the year.

Solar Radiation

Solar radiation observations continued without serious problems in 1981. Measurements with OG1 and GG22 pyranometers were terminated on 27 March in response to a request from Boulder. MLO's pyrheliometer and pyranometer responses were compared with those of circulating reference standard instruments in March and April. An ACR was added to the MLO complement of instruments in June. A defective filter block on the 13-channel radiometer was replaced by a newly recalibrated one in July, and in September the signals from radiometer channels 8, 12, and 13 were put on ICDAS channels 18, 17, and 20, respectively.

Meteorology

Meteorological measurements continued without major problems throughout the year.

Precipitation Chemistry

Precipitation chemistry and related programs continued normally through 1981.

Cooperative Programs

Most of the cooperative programs listed in table 1 continued through 1981 without major difficulties. The following items are worthy of special note: (1) A. Dittenhoefer, a visitor at MLO under the National Research Council Associateship program, completed his 18-mo visit to MLO in May and took a new position with Enviroplan, Inc., West Orange, N.J.; (2) equipment from the Max Planck Institute, Mainz, Germany, for measuring carbon monoxide failed on 26 January, and no further measurements were made during 1981; (3) J. Noxon, of

ERL in Boulder measured NO_x at MLO during several days in each of the months of April, June, and November; (4) A. Clarke, of the University of Washington, spent 4 weeks from 23 May to 19 June measuring the absorption properties of aerosols at MLO; (5) aerosol sampling by means of the streaker from Florida State University was indefinitely suspended on 22 July, when the motor failed and no replacement was available; and (6) in a special program, nine pairs of flask samples taken during a 3-wk period in July were sent to R. Rasmussen of OGC for analyses of their gaseous content.

2.1.3 Mauna Loa Meteorological Museum

J. Cross, a retired forestry specialist, continued to serve as a volunteer curator for the full year. The collection of the museum was increased during the year by the following items: (1) the slide rule owned and used for many years by the late H. Wexler; (2) a wind recorder of the type used in most weather stations in the United States beginning in the 1920's; (3) three boxes of books, pamphlets, tapes, and other materials on meteorological and astronomical subjects; (4) a rain gage of the weighing-bucket type; and (5) miscellaneous publications on various subjects in meteorology and related fields.

2.2 Barrow

2.2.1 Facilities

With the drastic reduction of operations at NARL there was great concern that the electrical power supplied to BRW would be discontinued. Several contingency plans were investigated in the event that NARL was completely shut down. For example, installation of a power line from the station to the Dewline station was suggested. The estimated cost for hauling and sinking power poles was over $30,000. Fortunately, it has become increasingly apparent that the USGS, required to maintain power to the local gas fields, will most likely operate the existing power generators at NARL and will eventually become the administrative agency for NARL. Arrangements are being made for the station to continue to receive power from NARL when the administrative transition is made.

In September, a 14- × 20-ft Wannigan hut was acquired from NARL and stationed approximately 100 ft north of the main building. With the addition of a garage door, it has become a convenient storage area for the snowmobile and all-terrain vehicle.

The access road running from the Dewline station to the observatory site is in need of significant repair. The road requires at least another layer of gravel and binder for it to be crowned and smoothed properly.

After losing many services from NARL, an imprest fund was granted the station chief to make moderate purchases and to facilitate the payment of certain services such as the telephone bill.

Through an interagency transfer, a 1979 GMC pickup truck was obtained from NARL. The 1973 International truck was excessed, and the Sidewinder all-terrain vehicle, which has countless problems from a frozen engine block to a flooded carburetor, may be excessed soon.

2.2.2 Programs

Programs carried out at BRW are listed in table 3. Comments on some selected programs follow.

Carbon Dioxide

The URAS analyzer performed well the entire year. Heat taping of the freezer hose to eliminate frost buildup has been successful.

A new system was initiated for sampling 2-ℓ flasks outdoors. A pair of flasks is sampled in parallel. These flasks are housed in a briefcase with a sampling line about 5 ft long, thus minimizing the risk of contamination from the observer.

Ozone

There were no major problems with the Dasibi surface ozone meter or the Dobson no. 76 spectrophotometer.

Halocarbons

Weekly flask sampling went smoothly.

Surface Aerosols

The Pollak CNC and the four-wavelength nephelometer performed well throughout the year. The G.E. CNC had a series of problems from inadequate wiring to a flooded casting and was in Boulder for repair for much of the year.

In December, BRW received a Knollenberg aerosol sprectrometer to measure the size distribution of aerosols. The laser head was malfunctioning, and the instrument was sent back to Boulder for repair.

Stratospheric Aerosols--Lidar

The lidar system did not function properly this year. With its complex method of operation, its extensive maintenance requirements, and the less-than-ideal location at NARL, this system will apparently require a great deal of attention to be operational.

Solar Radiation

Satisfactory solar radiation measurements were taken this year. In March two of the pyranometers (OG1 and GG22) were removed and shipped to Boulder as requested. The other two pyranometers (Q1 and RG8) remained in operation the entire year.

Meteorology

No significant problems were encountered. A temperature gradient system was received in December. One temperature probe will be placed near the top of the meteorological tower, and the other will be installed near the bottom. Calibrated together, they will detect any significant temperature gradient near the ground.

Table 3.--Summary of sampling programs at BRW in 1981

Program	Instrument	Sampling frequency
Gases		
Carbon dioxide	URAS-2T infrared analyzer	Continuous
	0.5-ℓ glass flasks, P[3]	1 pair wk^{-1}
	0.5-ℓ glass flasks, through analyzer	1 pair wk^{-1}
	5-ℓ evacuated glass flasks	1 pair wk^{-1}
Surface ozone	Dasibi ozone meter	Continuous
Total ozone	Dobson spectrophotometer no. 76	3 day^{-1}
Halocarbons	300-ml stainless steel flasks	1 pair wk^{-1}
Aerosols		
Condensation nuclei	Pollak CNC	Discrete
	G.E. CNC	Continuous
Optical properties	Four-wavelength nephelometer	Continuous
Solar Radiation		
Global irradiance	Eppley pyranometers: Q, RG8	Continuous
Direct irradiance	Eppley pyrheliometer: Q	Continuous
	Eppley pyrheliometer: Q, OG1, RG2, RG8	Discrete
Turbidity	Sunphotometer with 380- and 500-nm narrowband filters	Discrete
Meteorology		
Air temperature	Thermistor	Continuous
	Max.-min. thermometers	1 day^{-1}
	Hygrothermograph	Continuous
Soil temperature	Thermistor	Continuous
Temperature gradient	2 vertically separated thermistors	Continuous
Dewpoint temperature	Dewpoint hygrometer	Continuous
Relative humidity	Hygrothermograph	Continuous
Pressure	Capacitance transducer	Continuous
	Microbarograph	Continuous
	Mercurial barometer	Discrete
Wind (speed and direction)	Bendix Aerovane	Continuous
Precipitation Chemistry		
pH	pH meter (samples analyzed at MLO)	Discrete
Conductivity	Conductivity bridge (samples analyzed at MLO)	2 mo^{-1} (approx. Oct-May)
Cooperative Programs		
Total surface particulates (DOE)	High-volume sampler	Continuous (1 filter wk^{-1})
Aerosol chemistry (URI)	High-volume samplers	Continuous (one, 1 filter day^{-1}; the other, on an episodic basis)
Particulates (Carnegie-Mellon Univ.)	High volume sampler	Continuous (filter exposed on episodic basis)
Particulates (OGC, BNL, NBS)	High-volume sampler	Continuous (Jan-Apr)
Global radiation (SRL)	6 Eppley pyranometers	Continuous
Ultraviolet radiation (Temple Univ.)	Ultraviolet radiometer	Continuous
Carbon dioxide (SIO)	5-ℓ evacuated glass flasks	1 pair wk^{-1}
Precipitation gage (ASCS)	Wyoming shielded precipitation gage	2 mo^{-1}
Carbonaceous particles (LBL)	Dichotomous sampler (quartz and Millipore filters)	Continuous (1 set of filters wk^{-1})
	High-volume filter	Continuous (1 filter day^{-1})
Halocarbons (OGC)	5-ℓ stainless steel flasks	1 wk^{-1} (3 flasks $sample^{-1}$)
Incident and reflected radiation (Univ. of Alaska)	Up-down pyranometers	Continuous (program ended in Nov)
Magnetic fields (USGS)	Magnetometer observatory	1 station check wk^{-1}
Carbon-13 (USGS)	10-ℓ stainless steel flasks	1 pair mo^{-1}

Precipitation Chemistry

Snow samples were taken twice a month from January to May and October to December. Rain samples were taken on an episodic basis. After accumulating several samples, they were mailed to MLO for analysis.

ICDAS

A new multiplexer was installed in January. The entire system performed excellently. There was less than 2% downtime for the entire year.

Cooperative Programs

A program to measure ^{13}C began this year for the USGS. A pair of sampling tanks, used to store ambient air once a month, were sent to Denver for analysis. It was soon discovered that water was condensing inside the tanks. It was speculated that this condensation was forming during the sampling period. To remedy this situation the tanks were warmed by a torch during the sampling period.

Carnegie-Mellon University began a filter program of measuring particulates on an episodic basis when the air was coming from the Clean Air Sector (free of any local contamination sources such as the town of Barrow or the town dump).

Checking of the unattended USGS magnetometer site, located approximately 500 ft west of the station, was begun once a week. The date and time were routinely logged on the chart records, various electrical values were recorded, and any significant malfunctions were to be reported to the USGS office in Fairbanks.

LBL modified its carbon particulate sampling program by (1) adding a dichotomous filter sampler that uses two quartz and two Millipore filters, (2) moving the high-volume filter system indoors, and (3) eliminating the snow samples.

The precipitation gage sampling program included checking the gage at BRW and at the village of Atkasuk, about 60 mi south of Barrow. These monthly visits to Atkasuk were discontinued indefinitely to save observer time for work at BRW. An agreement has been made whereby the local school in Atkasuk will take the responsibility for checking the gage and will be reimbursed for its services by the state Soil Conservation Service.

2.3 Samoa

2.3.1 Facilities

No additions to SMO facilities were made by GMCC during 1981, but completion of the SEAREX project (discussed in sec 5.6) in August resulted in some additions. Specifically, the structures used for the SEAREX operation were retained with the exception of one, which was dismantled. Four small buildings remain, three located at the base of the stairs to Matatula Point and one on the ridge, adjacent to the GMCC remote sampling tower.

The orginal sampling tower at Matatula Point consisted of two GMCC sections and two sections belonging to R. Duce. The SEAREX project shipped in 15 additional sections and constructed a 10-section tower and a 7-section tower using the 2 sections belonging to Duce. When SEAREX was completed, 19 sections were shipped to New Zealand for the 1983 SEAREX operation; thus GMCC was able to construct a 5-section tower at the point. This tower is the primary sampling platform for the GMCC CO_2 program. The continuous analyzer sample line is mounted on the tower, and all CO_2 flask samples are obtained from the top level.

Additionally, the special high-voltage powerline stepdown transformer installed to provide power to the SEAREX operation at the point was not removed. The line was buried and the stepdown transformer was left in place in one of the remaining SEAREX buildings. This provides a valuable asset for possible future operations at the point, as a result of the increased electrical power capacity.

2.3.2 Programs

All 1980 programs are summarized in table 4. Additional comments follow.

Carbon Dioxide

The URAS-2T analyzer operated reliably all year, and the only equipment change involved installation of a new Hewlett-Packard chart recorder during February. An improved moisture removal system for the air line was installed during February when the condensation trap system in use since February 1978 was replaced by a freezeout trap assembly cooled by a CryoCool model CC100F. The freezer system is installed at the point, near the sampling tower, and it removes nearly all the water from sample air prior to passage through the long sample line to the analyzer. The Cincinnati Sub-Zero unit remained operational as an added protective trap system.

During June, a major modification occurred when SMO switched to CO_2-in-air reference gases during a visit by W. Komhyr and L. Waterman. Extensive testing of the CO_2 air sampling line was also conducted, using a large gas-sampling syringe that was filled at the point and carried back to the analyzer. The air sample was then injected through the Cincinnati Sub-Zero freezer system into the analyzer. Differences in CO_2 concentrations between air sampled by the syringe and air that had passed through the air sample line from the point were negligible. During September, a GMCC-SIO flask comparison program began. Weekly GMCC 0.5-ℓ and 5-ℓ flasks plus SIO 5-ℓ flasks are exposed at the point. GMCC semiweekly sampling was terminated with the onset of the intercomparison.

Ozone

Concurrent operation of the Dasibi and ECC sensors was continued until August, when the ECC program was terminated and the sensor was returned permanently to Boulder. The Dasibi ozone meter then became the primary surface ozone monitor.

A regular Dobson observational schedule was maintained all year, and no problems with the instrument (no. 42) were experienced.

Table 4.--Summary of sampling programs at SMO in 1981

Program	Instrument	Sampling frequency
Gases		
Carbon dioxide	URAS-2T infrared analyzer	Continuous
	0.5-ℓ glass flasks, P[3]	1 pair wk^{-1}
	0.5-ℓ glass flasks, through analyzer	1 pair wk^{-1}
	5-ℓ evacuated glass flasks	1 pair wk^{-1}
Surface ozone	Dasibi ozone meter	Continuous
	ECC meter (terminated Sep 81)	Continuous
Total ozone	Dobson spectrophotometer no. 42	3 day^{-1}
Halocarbons	300-ml stainless steel flasks	1 pair wk^{-1}
Aerosols		
Condensation nuclei	Pollak CNC	Discrete
	G.E. CNC	Continuous
Optical properties	Four-wavelength nephelometer	Continuous
Solar Radiation		
Global irradiance	Eppley pyranometers: Q, RG8	Continuous
	Eppley pyranometers (two): Q, on tilted mounts	Continuous
Direct irradiance	Eppley pyrheliometer: Q	Continuous
	Eppley pyrheliometer: Q, OG1, RG2, RG8	Discrete
Turbidity	Sunphotometer with 380- and 500-nm narrowband filters	Discrete
Meteorology		
Air temperature	Thermistor	Continuous
	Max.-min. thermometers	1 day^{-1}
	Hygrothermograph	Continuous
Soil temperature	Thermistor	Continuous
Dewpoint temperature	Dewpoint hygrometer	Continuous
Relative humidity	Hygrothermograph	Continuous
	Sling psychrometer	Discrete
Pressure	Capacitance transducer	Continuous
	Microbarograph	Continuous
	Mercurial barometer	Discrete
Wind (speed and direction)	Bendix Aerovane	Continuous
Precipitation	Polyethylene funnel, bottle	1 day^{-1}
Precipitation chemistry		
pH	Corning model 125 meter with semimicro combination electrode	1 day^{-1} (GMCC); 1 wk^{-1} (NADP)
Conductivity	Beckman model RC-16C meter	1 day^{-1} (GMCC); 1 wk^{-1} (NADP)
Cooperative Programs		
Carbon dioxide (SIO)	5-ℓ evacuated glass flasks	1 pair wk^{-1}
ALE project: CFC-11, CFC-12, N_2O, $CHCl_3$, CCl_4 (OGC)	HP5840A gas chromatograph	1 h^{-1}
CH_4, CO, CO_2 (OGC)	Carle gas chromatograph	3 h^{-1}
CH_3I, CH_3Cl, CH_4, CO (OGC)	Stainless steel flasks, 3 set^{-1}	1 wk^{-1}
Carbon-13 (USGS)	10-ℓ stainless steel flasks	2 pair mo^{-1}
Wet-dry deposition (NADP)	HASL wet-dry collector (new Chemetrics, Dec 81)	1 wk^{-1}, wet; 2 mo^{-1}, dry
Wet-dry deposition (EML)	HASL wet-dry collector (terminated May 81)	1 mo^{-1}
Bulk deposition (EML)	Plastic bucket	1 mo^{-1}

Surface Aerosols

The G.E. CNC operated all year with the exception of approximately a 1-mo period from late March to late April when the instrument was in Boulder for repair.

After an 18-mo absence from SMO, the four-wavelength nephelometer was returned and went back online 14 March. While in the United States, the instrument was fitted with a photomultiplier tube that does not require cooling. A marked improvement in instrument performance and reliability resulted.

Solar Radiation

During March, the GG22 and OG1 pyranometers were taken offline and returned to Boulder. Of the two pyranometers that remained in operation, the RG8 pyranometer was replaced in May because of a stained dome, and the quartz unit was exchanged in December after a systematic drift in the original SMO instrument calibration was discovered.

The GMCC traveling standard pyranometer and filter wheel pyrheliometer were intercompared during June and July.

Meteorology

The Aerovane was replaced in May. During September, a three-component anemometer was installed by G. Herbert, while on a station visit.

Precipitation Chemistry

Three collection protocols were maintained: (1) GMCC daily collections (bulk), (2) NADP weekly collection of wet deposition, and (3) EML monthly bulk collection.

Onsite measurements of pH and conductivity were performed on GMCC and NADP samples.

ICDAS

The data acquisition system operated routinely all year. Immunity to island power outages and fluctuations was significantly increased in July when the ICDAS UPS was modified to operate at 60 Hz by use of an internal quartz frequency source rather than the previous phase-locked loop method that tracked the island line frequency.

Cooperative Programs

The gas chromatograph from R. Rasmussen's ALE project at OGC was operational all year. A UPS was installed during May to eliminate disruptions caused by power outages. The Carle gas chromatograph was offline from 1 October through the end of the year. Weekly flask samples were collected for OGC all year.

SEAREX, a comprehensive program for measurement of sea-air exchange processes, was operational during January, February, June, July, and August 1981. All materials and equipment were then returned to the United States or shipped

to New Zealand for scheduled 1983 activity there. Details of SEAREX are discussed in sec. 5.6.

2.4 South Pole

2.4.1 Facilities

SPO continued operations for the 1981 season with few problems and little downtime in the CAF. There were some modifications made to the internal and roof layouts of the CAF; figs. 1 and 2 illustrate the new layouts. The GMCC Summary Report for 1978 (Mendonca, 1979, figs. 3 and 4) shows the old layouts. The changes made inside were (1) the removal of SIO CO_2 flasks from the storage cabinet, (2) the placement of the surface ozone equipment in a separate rack, and (3) the removal of WPL equipment and racks from the solar radiation room. These arrangements allowed for more storage space for SPO programs, and improved the environment for the surface ozone instruments. The electric field mill (removed 7 December 1980), the UV radiometer (discontinued), and the GG22 pyranometer (discontinued) no longer reside on the CAF roof. The University of Maryland's Atmospheric Chemistry Program (cooperative program) reduced the height of their three high-volume sampling stacks by 3-5 ft. The removal of the electric field mill and shortening of the sampling stacks may have reduced the amount of solar radiation data lost because of shadow interference.

Figure 3 shows the general layout of SPO and the area proposed by GMCC to NSF as the Clean Air Sector. Questions concerning the exact boundaries of the sector arose during the year. Specifically GMCC proposed that a Clean Air Sector be maintained upwind of the station, between 330° and 110° grid, and suggested if possible that no structures be installed in the sector. Further, the Science Sector between 110° and 150° should be maintained far enough upwind of the station to eliminate the possibility of detection of pollutants from temporary structures for scientific studies. Portable generators should not be placed in the Science Sector.

Measurements for both the Clean Air and Science Sectors begin at the grid NW corner of the CAF. During austral summer, aircraft activity extends into the Clean Air Sector. Allowances can also be made for temporary special projects that may require the use of the Clean Air Sector or Science Sector.

Electrical power to the CAF was adequate. In July 1981, two new electrical outlets were installed near the sampling stack to resolve the electrical problem of overloaded circuits from additional equipment.

The GMCC sampling stack did not require internal cleaning. A heat lamp was installed to alleviate ice buildup along the outer portion of the stack inside the CAF. The lamp, capable of being raised or lowered, slowly melted the ice without causing damage to the stack or affecting the air being sampled. In previous years, use of a heat gun, blow torch, hammer, and screwdriver was the method for melting or chipping the ice from the stack.

Two static mats, placed in front of and behind the ICDAS racks, and a humidifier were used throughout the year to suppress static discharge.

The first SPO air drop occurred on 22 June.

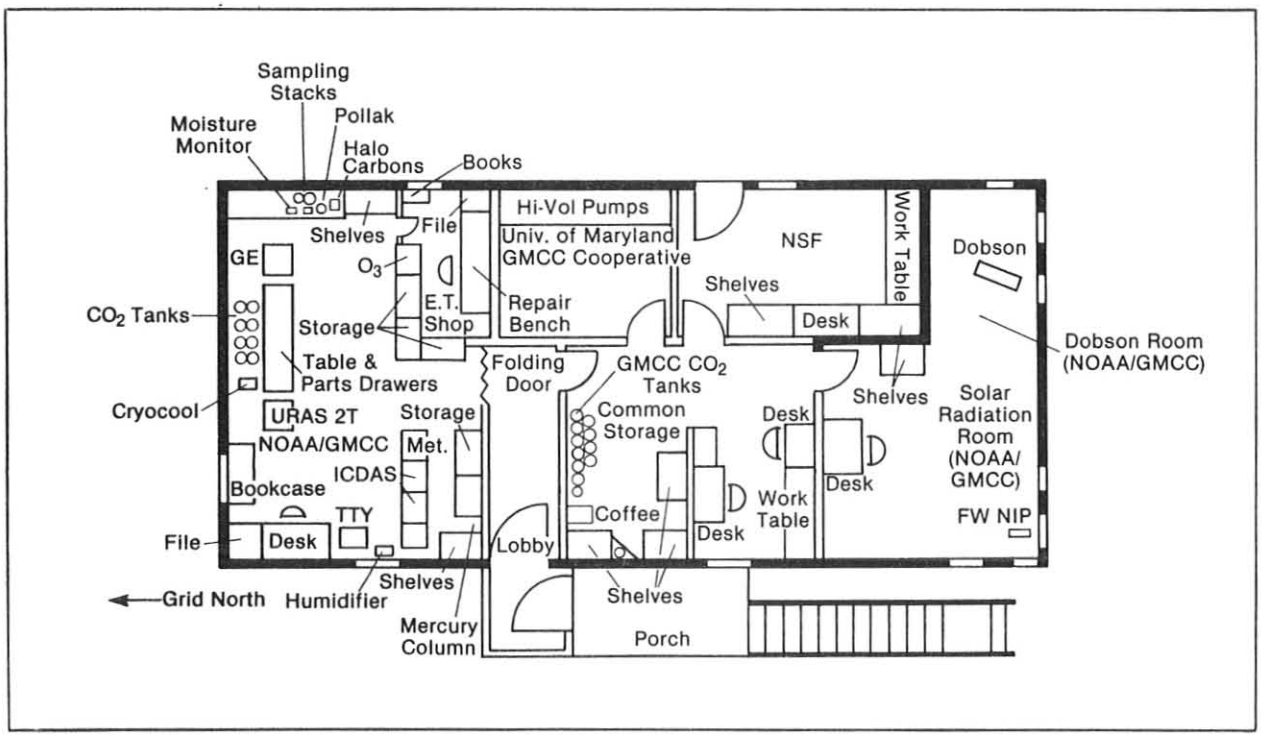

Figure 1.--Interior plan of CAF at SPO, 1981.

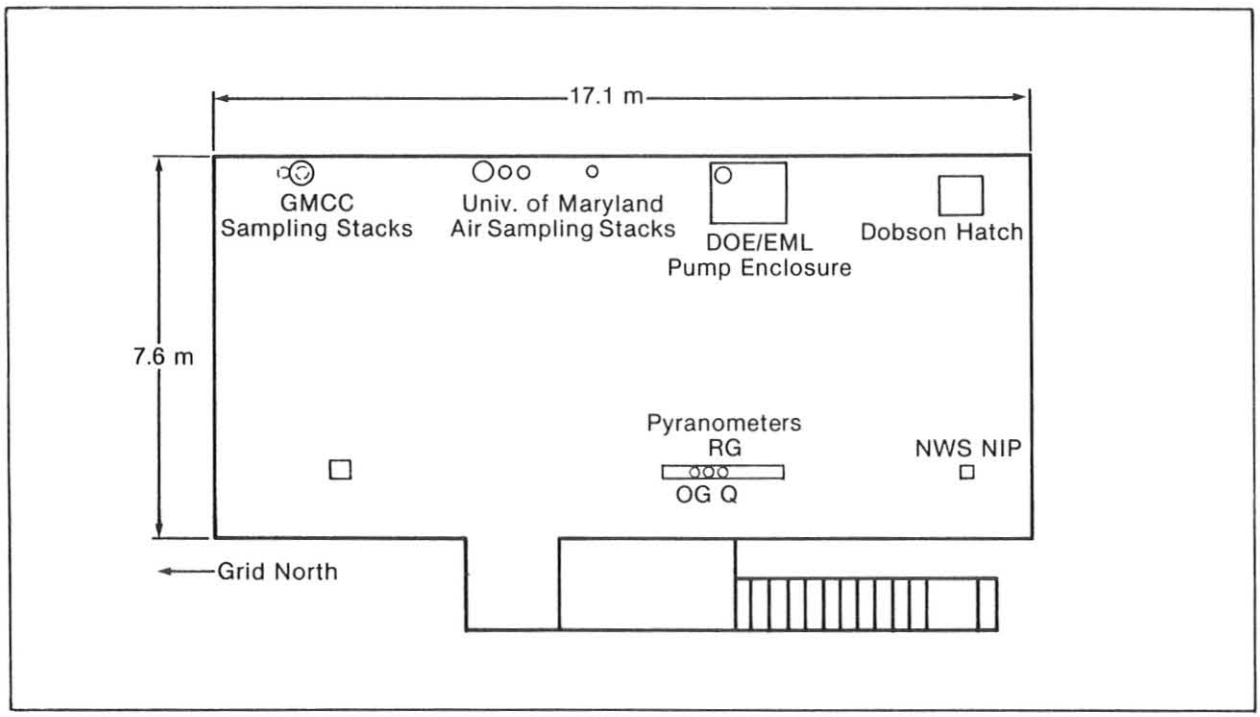

Figure 2.--Roof plan of CAF at SPO, 1981.

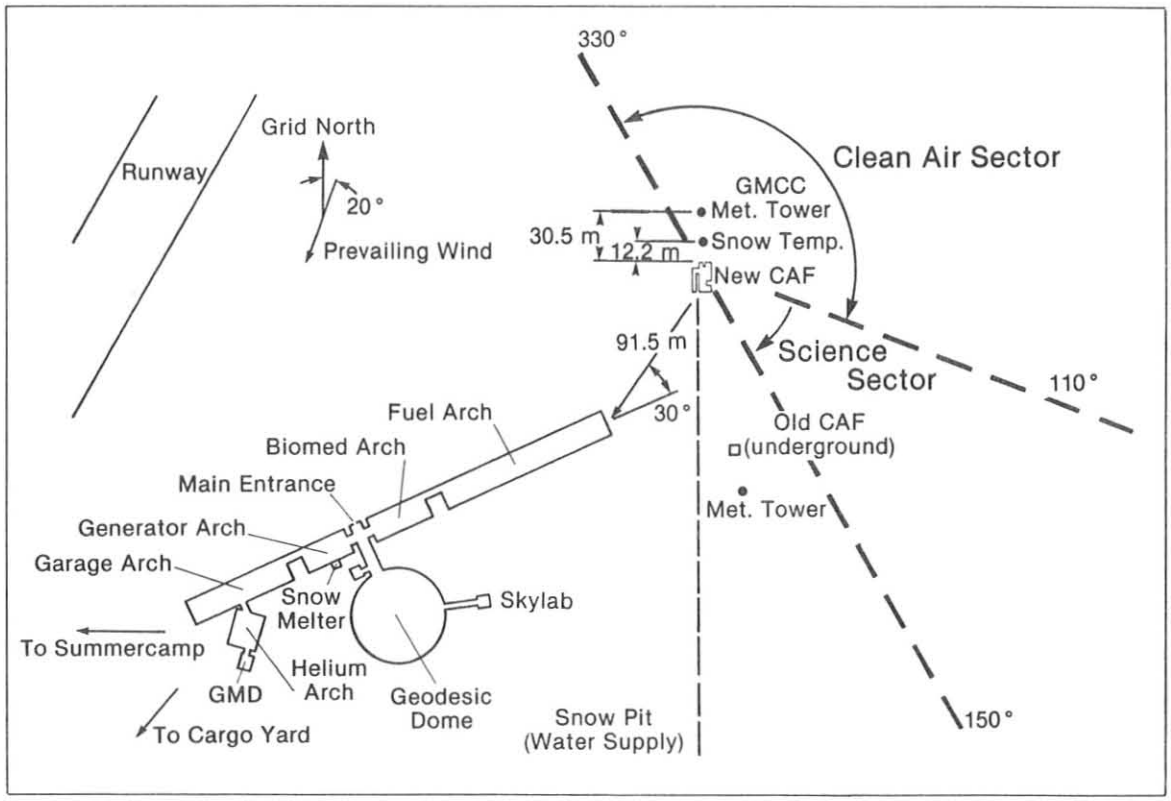

Figure 3.--Amundsen-Scott Station at South Pole, 1981.

2.4.2 Programs

SPO programs for 1981 are listed in table 5 and are briefly described below.

Carbon Dioxide

The CO_2 program operated well all season. The intercalibration of nitrogen and air standards was conducted as instructed on 3-5 December and 26-27 December 1980. The lid of the U-Tainer cold bath was redesigned 10 February to allow easier access to the thermometer and water traps. In early April a heat lamp was installed on the bench in front of the CryoCool unit to eliminate an ice buildup problem around the cryogenic probe. A precision drive for the chopper motor was installed 18 June to improve data quality and to eliminate the glitches believed to be caused by powerline frequency instability.

Discrete flask samples were alternately taken on the CAF roof and through the analyzer system until 16 April. The sampling sequence then changed to roof, analyzer, ground, analyzer, roof. The P^3 unit arrived at SPO on the air drop and was in operation 21 July. The sampling sequence was changed to roof, ground, analyzer, roof.

Zero drift occurred during the year as in previous years. It is believed to be temperature-induced, the main trouble source being the Chromalox heater

Table 5.--Summary of sampling programs at SPO in 1981

Program	Instrument	Sampling frequency	Remarks
Gases			
Carbon dioxide	URAS-2T infrared analyzer	Continuous	Jan 74-present (excl. Nov 78-Nov 79)
	0.5-ℓ glass flasks, P[3]	1 pair wk^{-1}	Jun 81-present
	0.5-ℓ glass flasks, through analyzer	1 pair wk^{-1}	Nov 79-present
Surface ozone	Dasibi ozone meter	Continuous	Jan 76-present
Total ozone	Dobson spectrophotometer no. 83	3 day^{-1}	Dec 63-present
Halocarbons	300-ml stainless steel flasks	1 pair wk^{-1}	Jan 77-Dec 79
		1 pair wk^{-1}, austral summer	Jan 80-present
		1 pair mo^{-1}, austral winter	Jan 80-present
Aerosols			
Condensation nuclei	Pollak CNC	Discrete	Jan 74-present
	G.E. CNC	Continuous	Jan 74-present
Optical properties	Four-wavelength nephelometer	Continuous	Jan 79-Dec 79 Jan 81-Dec 81
Solar radiation			
Global irradiance	Eppley pyranometers: Q, OG1, RG8	Continuous	Feb 74-present
Direct irradiance	Eppley pyrheliometers: Q, RG8	Continuous	Oct 75-present
	Eppley pyrheliometer: Q, OG1, RG2, RG8	Discrete	Jan 77-present
Turbidity	Sunphotometer with 380- and 500-nm narrowband filters	Discrete	Jan 74-present
Meteorology			
Air temperature	Thermistor	Continuous	Mar 77-present
Snow temperature	Thermistor	Continuous	Mar 77-present
Room temperature	Thermistor	Continuous	Jul 78-present
Water vapor density	Du Pont 303 moisture monitor	Continuous	Mar 77-present
Pressure	Capacitance transducer	Continuous	Dec 75-present
	Microbarograph	Continuous	Feb 80-present
	Mercurial barometer	Discrete	Jan 80-present
Wind (speed and direction)	Bendix Aerovane	Continuous	Dec 75-present
Cooperative Programs			
Carbon dioxide (SIO)	5-ℓ evacuated glass flasks	2 mo^{-1} (3 flasks $sample^{-1}$)	1957-present
Total surface particulates (DOE)	High-volume sampler	Continuous (1 filter wk^{-1})	May 70-present
Total surface particulates (EPA)	High-volume sampler	Continuous (1 filter wk^{-1})	May 70-present
Aerosol chemistry (Univ. of Maryland)	High-volume samplers	Continuous	Jan 79-present
Aerosol chemistry (URI)	High-volume samplers	Continuous	Jan 79-present
Halocarbons (OGC)	5-ℓ stainless steel flasks	3 $summer^{-1}$ (3 flasks $sample^{-1}$)	1980-present
Carbon-13 (USGS)	10-ℓ stainless steel cylinder	Discrete	Jan 81-present

behind the analyzer. Therefore a cardboard partition was placed between the analyzer and the heater early in the season, and a suggestion was made to the incoming crew to move the heater.

Ozone

Operation of the surface ozone program continued, with the addition of a Dasibi 1323 as the standard instrument. The Dasibi 1323 and the Mec-1000 ozone generator no. 205 were installed and online 17 December 1980. A new Watanabe Microservo recorder was installed on 20 January to replace the Rustrak recorder.

The Dasibi 1316 was tranferred to its own rack from the G.E. CNC rack on 18 September to correct for a high instrument temperature of about 40°C.

Surface Aerosols

The Pollak CNC operated well all year. The G.E. CNC was sent to Boulder for repair 10 November and returned to SPO and online 29 December 1980. It went down again 8 October 1981 and was returned to Boulder for repair.

The four-wavelength nephelometer obtained good results from January to December 1981. It arrived at SPO with minor damage from shipment and was online 28 January.

Solar Radiation

The quartz standard intercomparison using quartz secondary standard no. 12562 was conducted from 15 January to 5 February. Starting 19 September 1981, the GG22 pyranometer and the UV radiometer were discontinued.

Meteorology

There were no major problems with the meteorology program except the Du Pont 303 moisture monitor. The data from the moisture monitor are questionable. There were problems with the cells and difficulties in regulating the flow rate.

On 15 January the radiation shield was installed on the temperature sensor unit.

ICDAS

The NOVA 1220 was replaced with a newer NOVA 1220 on 9 January. Because of unrepairable mechanical parts, the teletype was replaced 13 May with a spare unit from the station Meteorology Office. All other ICDAS-related equipment operated continuously all year without difficulty.

3. CONTINUING GMCC PROGRAMS

3.1 Carbon Dioxide

3.1.1 Analyzer CO_2 Measurements

CO_2 measurements made with continuously operating NDIR gas analyzers were continued during 1981 at the four GMCC stations (BRW, MLO, SMO, and SPO). Data acquisition and processing procedures remained identical to those described in GMCC Summary Reports for 1977 and 1978 (Peterson, 1978; Mendonca, 1979). The complete record of continuous measurements at the four stations through 1981 is presented in table 6, in the form of provisional monthly mean CO_2 mole fractions, and plotted in fig. 4. These values, expressed in the provisional WMO 1974 CO_2-in-air mole fraction scale, are preliminary. Final values incorporating the best determination of carrier gas effects and final working-standard gas concentrations should be available early in 1983 for the full continuous record at each of the stations. Relative errors in the provisional values (table 6) are generally estimated to be less than 1 ppm, except for the first 3 years at BRW and occasional parts of the SPO record where pressure-broadening corrections have been made with less certainty, and at SMO where portions of the record require editing because of occurrences of sample line contamination. The questionable SMO data occurred from mid-October 1977 to early February 1978 and from mid-October 1978 to early February 1979. Systematic errors are believed to be less than ±1 ppm relative to an absolute CO_2 mole fraction scale. The provisional values of table 6 are a subset of the full record and have been selected to eliminate unreliable data resulting from measurement problems and to eliminate highly variable data that are probably representative of local pollution.

Table 6.--Provisional monthly mean CO_2 fractions (ppm) for BRW, MLO, SMO, and SPO

Year	Jan	Feb	Mar	Apr	May	Jun	Jul	Aug	Sep	Oct	Nov	Dec
BRW												
1973	--	--	--	--	--	--	324.4	322.6	325.6	330.3	334.1	334.4
1974	338.2	336.8	337.5	338.8	337.3	336.4	331.0	325.1	325.8	330.1	333.3	336.3
1975	338.3	340.6	338.8	338.4	339.2	336.3	328.8	324.6	325.8	329.7	335.3	336.8
1976	337.4	337.8	338.7	339.0	338.2	337.1	331.3	323.6	325.1	330.0	334.1	336.4
1977	336.7	336.7	338.1	339.0	339.2	337.7	330.1	326.1	327.9	331.6	334.7	338.8
1978	339.3	340.0	341.7	341.0	342.1	339.6	332.4	328.7	328.4	331.8	338.1	338.5
1979	339.0	340.3	341.6	341.4	341.9	340.9	332.3	327.2	329.2	332.3	337.5	340.4
1980	341.0	341.7	342.9	343.5	343.1	341.9	336.5	331.7	331.3	337.9	340.4	342.8
1981	343.3	344.6	343.7	345.1	346.1	343.6	336.2	331.1	333.0	337.8	340.3	343.9
MLO												
1974	--	--	--	--	332.9	331.7	330.5	328.5	326.9	326.8	327.9	329.3
1975	330.4	331.2	331.8	332.9	333.6	333.0	331.3	329.4	328.0	328.0	328.9	329.2
1976	331.3	332.3	333.1	334.4	334.5	334.0	332.1	330.1	328.4	328.3	329.9	331.4
1977	332.4	332.8	334.6	335.8	336.5	336.0	334.1	332.1	330.7	330.9	332.2	333.5
1978	334.6	335.0	336.3	337.5	337.8	337.6	335.9	334.1	331.8	332.0	333.4	334.7
1979	335.8	336.3	337.5	338.6	338.5	338.8	337.2	335.2	333.7	334.0	334.9	336.1
1980	337.4	337.9	339.5	340.3	341.0	340.8	338.7	336.8	335.1	335.2	336.4	337.5
1981	338.6	340.1	341.3	342.1	342.6	342.2	340.0	338.0	336.6	336.8	338.4	339.6
SMO												
1976	333.5	333.1	332.6	332.5	331.8	332.3	332.1	332.4	332.6	332.7	333.1	333.1
1977	333.1	332.7	333.5	333.4	334.0	334.9	334.4	334.3	334.1	335.3	335.4	336.7
1978	337.8	335.4	335.6	335.8	335.5	335.7	335.3	335.8	337.3	338.3	338.2	339.2
1979	--	340.6	335.8	336.5	335.9	336.2	336.7	336.6	336.6	336.9	337.0	337.2
1980	337.9	337.9	338.2	337.5	338.0	338.2	338.1	337.6	337.5	337.4	337.8	338.4
1981	338.7	339.0	338.3	339.1	338.4	339.1	338.9	339.0	339.0	338.7	339.1	339.5
SPO												
1975	329.8	329.8	329.8	329.4	329.1	329.7	330.5	331.2	331.6	331.9	331.1	330.0
1976	329.7	329.5	329.3	329.3	329.3	329.5	329.9	330.4	331.0	331.1	331.2	331.1
1977	330.6	331.5	331.3	331.4	331.4	331.6	331.9	332.3	332.6	333.0	333.0	332.6
1978	332.3	332.5	333.1	333.6	333.6	334.1	334.4	335.2	335.9	335.9	335.7	--
1979	--	--	--	--	--	--	--	--	--	--	--	--
1980	335.7	335.5	335.6	335.4	335.5	335.9	336.4	336.7	336.9	337.5	337.5	336.6
1981	337.3	337.2	337.3	337.3	337.5	337.8	338.1	338.3	338.6	338.4	338.2	337.7

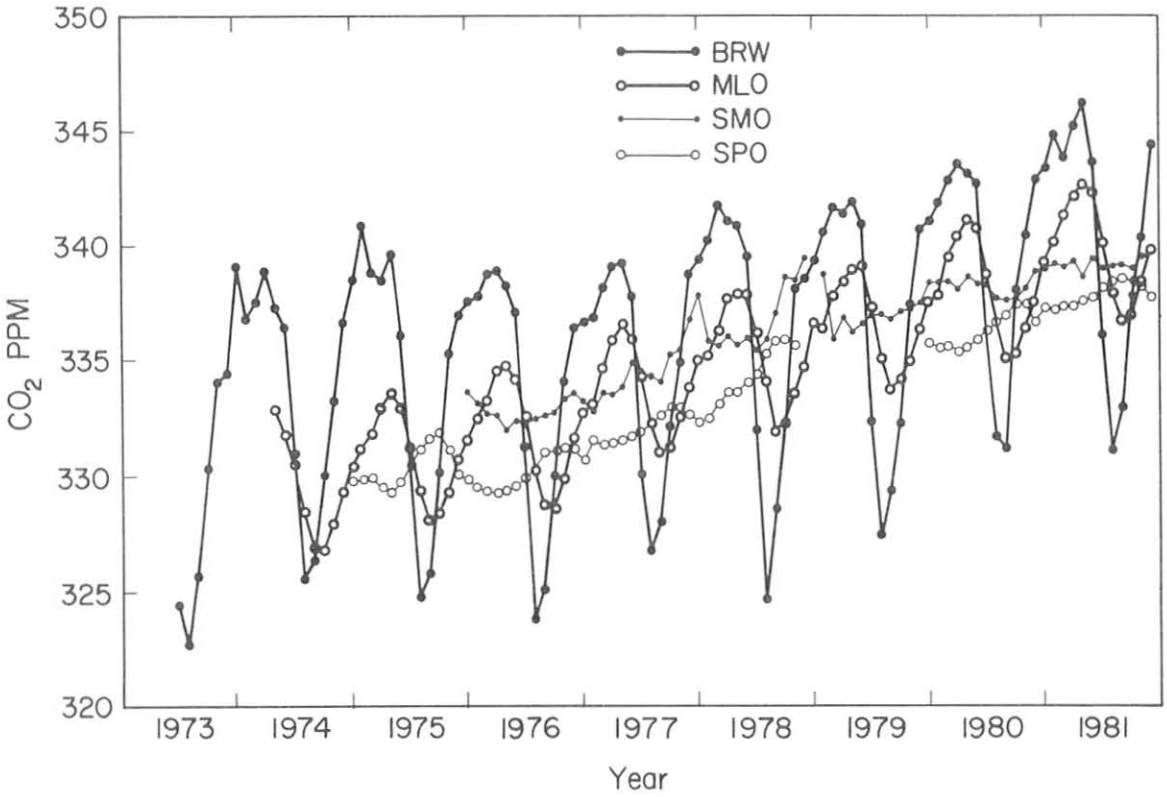

Figure 4.--Provisional monthly mean CO_2 mole fractions for GMCC observatories.

3.1.2 Flask Sample CO_2 Measurements

The GMCC CO_2 flask sampling program was expanded in 1981 to 20 stations, with startup sampling at Ocean Station M (66°N 02°E) and at Port Stanley, Falkland Islands (51°42'S 57°52'W). All stations active in 1981 are listed in the GMCC Summary Report for 1980 (DeLuisi, 1981, p. 20), with detailed station information (coordinates, elevation, and cooperating institutions and countries) given in the GMCC Summary Report for 1979 (Herbert, 1980, p. 19).

The edited flask data for 1979-1981 are presented in fig. 5 for the 20 flask stations in order of decreasing latitude. The data have been tightly edited for background conditions. Large portions of the period of severe contamination in 1979-1980 have been omitted entirely. The pair agreement criterion was chosen at ≤1 ppm. The record has also been scrutinized for large year-to-year changes in the seasonal pattern resulting from sample degradation due to long storage or from problems at the time of analysis. Occasional outlying values (≤2% of the data), although probably representing valid atmospheric concentrations, have been rejected from the selected set as not representative of background conditions. They were generally more than five standard deviations from the envelope of the selected data, as approximated by the dotted lines in fig. 5.

Edited in the manner described, the 3-yr flask record at most stations reveals a stable and characteristic seasonal pattern superimposed on a perceptible secular growth rate of ~1.4 ppm yr^{-1}. The fastest rate of CO_2 increase (~1.5 ppm yr^{-1}) is found at midlatitudes of the Northern Hemisphere, which is

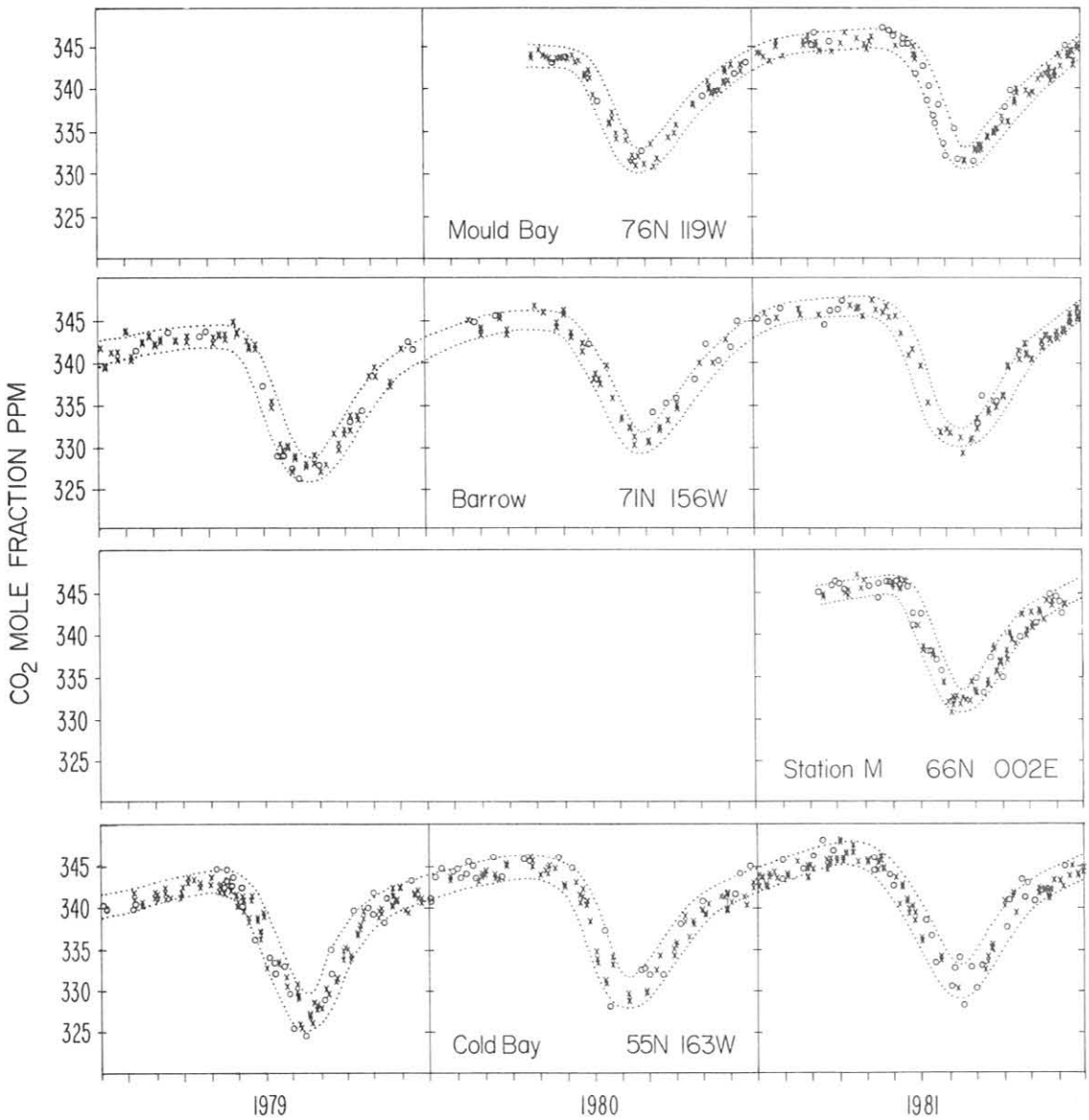

Figure 5.--Edited CO_2 flask data for 1979-1981 at 20 stations. Values are presented in the 1974 WMO CO_2-in-air mole fraction scale. The symbol × represents a reliable paired value; the symbol o represents a less-reliable, generally unpaired value. The dotted lines represent hand-drawn estimates of the envelope of the data, selected for background conditions.

consistent with the location of fossil fuel sources; significantly lower values (~1.2 ppm yr^{-1}) are observed for midlatitudes of the Southern Hemisphere.

The latitude dependence of the seasonal amplitude (fig. 6) reveals a maximum (~16 ppm) at high northern latitudes (~60°N) that is an order of magnitude greater than the mean for the Southern Hemisphere (~1.5 ppm). There is a clear indication of a stronger CO_2 seasonality at the Antarctic ice edge (2 ppm at Palmer Station, 65°S) than at the South Pole (1.5 ppm). In fig. 6, values for MLO (20°N, elev. 3400 m), NWR (40°N, 3750 m), Point Six Mountain (47°N, 2500 m), Azores (39°N 27°W, sea level, North Atlantic), and Station M

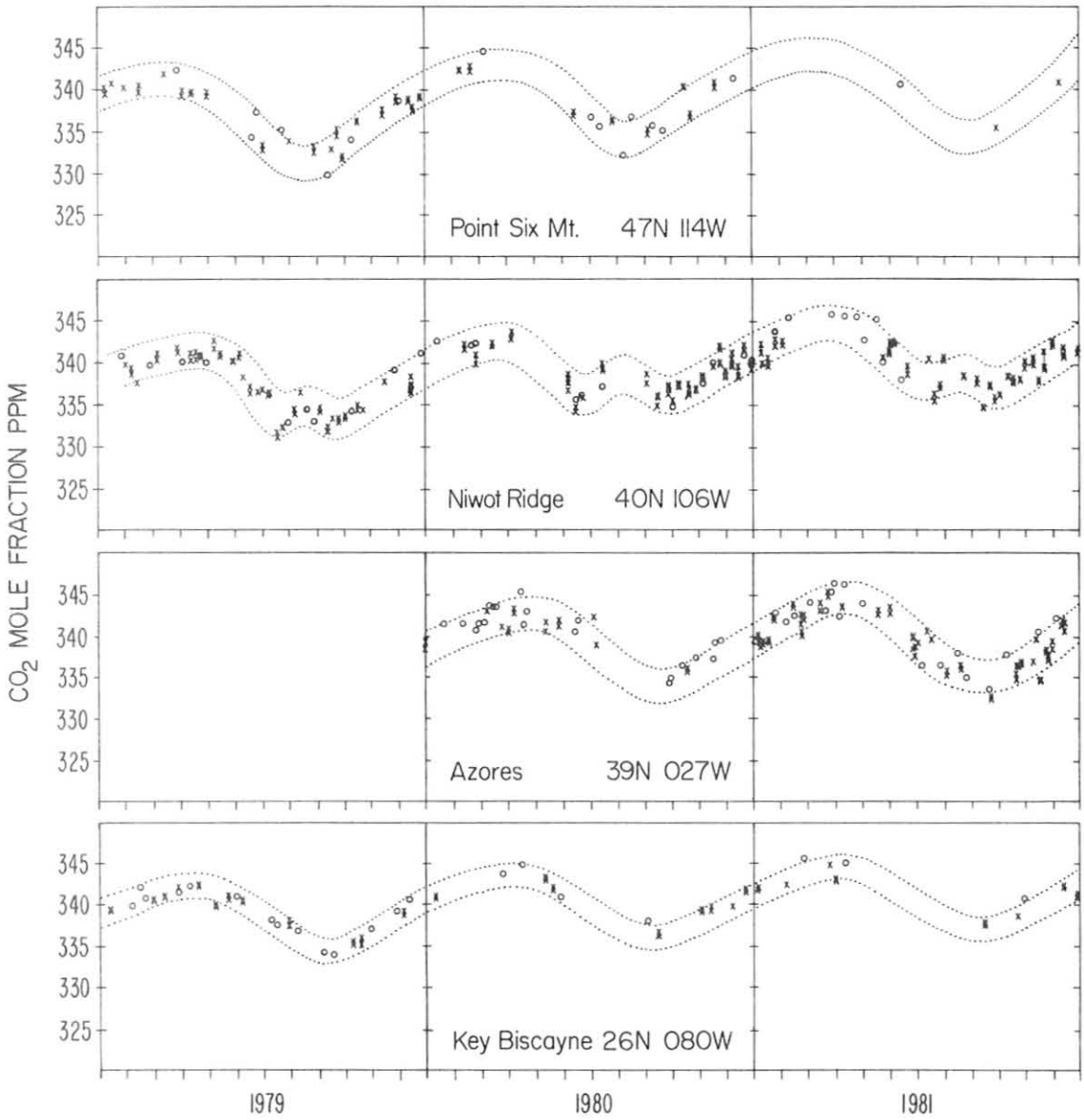

Figure 5.--Edited CO_2 flask data for 1979-1981 at 20 stations--Continued.

(66°N 02°E, sea level, North Atlantic) have been plotted with a different symbol (o) for comparison, but were not included in the fourth-order polynomial fit (smooth curve) to the data (*). Stations at higher elevations or very different longitudes (o) have smaller CO_2 seasonal amplitudes. The lower amplitudes at Azores and Station M in the North Atlantic suggest an ocean seasonality of ~2 ppm working out of phase with the dominant land biosphere seasonality at these latitudes. Weathership Papa (P) data are plotted for comparison. The seasonality for a sea level, midlatitude northern station will be available next year with startup data from Cape Meares, Ore.

Although the seasonal variations at several stations (Falklands, Cosmos, Key Biscayne, Azores, NWR, Point Six Mountain) are not yet well characterized, the full set of 20 stations reporting in 1981 may be synthesized to give a fair representation of the global CO_2 seasonality. Figure 7 presents a three-dimensional perspective on the global 1981 CO_2 distribution. Although some

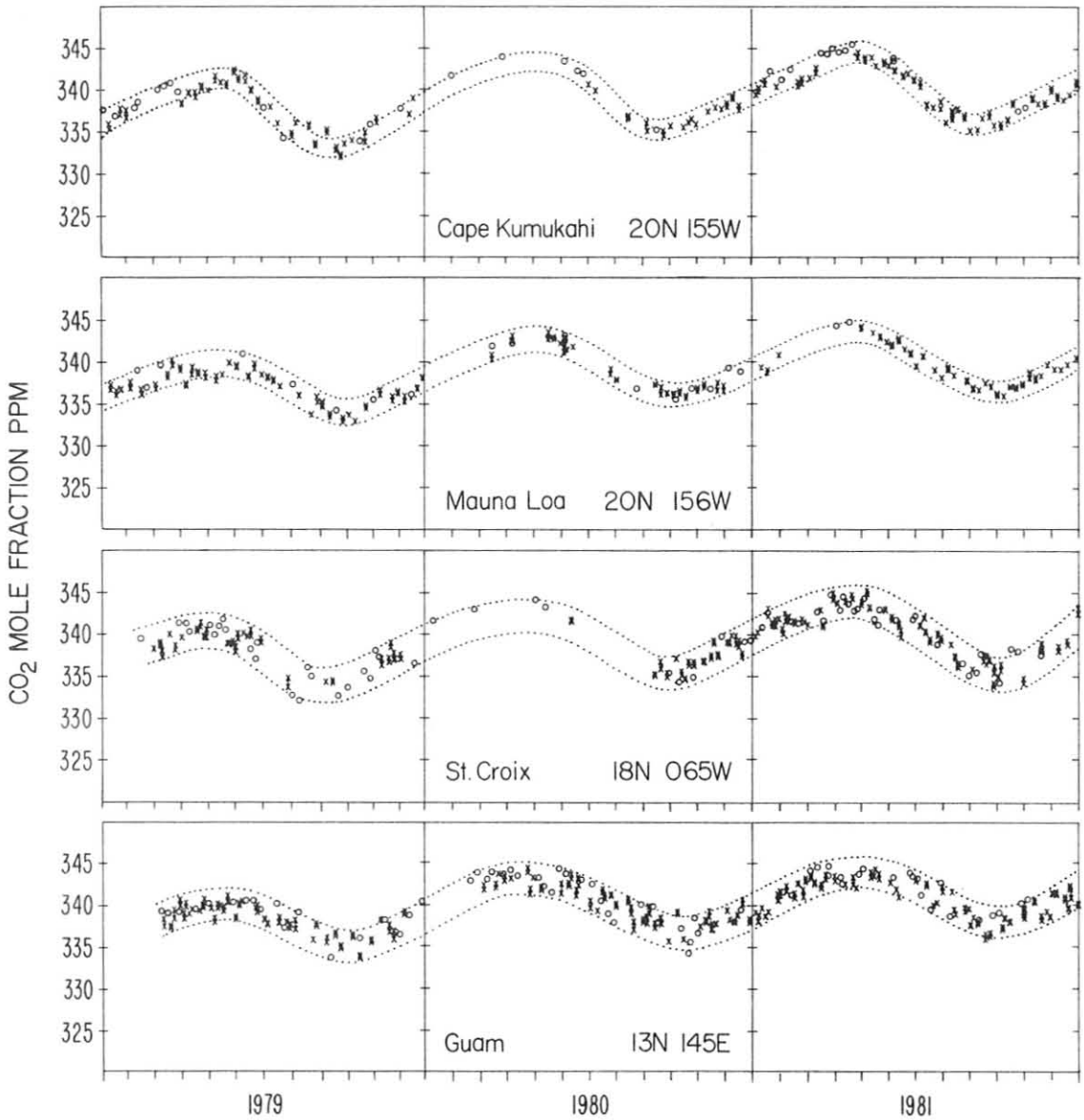

Figure 5.--Edited CO_2 flask data for 1979-1981 at 20 stations--Continued.

residual local bumpiness reflects the need for additional editing of outlying values, the major features of the global distribution are clear, especially the dominance of the Northern Hemisphere, high-latitude drawdown of CO_2 in late summer. This northern seasonality is transported across the equator to 15°-20°S. The "zero-phase" latitude, or effective equator for CO_2 seasonality is a flat trough at 15°-30°S. The most pronounced southern seasonality is in the latitude band 50°-70°S (Falklands to Palmer Station), and may well be related to seasonal variation of sea-ice cover and upwelling-downwelling in the Antarctic circumpolar current. Removing stations that are not at sea level and those in the Northern Hemisphere at very disparate longitudes would certainly smooth the Northern Hemisphere pattern. The secular increase has not been removed, so each latitude strip tends upward by ~1.3 ppm over the 1-yr timespan.

To improve the quality of flask samples collected for CO_2 analyses, several important changes were made during 1981 in the sampling methodology.

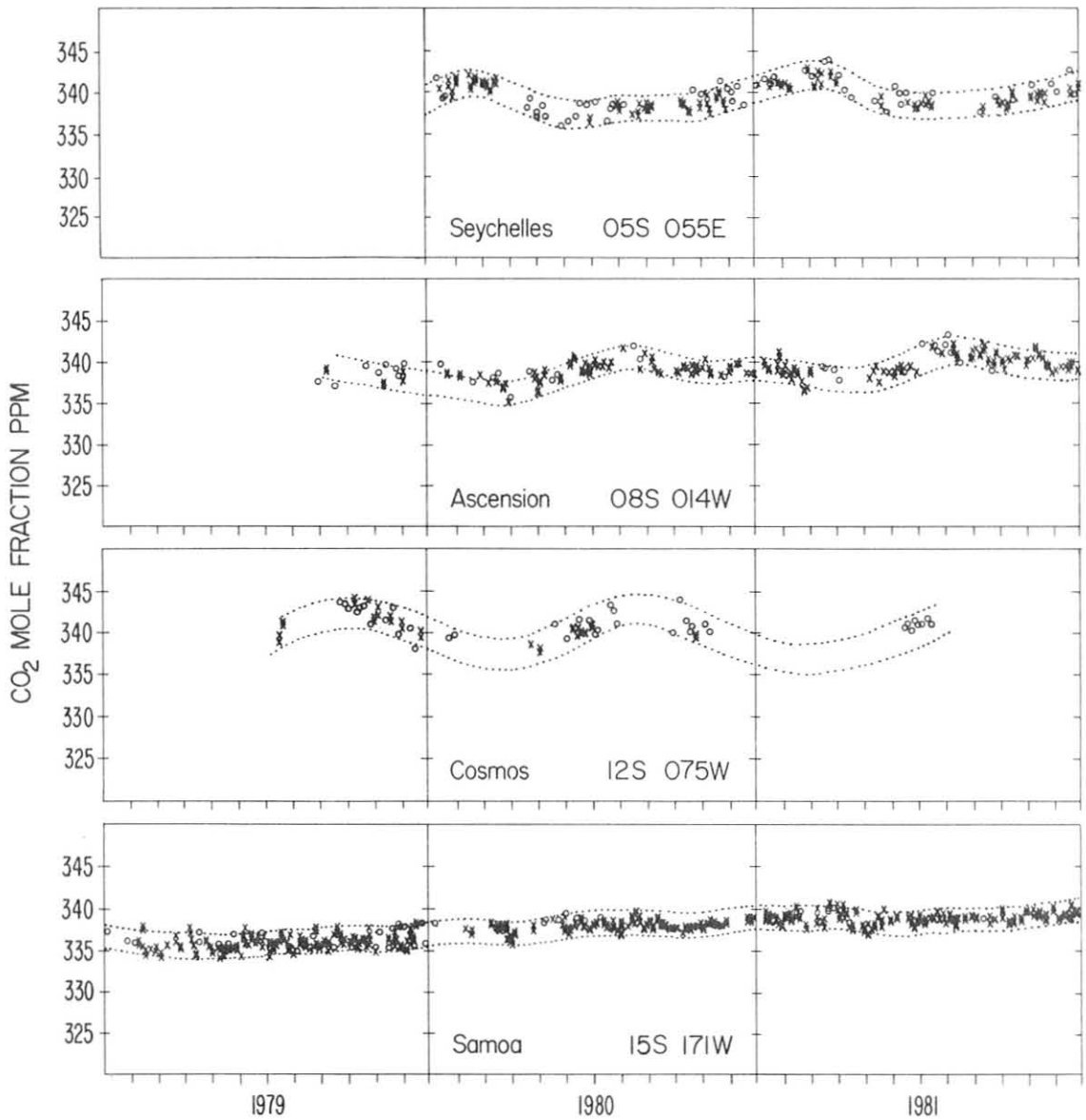

Figure 5.--Edited CO_2 flask data for 1979-1981 at 20 stations--Continued.

First, following the discovery that many of the glass flasks contained a powdery residue resulting from decomposition of traces of silicone grease during heat treating of the flasks, a program was initiated to reclean all flasks with an aqueous solution of hydrofluoric acid. Second, the method of flask preparation was changed from silicone-greased stopcocks and evacuated flasks to Apiezon-greased stopcocks and flasks initially evacuated and then filled to a slight positive pressure with a low-CO_2 reference gas prior to shipment to the sampling stations. Also in 1981, a small portable air-pumping system, P^3, was developed, tested, and deployed to all 20 stations. The system is used to collect pairs of air samples simultaneously in series in 0.5-ℓ glass flasks that are pressurized to approximately 1.3 atm. Introduction of the P^3 system dramatically improved pair sample agreement at most stations.

A milestone was reached in June 1981 when CO_2-in-N_2 calibration gases were replaced at MLO and SMO with CO_2-in-air calibration gases. Use of CO_2-in-N_2 had been discontinued in the GMCC flask sampling program in January

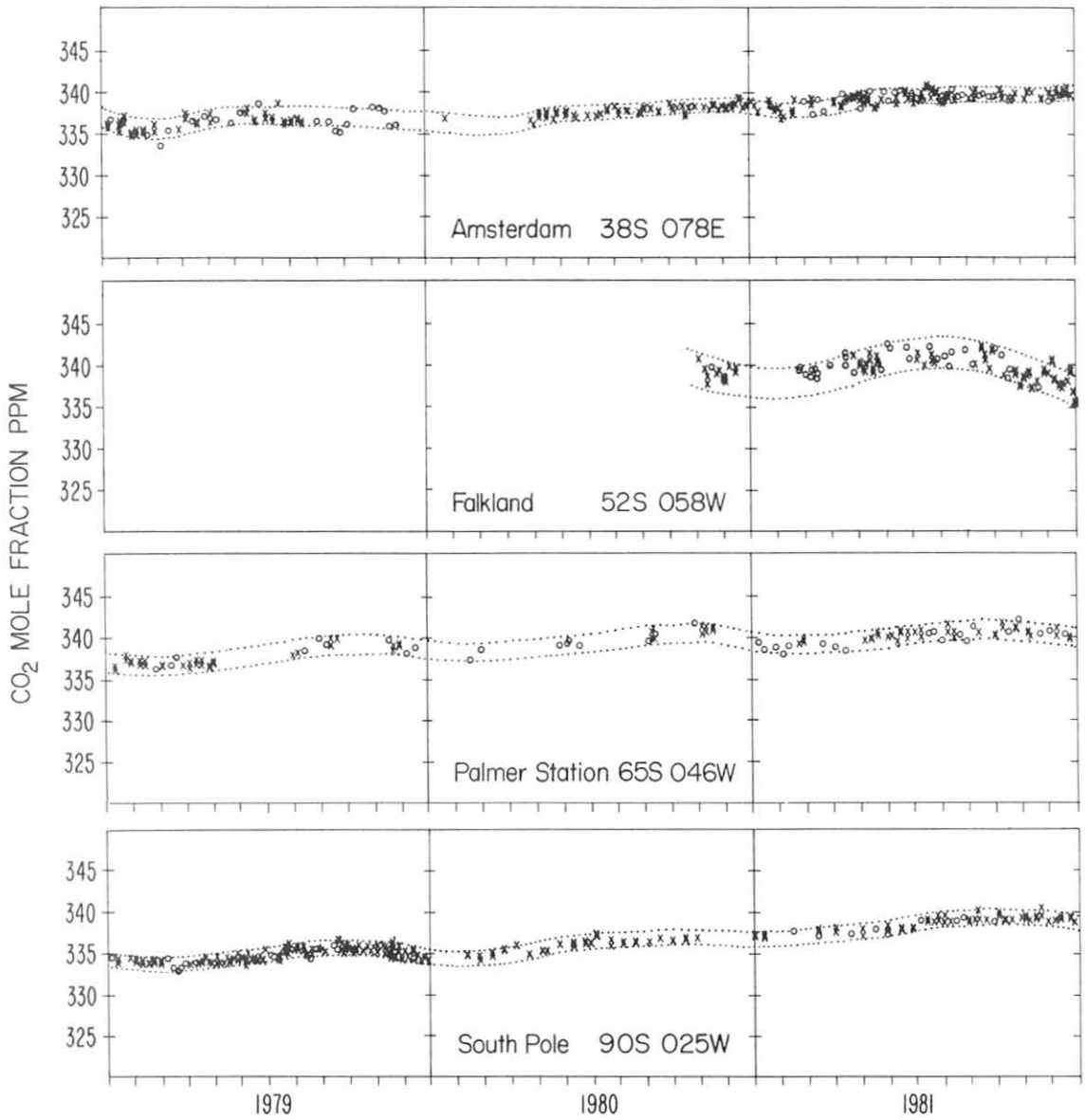

Figure 5.--Edited CO_2 flask data for 1979-1981 at 20 stations--Continued.

1979, and conversion to use of CO_2-in-air was made at BRW and SPO during middle and late 1980, respectively. The use of CO_2-in-air calibration gases eliminates the need to apply collision-broadening corrections to CO_2 data.

As a check on CO_2 flask sample data quality, several CO_2 data comparison programs were initiated in 1981 (Komhyr et al., 1982). One such program involves routine comparison of GMCC and SIO CO_2 flask sample data for BRW, KUM, MLO, and SMO. The GMCC and SIO samples are collected at these stations quasi-simultaneously, and data are exchanged without prior knowledge of the cooperating laboratory's results. For 54 sets of data compared during June through December 1981, the mean GMCC-SIO CO_2 concentration difference was 0.06 ppm. In a similar effort performed according to a WMO recommendation (WMO, 1981), a program was initiated late in 1981 with SIO whereby 12 GMCC flasks are sent to SIO for exposure four times each year. When sampling conditions are satisfactory, SIO collects CO_2 air samples in the GMCC flasks using GMCC techniques and, quasi-simultaneously, in SIO sampling flasks. GMCC flasks are returned

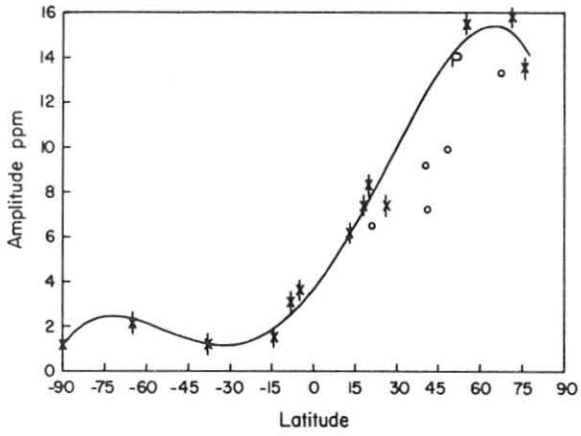

Figure 6.--Meridional distribution of the amplitude of the seasonal CO_2 concentration. The solid line is a fourth-order polynominal fit to the data (*), and the symbol o represents stations either not at sea level or at very disparate longitudes, which were not included in the fit. Weathership P data are plotted for comparison.

to Boulder for analysis, and SIO flasks are analyzed at SIO. Exchange of sample analysis data between the two laboratories is through WMO in Geneva.

Finally in yet another endeavor to assess CO_2 data quality, GMCC flasks and continuous analyzer data at BRW, MLO, and SMO were intercompared beginning in June 1981 when use of CO_2-in-air calibration gases was extended to all three stations. On the average, biases of only 0.1-0.2 ppm were observed (Komhyr et al., 1982). Such agreement in results is gratifying considering that the methodologies of flask and continuously operating analyzer CO_2 measurements differ significantly and that widely different environmental conditions are represented, namely, the humid, sea level atmosphere of SMO and the dry, rarefied air of MLO.

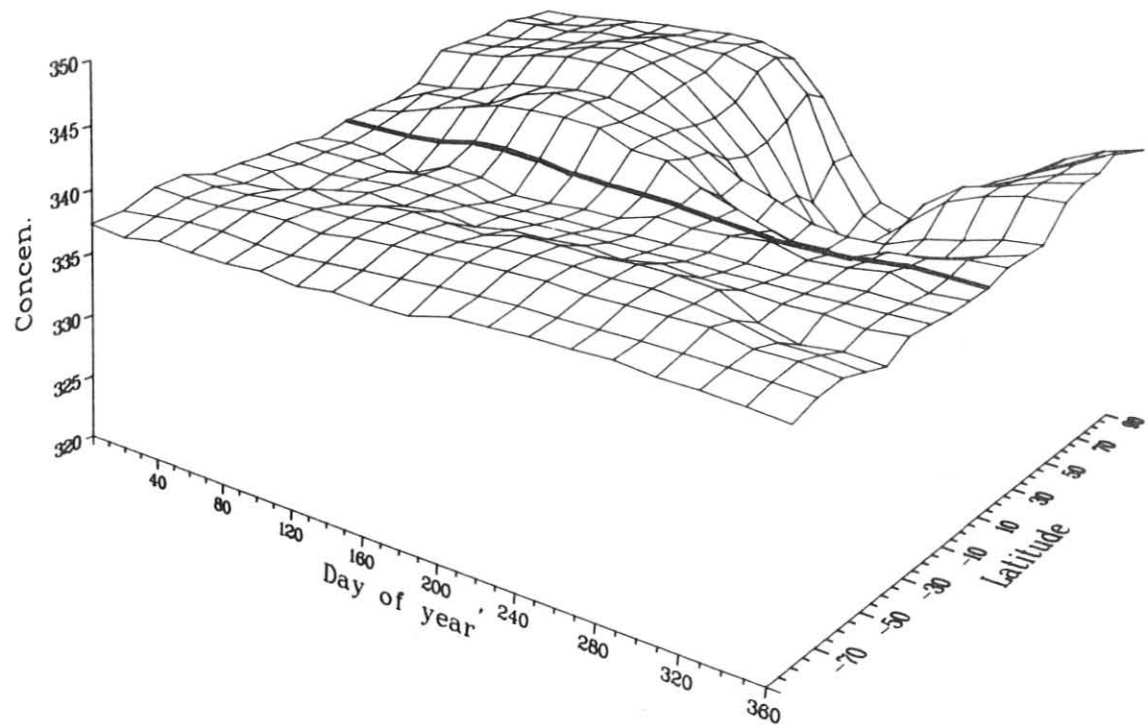

Figure 7.--Three-dimensional representation of the edited 1981 global atmospheric CO_2 distribution from the 20 flask sampling stations, a synthesis of the 1981 data presented for each station in fig. 5.

3.1.3 Miscellaneous

Thomas B. Harris retired in August 1981 after 34 years of government service, of which the last 10 years were in the GMCC program. Harris participated in the site selection of the GMCC observatories and was responsible for the operation of instrumentation in the CO_2 monitoring program.

3.2 Total Ozone

3.2.1 Routine Observing Program

Routine total ozone observations with Dobson ozone spectrophotometers were continued in 1981 at the four GMCC stations, one foreign cooperative station, three domestic cooperative stations, three NWS stations, and GMCC headquarters, Boulder. Table 7 lists the 12 stations, instrument numbers, the agencies responsible for taking observations, and observing time periods for which data are available.

During June, July, and August 1981, World Standard Dobson Ozone Spectrophotometer no. 83 was operated at MLO to check its calibration. No significant change was found. In September 1981 a trip was made to Nashville, Tenn., to erect a new 10-ft 6-in Ash Dome spectrophotometer shelter and to train station observers in the operation of the Dobson instrument. On 5 October 1981 observations of total ozone were reinstated at Tallahassee, Fla. They had been temporarily terminated at that station in May 1979.

3.2.2 Calibration Check of Dobson Spectrophotometers in the Global Network

In 1981 GMCC began a project in cooperation with the WMO Global Ozone Research and Monitoring Project. The global Dobson ozone spectrophotometer station network was divided into seven regions to check the calibration levels of those instruments in use throughout the world. A standard lamp power supply and two calibrated standard lamps will be shipped to each region. Upon

Table 7.--U.S. Dobson ozone spectrophotometer station network for 1981

Station	Period of record	Instrument no.	Agency
Bismarck, N.D.	1 Jan 1963-present	33	NOAA
Caribou, Maine	1 Jan 1963-present	34	NOAA
Tutuila Is., Samoa	19 Dec 1975-present	42	NOAA
Tallahassee, Fla.	2 Jun 1973-present	58	NOAA-Fla. State Univ.
Mauna Loa, Hawaii	2 Jan 1964-present	63	NOAA
Wallops Is., Va.	1 Jul 1967-present	38	NOAA-NASA
Barrow, Alaska	2 Aug 1973-present	76	NOAA
Nashville, Tenn.	1 Jan 1963-present	79	NOAA
Boulder, Colo.	1 Sep 1966-present	82	NOAA
White Sands, N.M.	5 Jan 1972-present	86	NOAA-Dept. of Army
Huancayo, Peru	14 Feb 1964-present	87	NOAA-Huancayo Obs.
Amundsen-Scott, Ant.	5 Dec 1963-present	80	NOAA

receiving the lamp unit, observers at each station will perform standard lamp tests on the Dobson instrument and determine the N-value for each lamp. Results of the tests will be sent to Boulder for analysis to determine the calibration status of each instrument and to identify instruments requiring recalibration.

3.2.3 Modernization and Calibration of Dobson Spectrophotometers

During 1981 GMCC personnel continued to participate in the WMO Global Ozone Research and Monitoring Project to upgrade the quality of Dobson spectrophotometers throughout the world. In June, Dobson instrument no. 64 from Potsdam, G.D.R, arrived in Boulder for modification and recalibration. New electronic circuitry and an electromechanical phase-sensitive rectifier were installed. After installation of an "air-space" optical wedge and alignment of optical components, instrument no. 64 was calibrated by direct comparison with the World Standard Dobson Instrument no. 83 and returned to Potsdam.

In August, U.K. instrument no. 41 arrived in Boulder for modification and recalibration. A provisional calibration showed it to be +2.7% out of calibration. The U.K. technician who accompanied the instrument to Boulder installed new solid state electronics and a new optical wedge. After alignment of the optical components, the instrument was calibrated by direct comparison with instrument no. 83 and returned to the United Kingdom.

Nashville, Tenn., instrument no. 79 and Tallahassee, Fla., instrument no. 58 were recalled to Boulder for minor modifications and recalibration. Results of intercomparisons made with these two instruments and instrument no. 83 indicated that the Nashville calibration was +3.33% in error, and the Tallahassee calibration was -2.62% in error.

3.2.4 Total Ozone Monthly Means

Daily 1981 total ozone values (applicable to local apparent noon) for all stations in the U.S. network have been submitted to and are available from the World Ozone Data Center, Atmospheric Environment Service, 4905 Dufferin Street, Downsview, Ontario M3H5T4. Table 8 lists monthly mean 1981 total ozone amounts for the NOAA observatories and cooperative stations.

Table 8.--Provisional 1981 monthly mean total ozone amounts (milli-atm-cm)

Station	Jan	Feb	Mar	Apr	May	Jun	Jul	Aug	Sep	Oct	Nov	Dec
Bismarck, N.D.	350	386	378	383	371	347	314	311	292	303	310	358
Caribou, Maine	390	381	427	435	401	386	364	333	321	320	335	339
Wallops Is., Va.	340	350	374	351	370	324	328	321	307	296	305	323
Tutuila Is., Samoa	256	254	260	256	263	265	264	258	268	268	272	266
Tallahassee, Fla.	-	-	-	-	-	-	-	-	-	279	281	287
Mauna Loa, Hawaii	241	251	268	288	281	278	269	269	268	264	254	254
Barrow, Alaska	-	-	432	-	387	368	350	320	327	-	-	-
Nashville, Tenn.	334	357	362	347	374	346	347	-	-	287	291	320
Boulder, Colo.	322	346	357	343	369	322	313	307	298	293	287	306
White Sands, N.M.	300	315	331	322	340	320	317	315	281	285	270	272
Huancayo, Peru	265	261	263	267	265	271	268	275	278	281	279	273

3.3 Ozone Vertical Distribution

3.3.1 Umkehr Observations

Umkehr observations yielding ozone profiles were continued at Boulder during 1981 with Dobson spectrophotometer no. 81. In December, regular measurements were begun using the automated Dobson instrument no. 61. The manual observations were continued during December to obtain comparison data.

Instrument no. 61 has been automated by mating an HP-85 computer to it for control and data processing. By controlling stepping motors to perform functions normally performed manually by an observer, the HP-85 selects the wavelengths at which observations are made and measures the difference in light intensity between strongly and weakly absorbing ozone lines. The shutter of the Ash Dome shelter has also been automated. (Precipitation detectors are used to keep the shelter closed during adverse observing conditions.) Umkehr observations are, therefore, completely automatic. Total ozone measurements have been semiautomated. After setting a sun director on the instrument's light inlet window and orientating the instrument correctly with respect to the sun, the operator merely activates a switch to initiate the total ozone measurement. About 2 minutes later the computer outputs the total ozone amount in Dobson units.

At the request of EPA and CMA, a proposal was written for automation of six additional Dobson spectrophotometers and establishment of a global automated Dobson instrument Umkehr observation station network by 30 April 1984. Data from the network are expected to provide information on possible long-term ozone destruction (e.g., by halocarbons) near 40 km. Data obtained will also be useful for comparison with satellite-derived atmospheric ozone vertical distributions.

3.3.2 Umkehr Data Analysis

Monthly mean ozone partial pressures derived from Umkehr observations for nine levels in the atmosphere are shown in fig. 8 for the 4 years of observations made in Boulder. In the layers below 4 mb a discernible annual variation exists. Below the 30-mb layer this cycle is associated with the wintertime poleward transport of ozone and shows a springtime maximum. Above 30 mb but below 4 mb the seasonal maximum occurs during the summer corresponding to a maximum in the photochemical production of ozone. In the two layers above 4 mb (note the much-expanded scale for these two layers in fig. 8) a semiannual cycle appears to predominate. It is in these top two layers that the largest percentage change due to the impact of halocarbons is expected. These data from Boulder show no readily discernible long-term trend for the 4 years of data shown.

3.3.3 ECC Ozonesonde Observations

A program was conducted during 1981 to extend balloon-borne ECC ozonesonde observations to the photochemically important stratospheric region of 40 km. The initial effort was concentrated in developing a reliable but inexpensive and easy-to-handle balloon vehicle system to carry the ozonesondes to desired heights. Some success was obtained with neoprene rubber balloons

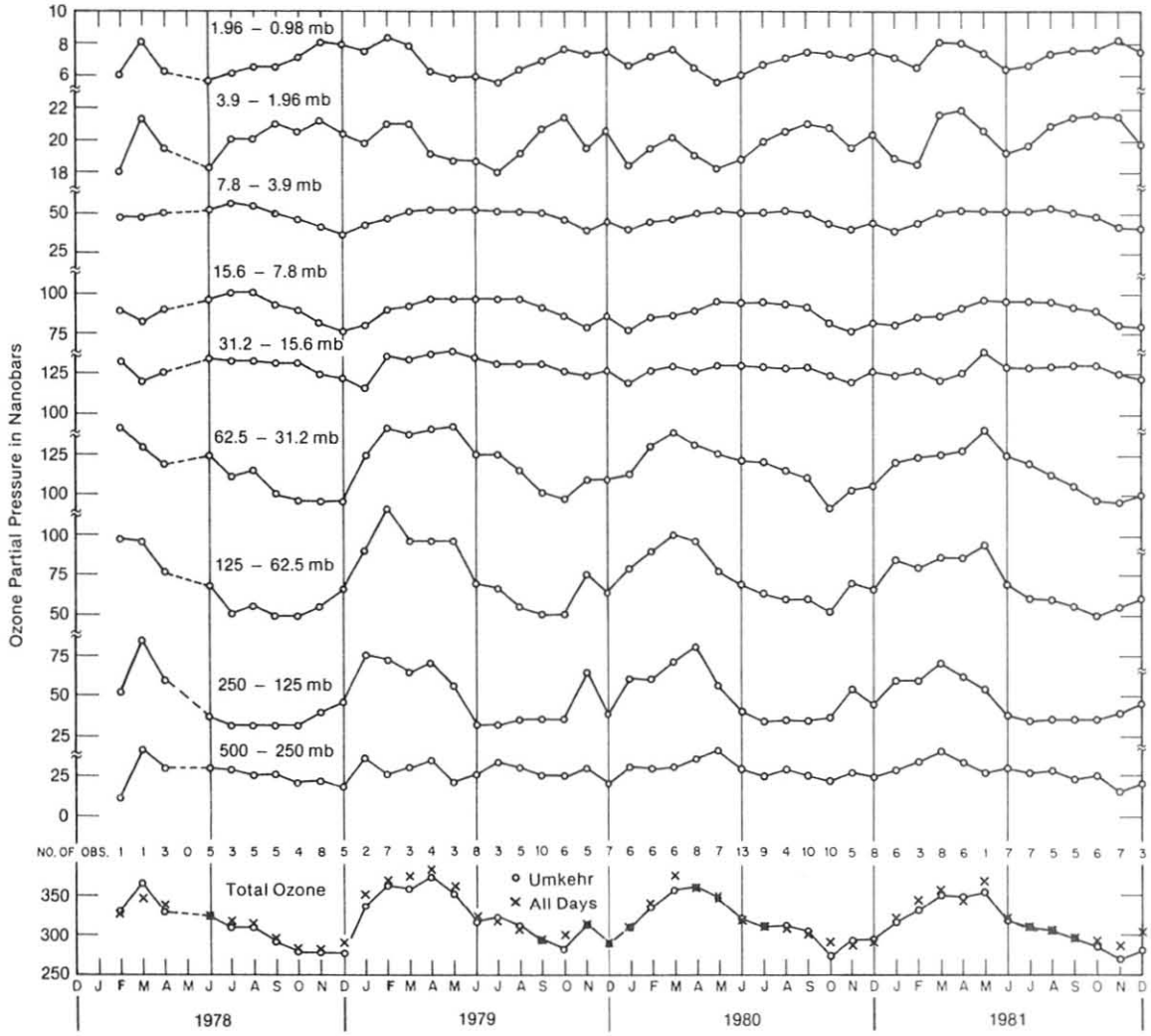

Figure 8.--Monthly mean ozone amounts at various levels in the atmosphere obtained from Umkehr observations in Boulder, Colo.

whose performance characteristics were found, however, to vary from batch to batch. Overall success rate in achieving 40-km heights was under 50%. In late 1981 a new plastic balloon material became commercially available that enabled balloons to be fabricated from material only about 0.006 mm thick. Whereas previously available plastic sheet balloons capable of carrying a 2-kg ozonesonde payload to 40 km weighed nearly 25 kg and required large amounts of helium, balloons made from the new material weigh only 7.5 kg and require only two tanks of helium for inflation (about 15 SCM). Success rate in using the new balloons has been nearly 100%.

Ozone vertical distributions to 40 km measured in Boulder during 1981 are shown in fig. 9. The soundings were made with Science Pump type 3A ECC ozonesondes. As a result of errors in pressure measurements above about 5 mb and variations in pumping efficiency from instrument to instrument, considerable

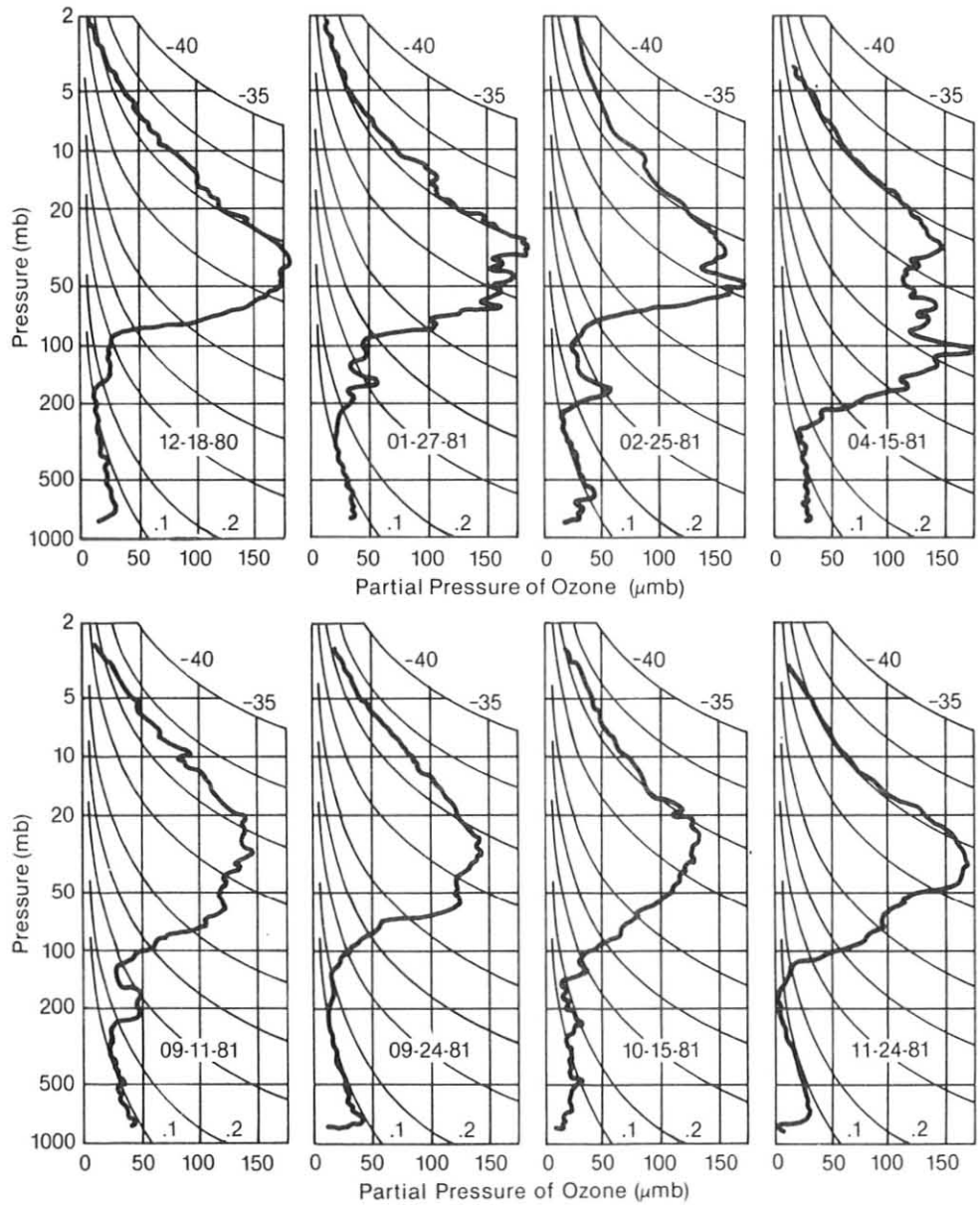

Figure 9.--High-altitude ECC ozone soundings made in Boulder, Colo., during 1981.

uncertainty exists in the reliability of the sonde data at altitudes above 10 mb. Recently, a new pump for ECC ozonesondes has been developed (Komhyr, 1981) that is expected to perform more reliably at high altitudes. Pump components are fabricated from TFE Teflon reinforced with 15% glass fibers. The piston and cylinders are of conventional design with circular cross sections, but the cylinder is fitted with externally located rubber rings that compress thin, flexible portions of the cylinder wall against the piston to form an effective piston-cylinder seal. Type 4A ECC ozonesondes are equipped with the new pumps. The new pumps are currently being tested to determine pumping efficiency at pressures of 100-2 mb.

3.4 Surface Ozone

Dasibi ozone photometers were operated at the four GMCC stations throughout the year. All of the station instruments have been intercompared with the GMCC standard photometer maintained in Boulder. In addition, three secondary standard instruments were established. One of the standards is to be maintained at SPO. The second will be used within the GMCC surface ozone network as a traveling standard for use in periodically calibrating station instruments at MLO, SMO, and BRW. When not in use as a traveling standard, this instrument will be located at MLO for more frequent calibrations of that station's instrument. The third standard is used in the GMCC ozonesonde program, and to check the stability of the Boulder standard photometer. Figure 10 diagrams the use of the Dasibi ozone photometers within the GMCC network.

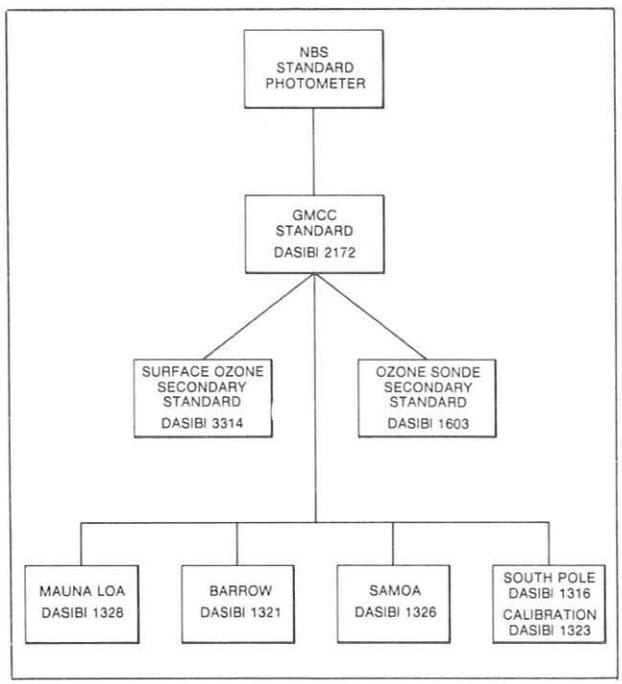

Figure 10.--Locations and uses of Dasibi ozone photometers in the GMCC surface ozone network.

Data for 1980 have not been processed but will be available in the future. The GMCC Summary Report for 1978 (Mendonca, 1979) and Oltmans (1981) describe shorter time scale variations in surface ozone at the GMCC observatories. With the addition of several more years of data it should be possible to investigate year-to-year variations in surface ozone.

3.5 Stratospheric Water Vapor

3.5.1 Operations

Balloon flights to measure stratospheric water vapor were made monthly during the year. Twelve successful flights were made in Boulder, and one flight was made in Palestine, Tex., as part of an international intercomparison of water vapor instruments. The measurements were made with frost-point hygrometers described in the GMCC Summary Report for 1978 (Mendonca, 1979).

3.5.2 Data Analysis

Figure 11 portrays the 13 water vapor soundings made during 1981. The mass mixing ratio of water vapor is plotted as a function of pressure for the region above the tropopause. The strong seasonal variation in the region around 100 mb and the relatively constant mixing ratio with altitude above 60 mb are noteworthy. During winter a minimum develops in the 14- to 16-km layer. The minimum weakens during the ensuing months and moves upward to the 19-km level by fall, where it disappears by year's end. A surprising feature is the appearance in October of a well-defined minimum, a feature that is seldom seen earlier than January in the Washington, D.C., soundings. This may be indicative of slightly different lower stratospheric airflow patterns over the two sites.

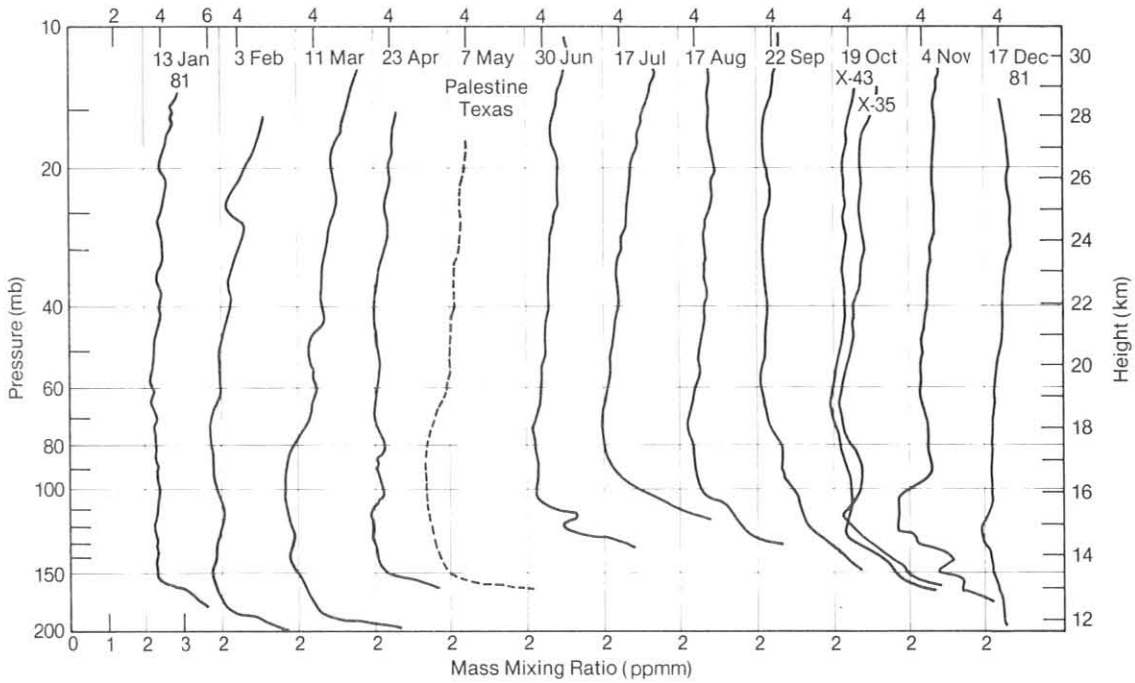

Figure 11.--Water vapor mass mixing ratio profiles for 12 soundings in Boulder, Colo., and 1 sounding in Palestine, Tex. Numbers along the top margin give volume mixing ratio in ppmv.

In October two water vapor sondes were launched within 3 hours of each other. Good quantitative agreement was achieved, with the differences lying within known measurement uncertainties.

The 12 soundings made in Boulder provide an opportunity to compare these measurements with soundings made from 1964-1980 at Washington, D.C., by NRL. At a level of about 60 mb the annual cycle in water vapor is relatively small, and as fig. 12 shows, the data from Boulder are somewhat less variable than earlier data from Washington, D.C. This reduced variability, which is typical of all altitudes, is probably a result of the improved instrumentation now being used.

An analysis of the data shown in fig. 12 reveals two important longer term cycles. If a 12-mo running mean is applied to these data (fig. 13), a

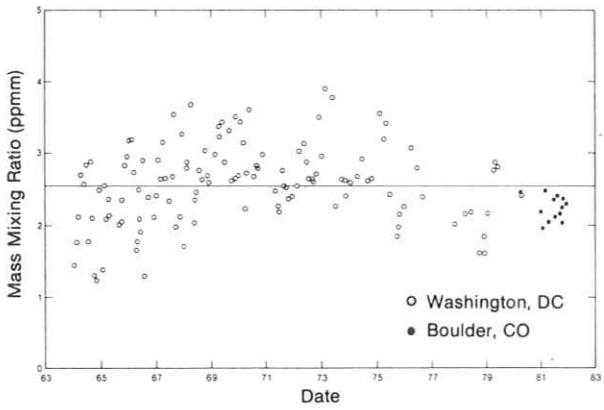

Figure 12.--Time series of water vapor mass mixing ratio at 60 mb for Washington, D.C. (open circles), and Boulder, Colo. (filled circles).

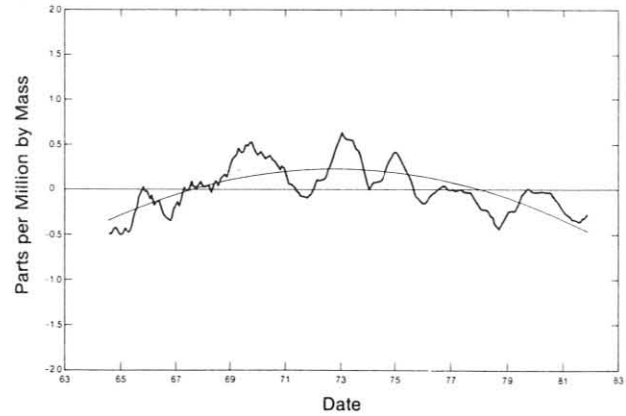

Figure 13.--The 12-mo running mean and parabolic trend of monthly water vapor mass mixing ratio at Washington, D.C., and Boulder, Colo. The long-term mean has been subtracted from the data.

quasi-biennial cycle is strongly suggested, especially after about 1971. Because a number of months of data are missing, especially in the late 1970's and in 1980, this finding must be considered preliminary. Comparison of this variation with the zonal winds at 50 mb at Ponape, located at about 7°N (fig. 14), shows that, since 1971, the minima in midlatitude water vapor concentration follow the minima in the Ponape zonal winds by about 10-12 months. This is consistent with the relationship between stratospheric ozone behavior at the quasi-biennial period (Oltmans and London, 1982).

Also shown in fig. 13 is a nonlinear trend fit to the data, which shows generally increasing values from 1964 to 1972 and decreasing values thereafter. By 1981 the Boulder values were nearly as low as those at the beginning of the observational series at Washington, D.C.

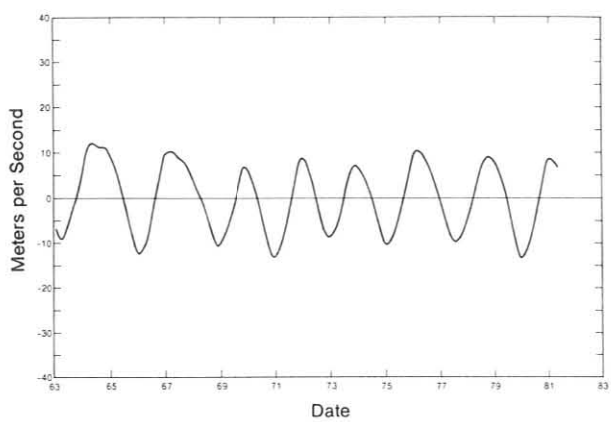

Figure 14.--The 12-mo running mean of the 50-mb zonal wind at Ponape (7°N).

3.6 Halocarbons and Nitrous Oxide

3.6.1 Operations

Routine collection of air in stainless steel flask pairs continued during 1981 at the four GMCC stations and at NWR. Samples were collected weekly at all stations except SPO where biweekly sampling prevailed. Sample quality was generally high, except at SPO where long storage time and extreme temperatures degraded the samples. Analysis of the air samples for CFC-11 (CCl_3F), CFC-12 (CCl_2F_2), and nitrous oxide (N_2O) continued at the Boulder chromatographic laboratory with few instrument problems and no procedural changes.

A used Perkin Elmer 3920 gas chromatograph, obtained in 1980, was totally reconditioned in 1981. Detectors were sent to Nuclear Sources and Services, Inc., for cleaning and testing. The electrometer circuit board was exchanged for a new one, all new carrier gas lines and controls were installed, temperature circuits were calibrated, oven insulation was improved, and a sampling valve was modified to provide on-column sample injection. After reassembly of the chromatograph, tests indicated that the detector response was high but sensitive to environmental temperature changes.

The chromatographic laboratory was reconfigured in December by installing all ancillary equipment in a rack between the two gas chromatographs. This has greatly facilitated sample analyses. Additions to the laboratory in 1981 were a spare pressure manometer system and flow controller system.

3.6.2 Calibration

The GMCC CFC-11, CFC-12, and N_2O secondary standard calibration gas tank (no. 3072) was sent to R. Rasmussen of OGC in April for its routine stability check. Results showed a decrease in CFC-11 and a continuing increase in CFC-12.

A question has been raised concerning the stability of the GMCC CFC-12 calibration secondary standard since no drift of this standard has been detected during calibration intercomparisons performed in Boulder relative to two other CFC-12 calibration gases. Tank no. 3072 gas has been intercompared quarterly with tank no. 3079 gas for 3 years and with tank no. 3088 gas for 4 years. This problem points to the neccessity of maintaining an independent calibration facility in Boulder for the halocarbon and N_2O monitoring programs.

An absolute calibration system for trace gases such as CFC-11, CFC-12, and N_2O was devised by W. Komhyr in 1979 (GMCC Summary Report for 1980, DeLuisi, 1981). As applied (e.g., to N_2O), the method involves preparation by gravimetric means of an N_2O/CO_2 gas mixture of accurately known mass ratio, and subsequent dilution of this mixture with N_2O- and CO_2-free air to approximately ambient air concentrations of these trace gases. From a determination of the absolute CO_2 concentration in this dilution mixture using accurately calibrated CO_2 gas standards and an NDIR analyzer, the N_2O concentration in the dilution mixture is readily inferred. CFC-11 and CFC-12 trace gases are calibrated by a similar method.

Preliminary work in implementing the calibration technology described above has already been accomplished. Calibration data obtained for N_2O indicate concentration values 10% lower than those obtained at OGC, but in agreement with those obtained by other researchers. These differences will be resolved in the near future.

3.6.3 Data Analyses

Selected 1981 data for CFC-11, CFC-12, and N_2O have been added to 4 years of previous data and are plotted in figs. 15, 16, and 17, respectively. Mean concentrations for 1981 and results of least-squares quadratic regression analyses of the 5-yr data sets for CFC-11 and CFC-12 are summarized in table 9. CFC-11 mean mixing ratios for 1981 are in the range of 188-205 pptv, with the highest concentration found at BRW. Regression analyses predict mixing ratios in the range of 135-154 pptv on 1 January 1977 and growth rates in the range of 11-14 pptv yr^{-1}. CFC-11 data for MLO show a slight but statistically significant decrease in growth rate. CFC-12 mean mixing ratios for 1981 are in the range of 321-345 pptv, with the highest concentration again found at BRW. Regression analyses predict mixing ratios in the range of 239-276 pptv on 1 January 1977 and growth rates in the range of 12-18 pptv yr^{-1}. CFC-12 data for BRW and SPO show statistically significant increases in growth rates. The CFC-12 data incorporate corrections for calibration gas drift as indicated by calibrations performed at OGC. It is likely that results for CFC-12 will change significantly following resolution of the gas calibration problem referred to in sec. 3.6.2.

Table 9.--Mean mixing ratios for 1981 and results of least-squares quadratic regression analyses of GMCC CFC-11 and CFC-12 data for 1977-1981*

Station	No. of obs.	Mean mixing ratio for 1981 (pptv)	Mixing ratio on 1 Jan 1977 (pptv)	Growth rate (pptv yr^{-1})	Growth rate change (pptv yr^{-2})†
CFC-11					
BRW	209	204.7	153.7 ± 0.45	11.33 ± 0.16	-
NWR	216	199.0	150.5 ± 0.47	10.78 ± 0.16	-
MLO	210	196.7	141.2 ± 0.80	14.36 ± 0.70	-0.45 ± 0.13
SMO	221	188.3	135.4 ± 0.40	11.76 ± 0.14	-
SPO	75	188.0	138.4 ± 1.89	11.02 ± 0.61	-
CFC-12					
BRW	190	345.4	274.4 ± 2.11	12.63 ± 1.64	0.70 ± 0.28
NWR	143	337.5	275.5 ± 1.42	13.78 ± 0.40	-
MLO	190	339.7	267.4 ± 1.22	16.08 ± 0.41	-
SMO	216	322.3	243.4 ± 0.83	17.53 ± 0.29	-
SPO	70	321.3	239.4 ± 3.30	12.09 ± 2.53	1.36 ± 0.44

*Coefficients are followed by their standard deviations.
†98% confidence interval.

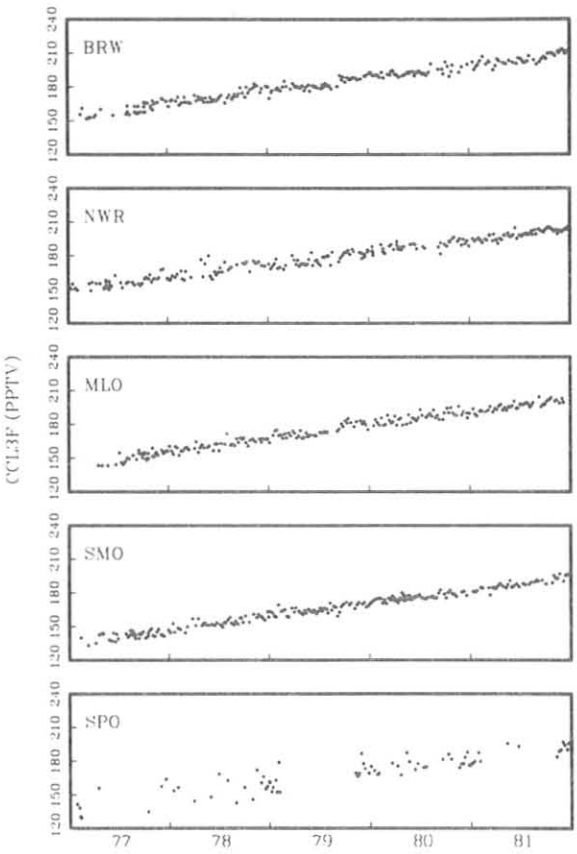

Figure 15.--GMCC's CFC-11 data record.

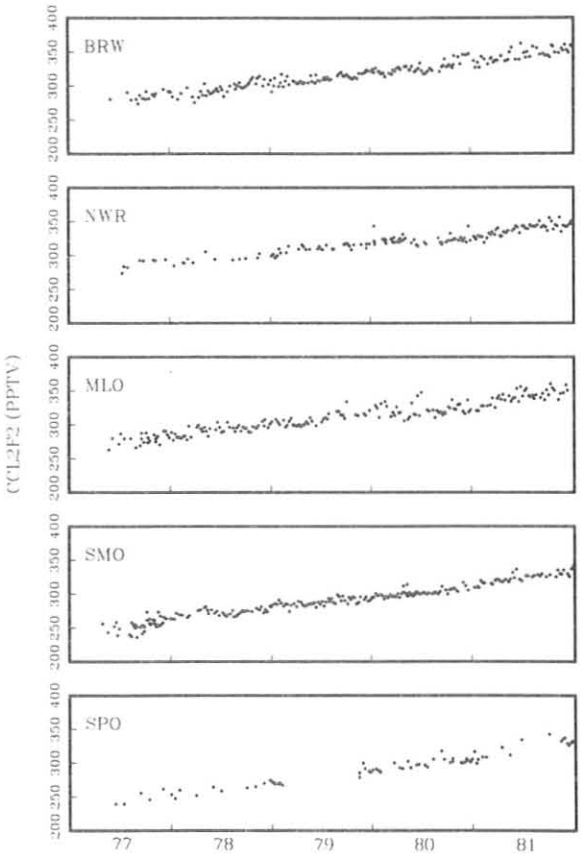

Figure 16.--GMCC's CFC-12 data record.

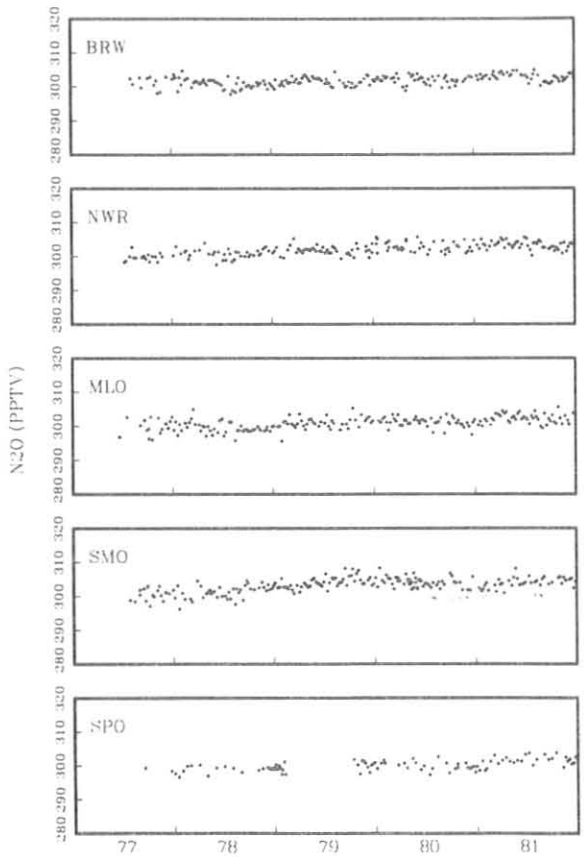

Figure 17.--GMCC's N_2O data record.

Table 10.--Mean mixing ratios for 1981 and results of least-squares quadratic regression analyses of GMCC N_2O data for 1977-1981*

Station	No. of obs.	Mean mixing ratio for 1981 (pptv)	Mixing ratio on 1 Jan 1977 (pptv)	Growth rate (pptv yr^{-1})	Growth rate change (pptv yr^{-2})†
BRW	199	302.5	300.4 ± 0.23	0.47 ± 0.08	-
NWR	187	303.2	298.5 ± 0.47	1.76 ± 0.37	-0.16 ± 0.06
MLO	199	302.0	298.9 ± 0.28	0.70 ± 0.09	-
SMO	197	304.1	297.4 ± 0.58	3.67 ± 0.45	-0.48 ± 0.08
SPO	94	301.1	297.6 ± 0.39	0.78 ± 0.11	-

*Coefficients are followed by their standard deviations.
†98% confidence interval.

Mean concentrations and summary results for similar regression analyses of the N_2O data are presented in table 10. N_2O mean mixing ratios for 1981 are in the range of 301-304 pptv, indicating that the gas is well mixed globally. Regression analyses predict mixing ratios in the range of 297-300 pptv on 1 January 1977. Growth rates are in the range of 0.5-1.8 pptv yr^{-1}, except for SMO, which shows the much larger growth rate of 3.67 pptv yr^{-1} that is not yet explained. N_2O data for NWR and SMO show small but statistically significant decreases in growth rates.

3.7 Stratospheric Aerosols--Lidar

3.7.1 Operations

Twenty-four successful lidar observations of the stratosphere were made during the second half of 1980, and 22 successful observations were made through 1981. The operational plan for lidar observations calls for an average rate of one observation every 2 weeks during unperturbed stratospheric conditions and an increase in the frequency of measurements where significant enhancements in stratospheric dust are detected.

3.7.2 Data Analysis

Lidar data for 1980 and 1981 have been processed and will be published, along with a summary, in a NOAA Technical Memorandum. A brief summary of the 1980-1981 observations is given here in terms of stratospheric dust optical depth integrated between approximately 13-15 to 28-30 km, which is the upper limit of the sounding.

Figure 18 shows a plot of stratospheric dust optical depth (λ = 694.3 nm) vs. time using the present data set. No range of uncertainty is given with these data; however, a comparison between these values and values of stratospheric dust optical depth for 1980 deduced from the MLO apparent transmission

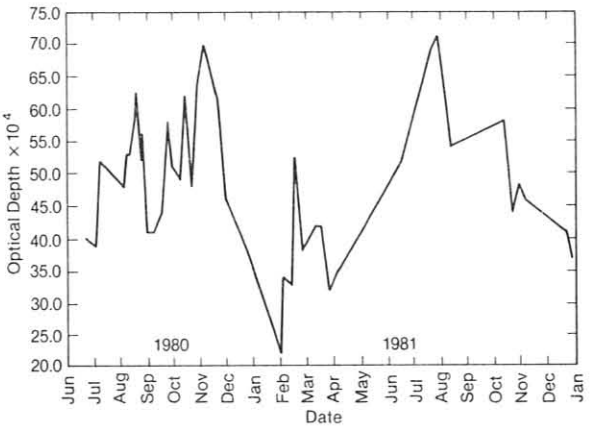

Figure 18.--Stratospheric dust optical depth (λ = 694.3 nm) at MLO as deduced from lidar observations during 1980 and 1981.

measurements showed that these values do not differ significantly. Determination of the uncertainty in lidar optical depth estimation by using other optical transmission measurements is planned.

The data plotted in fig. 18 reveal some interesting features. The first is that the variation in optical depth from minimum to maximum is about a factor of 3; the second is that the average optical depth of 0.005 (approximate) is what could be expected for an unperturbed stratosphere; and the third is that an increasing trend is seen during June to November in 1980 whereas the opposite is seen in the 1981 data. If an annual cycle in stratospheric dust optical depth does exist (as in the case of tropospheric dust optical depth), it may be easily disguised by volcanic eruptions that are expected to occur at random. As the size of the lidar data record is lengthened it may eventually be possible to isolate an annual cycle.

3.8 Surface Aerosols

The GMCC surface aerosol monitoring program during 1981 included the continuous measurement of CN concentration and integrated light scattering at BRW, MLO, SMO, and SPO. All data were recorded on magnetic tape and backup chart recorders. The data from the magnetic tape are available as both minute and hourly means. The Leeds and Northrup Speedomax 250 chart recorders print about three points per minute for each channel and provide information for quality control in addition to fill-data to cover downtime for the data acquisition system.

CN concentrations were measured using G.E. automatic CNC's (catalog no. 112L428) with modifications suggested by N. Ahlquist of the University of Washington. The modifications have resulted in improved sensitivity and reliability for these instruments and have been discussed in the GMCC Summary Report for 1976 (Hanson, 1977). Pollak CNC's (model P, BGI, Inc., Waltham, Mass.) are located at all sites as secondary standards to provide calibration for the automatic CNC's. A calibration check and a background compensation adjustment for the automatic CNC are performed daily. The calibration procedure is explained in detail by Bodhaine and Murphy (1980).

Light scattering was measured at the GMCC stations using specially constructed four-wavelength integrating nephelometers manufactured by MRI, Inc.,

Table 11.--Serial numbers of aerosol instruments at GMCC stations

Instrument	BRW	MLO	SMO	SPO
Pollak CNC	16	13	20	15
Nephelometer	105	103	106	107

Altadena, Calif. These instruments measure σ_{sp}, the scattering portion of extinction due to particles, simultaneously at 450-, 550-, 700-, and 850-nm wavelengths. Operation of the nephelometers is discussed in more detail in Hanson (1977) and Bodhaine (1979). Calibration of the nephelometers is performed at 2-mo intervals by filling them with CO_2 gas and adjusting the instrument outputs to agree with the known scattering coefficients of CO_2. Checks of the instruments' internal voltages are made daily. Weekly relative calibrations are performed using the internal calibration objects built into the instruments.

Table 11 gives the serial numbers of the Pollak CNC's and nephelometers located at the GMCC stations.

3.8.1 Barrow

The BRW Pollak CNC operated properly throughout 1981 without problems. Daily observations provided routine calibration checks for the G.E. automatic CNC. These observations have been keypunched and are available as a separate file on the Boulder computer. The G.E. CNC produced acceptable data for 89% of the hours in the year. Other than downtime for routine calibration and maintenance, the major periods of downtime were DOY 1-13, 111-113, and 305-314.

The nephelometer produced acceptable data for 97% of the year, with the only significant downtime occurring during DOY 7-13, 57, 106, 132, 237, and some minor intermittent problems occasionally during 290-309.

3.8.2 Mauna Loa

The MLO aerosol measurement program was started in September 1967 by B. Mendonca using Gardner counter SN826. Subsequently, A. Hogan of ASRC/SUNYA installed Pollak CNC SN13 (to be used to calibrate the G.E. automatic CNC), and routine Pollak CNC observations began in June 1974. All data taken with the Gardner and Pollak CNC's have been keypunched and are available on the Boulder computer.

The MLO Pollak CNC operated properly throughout 1981 without problems. Daily observations provided routine calibration checks for the G.E. automatic CNC. The G.E. CNC produced acceptable data for 87% of the year. The only significant downtime occurred during DOY 56, 59-61, 64-67, 80-81, 84-85, 165-166, 171-175, 344, 347-348, and 358-365. Most of these data could be recovered from the backup chart recorder.

The nephelometer produced acceptable data for only 37% of the year. Periods of downtime were DOY 45-61, 80-81, 109-110, and 143-365. In June the

instrument was shipped to Boulder and then to the University of Washington for repair, and was down for the remainder of the year.

3.8.3 Samoa

The SMO Pollak CNC operated properly throughout 1981 without problems. Daily observations provided routine calibration checks for the G.E. CNC. The G.E. CNC produced acceptable data for 88% of the year. The only significant period of downtime was DOY 80-114 when the instrument was shipped to Boulder for repair.

The SMO nephelometer produced acceptable data for 77% of the year. The instrument underwent modifications at the University of Washington to allow operation of a Hamamatsu photon-counting photomultiplier at room temperature rather than the RCA type C31034, which requires a thermoelectric cooler. The instrument experienced no significant downtime after it was installed on DOY 74.

3.8.4 South Pole

The SPO aerosol measurement program was started by A. Hogan in 1974 with the installation of Pollak CNC SN15, funded by NSF.

The SPO Pollak CNC operated properly throughout 1981 without problems except for the period DOY 59-64 when the humidification element in the instrument was dry. The G.E. CNC produced acceptable data for 73% of the year. Downtime occurred during DOY 283-365; on opening flight the instrument was shipped to Boulder for repair. The problem was unusual and was finally traced to a dirty meter switch that apparently was causing unpredictable feedback paths throughout the circuitry.

The nephelometer arrived at SPO in January 1981 with several broken components and an inoperable high-voltage power supply. The instrument was online DOY 30 and produced acceptable data for 64% of the year. Other than January, most of the downtime was caused by slow recovery of the instrument after a relative calibration.

3.8.5 Data Analysis

Data analysis has proceeded as described in the previous annual reports. All observer notes and chart recorder data are examined upon receipt in Boulder to assure proper instrument performance. Aerosol data are stripped from the monthly tapes made available by the A&DM group, and files of hourly means and 10-min graphics are produced. Missing data are then filled in, and necessary editing and calibration are applied. All aerosol data are available from GMCC in printout, microfiche, magnetic tape, or graphic form.

3.8.6 Discussion of Selected Data

Light scattering σ_{sp} and CN data for the four stations are presented in fig. 19. All available data were used to calculate monthly geometric means,

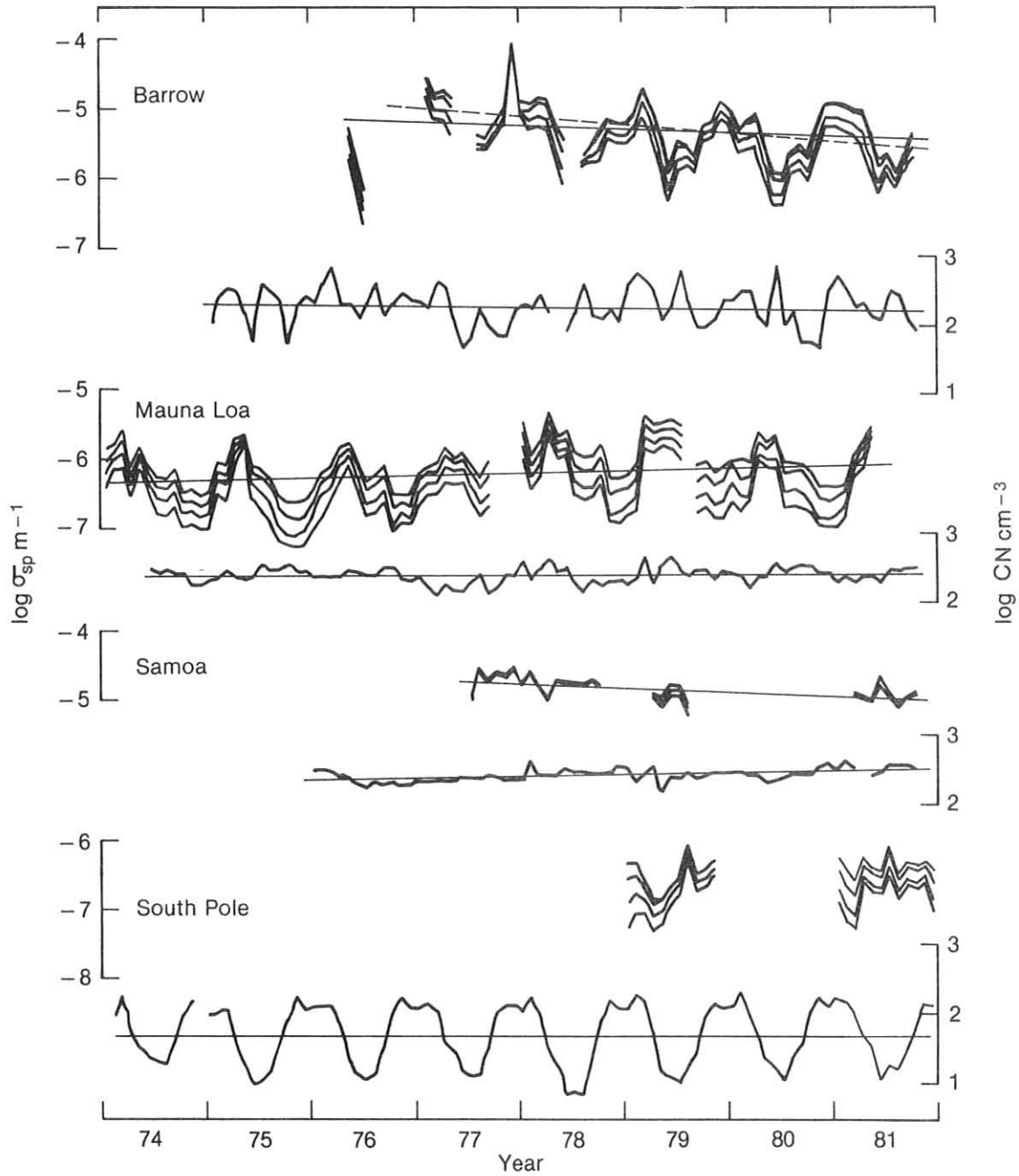

Figure 19.--Monthly geometric means of all light-scattering σ_{sp} and CN data acquired at BRW, MLO, SMO, and SPO. Only 0000-0800 LST data for MLO were used. Linear least-squares trend lines are shown for all data sets except SPO light scattering. The dashed line for BRW light scattering is the trend with 1976 data omitted. Details of the trend analysis are given in table 12.

Table 12.--Least-squares trend analysis of the common logarithms of the data given in fig. 19*

	Slope	Intercept	S.E.†	Trend yr^{-1}
BRW				
σ_{sp}(solid)	-0.00388	-5.037	0.4005	-10.0%
σ_{sp}(dash)	-0.00927	-4.637	0.3522	-23.0%
N	0.0000253	2.253	0.2824	0.7%
MLO				
σ_{sp}	0.00384	-6.340	0.3387	11.2%
N	0.00104	2.323	0.1164	2.9%
SMO				
σ_{sp}	-0.00413	-4.515	0.1198	-10.8%
N	0.00231	2.298	0.0181	6.6%
SPO				
N	0.0000172	1.684	0.4424	0.05%

*The scale of the abscissa in fig. 19 is such that January 1974 = 1 and December 1981 = 96.
†S.E. = standard error.

except for MLO, for which only 0000-0800 LST data were used to avoid possible local contamination from the upslope wind. A linear least-squares trend analysis similar to that given in last year's Summary Report (DeLuisi, 1981) was applied to the same data set updated by the 1981 data. The trend lines are shown in fig. 19, and the trend analyses are given in table 12.

Long-term trends are generally less pronounced in this year's analysis than in last year's, especially for BRW and SMO light scattering. In each case, an additional year of data made a large difference in the trend. Furthermore, in all cases the trend from the beginning nto the end of the record is smaller than the standard error of the data about the regression line.

General discussions of the annual cycles (or lack thereof) and other features of the data given in fig. 19 have appeared in the last several GMCC Summary Reports. Of note are the current years of SMO and SPO light-scattering data after rather long periods of instrument downtime. Figures 20 and 21 give a more detailed presentation of SMO and SPO aerosol data for 1981. SMO data continue at approximately the same level as in previous years and exhibit negative Angstrom exponents as before, suggesting a marine aerosol with a narrow size distribution. SPO light-scattering data show a minimum in April, and the austral winter is dominated by events similar to those first seen in

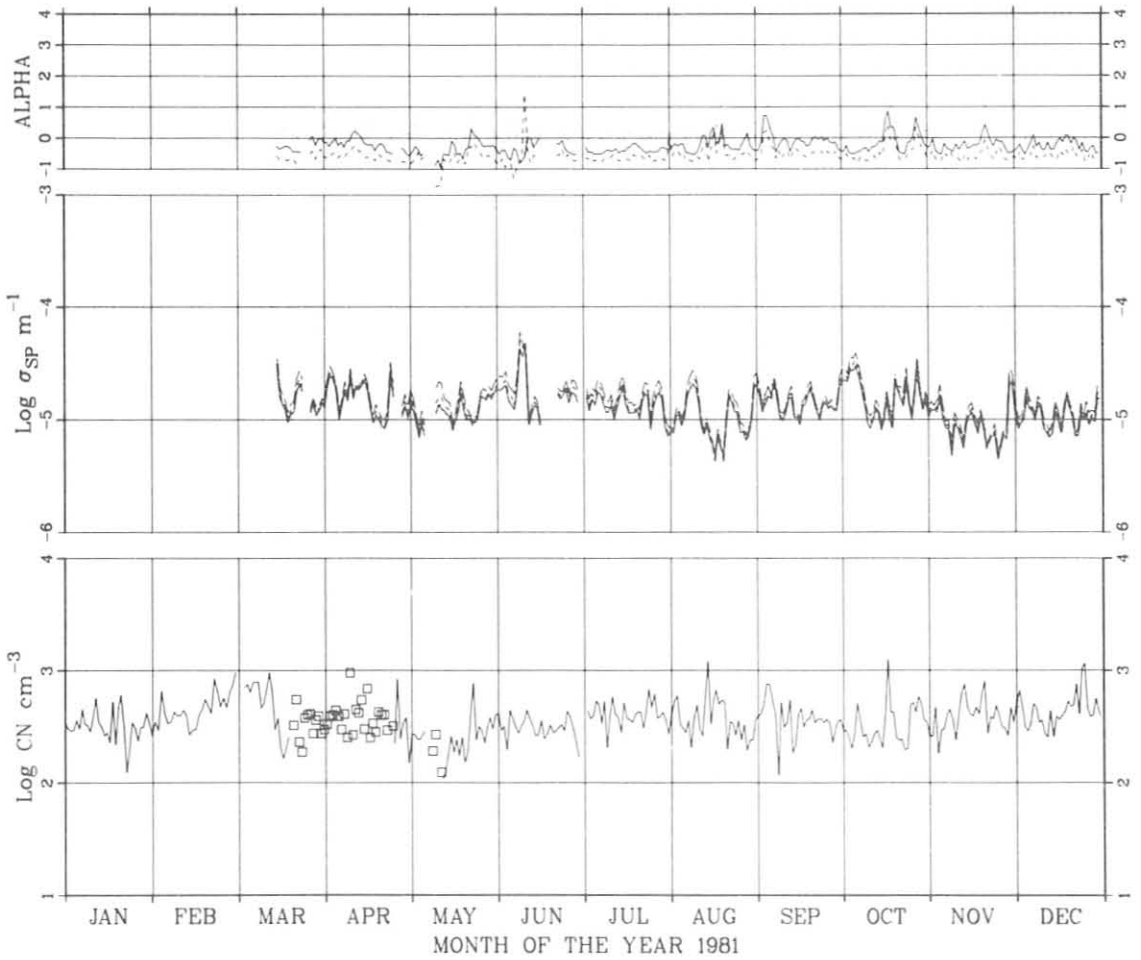

Figure 20.--Daily geometric mean CN concentration (bottom), four-wavelength light scattering (middle), and Angstrom exponent (top) for 1981 at SMO. For CN, the solid line is G.E. CNC data and the squares are Pollak CNC data. For light scattering, 450-nm data are dotted, 550-nm data are solid, 700-nm data are dashed, and 850-nm data are long-dashed. For Angstrom exponent, α_{12} is dotted, α_{23} is solid, and α_{34} is dashed.

the 1979 data (GMCC Summary Report for 1979, Herbert, 1980). These events most likely are caused by the transport of sea salt in the troposphere from coastal regions of the Antarctic continent. A summary of monthly geometric means of light scattering and CN concentration for all stations is given in table 13.

Figure 22 illustrates representative distributions of aerosols as a function of wind direction at the four GMCC stations. Each wind rose gives wind frequency and annual geometric mean values of CN and light scattering for 36 wind directions. In general, it is expected that CN data will be more

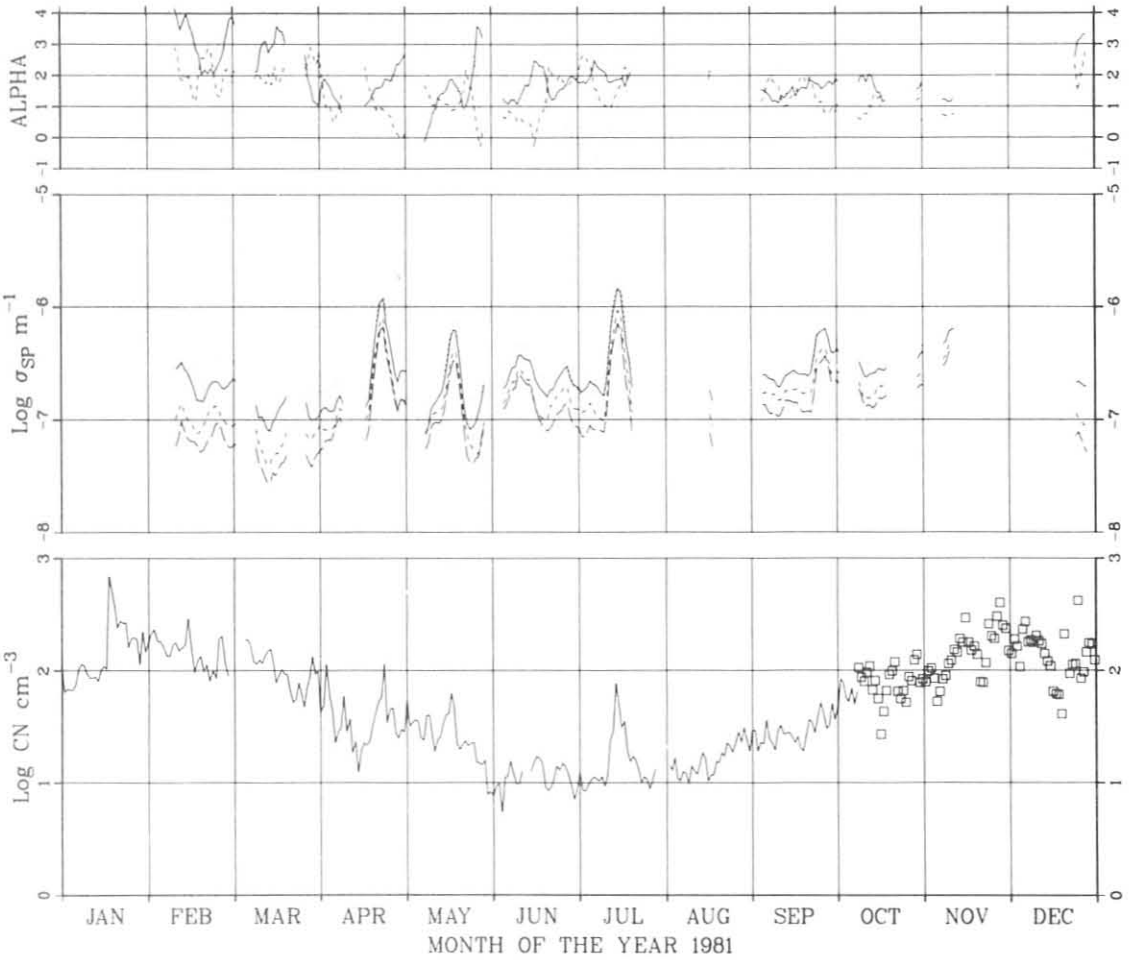

Figure 21.--Daily geometric mean CN concentration (bottom), four-wavelength light scattering (middle), and Angstrom exponent (top) for 1981 at SPO. For CN, the solid line is G.E. CNC data and the squares are Pollak CNC data. For light scattering, 450-nm data are dotted, 550-nm data are solid, 700-nm data are dashed, and 850-nm data are long-dashed. For Angstrom exponent, α_{12} is dotted, α_{23} is solid, and α_{34} is dashed.

sensitive to local pollution sources. A representative year was chosen for each station.

The BRW CN data clearly show the direction of the village, whereas light-scattering data appear not to respond to the village. MLO CN and light scattering both respond clearly to the upslope wind, and in addition, small peaks are evident when the wind is from the Mauna Loa caldera (about 200° bearing from MLO). SMO CN and light scattering are both higher to a small degree when the wind is from the island (SW) than from the ocean. South Pole data clearly show the effects of winds from the camp (SW).

Table 13.--Monthly geometric means of light-scattering and CN data for 1981 at all GMCC stations

Month	σ_{sp} m^{-1} (× 10^{-6})				CN cm^{-3}
	450 nm	550 nm	700 nm	850 nm	
BRW					
1	12.9	12.5	8.93	6.73	514
2	12.2	11.2	7.58	5.54	316
3	10.7	9.89	6.73	4.95	185
4	10.4	9.03	5.49	3.57	217
5	4.75	3.82	2.18	1.38	140
6	1.78	1.47	0.839	0.567	133
7	2.41	2.26	1.71	1.36	364
8	1.26	1.13	0.869	0.739	286
9	2.63	2.43	1.86	1.41	132
10	5.05	4.53	3.16	2.26	88
11	15.0	13.9	10.6	7.82	237
12	28.5	27.1	20.1	15.5	254
MLO					
1	0.471	0.336	0.183	0.118	195
2	0.154	0.150	0.101	0.0949	239
3	1.37	1.00	0.927	0.684	195
4	2.13	1.68	1.22	0.916	242
5	1.54	1.35	1.19	1.11	252
6	--	--	--	--	190
7	--	--	--	--	294
8	--	--	--	--	293
9	--	--	--	--	321
10	--	--	--	--	335
11	--	--	--	--	241
12	--	--	--	--	284
SMO					
1	--	--	--	--	329
2	--	--	--	--	447
3	15.0	14.3	15.3	17.3	451
4	15.8	14.7	15.3	17.2	317
5	12.4	11.8	12.8	14.7	251
6	16.2	15.8	17.3	19.5	305
7	13.2	13.0	14.3	16.3	405
8	10.4	9.75	10.2	11.2	366
9	15.2	13.8	14.1	15.4	367
10	16.7	15.7	16.3	17.7	323
11	9.45	8.87	9.36	10.5	381
12	11.0	10.4	11.1	12.4	440
SPO					
1	0.403	0.278	0.117	0.0565	139
2	0.362	0.208	0.0986	0.0618	144
3	0.237	0.134	0.0705	0.0473	98
4	0.326	0.220	0.154	0.123	35
5	0.252	0.184	0.126	0.102	25
6	0.309	0.249	0.172	0.141	11
7	0.378	0.343	0.207	0.150	15
8	0.265	0.208	0.127	0.0962	16
9	0.378	0.297	0.205	0.158	29
10	0.403	0.323	0.218	0.178	62
11	0.459	0.397	0.288	0.236	145
12	0.293	0.185	0.0998	0.0654	137

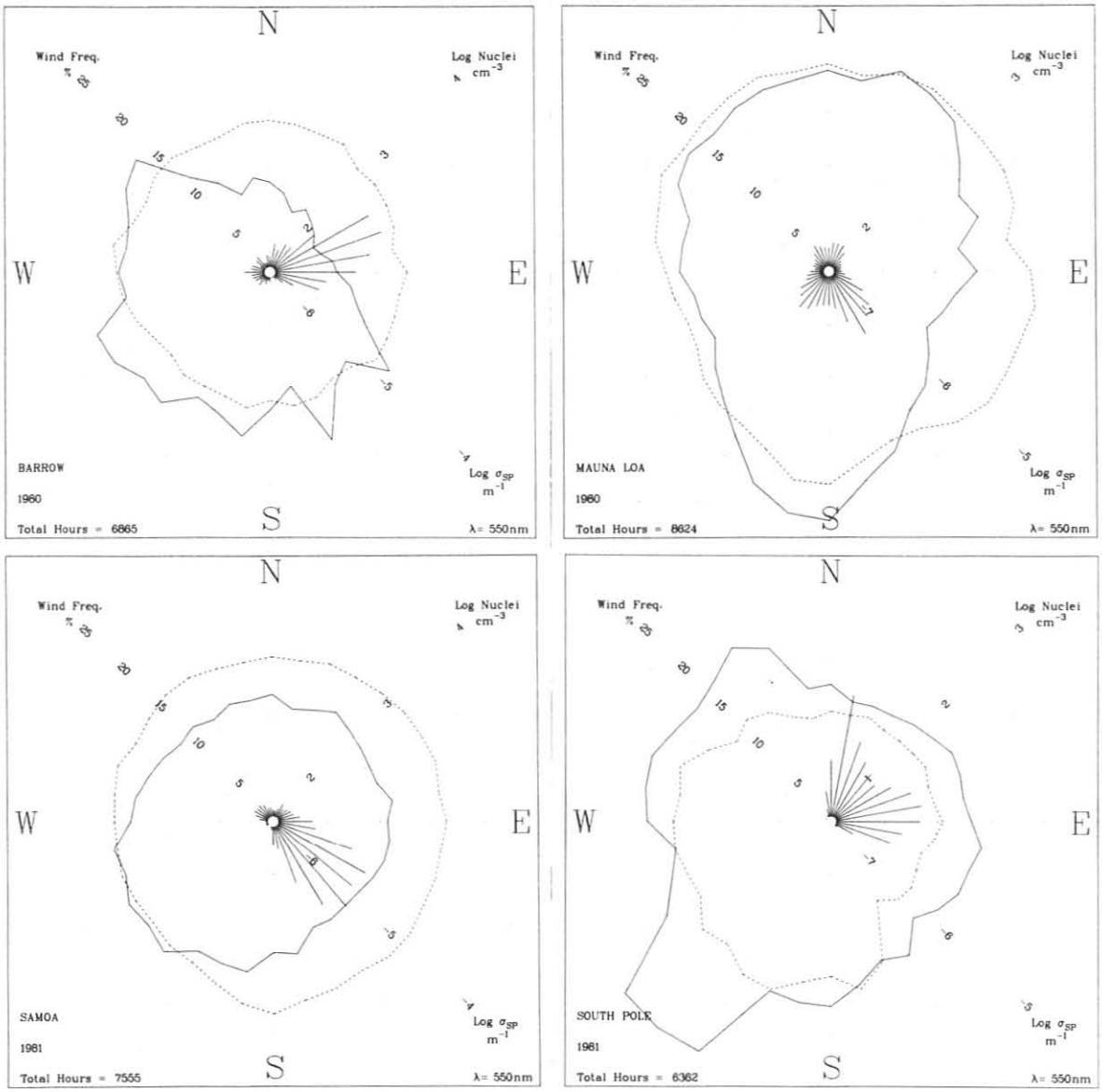

Figure 22.--Annual geometric mean CN concentration (solid), 550-nm light scattering (dashed), and wind frequency (center bars) for BRW, MLO, SMO, and SPO, all as a function of wind direction displayed on a 36-point wind rose.

3.9 Solar Radiation

3.9.1 Introduction

The GMCC solar radiation monitoring program consists of continuous and discrete measurements of several short-wave radiative quantities at the four baseline stations. The major components of the ground-based observing program have been in quasi-continuous operation since 1975-1976. Occasional data losses have occurred primarily as a result of data acquisition computer down-time, but also as a result of calibrations, obstructions to instrument field of view, solar tracking errors, and miscellaneous instrument failures. Some

Table 14.--Abbreviations for filter passbands of solar radiation instruments

Abbreviation	Filter
Q	Quartz, $280 < \lambda < 3{,}000$ nm
GG22	Schott glass, $400 < \lambda < 3{,}000$ nm
OG1	Schott glass, $530 < \lambda < 3{,}000$ nm
RG2	Schott glass, $630 < \lambda < 3{,}000$ nm
RG8	Schott glass, $695 < \lambda < 3{,}000$ nm

data losses are recoverable from the strip chart backup data-recording system but this is not routinely done. A nearly daily (5-7 days a week) documentation of the operation of the solar radiation instrumentation is maintained by the station personnel.

3.9.2 Instrumentation and Data Acquisition

A detailed summary of the initial instrument arrays at each station is given in the GMCC Annual Report for 1976 (Hanson, 1977). Additions and deletions to these instrument arrays are chronicled in subsequent GMCC annual reports. Table 14 gives the abbreviations for all of the filters used in Eppley solar radiation instruments in the GMCC program. The monitoring instruments as of December 1981, operating at the baseline stations, are given in table 15.

Table 15.--Solar radiation monitoring instruments, December 1981

Instrument*	Station				Comments
	BRW	MLO	SMO	SPO	
Eppley pyranometer					
Q	X	X	X	X	Continuous
RG8	X	X	X	X	Continuous
OG1				X	Continuous
Eppley pyrheliometer					
Q		X	X	X	Continuous
RG8				X	Continuous
Q	X	X	X	X	Discrete
OG1	X	X	X	X	Discrete
RG2	X	X	X	X	Discrete
RG8	X	X	X	X	Discrete
Sunphotometer					
380 nm, narrowband	X	X	X	X	Discrete
500 nm, narrowband	X	X	X	X	Discrete
Shaded pyranometer		X			
Solar IR hygrometer		X			

*See table 14 for abbreviations.

Table 16.--Calibration constants for solar radiation monitoring instruments

Instrument serial number	Type*	Filter†	Station	Basic calibration IPS§ (mV mW^{-1} cm^2)	ICDAS Zero offset (V)	ICDAS Scale factor ($mW\ cm^{-2}$)	ICDAS Ch. no.	Comments
12263	G	Q	BRW	0.0956	-0.020	11.51	16	
12267	G	RG8	BRW	0.0965	+0.007	11.48	19	
13913	NF	Q,OG1, RG2,RG8	BRW	0.0829	NA	NA	NA	
12616	G	Q	MLO	0.0794	-7.997	12.585	16	
10153	G	RG8	MLO	0.0767	-7.996	13.031	19	
2119	NT	Q	MLO	0.0295	-7.983	33.824	21	
13910	NF	Q,OG1, RG2,RG8	MLO	0.0825	NA	NA	NA	
12502	SG	Q	MLO	0.0952	-8.095	10.621	24	
12619	G	RG8	SMO	0.0791	-4.902	12.526	19	Online 9/81
11946	NT	Q	SMO	0.0810	-4.988	13.669	21	
13314	NF	Q,OG1, RG2,RG8	SMO	0.0829	NA	NA	NA	
12271	G	Q	SPO	0.1072	-7.896	9.213	16	
12269	G	OG1	SPO	0.1036	-7.949	9.421	18	
12270	G	RG8	SPO	0.0978	-7.802	10.085	19	
2968	NT	Q	SPO	0.0259	-7.912	38.72	21	
13912	NF	Q,OG1, RG2,RG8	SPO	0.0815	NA	NA	NA	
12617	G	Q	-	0.0810	NA	NA	NA	Traveling standard
13909	NF	Q,OG1, RG2,RG8	-	0.0774	NA	NA	NA	Traveling standard

*Type: G--global pyranometer; NT--NIP, continuous tracking; SG--shaded pyranometer; NF--NIP filter wheel, handheld.
†See table 14 for abbreviations.
§IPS = International Pyrheliometric Scale.
Note: For absolute radiation scale, divide basic calibration by 1.026 or multiply scale factor by 1.026.

Table 16 gives the current calibration information for most of these instruments. The ICDAS constants take into account amplified instrument signals and a zero offset used by ICDAS. Radiation quantities in engineering units ($mW\ cm^{-2}$) can be obtained from the ICDAS-recorded minute-averaged voltages by means of

$$EU = (V - OS) \cdot SF \quad ,$$

where EU = engineering units, V = recorded voltage, OS = offset voltage, and SF = scale factor. The ICDAS constants vary slightly with time and are routinely monitored, but long-term changes (except for amplifier replacements) are less than 0.1%.

Table 17.--Field instrument intercomparison with traveling standard*

Station	Inst. type†	1976	1977	1978	1979	1980	1981
BRW	G	0.994	0.997	-	1.014	-	1.0092
BRW	NF	-	1.0039	-	1.0038	-	1.0058
MLO	G	1.0016	1.0031	1.0041	1.0091	1.0081	1.0069
MLO	NF	-	1.0071	1.0097	1.0056	1.0016	1.0089
MLO	NT	-	0.998	1.0079	1.0039	1.0054	0.9975
SMO	G	0.990	-	1.010	1.0216	1.0343	1.0494
SMO	NF	-	1.011	1.0123	1.0075	-	1.013
SMO	NT	-	-	-	-	-	0.989
SPO	G	-	0.9905	0.9961	0.9870	-	0.985
SPO	NF	-	-	0.9978	-	0.9959	-
SPO	NT	-	-	1.0706	1.07§	1.07§	1.07§

*Ratio of standard instrument to station instrument.
†See table 16 for abbreviations.
§Comparison between station NF and NT.
Note: All instruments have quartz filters.

3.9.3 Instrument Intercomparison and Intercalibration

The basic instrument calibrations, originally supplied by the manufacturer, are monitored in two ways: intercomparison with similar instruments at the station and intercomparison with GMCC-maintained traveling standard instruments. The traveling standards are in turn intercompared with instruments maintained in Boulder and intercalibrated by the NOAA Solar Radiation Facility. Only the nonspectral pyranometers and pyrheliometers are intercompared and intercalibrated in this manner. Calibration of the broadband spectral instruments depends on a combination of a nonspectral calibration of the instrument sensor and a filter factor. Narrowband spectral instruments can be self-calibrated using the Sun as a constant source, but they generally have had a calibration transferred from a reference instrument.

A summary of the intercomparison ratios between the traveling standards and the station quartz pyranometers and pyrheliometers is given in table 17. The ratios are obtained from side-by-side measurements over the period of several days, which result in several thousand simultaneous measurements per comparison for the pyranometers and 20-40 points for the pyrheliometers. The only departure significantly greater than 1% over the 6-yr record is for the pyranometer at SMO that was replaced at the end of 1981 because of its apparent calibration drift. The affected data at SMO were corrected for this drift before being archived.

3.9.4 Pyranometer Data

Solar radiation data can be summarized and presented in numerous ways. The generally known dependency of surface-received solar radiation on highly variable quantities such as solar position, time of day, time of year, amount and type of cloudiness, and surface albedo, in addition to atmospheric composition, makes straightforward presentation of all the GMCC data impractical here.

Table 18.--Monthly average of daily total received solar radiation on a horizontal surface × 10^3 kJ m^{-2} absolute scale*

	BRW		MLO		SMO		SPO	
	Q	RG8	Q	RG8	Q	RG8	Q	RG8
1979								
J	0.07	0.0	19.7	10.4	20.8	10.1	32.8	16.9
F	0.94	0.47	16.5	7.75	22.7	11.7	19.1	11.0
M	6.03	3.06	25.1	13.3	21.6	10.7	3.74	2.16
A	13.8	6.86	27.0	14.9	17.6	8.91	0.0	0.0
M	19.6	8.86	28.1	15.1	16.2	8.21	0.0	0.0
J	20.1	9.68	28.1	15.4	14.8	7.60	0.0	0.0
J	18.3	8.49	27.3	14.9	15.0	7.44	0.0	0.0
A	8.2	3.98	27.3	14.8	19.4	9.85	0.0	0.0
S	4.9	2.29	24.2	13.2	19.2	9.66	1.32	0.82
O	1.09	0.44	17.3	9.32	18.2	9.00	10.7	5.66
N	0.125	0.06	17.5	9.02	23.0	11.5	28.4	14.5
D	0.00	0.0	17.8	9.83	20.5	9.93	35.1	17.8
1980								
J	0.019	0.01	19.8	10.6	9.4	8.96	32.0	16.6
F	0.896	0.43	23.9	12.4	19.4	9.57	16.7	9.17
M	5.19	2.98	18.5	10.3	20.8	9.92	5.26	3.48
A	13.6	6.49	29.3	15.2	17.2	8.26	0.0	0.0
M	20.0	8.39	26.0	13.8	12.7	5.96	0.0	0.0
J	21.3	9.54	26.7	14.5	12.8	6.03	0.0	0.0
J	15.5	7.67	24.6	13.3	14.7	7.00	0.0	0.0
A	M	M	27.4	15.0	14.4	6.67	0.0	0.0
S	M	M	21.7	11.7	17.0	8.23	1.82	M
O	1.71	0.73	21.5	12.3	18.0	9.44	10.2	5.45
N	M	M	21.6	12.0	20.8	10.3	27.8	14.2
D	0.00	0.00	19.6	11.0	23.6	10.5	36.9	18.5
1981								
J	0.064	0.0	21.0	11.9	20.2	9.62	31.1	15.8
F	0.911	0.46	23.7	13.3	20.6	9.88	19.3	10.1
M	5.90	2.89	27.0	15.2	19.4	9.32	M	M
A	13.2	6.30	26.1	14.5	14.2	6.58	0.0	0.0
M	18.7	8.39	30.3	16.9	15.3	7.19	0.0	0.0
J	21.2	9.92	29.8	16.5	14.5	7.06	0.0	0.0
J	13.9	6.49	29.6	16.5	16.7	8.09	0.0	0.0
A	11.1	5.16	26.9	14.8	17.1	8.15	0.0	0.0
S	4.87	2.29	23.7	13.1	19.5	9.35	1.44	0.77
O	1.52	0.93	22.2	12.6	18.5	8.62	12.0	6.50
N	0.18	M	19.4	11.5	19.7	9.22	28.2	14.5
D	0.00	0.00	19.2	10.8	20.0	9.65	34.0	15.4

*See table 14 for filter abbreviations.
Note: M = missing data.

Examples of several days' worth of minute-by-minute pyranometer data were given in the GMCC Summary Report for 1979 (Herbert, 1980). Pyranometer data are being archived on a yearly basis at NCC. These data are archived as hourly integrals of total energy received in the Research-Cooperator format. None of the known sources of variability were removed except some instrument-related errors. The data are not corrected for possible instrument errors due to cosine response or ambient temperature variations, however. A summary of the archived pyranometer data for 1979-1981 is given in table 18. Prior to 1981, OG1 and GG22 pyranometer data were also archived.

Table 19.--Pyranometer ratios averaged for 1979-1980

Station	GG22/Q	OG1/Q	RG8/Q
BRW	0.913 ± 0.015	0.716 ± 0.033	0.474 ± 0.046
MLO	0.958 ± 0.028	0.746 ± 0.029	0.544 ± 0.033
SMO	0.918 ± 0.013	0.714 ± 0.026	0.483 ± 0.032
SPO	0.925 ± 0.021	0.702 ± 0.031	0.514 ± 0.031

The spectral resolution of the archived pyranometer data can be demonstrated by taking the ratios of the values from the cutoff filters to the values from the quartz pyranometer. These ratios averaged for all of 1979 and 1980 hour by hour for all-sky conditions are given in table 19. The indicated range is one standard deviation; the number of points is about 6,000 for each ratio.

Temporal variations in the ultraviolet spectrum would be reflected in the GG22/Q ratio whereas changes in the solar infrared regions are reflected in the RG8/Q ratio. Ozone and water vapor are the two main atmospheric constituents responsible for variations in the UV and solar IR, respectively. A more quantitative analysis of these ratios would be complicated by the presence of cloudy and diffuse sky as well as by variable path length data included in the averages.

3.9.5 Pyrheliometer Data

Pyrheliometer measurements of the direct sun intensity normal to the light path are made for a more complete picture of the nature of solar radiation reaching the Earth's surface. The measured direct radiation is a single component of the total radiation measured by the pyranometers. Pyrheliometer measurements are useful in determining the cloud-free atmospheric influence on surface-based solar radiation measurements. Unlike the total or all-sky measurements of the pyranometer, the pyrheliometer measurements can be reduced to remove nearly all of the known sources of variability except for those due to atmospheric composition and to the variability of the output of the Sun itself. Figure 23 shows a 5-yr summary of broadband filter wheel NIP data on the absolute radiation scale corrected to 1 A.U. for each station. Each point plotted, with the number of observations and standard deviation, is the average of all data falling within a 0.2 relative air mass (M_R) interval. These measurements are normally made 2-3 times per day, sky conditions permitting. Better time resolution in the presentation of these data would be necessary for detailed discussion, but they are presented in this manner as a summary and for use as reference levels. The decrease in intensity with decreasing air mass at MLO is attributed to local diurnal cycles in water vapor and aerosols.

The continuously tracking and recording pyrheliometers at the baseline stations permit the calculation of a relative atmospheric transmission factor, after the technique of Ellis and Pueschel (1971). The technique uses the ratios of the measured solar intensity at consecutive-integer relative air masses, and averages these ratios for a given morning or afternoon. The air mass values traditionally used are 5, 4, 3, and 2. The resulting transmission

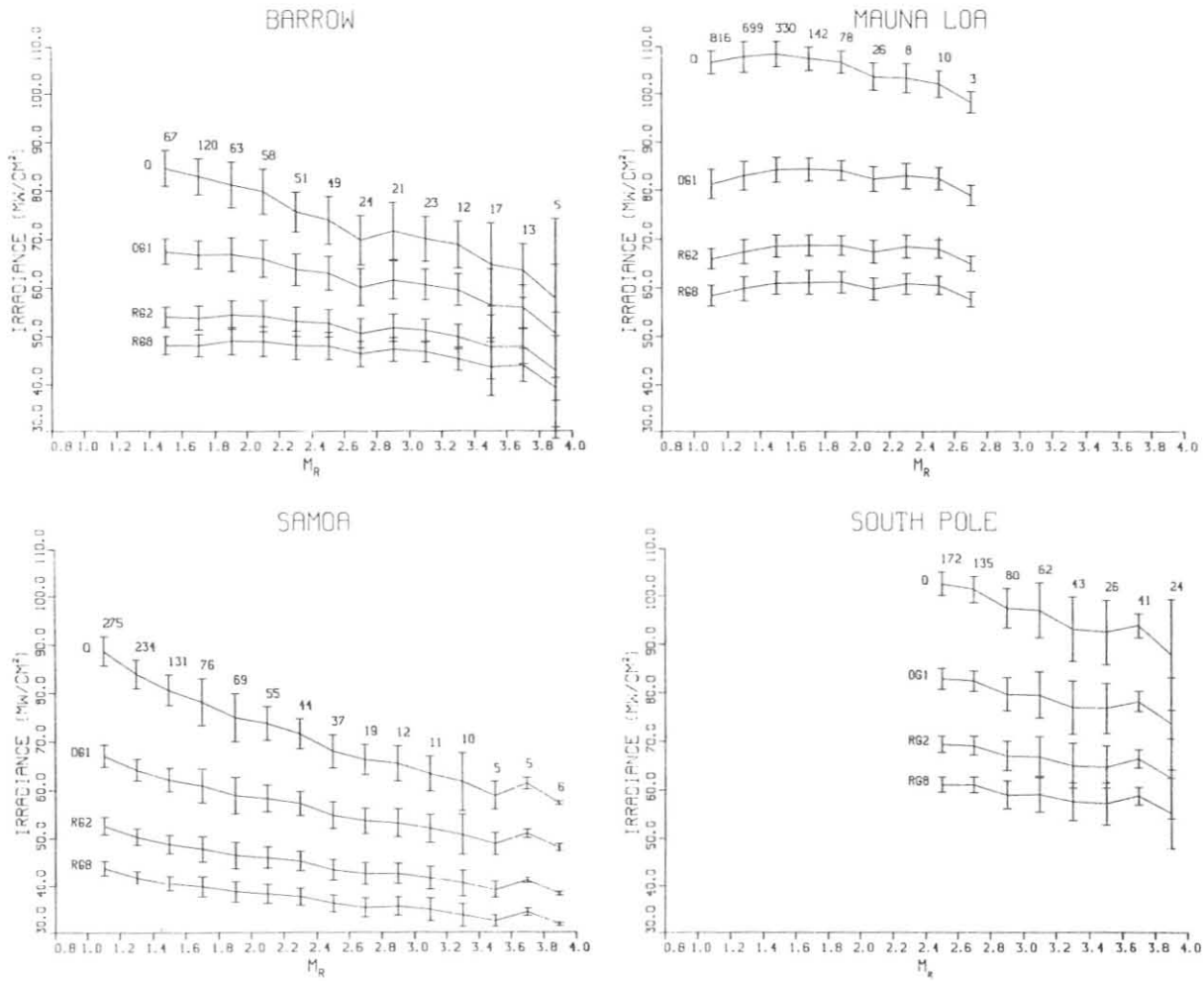

Figure 23.--Direct irradiance averaged for 1976-1980 for filters Q, OG1, RG2, and RG8 at (a) BRW, (b) MLO, (c) SMO, and (d) SPO. Variability bars show one standard deviation. The number of observations is given along the bar for each indicated air mass interval.

factor or apparent transmission is independent of instrument calibration, independent of instrument drift on time scales longer than one day, independent of the extraterrestrial irradiance, but dependent on air mass. As a long-term monitor of relative atmospheric transmission, the parameter is compared day to day at the same air mass values. Of the four baseline stations, only MLO has proved suitable for the long-term calculation of the apparent transmission factor. Analysis of the long-term record at MLO, starting in 1958, has been given by Mendonca et al. (1978) and Bodhaine et al. (1981b).

The 1980 and 1981 monthly average values of MLO apparent transmission are presented in table 20. Beginning in March 1981 the values are derived by computer from the data recorded on magnetic tape at the station. Visual inspection of the strip chart records is still required to ensure that only cloud-free days are used in the calculation. A careful comparison was made between the computer-derived values and the previously hand-determined values to ensure consistency of the record.

Table 20.--MLO apparent atmospheric transmission
(morning only)

	Hand calculated	Computer calculated
1979		
Sep	0.933	-
Oct	0.929	-
Nov	0.924*	-
Dec	0.933	-
1980		
Jan	0.935	-
Feb	0.934	-
Mar	0.931	-
Apr	0.925	-
May	0.923	-
Jun	0.927	-
Jul	0.929	-
Aug	0.928	-
Sep	0.931	-
Oct	0.932	-
Nov	0.930	-
Dec	0.931	-
1981		
Jan	0.933	-
Feb	0.934	-
Mar	0.927	0.931
Apr	0.929	0.927
May	0.932†	0.929
Jun	0.930	0.926
Jul	0.929	0.929
Aug	0.930	0.929
Sep	0.931†	0.930
Oct	0.929	0.929
Nov	0.931	0.931
Dec	0.933	0.931

*Less than five days.
†Edited data.

3.9.6 Special Projects

During 1981, and extending into 1982, several special projects were undertaken by the GMCC ARM group. Table 21 shows the new or special short-term measurements conducted during 1981. Some of these measurements were carried out for instrument testing and performance analysis only (Boulder-based measurements). The results of the water vapor meter measurements and an intercomparison of various sunphotometers are reported in secs. 4.11 and 4.12. Data from most of the programs indicated in table 21 are not ready for presentation at this time. Only the results of the active cavity pyrheliometer measurements at MLO and Boulder are given in the following.

An Eppley Kendall ACR is a self-calibrating radiometer directly comparable with the Eppley NIP's because of their equal fields of view and calibrated spectral ranges. The absolute accuracy of the ACR is limited only by

Table 21.--Experimental and event measurements

	BRW	MLO	SMO	SPO	Boulder	Whiteface Mt., N.Y.
Eppley narrowband & broadband NIP (13 channels)		X				
Spectral albedo	X			X		
Spectral diffuse sky/direct solar	X	X			X	X
Spectral extinction	X	X	X	X	X	X
Total H_2O		X		X	X	
Active cavity pyrheliometer		X			X	

the geometry of the optical system and the ability to measure voltage and current. International intercomparison of these instruments has shown that instruments of different design and manufacture all agree to within ±0.5%, and most agree to ±0.25%.

GMCC Eppley Kendall ACR no. 12843 was compared with TMI ACR no. 67502 of the NOAA Solar Radiation Facility on 31 December 1980 and 6 April 1981. ACR no. 67502 is the primary standard of the calibration facility and has participated in many international ACR intercomparisons held in Davos, Switzerland. The 31 December comparison showed a 0.003% ± 0.026% difference between the two instruments. A sensitivity of ACR no. 12843 to air currents was observed during the intercomparison, and some obviously affected data were removed when compiling the comparison ratio.

Before the 6 April intercomparison, an insulating jacket and sun shade were fitted to the GMCC ACR. These additions appeared to greatly reduce the air current sensitivity of the instrument. The 6 April intercomparison showed a 0.020% ± 0.011% difference, essentially unchanged from the 31 December comparison.

ACR no. 12843 was sent to MLO for long- and short-term intercomparisons with the tracking NIP no. 2119. (The calibration constant of the NIP was 0.0288 mV mW^{-1} cm^2 on the absolute scale.) The results of the monthly average difference between these two instruments are given below.

$$\frac{ACR - NIP}{ACR} \times 100$$

Jun	0.40% ± 0.16%
Jul	0.58% ± 0.20%
Aug	0.59% ± 0.14%
Sep	0.44% ± 0.18%
Oct	0.60% ± 0.09%
Nov	0.67% ± 0.17%
Dec	0.40% ± 0.10%
Average	0.53%

These data represent excellent agreement between a quartz-window, normal incidence pyrheliometer and an ACR, especially in the relative sense where the month-to-month variability was less than 0.3%. However, most of the comparison measurements were taken near midday so the agreement cannot be projected over an entire day. These measurements are continuing in an effort to maintain the current calibration of the MLO NIP and to back-calibrate the entire 26-yr NIP record for MLO.

Late in 1981 plans were initiated to develop a semiautomated solar observatory at MLO. The observatory will be housed in the 16-ft Ash Dome currently housing the MLO lidar, which will be moved to a new building. The observatory dome will house a precision active solar-tracking spar, data acquisition system, several radiometers, and a semiautomated dome controller. The observatory is expected to be put into operation in late 1982. A prototype observatory will first be operated in Boulder.

The high-spectral-resolution atmospheric transmission model, LOWTRAN 5.0 (Kneizys et al., 1980), has been combined with an extraterrestial solar intensity spectral curve to aid the theoretical calculation of surface-received direct solar radiation at GMCC stations. The SOLTRAN (LOWTRAN and SOLAR SPECTRUM) model along with a nonspectral model of diffuse and direct solar radiation (Bird and Hulstrom, 1981) have proved useful in data quality control and research.

The design adaptation and fabrication of a high-precision three-wavelength sunphotometer was begun by the ARM group in late 1981. The design is basically that provided by C. Fröhlich, which satisfies WMO's recommendations for instruments that measure background levels of turbidity or optical depth. Current plans call for this instrument to be used as a standard against which all narrowband spectral measurements at GMCC will be referenced. The instrument will be tested and calibrated at the new solar observatory facility at MLO.

Several designs of a narrowband spectral radiometer have been tested in an effort to measure the ratio of diffuse sky flux to direct solar flux. Measurement of this ratio permits determination of the aerosol absorption occurring in a sufficiently optically thick event. The diffuse component can be either the global (2π) field or a narrow (few-degree) field, with the resulting absorption determined by observational agreement with radiative transfer models. The diffuse/direct radiometers have been or will be used in field programs at BRW, MLO, Boulder, and Whiteface Mountain.

3.10 Station Climatology

3.10.1 Instrumentation and Data Processing

A description of meteorological instrumentation and data processing appears in last year's Summary Report (DeLuisi, 1981). Meteorological data from the GMCC stations are stored in tabular form on microfiche and on magnetic tape. The listings on microfiche are organized by station, date, time, and variable. The hourly average values, scaled in metric units, for a single GMT day, are listed on a single frame. The variables include resultant wind direction and speed; station pressure; and air, ground, and dewpoint temperatures. Listings of data on microfiche are available 6 months following the

end of the year. Data are also stored on magnetic tape and can be supplied if a large volume is needed.

3.10.2 Barrow

BRW is located about 9 km southwest of Point Barrow on a small rise in the tundra between two saltwater lagoons. With the Arctic Ocean to the north, east, and west, and relatively level tundra stretching more than 200 km to the south, there are no local topographic barriers to redirect the wind field. A uniform snow and ice cover hides the Alaskan shoreline for 8 months of the year. Except for stormy periods that bring westerly winds, the surface winds are generally northeasterly in response to the general circulation around the two dominant continental high-pressure regions in the Arctic. A low-level inversion (0.1-1 km) separates the more easterly surface winds from more northerly winds aloft (Miller, 1981a). In a recent study of the wind climatology along the Alaskan North Slope, Kozo (1980) found evidence of a turning of the wind in the surface layer as the result of a baroclinic effect caused by the Brooks Range to the south. The effect is such that east of BRW, where the mountain barrier is close to the coast, the winds are turned to the south, whereas at BRW surface winds are northeasterly. Surface winds during the summer months are influenced by a local sea breeze along the Beaufort Sea (Kozo, 1979).

The histograms of the hourly average resultant wind speed as a function of direction (fig. 24) for 1977-1980 and for 1981 show excellent agreement. Except for the predominance of the five most easterly directions, the distribution is surprisingly symmetrical. For the period 1977-1980, easterly sector winds (NE, ENE, E, ESE, and SE) occurred 55% of the time, whereas for winds

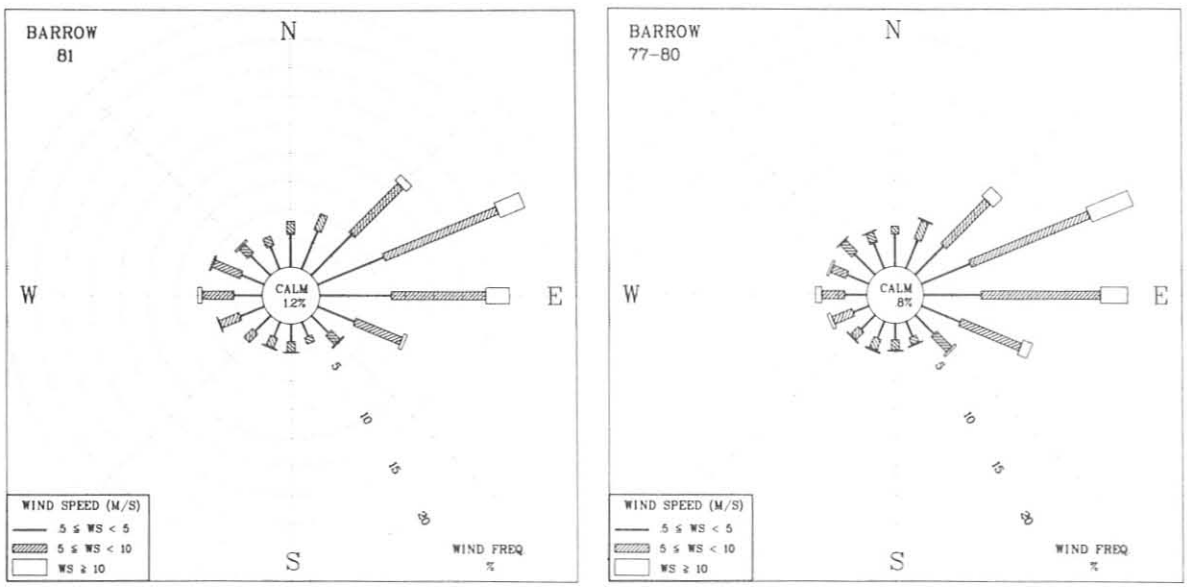

Figure 24.--Wind rose of surface winds for BRW for 1981, left, and 1977-1980, right. The distributions of the resultant wind direction and speed are in units of percent occurrence for the year and 4-yr period, respectively. Wind speed is shown as a function of direction in three speed classes.

Table 22.--1981 BRW monthly climate summary*

	Jan	Feb	Mar	Apr	May	Jun	Jul	Aug	Sep	Oct	Nov	Dec
Prevailing wind direction	ENE	ENE	ENE	E	ESE	E	W	ENE	ENE	ENE	ENE	ENE
Average wind speed ($m\ s^{-1}$)	6.3	6.0	6.7	4.4	5.3	5.0	5.3	4.6	4.8	6.1	5.7	5.8
Maximum wind speed† ($m\ s^{-1}$)	14	14	18	10	12	11	13	11	11	16	19	15
Direction of max. wind† (deg.)	85	95	95	110	310	70	195	255	50	85	85	70
Average station pressure (mb)	1002.1	1016.3	1014.4	1015.8	1014.7	1010.1	1013.9	1007.9	1012.1	1013.8	1009.1	1009.0
Maximum pressure† (mb)	1025	1044	1033	1042	1029	1019	1018	1030	1028	1030	1026	1041
Minimum pressure† (mb)	986	993	1000	995	993	999	983	992	998	1002	989	975
Average air temperature (°C)	-18.6	-26.2	-23.5	-17.2	-4.1	0.9	4.1	3.6	-3.5	-9.1	-18.5	-23.4
Maximum temperature† (°C)	-7	-10	-8	0	3	12	17	15	6	-2	-5	-9
Minimum temperature† (°C)	-33	-38	-38	-32	-17	-4	-3	-1	-12	-21	-29	-33

*Instrument heights are as follows: wind, 16 m; pressure, 9.5 m (MSL); air and dewpoint temperature, 3 m. Wind and temperature instruments are on a tower located 25 m northeast of the main building.
†Maximum and minimum values are hourly averages.

10 $m\ s^{-1}$ or greater the occurrence from this quadrant is 75% (Harris and Herbert, 1980). As in previous years, the prevailing wind is east-northeasterly, and sometimes northerly and westerly in December. Table 22 gives a monthly breakdown of average and extreme values of wind, air temperature, and station pressure. The most striking feature in the 1981 data summary is the anomalously low pressure and the warm temperature in January. The pressure was 12.5 mb below the 6-yr average ending in 1981. The January temperature was 4°C warmer than the average for the last 6 years. The maximum hourly average wind speed was reported in November to be 19 $m\ s^{-1}$. Recent studies indicate that the station pressures measured with the pressure transducer at BRW are on the order of 2.5 mb low.

3.10.3 Mauna Loa

Throughout much of the year the midtropospheric winds in the south-central Pacific are determined by the position of the Pacific anticyclone. This is especially the case in the summer months when the anticyclone is in its northernmost position and the winds in the vicinity of Hawaii are light and easterly. During the winter months the Pacific anticyclone moves farther south and diminishes in size, allowing the southern extent of the midlatitude cyclones to pass the islands. This period is characterized by a much higher occurrence of westerly winds at all levels. In the transition periods between these two dominant patterns, stronger easterly winds are commonly observed. A recent study of the beginning point of 10-day back trajectories from MLO shows this seasonal breakdown (Miller, 1981b). The largest percentage of the trajectories originate to the east of MLO during the summer months and to the

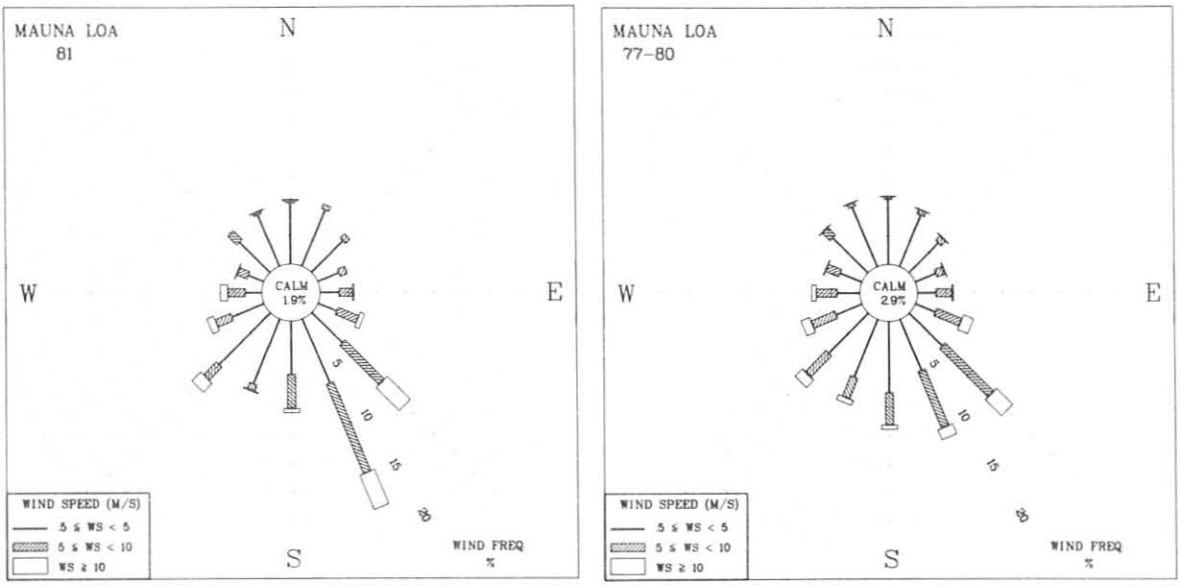

Figure 25.--Wind rose for MLO for 1981, left, and 1977-1980, right. See legend for fig. 24.

northwest during winter months. The highest percentage of long trajectories (greatest number beginning beyond 2,000 km from MLO) also occurs in the winter. Significant year-to-year variations are also observed.

The surface wind (10-m height) measured at the observatory represents a more complex flow regime. For much of the time the synoptic-scale pressure gradient influence is overpowered by the local influence of surface heating and cooling causing a diurnal upslope-downslope flow (Mendonca, 1969; Miller, 1978). In even more well-defined flow situations, the twin peaks of Mauna Kea and Mauna Loa redirect the flow. This is illustrated in part by systematic differences between the climatology of trajectory source points and the wind distribution at the observatory, as in fig. 25. The combined wind distribution from 1977 through 1980 shows a much higher occurrence of winds with a southerly component than does the trajectory analysis. While the synoptic-scale flow pattern is more easterly or westerly, the effect of Mauna Loa is to redirect stronger winds from aloft down the slope with a more southerly component. The departure from symmetry in the distribution of the southerly winds is to the south-southwest, the exact direction of the summit of Mauna Loa. Higher wind speeds ($\geq$10 m s^{-1}) occur most commonly (80% of the time) with stormy periods and are almost exclusively confined to the southerly directions. Of particular interest is the relatively large frequency of occurrence of winds greater than 10 m s^{-1} from the south-southeast. The upslope-downslope winds are generally represented by speeds of 5 m s^{-1} or less. Such conditions occur approximately 62% of the time. Calm conditions (wind speed <0.5 m s^{-1}) occur 2.9% of the time on the basis of the 4-yr average. It is of interest to note that the January 1981 temperature at MLO is 3.5°C warmer than the 6-yr average ending in 1980. Monthly mean and extreme values for wind, pressure, and temperature are given in table 23. Temperature measurements are made at MLO using instrumentation similar to that at BRW.

Table 23.--1981 MLO monthly climate summary*

	Jan	Feb	Mar	Apr	May	Jun	Jul	Aug	Sep	Oct	Nov	Dec
Prevailing wind direction	SW	SW	SSE	SSE	NW	SE	SSE	SSE	SSE	SW	SSE	SSE
Average wind speed ($m\ s^{-1}$)	5.3	7.6	5.0	4.5	4.9	7.5	4.3	4.4	4.4	3.4	5.0	5.1
Maximum wind speed† ($m\ s^{-1}$)	15	17	14	13	10	16	12	14	12	12	14	17
Direction of max. wind† (deg.)	260	225	160	150	295	150	155	145	155	355	150	165
Average station pressure (mb)	680.6	679.6	681.1	680.8	681.4	681.9	681.7	681.9	681.7	681.1	681.7	680.5
Maximum pressure† (mb)	685	686	685	685	685	686	684	685	684	685	686	683
Minimum pressure† (mb)	676	670	678	676	678	679	678	679	678	677	678	676
Average air temperature (°C)	7.3	6.0	5.8	6.1	9.2	9.3	9.9	8.7	8.0	7.4	7.2	6.0
Maximum temperature† (°C)	16	16	15	18	18	21	20	19	17	16	17	15
Minimum temperature† (°C)	1	-2	-2	-1	-1	1	3	2	1	0	1	-1

*Instrument heights: wind, 10 m; pressure, 3399 m (MSL); air and dewpoint temperature, 2 m. Wind and temperature sensors are located approximately 15 m southwest of the main building on a tower. Pressure sensors are located in the observatory building.
†Maximum and minimum values are hourly averages.

3.10.4 Samoa

Since February 1977 both the anemometer and thermometer have been located on the sampling tower atop Lauagae Ridge. The anemometer is positioned on top of the tower at a height of 14 m, and the thermometer for measuring air temperature at a height of 4 m above ground. The dewpoint temperature is measured from air samples drawn from the sampling stack. The wind distribution for the first 4 years of this period is displayed in 16 classes of wind direction and three classes of speed (fig. 26). The southwesterly trade winds dominate the airflow at Cape Matatula, occurring 68% of the time in 1981. This compares with 73% for directions east through south for the first 4 years of this period. For 1981 winds from the northwest quadrant (west through north) occurred 17% of the time. This is the same as that observed for the preceding 4 years.

Seasonal variations of all other meteorological variables are small (table 24) in comparison with the other GMCC stations. Only slightly higher winds and cooler temperatures occur in the winter than in summer. The annual average pressure, temperature, and resultant wind speed for 1981 were 1000.2 mb, 27.0°C, and 4.6 $m\ s^{-1}$, respectively. These values compare with 1000.3 mb, 27.3°C, and 4.6 $m\ s^{-1}$, respectively, for the previous 4 years.

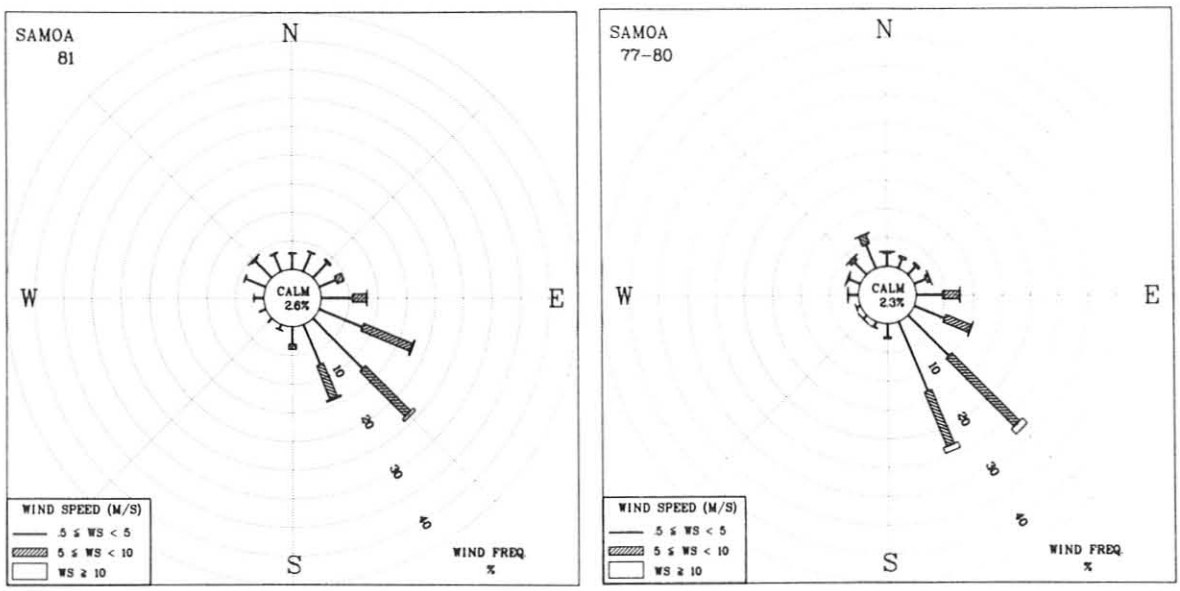

Figure 26.--Wind rose for SMO for 1981, left, and 1977-1980, right. See legend for fig. 24.

Table 24.--1981 SMO monthly climate summary*

	Jan	Feb	Mar	Apr	May	Jun	Jul	Aug	Sep	Oct	Nov	Dec
Prevailing wind direction	SE	SE	SE	SE	SE	SE	ESE	ESE	ESE	SSE	SSE	SSE
Average wind speed ($m\ s^{-1}$)	2.9	3.3	2.7	3.4	5.3	4.7	5.6	4.2	4.3	4.4	3.0	3.6
Maximum wind speed† ($m\ s^{-1}$)	11	13	16	10	12	12	11	10	11	12	10	11
Direction of max. wind† (deg.)	145	320	150	325	140	135	120	60	120	160	155	355
Average station pressure (mb)	998	996.5	998.2	1000.2	1001.6	1001.9	1002.2	1002.4	1002.3	1001.2	999.8	998.4
Maximum pressure† (mb)	1003	1002	1004	1006	1006	1007	1006	1007	1007	1006	1005	1005
Minimum pressure† (mb)	994	988	980	995	996	997	998	998	998	995	996	992
Average air temperature (°C)	28.7	27.5	27.2	27.0	27.0	26.5	25.9	26.3	26.8	26.4	27.1	27.1
Maximum temperature† (°C)	32	33	31	31	31	31	31	31	31	31	30	30
Minimum temperature† (°C)	25	23	23	23	24	24	22	23	23	23	24	23

*Instrument heights: wind, 14 m; pressure, 30 m (MSL); air and dewpoint temperature, 7 m. Wind and temperature sensors are located atop Lauagae Ridge, a distance 110 m northeast of the station. Pressure sensors are located in the station.
†Maximum and minimum values are hourly averages.

3.10.5 South Pole

The extent, depth, and duration of the Antarctic winter is clearly depicted by the very cold average monthly temperatures from April through September at SPO. Minimum temperatures observed during these months are consistently below -70°C (-94°F). See table 25 for 1981 results. The very persistent surface wind from a grid northeasterly direction is another dominant climatological feature of the pole station. This is an inversion wind most of the year, flowing down the Antarctic ice dome. The speed is typically about 6 m s^{-1}. The station is located on the Amundsen-Scott plateau, at an elevation of 2.84 km. The plateau exhibits little topographic relief within a 100-km radius of the station, and is near the western edge of the main ridge of eastern Antarctica. The highest point (elev. 4 km) on the plateau is about 900 km east-northeast of the geographical South Pole.

Figure 27 displays, in polar coordinates, the distribution of the wind as a function of speed and direction. In previous years the most prevalent wind direction has been east-northeasterly. The most prevalent direction in 1981 was north-northeasterly. This is due in large part to a marked increase in the percentage of stronger winds ($\geq$10 m s^{-1}) that are predominantly from the north. During the previous 4 years, wind speeds $\geq$10 m s^{-1} have occurred 2% of the time. In 1981 wind speeds $\geq$10 m s^{-1} occurred 7.9% of the time. Calm conditions (wind speeds <0.5 m s^{-1}) occurred 0.2% of the time.

The full extent of the austral winter on the Antarctic plateau is shown in the eight monthly average air temperatures that are below the annual average (-48.6°C); see table 25. The maximum hourly average temperature in 1981 was -18.4°C (DOY 364) and the minimum temperature was -75.6°C (DOY 256). The air temperature was measured with a platinum resistance thermometer (no. 954 PL-C, Stow Laboratory, Hudson, Mass.) in a naturally ventilated radiation shield (no. 43103A, R. M. Young, Traverse City, Mich.) at a height of 2 m.

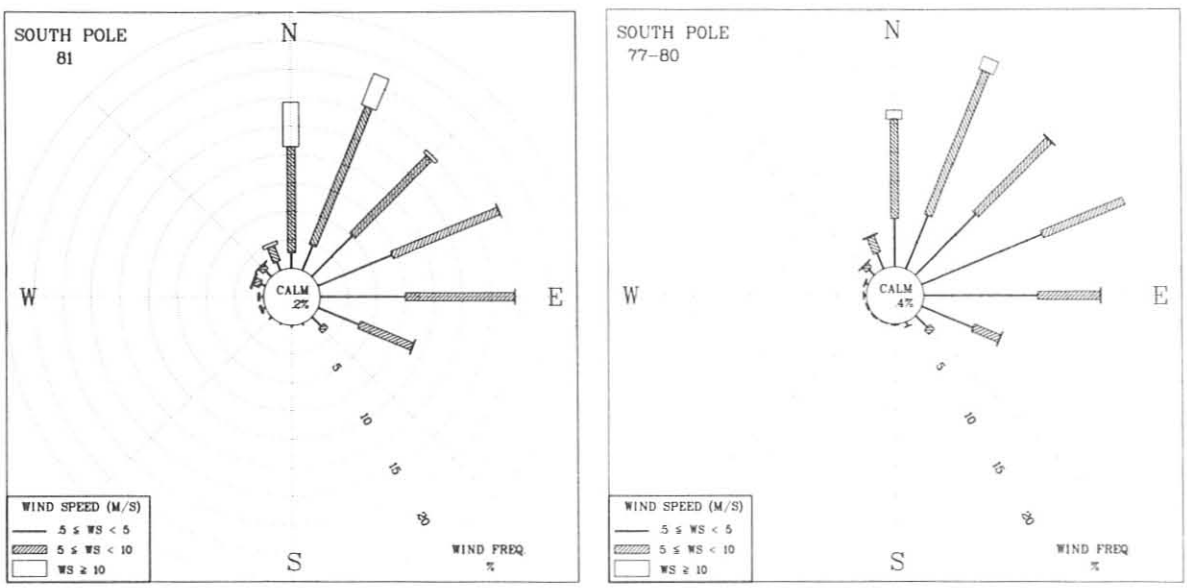

Figure 27.--Wind rose for SPO for 1981, left, and 1977-1980, right. See legend for fig. 24.

Table 25.--1981 SPO monthly climate summary*

	Jan	Feb	Mar	Apr	May	Jun	Jul	Aug	Sep	Oct	Nov	Dec
Prevailing wind direction	N	NNE	ENE	E	N	NNE	N	ENE	NNE	NE	NNE	NE
Average wind speed ($m\ s^{-1}$)	5.5	5.8	6.2	6.5	7.1	7.5	7.8	8.3	6.0	5.1	5.2	4.7
Maximum wind speed† ($m\ s^{-1}$)	11	11	13	11	14	13	14	16	14	12	11	9
Direction of max. wind† (deg.)	15	10	110	11	295	10	345	10	20	15	25	30
Average station pressure (mb)	684.7	681.2	684.5	675.7	677.4	674.1	678.9	681.1	669.8	672.2	673.9	678.3
Maximum pressure† (mb)	694	694	697	704	688	692	693	699	685	692	684	688
Minimum pressure† (mb)	669	674	672	650	666	658	665	663	660	654	660	668
Average air temperature (°C)	-26.5	-39.4	-53.3	-59.5	-54.5	-58.8	-56.2	-54.6	-61.4	-54.1	-39.5	-25.8
Maximum temperature† (°C)	-21	-30	-38	-37	-32	-45	-40	-42	-46	-41	-27	-18
Minimum temperature† (°C)	-38	-48	-66	-73	-71	-74	-70	-67	-76	-67	-52	-34

*Instrument heights: wind, 10 m; pressure, 2850 m (MSL); air temperature, 2 m. The anemometer and thermometer are located on a mast 30 m grid north of the Clean Air Facility. Pressure measurements are made inside the facility.
†Maximum and minimum values are hourly averages.

3.11 Precipitation Chemistry

Routine and special measurements of precipitation chemistry continued at both GMCC baseline sites (MLO and SMO) and at regional sites. The routine measurements at GMCC sites are important in measuring the year-to-year variations of acidity and in detecting possible long-term trends in precipitation chemistry. Recent studies have confirmed that the acidity level at other remote sites is similar to that found at GMCC baseline sites (pH 4.5-5.0) (Galloway et al., 1982). Limited, special onsite chemical analyses, in addition to pH and conductivities, were performed at MLO and SMO.

3.11.1 Baseline Measurements

This is the first full year that MLO and SMO have participated in NADP. Data from these weekly collections have been reported in the NADP quarterly report.

Onsite research measurements have continued, particularly at MLO and SMO. At these stations shorter term collections are made and samples are analyzed for the major ions on the ion chromatograph. The monthly average pH values for measurement sites on the island of Hawaii are shown in fig. 28. Site descriptions have been documented in the GMCC Summary Report for 1977 (Peterson, 1978).

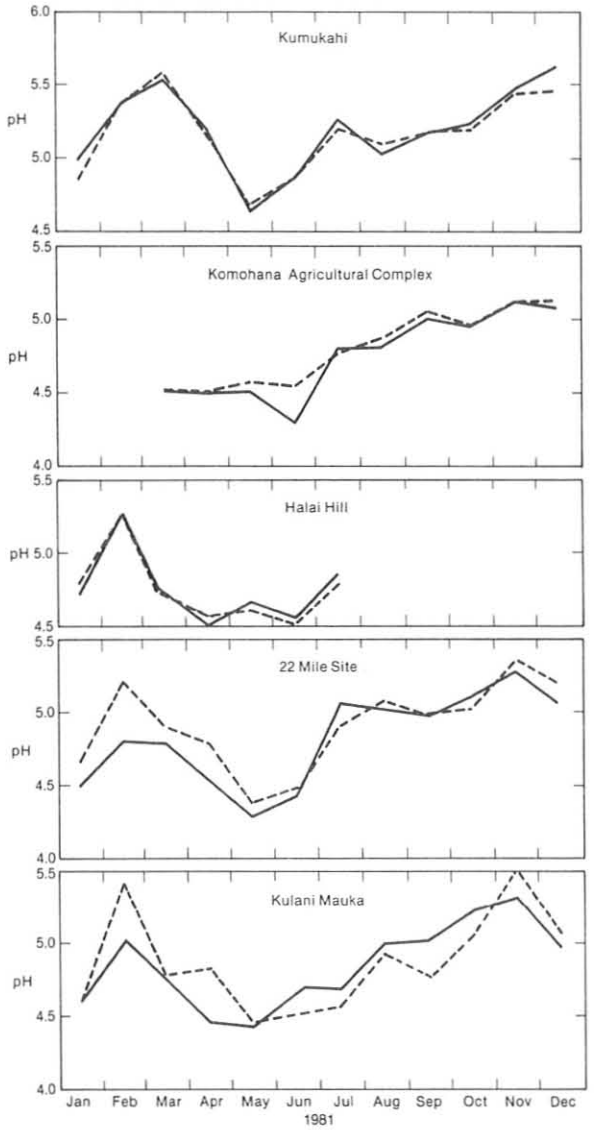

Figure 28.--The monthly average pH values for measurement sites on the island of Hawaii.

3.11.2 Regional Measurements

The 10 WMO regional sites are also a part of NADP. A summary of their annual average pH and ion concentrations is given in table 26.

3.11.3 Washington, D.C., Network

The pH data from six sites in the Washington, D.C., area are shown in fig. 29.

Table 26.--Average ion concentration and pH values at WMO regional sites from January 1981 to December 1981

WMO regional sites	pH	SO_4	NO_3 (mg ℓ^{-1})	Cl
Alamosa, Colo.	5.05	2.05	1.86	0.79
Bishop, Calif.	5.87	1.25	0.53	0.81
Caribou, Maine	4.51	2.20	1.79	0.23
Huron, S.D.	5.69	3.17	1.73	0.76
Meridian, Miss.	4.75	2.97	1.56	0.96
Pendleton, Ore.	5.64	0.45	0.96	0.30
Princeton, N.J.*	4.38	4.43	2.15	0.50
Raleigh, N.C.	4.52	4.70	2.76	0.84
Salem, Ill.	4.33	4.76	2.32	0.46
Victoria, Tex.	5.01	1.75	0.95	0.58

*Since moved to Washington's Crossing, N.J.

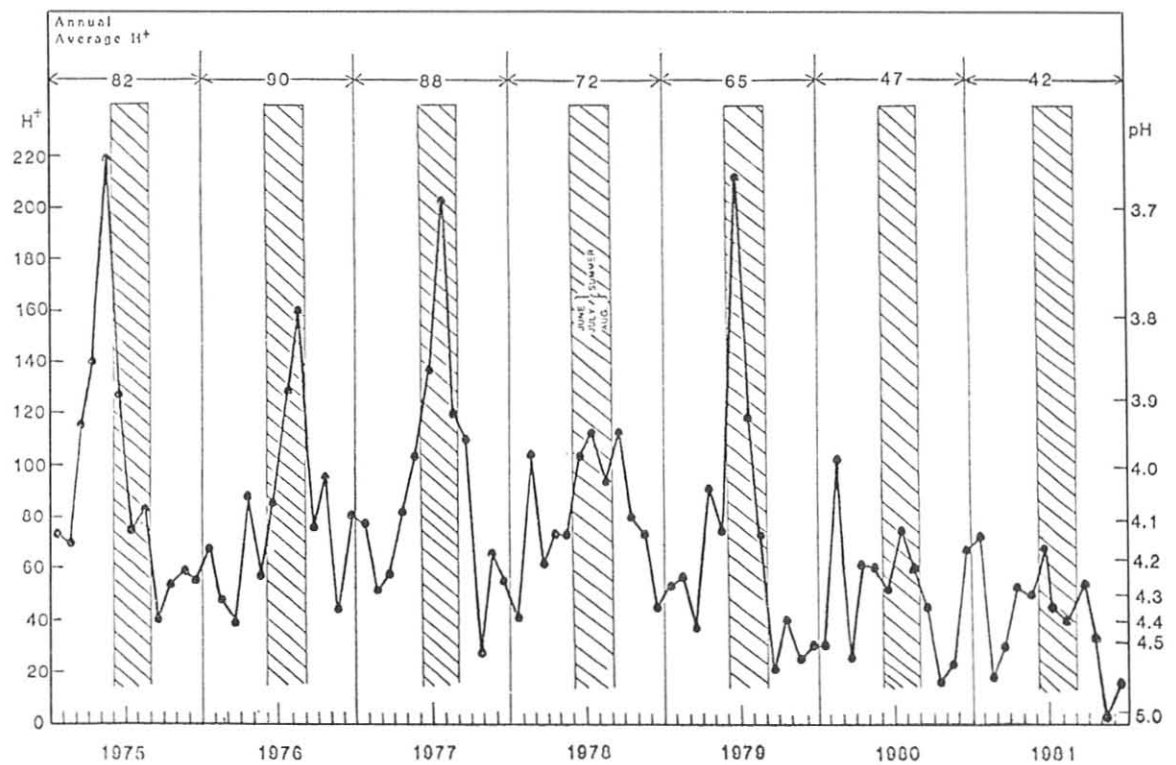

Figure 29.--Weighted monthly average H^+ concentration (μmol $\ell^{-1} \times 10^6$) and pH for the Washington, D.C., network from 1975 through 1981. The weighted annual average H^+ concentration is also given by the numbers at the top of the figure.

3.12 Data Management

3.12.1 ICDAS

Each GMCC observatory records continuous data on magnetic tape using a minicomputer system called ICDAS. The A&DM group within GMCC oversees this system, which has been fully operational for more than 5 years. The overall performance of ICDAS in 1981 was the best since its installation. The average downtime for the four stations was about 3% or only 11 days out of the year. The performance statistics for the individual stations are as follows: SPO, 98.3%; SMO, 97.2%; MLO, 93.1%; and BRW, 98.6%.

The main reasons for ICDAS downtime were power problems at MLO and SMO, a faulty multiplexer at BRW, and magnetic tape drive maintenance at MLO and SPO. In the middle of July an uninterruptable power supply installed at SMO solved most of the power problems there. This power supply was modified to run under internal oscillator frequency control rather than line frequency control.

Noise levels within ICDAS were quite low by the end of 1981. This is attributed to the "quiet" linear power supplies now in all the NOVA's and the fact that most ground loops and loose connections have been found and removed.

3.12.2 Reduction Facility

Initial processing of station data tapes takes place in the reduction facility in Boulder. In 1981 A&DM renovated the reduction facility by upgrading both its hardware and software. The new hardware consists of a faster minicomputer (NOVA 4), a Winchester disk drive, and a hardware multiply-divide board for faster computations. The programs that check and copy the station tapes were converted from BASIC to FORTRAN, giving a significant run-time savings. Because of the larger disk drive we are now able to operate under Data General's RDOS, which is more powerful than the previous operating system.

A DECtape II (TU-58) cassette drive identical to those in the microprocessor-based data systems (see sec. 3.12.3) was installed in the reduction facility. The software needed to link the cassettes to the NOVA was written so that data recorded on cassettes can be processed in the reduction facility.

In addition to standard tape processing, the A&DM group continues to support special projects, with the use of the reduction facility. For example, a procedure was developed to decode and unpack the data tapes from the aerosol spectrometer. These data tapes will be routinely translated to a form readily useable on the CDC 750 computer.

Finally, the A&DM group has upgraded the documentation for the reduction facility. The convenient central location of these manuals and instructions will make training for newcomers and students an easier task.

3.12.3 IICAMS

In the fall of 1978 members of the A&DM staff began design of a gas flow controller using microprocessors for the CO_2 program. The controller was completed early in 1979 and has been in operation since (Harris et al., 1980).

The success of this effort led to the procurement of a microprocessor development laboratory and the subsequent development of a controller for CO_2 gradient measurement at MLO. Since the construction of these first controllers, the Z80 microcomputer has been adapted as standard along with the STD-Z80 bus. A standard bus allows simple plug-in access of such items as clocks, memory, analog-to-digital converters, input-output ports, and other standard function boards. This collection of hardware and operational software has been named IICAMS. Current plans are to begin replacing ICDAS, project by project, early in 1984.

IICAMS consists of the following: CPU, programmable memory, battery-powered memory, clock and serial input-output port for access to the front panel, and cartridge tape drive. The preformatted DECtape II has been selected as a recording medium. It offers maximum reliability and a simplified mechanical design. The front panel is modular in design, providing a standard 10-character keyboard and 8 special-function switches. The analog-to-digital converter is available with a programmable gain option. The entire unit requires only 7 in of a standard equipment rack. The software will be programmed into PROM so the system will restart automatically after a power failure. Variables produced by the system will be stored in memory that is backed up by battery. The clock is also battery powered and will maintain the time for 5 days without recharging. The batteries in the memory and the clock will require changing every 24 months or so. A function switch will be assigned to the three primary peripherals (clock, A/D converter, and cartridge tape) to allow access and control. Four function switches will be reserved for the use of individual programs.

3.12.4 Archiving

Table 27 lists the GMCC data archived at the WDC-A in Asheville, N.C. Except for tapes written in Research-Cooperator format, each archive tape contains a preamble in card-image format that describes the data. Copies of the tapes can be obtained from User Services Branch, D5421, National Climatic Center, Asheville, NC 28801 (FTS 672-0682 or (704) 258-2850, ext. 682). GMCC archive tapes are located in tape deck no. 9708.

In addition to these data tapes, GMCC has archived all available CO_2 flask data from stations in the CO_2 flask network, through 1978, in a yearly WDC-A publication, "Global Monitoring of the Environment for Selected Atmospheric Constituents."

Table 27.--Inventory of GMCC data tapes at World Data Center-A

No.	Tape name	Date of issue	Parameter	Station	Period of data
1	MLONF1	12/09/77	Volumetric light scattering	MLO	1974-1976
2	GPOLO1	1/16/78	Condensation nucleus concentration	BRW MLO SPO	1975-1976 1975-1976 1975-1976
3	A78076	3/17/68	Solar irradiance	MLO	1977
4	A78083	3/24/78	Solar irradiance	SMO	1977
5	A78100	3/10/78	Solar irradiance	BRW	1977
6	A78104	4/14/78	Solar irradiance	MLO	1976
7	A78132	5/12/78	NIP radiation	BRW, MLO, SMO, SPO	1977
8	A78139	5/19/78	Wind, pressure, temperature, humidity	BRW, MLO, SMO, SPO	1977
9	A78146	5/26/78	Solar irradiance	SMO	1976
10	A78160	6/09/78	Solar irradiance	SPO	1976-1977
11	A78230	8/18/78	Solar irradiance	BRW	1976
12	A78272	9/19/78	Solar irradiance	BRW, MLO	1978, first half
13	A78279	10/06/78	Solar irradiance	SMO	1978, first half
14	A79127	5/07/79	Solar irradiance (Research-Cooperator format)	SMO	1976
15	A79128	5/07/79	Solar irradiance (Research-Cooperator format)	SMO	1977
16	A79208	7/27/79	Solar irradiance	MLO	1978, second half
17	A79222	8/10/79	Solar irradiance	SMO	1978, second half
18	A80010	1/25/80	Carbon dioxide	MLO	1974-1978
19	A80011	1/25/80	Carbon dioxide	SPO	1976
20	A80012	1/25/80	Carbon dioxide	BRW	1973-1978
21	A80036	2/05/80	Solar irradiance	BRW	1978, second half
22	A80075	3/16/80	Solar irradiance	SPO	1978
23	A81128	6/10/81	Solar irradiance	MLO	1979
24	A81155	6/10/81	Solar irradiance (Research-Cooperator format)	SMO	1979
25	A81155	6/10/81	Solar irradiance (Research-Cooperator format)	BRW	1979
26	A81170	7/09/81	Solar irradiance (Research-Cooperator format)	SPO	1979
27	A81190	8/12/81	Solar irradiance (Research-Cooperator format)	BRW	1980
28	A81193	8/12/81	Solar irradiance (Research-Cooperator format)	MLO	1980
29	A81201	8/12/81	Solar irradiance (Research-Cooperator format)	SMO	1980
30	A81211	8/12/81	Solar irradiance (Research-Cooperator format)	SPO	1980

3.13 Atmospheric Trajectories

3.13.1 Introduction

In 1976 an atmospheric trajectory program developed by J. Heffter and A. Taylor (GMCC Summary Report for 1976, Hanson, 1977, p. 60) became operational. This program runs on the NMC computer in Suitland, Md., and produces printed plots. In 1981 J. Harris of GMCC modified the program to run on the NOAA CDC 750 computer in Boulder so that the GMCC group would have easier access to trajectories. At the same time the program and the output plots were tailored to suit the needs of the scientists in Boulder. Although the accuracy of the trajectories is limited by the quality of the input data and the simplicity of the model, these trajectories, when used in conjunction with other meteorological parameters, can be an effective research tool to indicate large-scale airflow patterns.

The new version of the trajectory program is called GAMBIT for gridded atmospheric multilevel backward isobaric trajectories. As the name implies, the trajectories produced are computed from analyzed winds along constant pressure surfaces. Trajectories at two or three standard levels are computed, then displayed on a map. Although earlier versions of the program computed trajectories by averaging the winds through a selected layer, multiple trajectories at standard pressure levels were found to be preferable. In fact, the average-layer technique could yield trajectories that are not realistic. At MLO for example, when northeast trades dominate the lower levels and westerly winds prevail in the upper levels, there is no meaningful average between these two distinct wind regimes.

3.13.2 The GAMBIT Program

NCAR in Boulder now furnishes the meteorological input data on magnetic tapes (Jenne, 1975). These data, originating from NMC, are analyzed winds at 10 standard pressure surfaces: 1000, 850, 700, 500, 400, 300, 250, 200, 150, and 100 mb. As of the end of 1981, 5 years of data (1976-1980) were obtained from NCAR with two data records (0000 and 1200 Z) for each day. The raw gridded data are packed in a dense binary format (NMC, 1979). As standard procedure, only the first four levels (1000, 850, 700, and 500 mb) are unpacked. If upper levels are needed they are handled as a special case. As the data are unpacked, the order of the records is checked and one or two missing records are filled by interpolation. Interpolation has been necessary for only a few percent of the data. A gap of three or more records (>24 hours) constitutes a break in the data. Trajectories must terminate where there is a break in the data, but for the 5-yr period only two breaks occurred: 2 days starting 7 August 1980, and the last 1½ days of 1980.

The wind data are available in the form of U and V components on a 65 × 65 grid called the NMC grid for the Northern Hemisphere (fig. 30). The grid is a square matrix overlaying a polar stereographic projection of the hemisphere with a resolution of about 200 km per grid unit at the equator to about 400 km per grid unit at the pole. The wind data are computed by NMC's Optimum Interpolation Analysis Model (personal communication, R. Jenne, NCAR, 1981). The model starts with a forecast for the time period and then modifies this according to meteorological observations reported from around the globe. As might be expected, observations are sparsest near the Arctic and densest

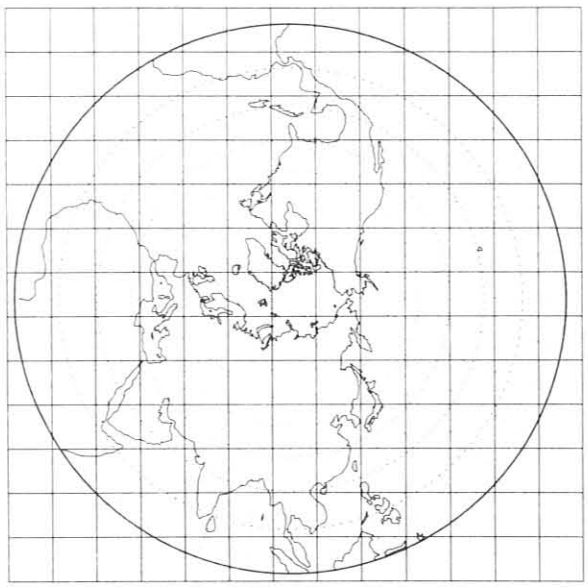

Figure 30.--The 65 × 65 NMC grid for the Northern Hemisphere. Grid point (0,0) is in the lower left corner. Every fifth grid line is shown.

over well-populated landmasses. Where the model has fewer real observations to constrain it, the wind data it produces may be less reliable, so that trajectories in these areas should be cross-checked with other data sources.

The basic computations that convert U, V wind components on the NMC grid to a trajectory segment are identical to those in previous versions of the trajectory program (Heffter and Taylor, 1975). A 10-day trajectory consists of eighty 3-h trajectory segments placed end to end. To compute one 3-h segment, the endpoint of the last 3-h segment is located with respect to the NMC grid; i.e., (latitude, longitude) is converted to (x, y). The wind is calculated at (x, y) using bilinear interpolation from the four grid points surrounding (x, y). The iterative scheme used to approximate the values of U and V representative of the 3-h period is the modified Euler method. These values are assumed constant for 3 hours to obtain the 3-h segment and the new endpoint.

3.13.3 Plotting the Trajectories

Three forms of the plotting program are now in use. The first type, shown in fig. 31, plots trajectories for one arrival time, 0000 or 1200 Z (shown here for 0000 Z), and three standard levels. The lowest level, in this case 850 mb, is marked L; the middle level (700 mb) is M; and the upper level (500 mb) is U. A character, either the letter indicating level or a number, appears every 12 hours along the trajectory. The number gives the time in days for an air parcel to travel from that point to the origin. The second type of plot (fig. 32) shows trajectories for two standard levels and two arrival times (0000 and 1200 Z) during the day. Again the identifying letters alternate with numbers showing number of days back. The legend at the top shows that A and B arrive at 0000 Z, that C and D arrive at 1200 Z, and that levels 700 and 500 mb are plotted. Finally, the third type of plot (fig. 33) displays all trajectories for a selected level over a given time period. This output is useful for climatological and case studies where one is concerned with general airflow patterns, not individual trajectories. Although these three types of plots cover most needs, other types are possible.

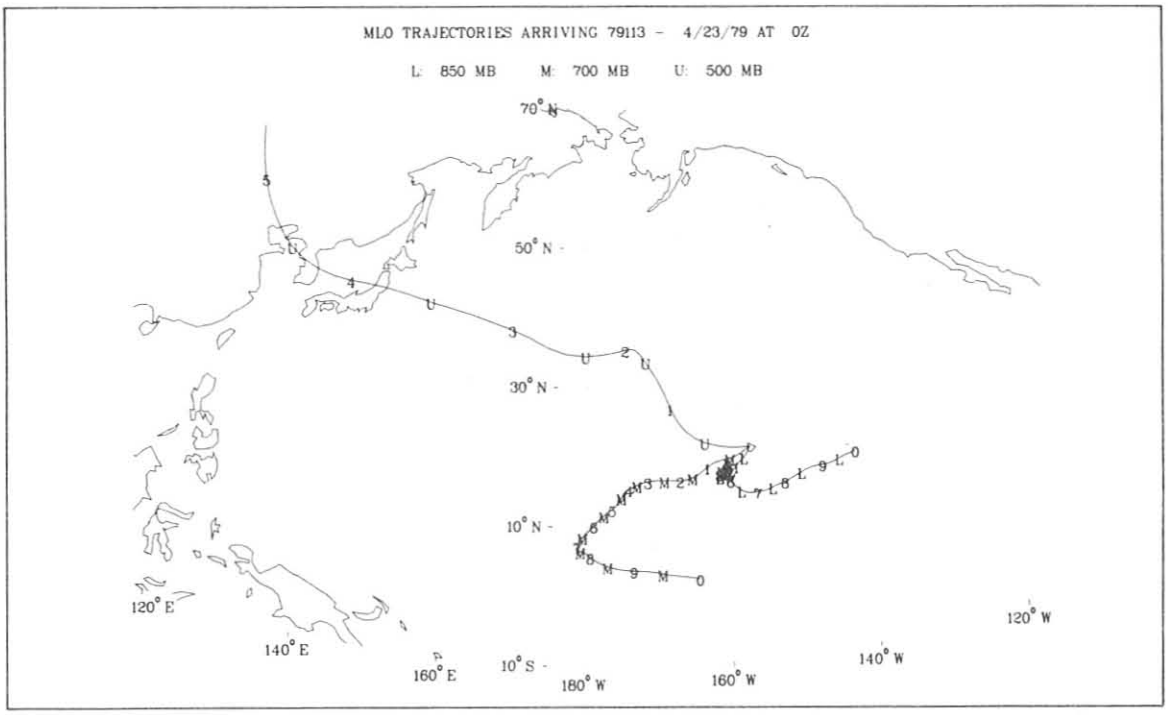

Figure 31.--Sample plot of MLO trajectories for one arrival time and three isobaric surfaces.

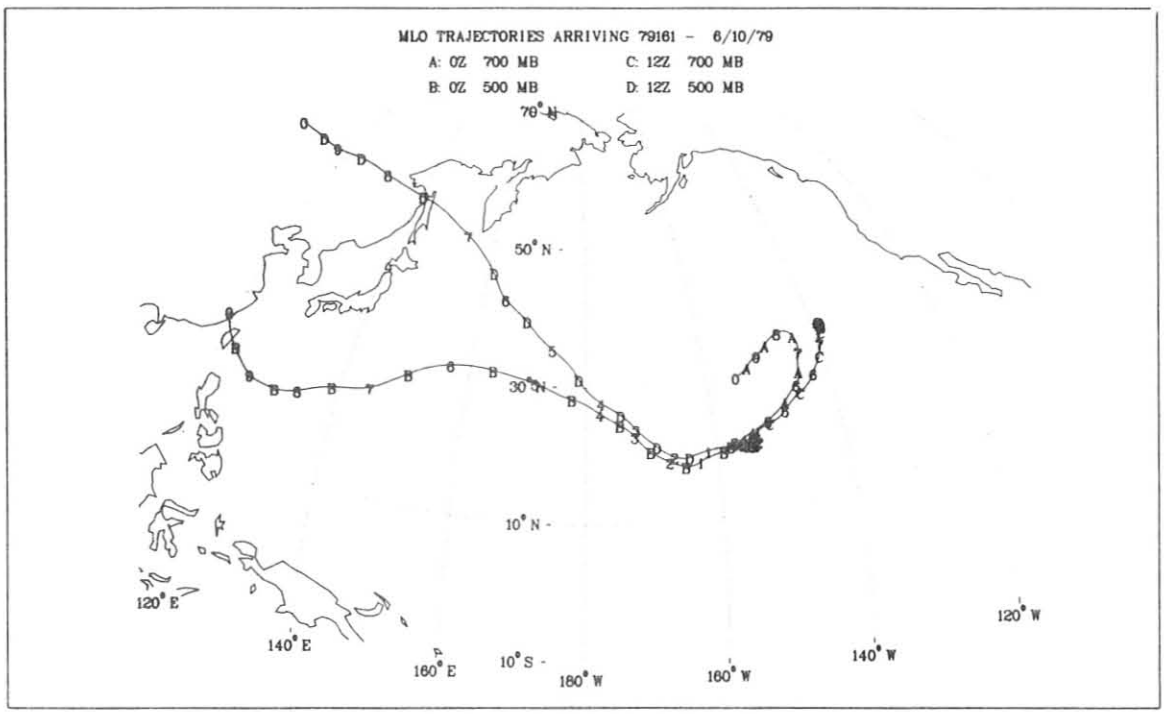

Figure 32.--Sample plot of MLO trajectories for two arrival times and two isobaric surfaces.

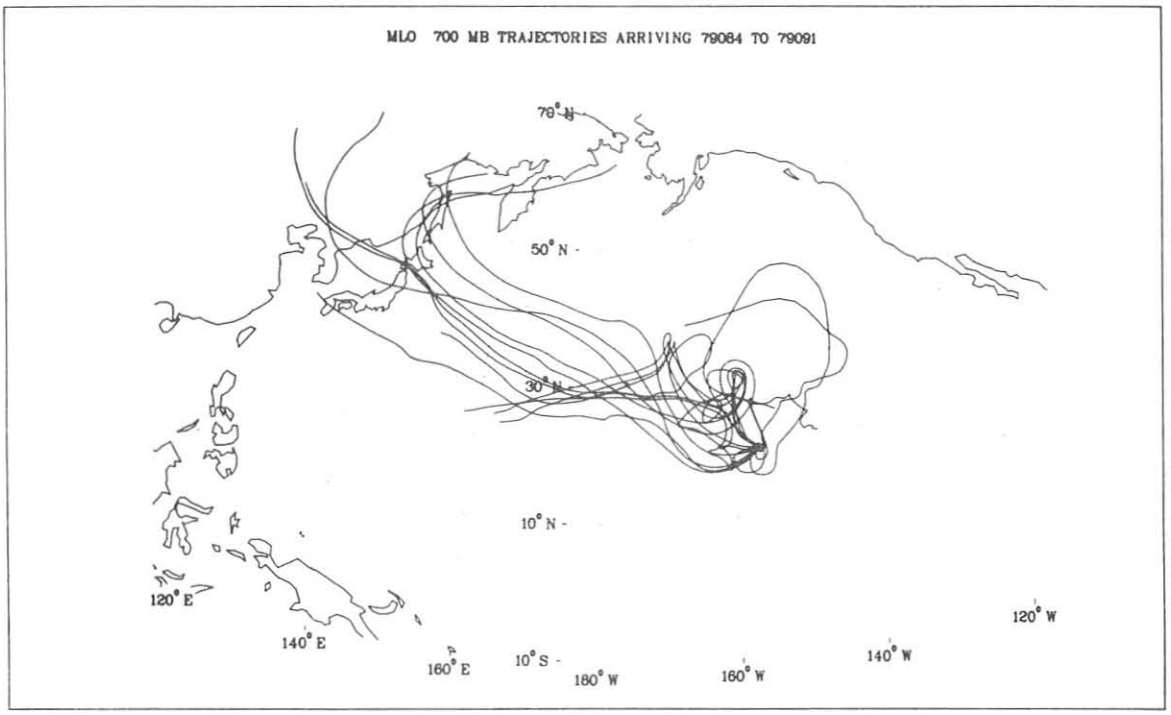

Figure 33.--Sample plot of MLO trajectories arriving over a period of 8 days along one isobaric surface.

The trajectory endpoints are computed and saved on magnetic tape. Once on magnetic tape they may be plotted any number of times in any desired form. Next year archival of the entire set of trajectory endpoints for MLO and Bermuda (1976-1981) on magnetic tape is planned. Trajectories for other origins will be computed as the need arises. The GAMBIT program will be modified in the future to accept the NMC 2.5° global analyzed winds so that not only trajectories for SMO and other points in the Southern Hemisphere can be computed, but also data can be available to investigate cross-equatorial flow.

4. SPECIAL PROJECTS

4.1 Modeling the Atmospheric CO_2 Concentration

On a global scale the change of CO_2 concentration during the year is caused by (1) combustion of fossil fuels that can have a seasonal variation, for example, due to space heating in northern latitudes; (2) biospheric uptake and output due to amount of biomass, which is a function of changing seasons, land/ocean ratios, climate patterns, soil fertility, etc.; (3) oceanic uptake and output, which is a function of presence of ice, concentration of CO_2 in water, water temperature, wind speed, biological activity in the ocean, ocean circulation, etc.; and (4) atmospheric mixing, which transports excess CO_2 produced at one location to other locations throughout the atmosphere.

Each of the above four causes of variation is considered in modeling atmospheric CO_2 concentrations. The four ingredients of the model are listed below.

(1) Atmospheric mixing. A two-dimensional atmospheric diffusion model (Machta, 1974) has been adapted for use in CO_2 modeling. It has 26 vertical layers and 9 latitude bands. Mixing coefficients are derived from bomb debris data and other diffusion studies.

(2) Oceanic uptake. As shown in fig. 34, two oceanic layers were added to the Machta atmospheric diffusion model. The first layer, the mixed layer, has variable depth while the depth of the second layer is held constant. The relation between concentration of CO_2 species in the ocean water and the partial pressure of CO_2 now assumes a constant total alkalinity. The model calculates hydrogen ion activity, then computes the proportion of CO_2 to total dissolved inorganic carbon by using equilibrium constants, which are a function of salinity and water temperature, for dissociation of CO_2 in water.

The flux from ocean water to the atmosphere is a part of the model that will vary parametrically. At present, the flux is a function of differences of partial pressure of CO_2 in the air and in the water multiplied by a function of wind friction velocity. Initial values of total dissolved inorganic carbon will be varied in the model. Ice coverage will be added to oceanic areas as a function of time as determined from sea ice records.

(3) Biospheric CO_2 fluxes. Fluxes to and from the biosphere will be parameters in the model and will be varied in numerical experiments. One example of biospheric fluxes is shown in fig. 35.

(4) Fluxes of CO_2 from combustion of fossil fuels. These have been tabulated by Rotty (1982) as a function of latitude as shown in fig. 36 and will be used to specify anthropogenic CO_2 contributions.

By variation of unknown parameters, the model can be compared with concentration data to obtain ranges of global oceanic fluxes and biospheric fluxes. Then by evaluating the data, planning sampling strategy, and estimating global oceanic and biospheric fluxes, adjustments can be made such that model and sampled CO_2 concentrations agree within some range of uncertainty.

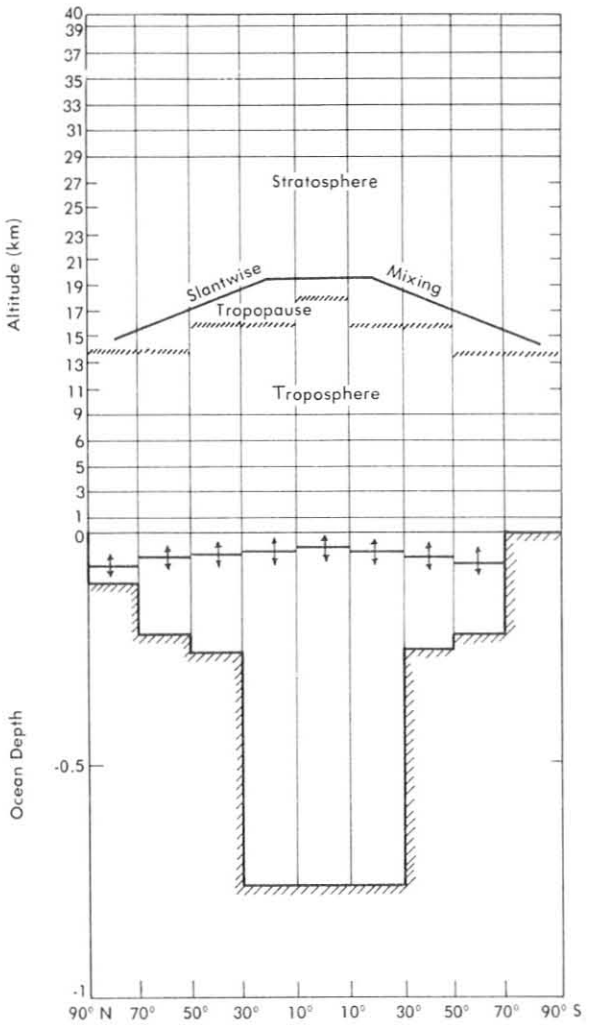

Figure 34.--Schematic presentation of the two-dimensional atmospheric-ocean CO_2 diffusion model. The upper part of the figure (atmospheric diffusion) is after Machta (1974).

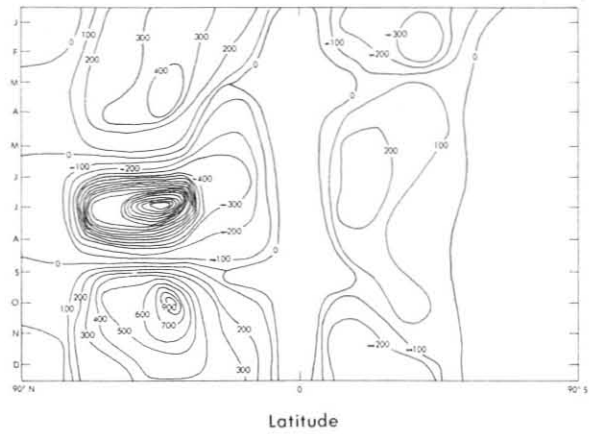

Figure 35.--Biospheric fluxes (Tg mo^{-1}, 20° latitude band) as a function of latitude and time of year.

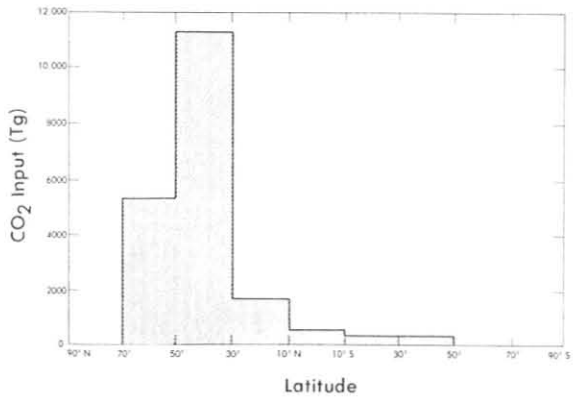

Figure 36.--Industrial CO_2 input per year (Tg yr^{-1}), after Rotty (1982).

4.2 Analysis of SPO's CO_2 Record for 1976-1980

4.2.1 Introduction

The South Pole, being extremely distant from sources and sinks of CO_2 and therefore relatively free of sources of short-term CO_2 variability, is one of the most desirable sampling locations in the world. Its record of CO_2 concentration is a smooth history representative of a large part of the globe. However, its remoteness and extreme environmental conditions offer difficulties in obtaining data. The CO_2 concentration data record for 1976-1980 had three discontinuities of concentrations corresponding to changes of infrared sources in the continuous analyzer and in a change of reference gas from CO_2-in-nitrogen to CO_2-in-air.

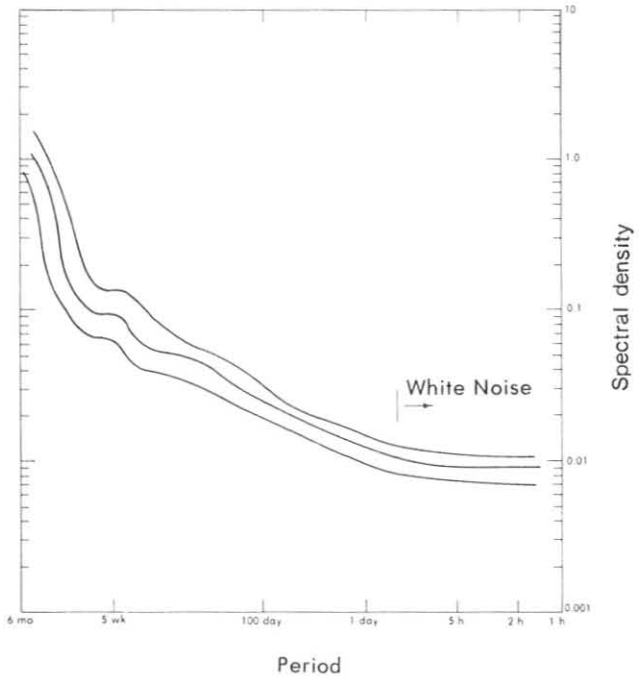

Figure 37.--Spectrum of atmospheric CO_2 hourly mean variability.

4.2.2 Variability of CO_2 at SPO

Minute-to-minute variability of CO_2 was found to be practically nonexistent at SPO. All variability of a minute-or-less time scale was explained by instrumental noise. Variability of hourly means of CO_2 for 1976 (a year when no discontinuties and little downtime occurred) is shown in fig. 37. Three conclusions were drawn from the 1976 data.

(1) Variability on time scales smaller than 12 hours is white noise. There is very little power for variations having time scales smaller than 75 hours.

(2) On the basis of a study of residuals for the fitted function,

$$f(t) = a + bt + ct^2 + dt^3 + e \sin\left(\frac{2\pi t}{365}\right) + f \cos\left(\frac{2\pi t}{365}\right) + g \sin\left(\frac{4\pi t}{365}\right) + h \cos\left(\frac{4\pi t}{365}\right),$$

where t = day of year, a-h are coefficients determined by the least-squares fit, and f(t) is the predicted CO_2 concentration, no significant spectral peaks were left for a single year's fit. Thus it is felt that the above function can adequately describe the SPO CO_2 record for 1 year.

(3) With the exception of instrumental failure or obvious contamination, no residual for a fit of 12-hourly values was larger than 0.1 ppm.

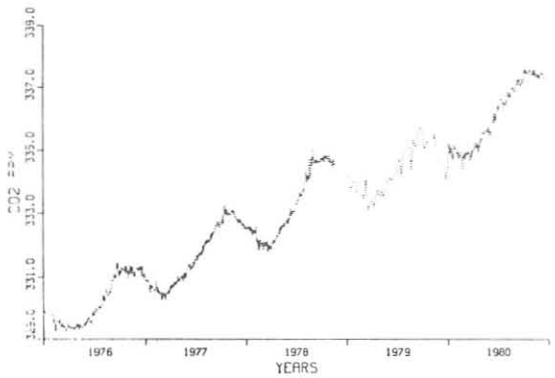

Figure 38.--Selected SPO daily CO_2 means.

4.2.3 Data Selection and Discontinuity Removal

A data selection method followed from point (3) in sec. 4.2.2: 12-hourly mean CO_2 values were fitted linearly, and residuals larger than 0.1 ppm were removed. The discontinuities of the data were removed by an exponentially decaying correction, which assumes that the value for CO_2 was accurate before the infrared sources in the continuous analyzer were changed.

4.2.4 Data Record

The corrected record of atmospheric CO_2 concentration is shown in fig. 38 for 1976-1980. The data are reported in the 1974 SIO mole fraction scale. An estimate of the annual mean CO_2 increase from these preliminary data is 1.4 ppm yr^{-1}. This number is slightly larger than the 1.3 ppm yr^{-1} value for the linear coefficient of increase reported by Keeling et al. (1976) for the period 1957-1971. The annual mean range after the linear increase is removed from the record is approximately 1.7 ppm.

4.3 Atmospheric CO_2 Variations Measured in the North Pacific Region and the Southern Oscillation

Recent research has shown that the rate of change of CO_2 concentrations at SPO, Fanning Island, MLO, and Weather Station P (Papa) correlate with an index of the Southern Oscillation and the associated El Niño phenomenon (Bacastow et al., 1980). These authors further suggest that the relatively weak El Niño of 1975 as well as the fully developed El Niño of 1976 were linked to atmospheric CO_2 anomalies measured at these locations. To continue this line of research, CO_2 concentration data from the GMCC baseline stations, BRW and MLO, and from Station P were analyzed. Although the data sets were different from those used by Bacastow et al., the data were analyzed in a similar manner. The resulting inverted time derivatives of the CO_2 anomalies are shown in fig. 39.

Figure 39 shows a similarity in the structures of the CO_2 anomaly derivative curves, which supports the view that these stations are measuring hemispheric-scale CO_2 perturbations. The CO_2 anomaly in 1975 (the dip in the three curves) decreases with increasing latitude. This feature is evident in the BRW record, but its magnitude is quite small. In contrast, the 1976-1977

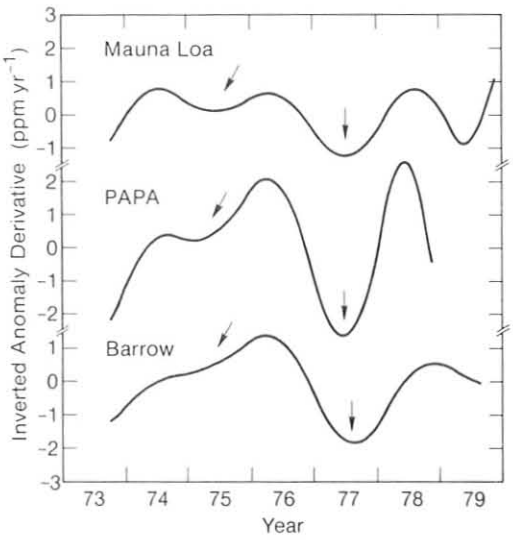

Figure 39.--Inverted time derivatives of the CO_2 anomaly curves (in the manner of Bacastow et al., 1980) at MLO, Weather Station P, and BRW. The CO_2 anomalies are the differences between observed monthly average CO_2 concentrations and the detrended long-term CO_2 record at each location. Long-term growth rate factors of 1.0019 for BRW and Station P and 1.00423 for MLO were used in these calculations. The apparent responses to the 1975 El Niño and the 1976-1977 anomaly are indicated by arrows.

CO_2 anomaly is quite prominent, and its greatest amplitude is at Station P. Moreover, the phase of the anomaly minimum at Station P slightly precedes that at the other two locations. This evidence suggests, but does not prove, that different forcing functions produced the two anomalies.

Other researchers have shown that the 1976 decrease in the slope of the long-term atmospheric CO_2 concentration records from BRW, Station P, and MLO are significantly correlated with coincident SST DN in the North Pacific Ocean (Hanson et al., 1981; Schnell et al., 1981). At BRW, this decrease was of such magnitude that the annual average CO_2 concentration in 1976 was 0.1 ppm lower than in 1975 (Peterson et al., 1982). The correlation patterns between the CO_2 DN and SST DN for MLO are shown in fig. 40. In this figure, the positive correlation patterns (no lags) in the North Pacific in 1976 are worthy of note.

In an extension of the above analysis, correlations between the Southern Oscillation and SST DN were calculated, with the results shown in fig. 41. The shaded areas indicate zones of positive correlation of +0.6 and larger. By comparing figs. 40 and 41, a marked similarity in the areas of high positive correlation may be observed for 1974 and 1976. Point correlations of +0.9 occur in similar locations in the same years in both series.

These correlations between the Southern Oscillation and both the North Pacific CO_2 DN and the North Pacific SST DN suggest that each is either responding to some other undocumented forcing or that one influences the others. It is known that the Southern Oscillation is positively coupled to the North Pacific pressure-wind system (i.e., weather) and that these teleconnections affect broad areas of the North Pacific (White and Walter, 1973). If the Southern Oscillation is directly influencing annual CO_2 concentrations in the North Pacific, the mechanism by which it does so is unclear.

One possible mechanism is abnormal seasonal SST. The theoretical atmospheric CO_2 response to ocean cooling is a decrease in the slope of the long-term CO_2 trend. Conversely, an abnormal ocean warming increases the slope of

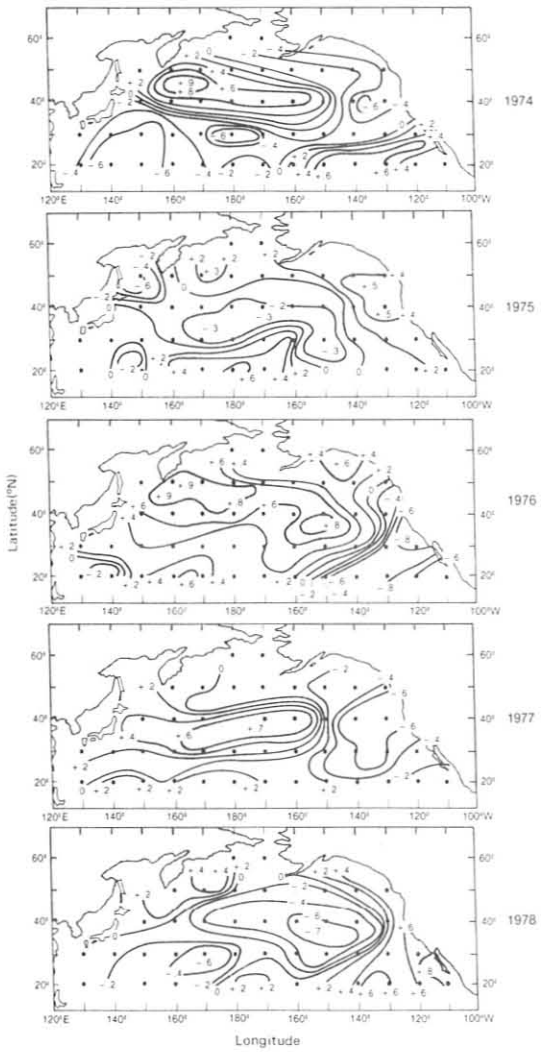

Figure 40.--Correlations of MLO CO_2 DN with SST DN, year by year for the period 1974-1978. Shading indicates correlations ≥0.6.

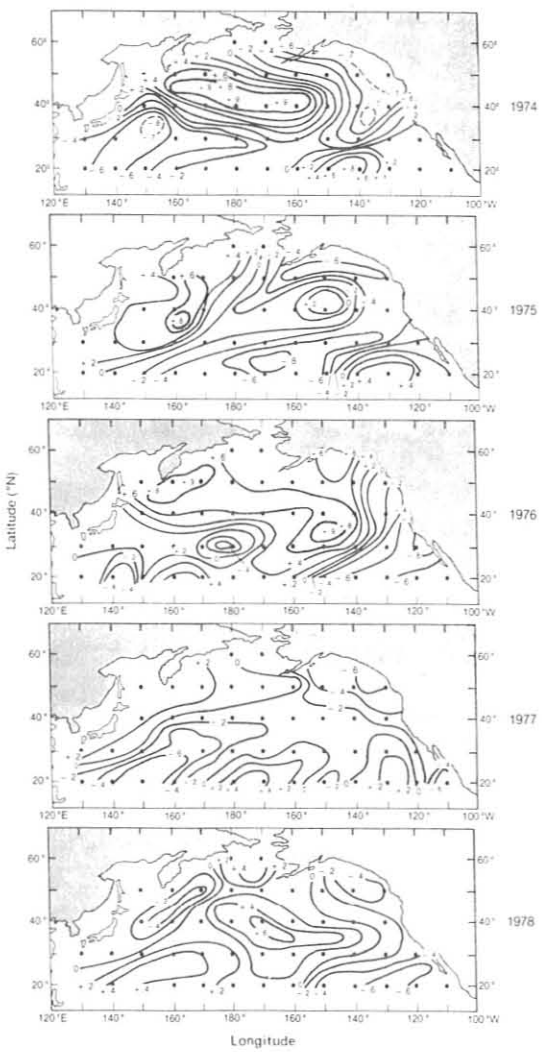

Figure 41.--Correlations of the Southern Oscillation Index with SST DN, year by year for the period 1974-1978. Shading indicates correlations ≥0.6.

the trend. Both the CO_2 anomaly derivative studies and the DN studies for CO_2 and SST presented above support the suggestion that abnormal seasonal SST's affect atmospheric CO_2 concentrations in the Pacific basin.

Further, if one accepts that the Southern Oscillation is related to seasonal North Pacific weather, and that these weather patterns influence SST, the correlation patterns discussed above may be explained. Other explanations for the CO_2 DN's, such as changes in hemispheric-scale flow or changes in global mixing of fossil fuel CO_2, are being studied.

4.4 CO_2 Flux Estimation at BRW

A new CO_2 inlet line was mounted 0.3 m above the tundra at BRW in June 1981. Samples of 5-min duration are passed through the continuous CO_2 analyzer once an hour on the half-hour; the remaining time of the analyzer is devoted to ambient air sampling from the line mounted 10-m above the tundra, and to calibration. In conjunction with the regular CO_2 concentrations measured at 10 m, the data from the ground line allow for rough estimates of CO_2 flux into and out of the tundra. This in turn provides a means for determining the role of Arctic tundra vegetation in the global CO_2 cycle.

CO_2 mean concentrations measured at the two levels (plotted in LST and in the 1974 mole fraction scale) are shown in fig. 42 for a 1-wk period in August 1981. In this figure, a high-amplitude diurnal cycle is evident in the ground line data, and a diurnal cycle of lesser amplitude is in the upper-line data. A general trend of decreasing average CO_2 concentration is present in the upper-line data; this reflects the annual summer CO_2 drawdown observed at BRW.

The difference in CO_2 concentration between the upper and lower lines is shown in fig. 43 for the same period as in fig. 42. CO_2 values below the zero line represent periods when smaller CO_2 concentrations were measured near ground level, and values above the zero line represent periods when ground level CO_2 concentrations were higher. For this week in August there were more hours when the CO_2 concentration was lower nearer the ground than the opposite.

CO_2 fluxes into and out of the tundra were estimated using the CO_2 concentration differences in fig. 43 along with measured wind speeds and derived

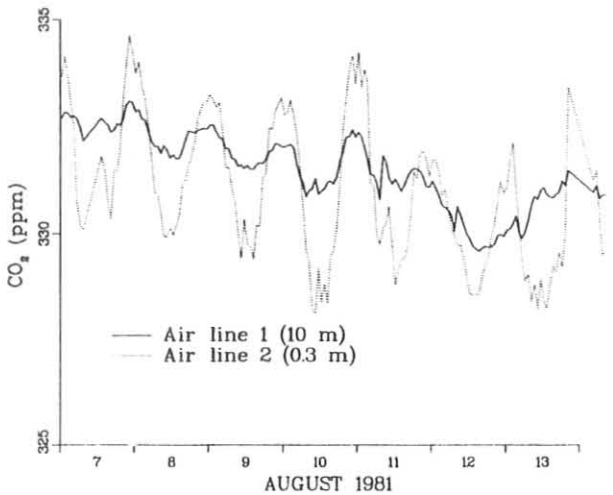

Figure 42.--Hourly mean CO_2 concentrations measured at two levels at BRW. The inlet to the lower line is 0.3 m above the tundra vegetation; the height of the vegetation is an average 0.2 m. The CO_2 concentrations measured at the 10-m height constitute the atmospheric CO_2 record for BRW. Time is given in LST.

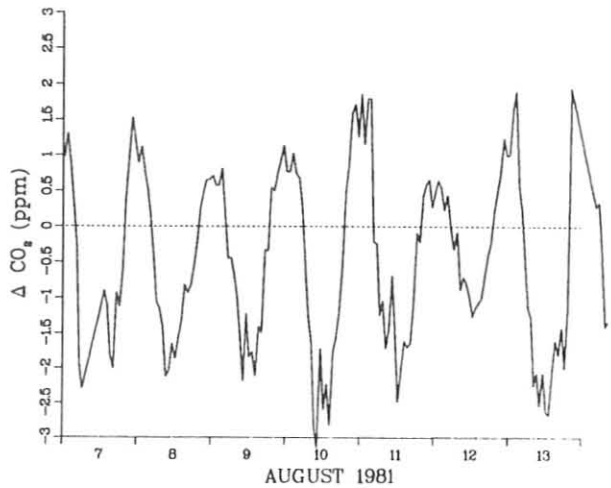

Figure 43.--CO_2 concentration measured at 0.3 m minus that at 10 m. Negative values represent periods of CO_2 uptake by the vegetation, and positive values represent CO_2 egress from the vegetation. Time is given in LST.

mixing coefficients. These estimations are necessarily rough because (1) CO_2 concentration data were not obtained at exactly the same time for the two heights sampled; (2) wind data were obtained at only one height (10 m); and (3) temperature stratification data were not available. Nonetheless, estimates of CO_2 vertical fluxes were calculated using the method of Sehmel and Hodgson (1976). The vertical CO_2 flux was expressed as

$$F = u_* (\chi_{hi} - \chi_{lo})\rho_a \Big/ \int_{Z_{lo}}^{Z_{hi}} dz/(E + D) \ .$$

The values of χ_{hi} and χ_{lo} are mass mixing ratios of CO_2 at the high and low vertical heights Z_{hi} and Z_{lo}; E and D are particle eddy diffusivity and Brownian diffusivity, respectively; u_* is wind friction velocity; and ρ_a is the density of the air. The integral in the denominator was evaluated to be 8 for a slightly unstable condition of Monin-Obukhov length L = -5,000 cm. With assumed values of aerodynamic roughness height Z_0 = 0.5 cm, and Monin-Obukov length L = -5,000 cm, the relationship

$$u_* = 0.0534\ \bar{u}_{10m}$$

was obtained, where $\bar{u}_{10m}$ is the hourly mean wind speed at the 10-m height.

Thus the approximation

$$F = \bar{u}_{10m} (C_{lo} - C_{hi}) \cdot 1.24 \times 10^{-9} \text{ g cm}^{-2} \text{ s}^{-1}$$

was made, where $\bar{u}_{10m}$ is measured in meters per second, and C_{lo} and C_{hi} are dimensionless volume mixing ratios.

Hourly CO_2 fluxes for the months of July, August, and September are shown in fig. 44, where negative values represent CO_2 uptake by vegetation and positive values represent egress of CO_2 from the vegetation layer. Notice that the amplitude of the daily CO_2 flux cycle increases through the last week of July and then becomes relatively steady for a month. In the last week of August, the amplitudes of the cycles are decreasing until they approach noise levels in late September. The high-amplitude cycles correspond to the peak in the growing season of vegetation on the tundra.

The fluxes of CO_2 measured at BRW ranged from 0 to 1×10^{-8} g cm^{-2} s^{-1}, with a few excursions in excess of 2×10^{-8} g cm^{-2} s^{-1} during the peak growing season. These estimates are in qualitative agreement with those obtained by Coyne and Kelley (1975) who measured summertime CO_2 fluxes from 0 to 1.6×10^{-8} g cm^{-2} s^{-1} over tundra near Pt. Barrow. CO_2 flux measurements over growing vegetation in lower latitudes suggest that the fluxes generally do not exceed 3×10^{-8} g cm^{-2} s^{-1} (Verma and Rosenberg, 1976).

The integral of the CO_2 flux at the 0.3-m height was calculated for the period from snow melt (20 June 1981) until the ground line became buried in snow (23 October 1981). The results are shown in fig. 45 in conjunction with atmospheric CO_2 concentrations measured at the 10-m height. From this figure observe that atmospheric CO_2 is being deposited in the vegetation from early July to mid-August, at which point the vegetation becomes a net contributor of

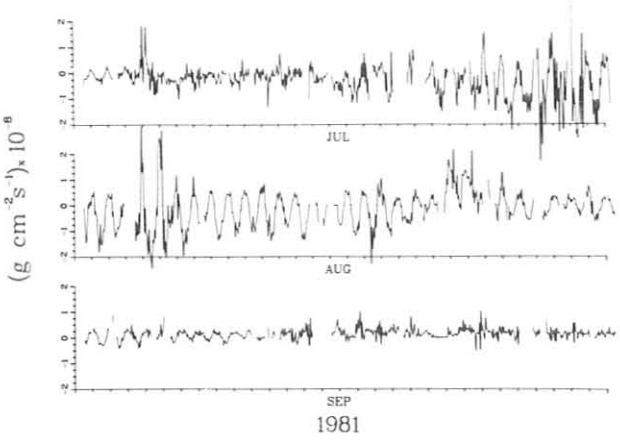

Figure 44.--Hourly CO_2 flux values for the growing season at BRW. Negative values represent periods of CO_2 uptake by the vegetation, and positive values represent CO_2 egress from the vegetation. Time is given in LST.

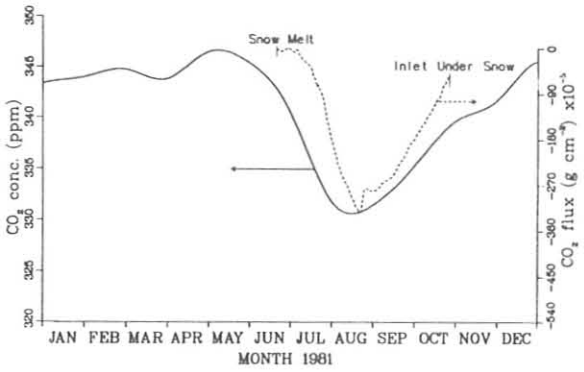

Figure 45.--Hourly mean CO_2 concentrations at BRW (smooth line, 10 m) and the integral of the net hourly CO_2 fluxes illustrated in fig. 44 (broken line, 0.3 m). The spring drawdown of the CO_2 cycle is seen to occur some months prior to snowmelt at BRW. In the fall, the rise in the annual CO_2 cycle is later than, and continues well past, the time the tundra is frozen and covered with snow.

CO_2 to the atmosphere. The fact that the integral does not return to 0 has a number of possible explanations: (1) the mixing coefficients used were incorrect and/or were not constant over a day or over the growing season (likely); (2) decomposition of local vegetation was not complete at the time of snowcover (possible); or (3) a net annual positive fixation of CO_2 by the tundra occurred (unlikely).

The question of whether CO_2 release through decomposition of the local vegetation was in balance with CO_2 fixation earlier in the growing season is difficult to answer without accurate determination of the mixing coefficients. Uncertainty in the mixing coefficients will be considerably reduced in the 1982 CO_2 data flux calculations because data will be available from a second temperature sensor and a new anemometer that have been installed at the height of the ground CO_2 line. Research on the CO_2 budget for Arctic flora (Coyne and Kelley, 1974) has shown that at soil temperatures warmer than -7°C there is subnivean release of CO_2 from the tundra. Much of this CO_2 is apparently released to the atmosphere when the snow melts the following spring. Assuming that this occurred in the fall and winter of 1981 may explain the shortfall of released CO_2 evidenced in fig. 45. Analyses of the CO_2 fluxes released during the thaw of 1982 should provide further information on the matter.

The possibility that there is a net annual excess fixation of CO_2 by the Arctic tundra is remote because then the biomass would double in about 5 years, on the basis of the values presented in fig. 45. This has not been observed. Even if there were a net positive CO_2 fixation in any year, excess decomposition in subsequent years could very well balance the equation or produce a deficiency, depending on the moisture and temperature pattern of that particular season.

In fig. 45, the observed BRW CO_2 cycle is seen to begin its annual spring decrease in early April, about 2 months prior to snow melt. In the fall, the annual cycle is still rising 2.5 months after ground freeze and snow cover. It may be stated with some assurance that vegetation on the tundra is not consuming CO_2 in April or May. In July, the annual CO_2 drawdown becomes relatively steep, which may reflect the consumption of CO_2 by local vegetation. In the fall, the annual cycle is still rising months after the time expected for high-latitude snow cover to considerably reduce or terminate plant decomposition and soil-to-atmosphere transfer of CO_2.

The annual CO_2 cycle at BRW does exhibit the expected timing of growth and decay of vegetation in a 50°-60°N latitude band. Coincidentally this same latitude band encompasses the zone of the largest nonequatorial net primary productivity of CO_2 on Earth (Box, 1978). Also, in terms of gross and net primary productivity, and seasonal primary productivity of CO_2 rate, Schnell and Harris (1981) have shown that CO_2 fixation and release by tundra vegetation do not adequately account for the amplitude of the CO_2 cycle observed at latitudes in the region of 70°N.

In summary, it appears that both the timing and amplitude of the BRW CO_2 cycle can be explained if it is assumed that the cycle reflects the growth and decay of vegetation at lower latitudes.

4.5 Air Mass Types Associated With Extremes in Winter CO_2 Concentration at BRW

The relation between winter CO_2 concentration at BRW and air mass type was studied to supplement an earlier study of CO_2 variability based primarily on trajectories (Peterson et al., 1980). Fifteen cases of the largest deviations (up to 3 ppm) of CO_2 concentration from average, for a 3-mo period, were considered. Information about the horizontal and vertical structure of the atmosphere was combined to characterize air masses associated with these CO_2 anomalies. This information included (1) NWS radiosonde winds, temperature, and moisture from Barrow; (2) pressure, height, and temperature fields obtained from NMC maps; (3) meteorological variables at BRW; and (4) air mass trajectories.

Two broad regions were identified as the sources of air masses associated with the CO_2 anomalies at BRW: the Arctic and North Atlantic regions. Arctic air masses were recognized by cold temperatures, low moisture, and long residence times in the Arctic. These air masses were found to be high in CO_2 and aerosol mass loading. The modified oceanic air masses, characterized by relative warmth and moisture, were, in contrast, low in CO_2 and aerosol mass loading.

During low-CO_2 episodes, oceanic air centered between 950 and 850 mb flowed into the Arctic. Pacific air was brought northward over Pt. Barrow by intense cyclonic circulations in the Bering Sea-Aleutian-Gulf of Alaska region and/or high-pressure systems over Alaska and western Canada. Intense cyclones over eastern Canada were responsible for the less-frequent arrival of air from the North Atlantic region. At the same time, the surface layer of the atmosphere, being dominated by high pressure over the North American or Siberian sectors of the Arctic Basin, was relatively cold and dry. Surface temperatures were 10°-15°C cooler than at the top of the consequent surface-based

inversion layer. With the modified oceanic air aloft, moisture levels in this surface-based Arctic air layer, although at considerably lower levels, tended to follow those aloft. This provided evidence of eddy turbulence and/or gaseous diffusion through the inversion layer. The surface-based Arctic layer varied in depth, and on a few brief occasions, increases of surface temperature and moisture to levels comparable with those of the Pacific or Atlantic air aloft indicated the actual elimination of the Arctic layer. On these occasions, the high aerosol light-scattering values typical of Arctic air during winter at BRW diminished to values approaching those typical of summer (Murphy and Bodhaine, 1980).

In high-CO_2 episodes, Arctic air was present in a deeper layer, usually extending through the entire depth of the troposphere. The Arctic air was drawn into the BRW area by cyclonic circulations over the North American sector of the Arctic Basin and/or anticyclones over the Arctic Ocean or Siberia. The trajectories suggested residence times in the Arctic of longer than 10 days for these air masses. Low-CN counts for some of these cases, implying a well-aged aerosol, suggested a long residence time over the Arctic Ocean, whereas higher CN counts for other of these cases and southeasterly airflow suggested fresher aerosol from Arctic land areas such as Alaska and Canada.

Regarding the high-CO_2 concentrations with deep Arctic air masses, the long residence times in the Arctic seem consistent with both a natural CO_2 source from the Arctic Ocean (Kelley and Gosink, 1979) and a polluted Arctic air reservoir (Barrie et al., 1981). In future studies, surface ozone data and daily air chemistry samples obtained at BRW (GMCC Summary Report for 1980, DeLuisi, 1981, pp. 113-116) may clarify the relative importance of midlatitude anthropogenic sources and the Arctic Ocean with regard to CO_2 concentration at BRW.

4.6 Calibration of Pollak Condensation Nucleus Counters

4.6.1 Introduction

The Pollak CNC (Metnieks and Pollak, 1959) has been adopted as a secondary standard for all CN measurements at the GMCC stations. A Pollak CNC is located at each GMCC station and is compared daily with the G.E. automatic CNC to ensure that the calibration of the automatic instrument is maintained over a long time period. The original calibration of the Pollak CNC (Pollak and Metnieks, 1960) used a photographic absolute CNC, and it has since been assumed that any instrument manufactured to Pollak's specifications would inherently have the same calibration.

4.6.2 Results

The seven Pollak counters used in the GMCC program were manufactured by BGI, Inc., Waltham, Mass., to the exact specifications given by Metnieks and Pollak (1959). These instruments have BGI serial numbers 13, 15, 16, 19, 20, 21, and 22. To ensure calibration of the Pollak counters, GMCC maintains a photographic CNC similar to the one described by Winters et al. (1977) and a mobility analyzer similar to that of Liu and Pui (1974).

During the summer of 1981, a laboratory experiment was performed in which three Pollak counters (SN 19, 21, 22) were compared with the GMCC differential mobility analyzer. The results of this experiment were reported by Miller and Bodhaine (1982a). The aerosol generation scheme, shown in fig. 46, used an atomizer to generate a polydisperse aerosol, a differential mobility analyzer to select a monodisperse aerosol of a given size, and an electrical aerosol detector to measure aerosol concentration. This system can be used to generate a monodisperse aerosol in the size range of about $0.01 < d < 0.1$, where d is the aerosol diameter in micrometers.

The results of the experiment are shown in fig. 47. The three GMCC Pollak counters were within about 7% of each other and coincided almost exactly with the results of a similar experiment by Liu et al. (1975). The Pollak CNC concentrations were about 30% lower than the electrical aerosol detector concentrations.

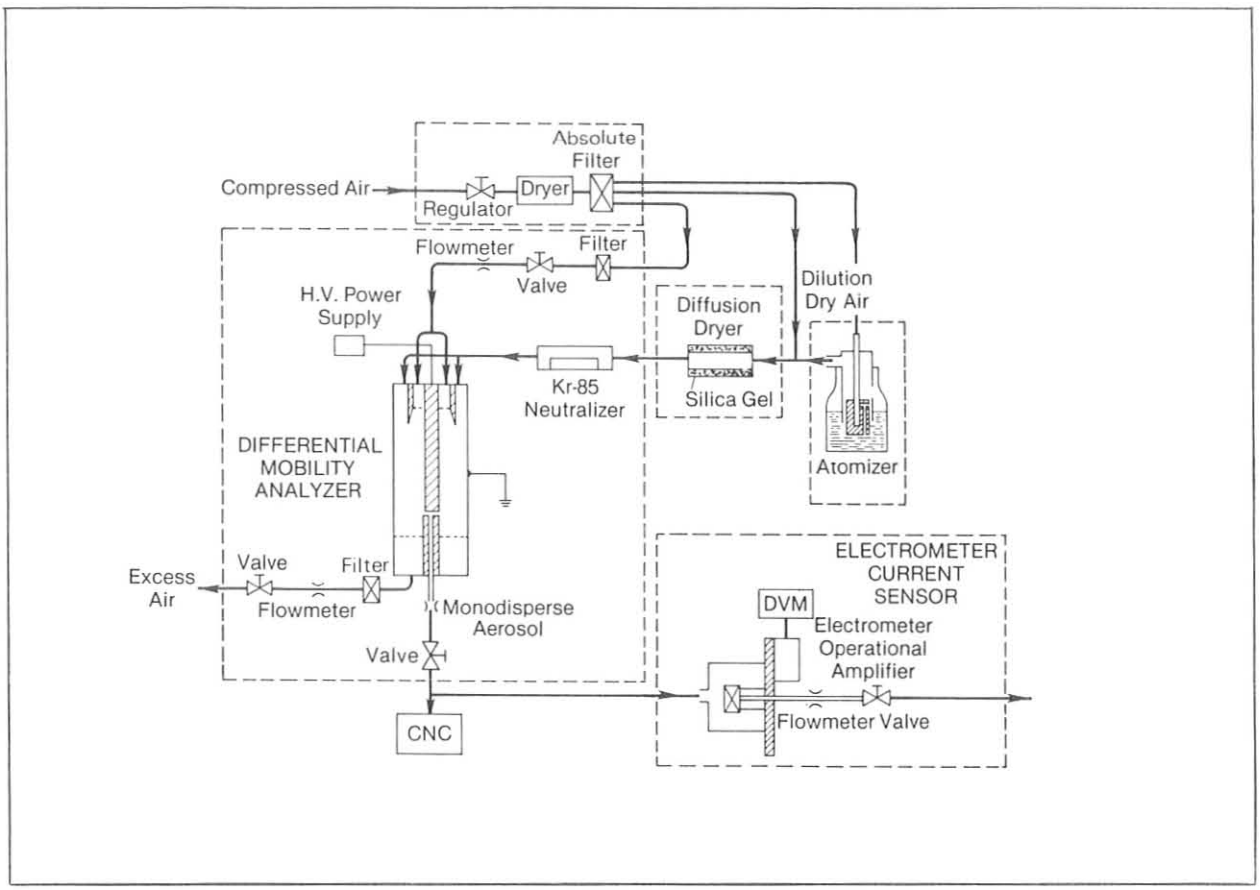

Figure 46.--Diagram of the monodisperse aerosol generation scheme.

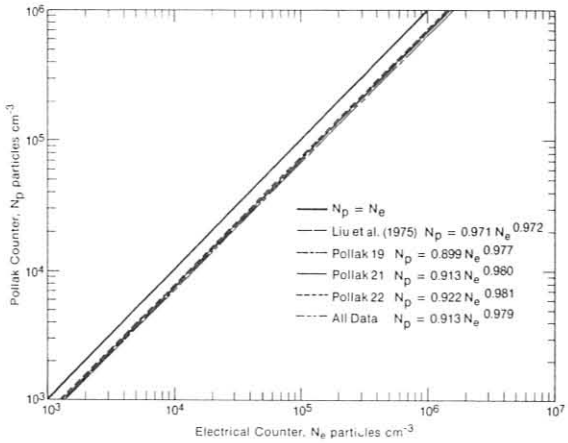

Figure 47.--Intercomparison of Pollak CNC calibrations.

4.7 Supersaturation and Expansion Ratios in Condensation Nucleus Counters

4.7.1 Introduction

In Aitken's experiments in 1880 on the physics of condensation processes (Knott, 1923), he concluded that "if there was no dust in the air there would be no fogs, no clouds, no mists, and probably no rain." In the next few years Aitken constructed several instruments, each of which produced an expansion of an air sample. The resulting supersaturation caused droplet growth on the "dust particles" in the air. His final version, the Aitken pocket counter, was used for many years as the only available measurement device for CN.

Subsequent work by Wilson (1897), Scholz (1931), Bradbury and Meuron (1938), and Nolan and Pollak (1946) led to the development of the photoelectric CNC in its present form (Pollak and Metnieks, 1960). It is this instrument that was adopted as the GMCC reference standard for CN measurements. A historical review of the development of CNC's has been presented by Miller and Bodhaine (1982b).

In the course of their review, Miller and Bodhaine discovered inconsistencies in the methods of calculation of expansion and supersaturation in CNC's. Interestingly, the confusion in the literature arose from a lack of appreciation of a thermodynamic process known as a free expansion.

4.7.2 Expansion and Supersaturation

An expansion instrument may be constructed to operate adiabatically by two different thermodynamic processes, apparently first explained by Herzog (1935). In a volume-defined expansion produced by a moving piston, work is done by the piston and the internal energy of the gas changes. In a pressure-defined expansion, or free expansion, in which the initial volume is allowed to expand into an adjacent evacuated vessel by means of a valve, no work is done on the gas and the internal energy does not change. The instruments of Aitken, Wilson, and Scholz were all piston operated, whereas the Pollak counter and the Gardner counter are both free-expansion instruments.

In the case of a piston-operated instrument, the relationship between the initial and final pressures and temperatures is given by

$$\frac{T_f}{T_i} = \left(\frac{P_f}{P_i}\right)^{\frac{\gamma-1}{\gamma}} , \tag{1}$$

where γ is the ratio of the specific heat of air at constant pressure to that at constant volume. The relationship between the initial and final pressures and volumes is given by

$$\frac{P_f}{P_i} = \left(\frac{V_i}{V_f}\right)^{\gamma} . \tag{2}$$

In the case of a pressure-defined instrument in which the sample volume is allowed to expand by means of a valve, the relationship between pressures and temperatures is still given by (1). However, the relationship between pressures and volumes, derived by Herzog (1935), is complicated and is not given by (2). In the case of a Pollak counter, which is expanded to the atmosphere, the final volume is not defined and the temperature depression must be calculated from (1). In the special case of a Gardner counter, which expands to an evaculated chamber, the relationship between pressures and volumes is given by

$$\frac{P_f}{P_i} = \frac{V_i}{V_f} ,$$

from which the temperature depression may be calculated using (1).

Saturation ratio in an air sample is defined as the ratio of the actual water vapor pressure to the saturation vapor pressure in the sample. Therefore, the saturation ratio achieved in an instrument after expansion is found from

$$S = \frac{e}{e_s(T_f)} ,$$

where e is the water vapor pressure immediately after expansion (but before condensation) and e_s is the saturation vapor pressure of the sample after expansion and at the final temperature. Since the air sample is saturated before the expansion,

$$\frac{e}{e_s(T_i)} = \frac{P_f}{P_i}$$

and

$$S = \frac{e_s(T_i)}{e_s(T_f)} \frac{P_f}{P_i} . \tag{3}$$

Equation (3) is the correct expression to calculate the saturation ratio achieved in either a piston-operated or a free-expansion-type instrument. An equivalent expression for use only in a piston-operated instrument is

$$S = \frac{e_s(T_i)}{e_s(T_f)} \left(\frac{V_i}{V_f}\right)^{\gamma}$$

Supersaturation is defined as the excess above a saturation ratio of 1 and is sometimes expressed as a percent. In general, therefore,

$$SS = S - 1$$

$$SS(\%) = (S - 1) \times 100 \ .$$

A more complete discussion of the theory of expansion, supersaturation, and condensation can be found in Miller and Bodhaine (1982b).

4.8 Correction to Long-Term Umkehr Data Using the MLO Solar Transmission Record

4.8.1 Introduction

The high sensitivity of MLO solar transmission measurements to stratospheric aerosols lends itself as a source for a virtually continuous set of optical thickness data for stratospheric dust. As far as can be determined, there exists no comparable data set for the Northern Hemisphere that is as long as the MLO record (1957 to the present). Rather coincidentally, systematic Umkehr observations of the vertical profile of ozone were started at several stations in the Northern Hemisphere near the same time as the MLO transmission measurements were started. Consequently, it is possible to investigate the relationship between stratospheric aerosol-induced errors and specific features seen in the long-term Umkehr ozone profile data. This report briefly describes the preliminary results of such an investigation.

4.8.2 Results

Figure 48 shows a slightly smoothed plot of the entire record of monthly averaged solar transmission measurements made at MLO. Details of the record are given by Mendonca et al. (1978). On the assumption that the span of years preceding the eruption of Agung in 1963 was representative of a climatically quiescent period during which the stratospheric dust was of a background character, it is possible to estimate enhancements in stratospheric dust optical thickness whenever a departure (decrease) in transmission from the mean of the quiescent period occurs.

Figure 49 shows departures from the 2-yr average of the pre-Agung quiescent period. The 2-yr average means that a 2-yr cycle rather than the annual cycle has been removed because there appears to be some indication that a biennial cycle exists in the transmission record, although this has yet to be proved. The departures shown in fig. 49 essentially represent an estimate of the optical thickness of a stratospheric dust enhancement. From Beer's law an estimate of optical thickness $\Delta\tau_t$ is given by

$$\Delta\tau_t = - \frac{\Delta T}{T} \ ,$$

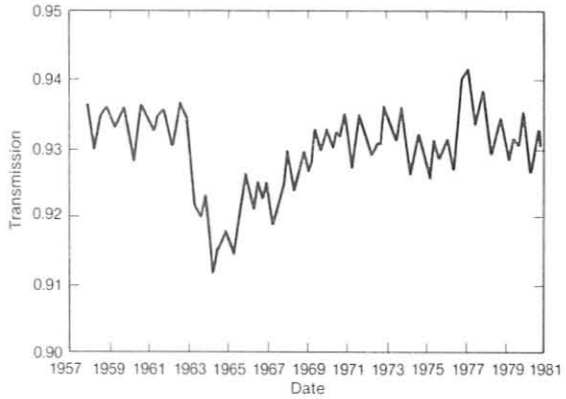

Figure 48.--Plot of monthly averaged transmission measured at MLO. The plot has been slightly smoothed.

Figure 49.--Plot of transmission differences after subtracting 2-yr cycles calculated for the quiescent period prior to Agung. Data from fig. 48 were used.

where T is the mean transmission and ΔT is the departure in transmission. However, this optical thickness is representative of the solar flux integral over all wavelengths in the solar spectrum whereas a value near 330 nm is required here. Model calculations of transmission using LOWTRAN show that $\Delta\tau_t$ is best applicable at a wavelength somewhere between 700 and 800 nm, and that at 330 nm the optical thickness is approximately 2 times greater than the transmission for all wavelengths. Figure 50 is a plot of $\Delta\tau_t$ vs. time. Multiplication of $\Delta\tau_t$ by 2.2 will give the value of the optical thickness at 330 nm.

The error to Umkehr observations (made in the Northern Hemisphere) is estimated using $\Delta\tau_t$ and the results of Dave et al. (1980), and invoking the reasonable assumption that the error is linear with optical thickness. Figure 51(a) shows four panels of average ozone concentration in Umkehr layer 9 using data from six stations located in Europe and Japan. The ordinate represents departures from the long-term average with the annual cycle removed, and the abscissa is time in years. The uppermost plot is the uncorrected basic data; the next includes the stratospheric aerosol correction; and the lower two plots are unweighted, seven-point smoothed versions of the corresponding plots above. Some obvious differences are seen between the uncorrected and

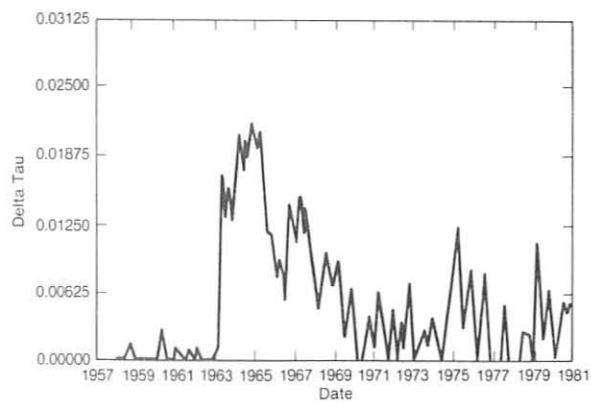

Figure 50.--Estimates of enhancements in stratospheric dust optical depth $\Delta\tau_t$ at MLO using data from fig. 49.

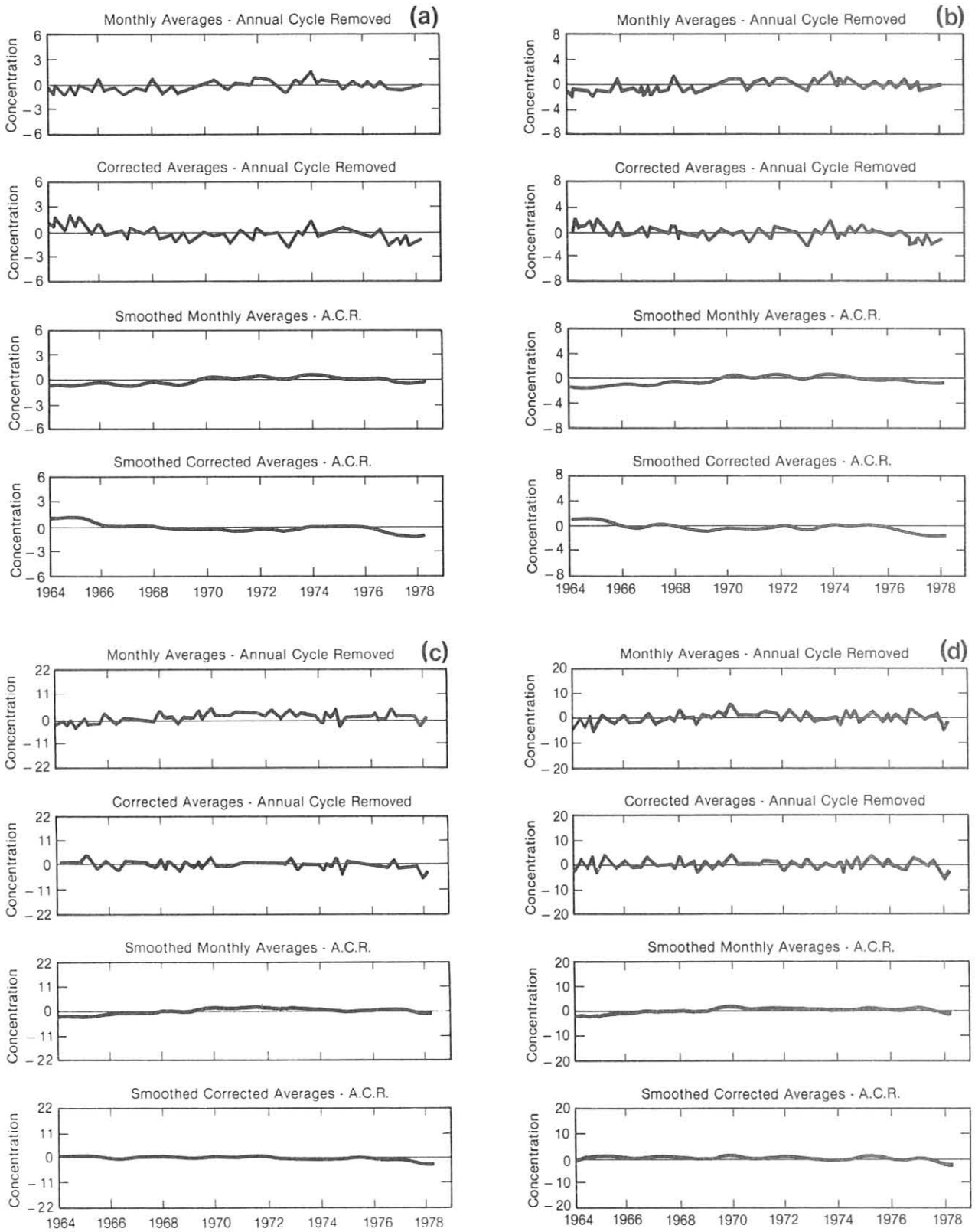

Figure 51.--Umkehr data for three stations in Europe (35, 68, and 70) and three stations in Japan (7, 12, and 14) for (a) layer 9, (b) layer 8, (c) layer 7, and (d) layer 6. Data are in terms of concentration (μmb) departures from the mean vs. time with the annual cycle removed.

corrected plots. There is reason to believe that the corrections made in 1964 and 1965 may be overestimated, because a stratospheric dust gradient probably existed between the latitude of MLO (19°N) and the European and Japanese stations (located between 30° and 50°N).

Figures 51(b-d) are similar to fig. 51(a), but show results for layers 8, 7, and 6, respectively. No corrections were made to layer 5. Note that the magnitude of the correction decreases as the layer altitude decreases.

4.8.3 Conclusion

The MLO transmission data are useful for correcting Umkehr ozone profile errors caused by the presence of stratospheric dust. However, the latitude differences between MLO and the Umkehr stations probably introduce a bias in the corrections because a latitude gradient of dust concentration may exist. Further work on the horizontal diffusion of stratospheric aerosol will be needed in the present correction procedure. In the future, it would be wise to have stations measuring stratospheric dust at several different latitudes between 30° and 50°N.

4.9 Comparisons between Backscattered Ultraviolet, Standard Umkehr, and Short Umkehr Measurements of Ozone Concentration

A comparison of ozone concentration at 45 km (Umkehr layer 9) observed coincidentally with the BUV and Umkehr measurement methods was presented by Fleig et al. (1981). The comparison consisted of an annually averaged percent deviation of the BUV with respect to the Umkehr from 1970 to 1977. This comparison is shown in fig. 52 as the dashed plot. The year 1977 was omitted because only a few comparisons were possible. The plot shows an obviously increasing difference with time until 1975 when a rather serious departure from this trend occurred. This happened to be during the time of enhancement in stratospheric dust from the eruption of DeFuego (fall 1974).

The MLO transmission data were used to correct Umkehr measurements made during the period of comparison. The corrected comparison is shown as the solid-line plot. The correction for stratospheric dust not only lowers the

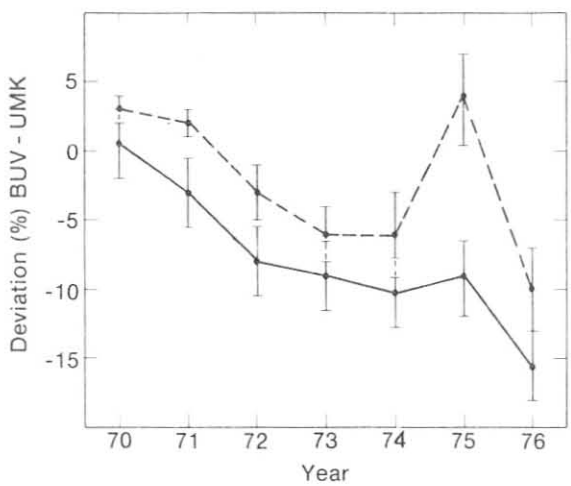

Figure 52.--Comparison between BUV and Umkehr (UMK) observations of ozone in Umkehr layer 9 over Arosa, Switzerland. Points are annual averages in terms of percent difference with the Umkehr as a reference. The dashed line is the comparison published by Fleig et al. (1981); the bars are for standard error. The solid line is the result of stratospheric aerosol error corrections to the Umkehr; bars are for 2.5% uncertainty in optical depth.

Table 28.--Comparison of SBUV, Umkehr, and short Umkehr observations using 1978 Boulder data

Layer no.	UMK-SBUV* (%)	Short-UMK† (%)	Short-SBUV (%)
9	3.8	-0.3	3.5
8	-6.3	7.5	0.7
7	-3.7	0.64	-3.1
6	10.5	-12.5	-3.3
5	9.1	-12.1	-4.1
4	-6.8	11.7	4.1
3	1.1	24.3	25.7
2	27	8.6	37.9
1	-43	-5.1	-45.9

*SASC (1981).
†Mateer and DeLuisi (unpublished).

original comparison by 5%, but also removes most of the large anomalous departure seen in 1975. On the whole, the BUV ozone data appear to have changed by 15% during the 7-yr period.

Another type of comparison between coincident SBUV and Umkehr observations was given in an informal report by the Systems and Applied Sciences Corporation (SASC, 1981) BUV data processing team. Their comparison is shown in the second column in table 28. The data are from the SBUV and the Boulder Umkehr (UMK); SBUV is the reference for the difference. The third column shows a comparison between concurrent short and standard Umkehr measurements also made at Boulder (C. Mateer and J. DeLuisi, unpublished), but not necessarily during the time of the SBUV fly-by. By use of this comparison, the Umkehr-SBUV comparison was transformed into a short Umkehr-SBUV comparison, and an improvement is noted in layers 4-9 where agreement is now 4% or better. The improvement is most likely due to the use of better ozone absorption coefficients and ozone profile statistics in the short Umkehr inversion. No improvement is noted in layers 1-3 where the Umkehr is very insensitive to ozone, and in fact, the agreement is worse than that of the standard Umkehr. At this time the marked disagreement cannot be explained, but an investigation of the cause is planned. Before this is done, however, an attempt will be made to use coincident SBUV and short and standard Umkehr measurements to repeat the type of comparison done for fig. 52. The use of coincident data will give assurances that a time-dependent bias is not responsible for the present result.

These kinds of comparisons appear to hold promise as means for monitoring changes in BUV response to stratospheric ozone. It is extremely important that a BUV satellite be continuously checked for performance changes if the measurements are to be used to search for trends in upper-stratospheric ozone.

4.10 Cloud Chemistry and Radiation Experiment at Whiteface Mountain, N.Y.

4.10.1 Introduction

A summer experiment on Whiteface Mountain was organized by scientists from NOAA and from ASRC at Albany to investigate possible augmentation of cloud absorption of solar radiation caused by aerosol scavenging in the cloud. Cloud-droplet size spectra have been observed to be altered by aerosols from anthropogenic sources (Barrett et al., 1979). Thus, if these aerosols possess significant radiation absorption properties, then the solar radiation absorbed by the clouds is likely to be increased whether the aerosols are distributed in the cloud water or remain as aerosols interspersed among the cloud droplets.

The basic research strategy employed in the summer experiment was to (1) collect cloud water at the Whiteface Mountain ASRC facility and analyze the residue, after evaporation of the water, for optical absorption; (2) identify chemically the nonaqueous constituents of the cloud water; (3) characterize the optical properties of the free aerosols by collection and laboratory analysis, by measuring their size distribution, and by measuring their optical extinction properties using sunphotometry; (4) compute the optical properties of the modified cloud using Mie theory and the results of (1) and (3); and (5) estimate the excess absorption of solar radiation by the cloud, using radiative transfer calculations.

4.10.2 Preliminary Results

Preliminary results from the basic strategy are given in table 29, which partially summarizes the nature of the substances in the cloud water. Figure 53 shows the imaginary (or absorption term) of the complex refractive

Table 29.--An example of some characteristics of the cloud water sampled at Whiteface Mountain

Chemistry analysis*

F^-	Cl^-	NO_3^-	$SO_4^=$	Na^-	NH_4^+	K^+
1.06	2.8	0.5	2.4	1.9	0.3	3.3

Microscopical analysis

Biological	50%	
Mineral	35%	
Industrial	15%	(black, yellow, red)

SEM analysis

(1) Sulfate is an integral part of the cloud water.
(2) There is evidence of upwind industrial pollution.
(3) Naturally occurring organic aerosol makes identification of industrial or local pollution sources difficult during the summer.

*Ion chromatography (ppm), 26 June 1981.

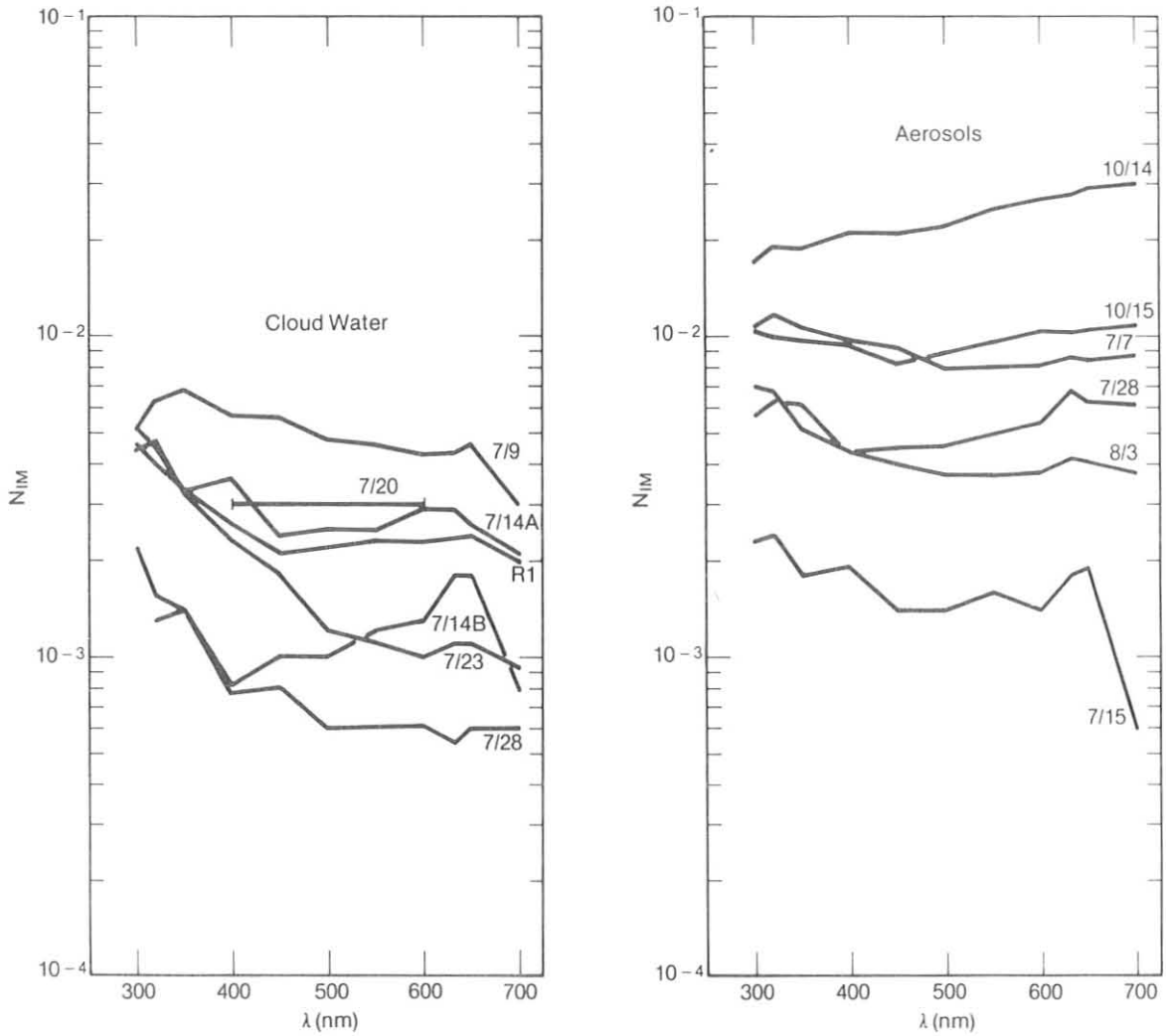

Figure 53.--Imaginary term N_{IM} of the complex refractive index of cloud water residue (left) and free aerosol (right). The real term is fixed at 1.5. R1 designates a rime ice sample (collection time unknown).

index N_{IM} of the substances extracted from cloud water (left figure) and the free aerosol (right figure) vs. wavelength. An N_{IM} of 0.01 is considered to be quite strong and approaches that found in an urban atmosphere. An apparent relationship between N_{IM} and cloud water pH (measured at Whiteface) seems quite real. An example of such a relationship is seen in fig. 54 in which N_{IM} data at 500 nm from fig. 53 have been plotted vs. pH. The horizontal bars represent the maximum and minimum of the pH values that constituted the average of a large number of readings. If anthropogenically derived aerosols are more strongly absorbing, very likely because of the presence of black carbon, then it is also likely that the pH decrease is due to anthropogenic sources.

Further confirmation of the relationship between absorption and pH is seen in fig. 55 where attenuation of light (or filter blackness) vs. hydrogen ion concentration is plotted. Note that the rainwater samples from Illinois are included in these data.

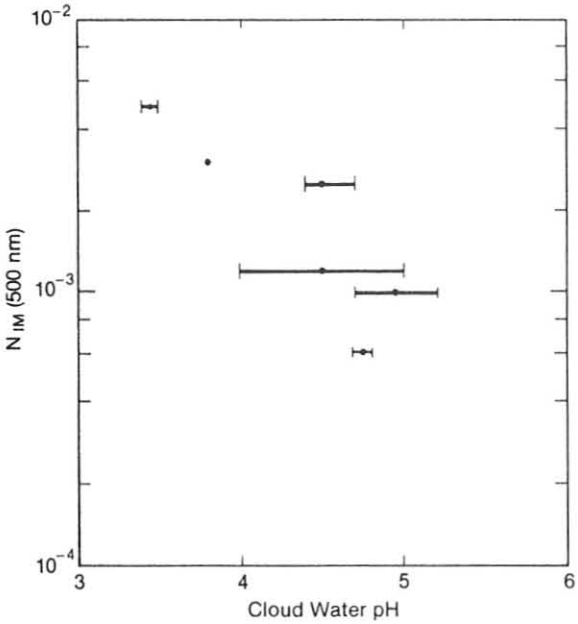

Figure 54.--A series of points that imply a relationship between N_{IM} (see fig. 53) and acidity (pH) of cloud water. Horizontal bars represent the maximum and minimum of the pH values that constituted the average of many readings.

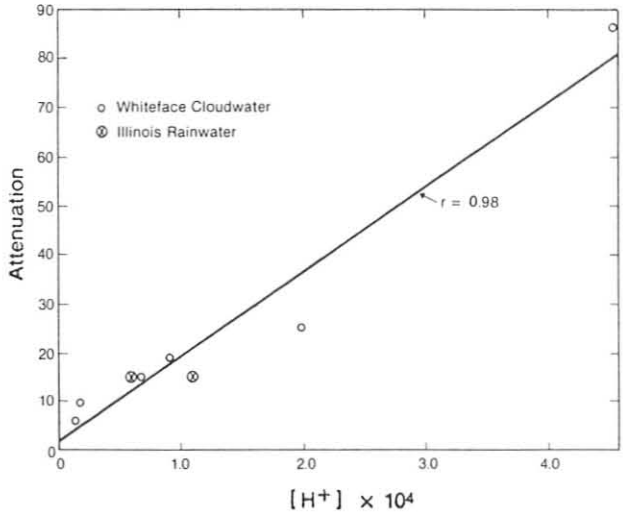

Figure 55.--A series of points that implies a relationship between absorptivity of cloud water residue and the hydrogen ion concentration of cloudwater. Correlation coefficient r is given (H. Rosen, personal communication).

Table 30.--Calculations* of cloud optical properties using cloud water residue data

	Case	Mass† (mg)	B_{ext}§ (cm^{-1})	W_0**
Droplet Mode				
	I	40	2.2805×10^{-4}	0.999974
	II	22	2.2805×10^{-4}	0.999987
	III	3	2.2805×10^{-4}	0.999996
Accumulation mode				
	-	-	6.355×10^{-7}	0.955
Combined mode				
	I	40	2.2864×10^{-4}	0.99985
	II	22	2.2864×10^{-4}	0.99986
	III	3	2.2864×10^{-4}	0.99987

*Calculations were performed by E. Barrett of ERL.
†Mass of residue per 2 ℓ of collected cloud water.
§B_{ext} = optical extinction.
**W_0 = albedo of single scatter.
NOTE: Index of refraction used in these calculations was N = 1.55 - 0.009i, as measured by E. Patterson of the Georgia Institute of Technology.

Table 31.--Calculated fractional absorption in a cloud*

Optical depth	Thickness	Absorption for $W_{\bar{0}} = 0.9999$	Absorption for $W_{\bar{0}} = 0.999$
8	0.35	0.0009	0.0081
16	0.7	0.0015	0.0148
32	1.4	0.0029	0.0272
64	2.8	0.0055	0.0467

*Initial input variables: G = 0.85 is the Henyey-Greenstein factor; $\theta_{\bar{0}} = 60°$ is the solar zenith angle; and $F\downarrow = 0.5$ is the value of the incident solar flux.

Typical size distribution measurements of the free aerosol and cloud droplets, made at Whiteface, were used to calculate the albedo of single scattering $W_{\bar{0}}$ shown in table 30. In the droplet and combined modes, Cases I, II, and III refer to the mass per unit volume of cloud water. B_{ext} is the extinction optical thickness.

The optical characteristics of free aerosols are given in table 30 under the heading "Accumulation mode," and the optical characteristics of the combined droplet and accumulation mode are given under the heading "Combined mode." A comparison between results for the droplet mode and the combined mode show an order of magnitude difference in $W_{\bar{0}}$.

The impact on the absorption of solar radiation in a cloud can be illustrated by a model calculation of fractional cloud absorption for two different values of $W_{\bar{0}}$ and four different optical thicknesses. Calculations were done by M. King of NASA, Goddard. His calculations are shown in table 31. In this table "G" stands for the Henyey-Greenstein or g factor, $\theta_{\bar{0}}$ is the solar zenith angle, and the incident flux $F\downarrow$ is 0.5 of the solar constant. The cloud optical depth is transformed into linear thickness using the calculated volume extinction given in table 30. The $W_{\bar{0}}$ values calculated from the Whiteface Mountain experiment are in the range used for the calculations in table 31, so it is believed that these results represent reasonable estimations of the increased solar radiation absorption in clouds caused by aerosols scavenged and released in cloud processes. However, there is no doubt that a greater amount of experimental work is needed to develop a clearer understanding of the range and variability of the cloud properties observed, and the reliability of the estimated cloud radiative properties.

The following were participants in the 1981 Whiteface Mountain experiment.

ERL

E. Barrett
B. Bodhaine
J. DeLuisi
E. Dutton
B. Mendonca
R. Pueschel
L. Stearns

SUNY

R. Castillo
R. Cheng

Other universities

T. Cahill
E. Patterson
H. Rosen

4.11 Calibration of a Solar Infrared Hygrometer

Five solar infrared hygrometers were acquired by GMCC in 1976-1977. Properly calibrated, these instruments accurately measure narrowband absorption of solar radiation by atmospheric water vapor, from which total vertical water vapor amounts can be inferred. Although a prototype instrument had been satisfactorily calibrated by means of a sophisticated theoretical approach and substantiated by high-altitude aircraft measurements, the instruments delivered to GMCC had no calibration. The prototype calibration was destroyed by an electrical malfunction before it could be transferred to the GMCC instrument. Lacking facilities to repeat the original prototype calibration, a semiempirical approach has been used in an effort to perform a reasonable calibration of the GMCC solar hygrometers.

The basic instrument consists of two narrowband interference filters with an optical arrangement such that the solar radiation passing through each filter is alternately allowed to fall on a single gallium arsenide detector. A background signal is subtracted from each filter channel signal by the use of a chopper wheel rotating at 30 Hz in front of the detectors. The resulting signal is demodulated, yielding two 0- to 10-V signals, each linearly proportional to the solar intensity in the respective band passes. The instrument optics are sealed against the weather and heated to a constant temperature above ambient temperature.

The principle of the instrument involves the measurement of the ratio of solar intensities in two nearby spectral bands, one (1.1344 μm) with strong water vapor absorption and the other (1.060 μm) with virtually no water vapor absorption. Then if all other of the attenuator's extinction ratios between bands are constant, the variability of the measured intensity ratio is due entirely to water vapor. This is expressed mathematically by the calibration equation, which is combined with the total water vapor inference expression as derived in the following.

The extinction of monochromatic electromagnetic radiation is expressed by Beer's Law:

$$I_\lambda = I_{\dot{0}\lambda}\, e^{-\tau_\lambda m} \quad , \tag{4}$$

where I_λ = spectral intensity as depleted by the medium, $I_{\dot{0}\lambda}$ = spectral intensity before entering the medium, τ_λ = optical parameters of the medium, and m = relative path length through the medium (air mass). This expression holds for atmospheric cases in narrow spectral intervals that only approximate monochromatic radiation, except where water vapor is a dominant absorber in the interval. An expression often given, equivalent to (4) but describing extinction due to atmospheric water vapor, is

$$I_\lambda = I_{\dot{0}\lambda}\, e^{-(\tau_w m)^n} \quad ,$$

where τ_w is vertical optical depth of water vapor and n is a variable depending on the particular band and bandwidth under consideration.

For any given spectral band in the atmosphere, the extinction of sunlight will be caused by several attenuators, and the cumulative effect is given by

$$I_\lambda = I_{\dot{0}\lambda} \cdot e^{-m\Sigma\tau_{\lambda_i}} \cdot e^{-(\tau_w m)^n} \quad .$$

Taking the ratio of two wavelength (λ_1, λ_2) bands, one containing H_2O and the other the same attenuators except H_2O, gives

$$\frac{I_{\lambda_1}}{I_{\lambda_2}} = \frac{I_{\bar{0}\lambda_1}}{I_{\bar{0}\lambda_2}} \frac{e^{-m\Sigma\tau_{\lambda_{1_i}}} e^{-(\tau_w m)^n}}{e^{-m\Sigma\tau_{\lambda_{2_i}}}} \quad . \tag{5}$$

Now considering the GMCC solar IR hygrometer with its linear-with-intensity voltage output and the assumed constant ratio between wavelengths of Rayleigh and aerosol optical depth, (5) becomes

$$\frac{V_1}{V_2} = \frac{V_{\bar{0}1}}{V_{\bar{0}2}} C' e^{-(\tau_w m)^n} \quad , \tag{6}$$

where V_1, V_2, $V_{\bar{0}1}$, and $V_{\bar{0}2}$ are voltages associated with I_{λ_1}, I_{λ_2}, $I_{\bar{0}\lambda_1}$, and $I_{\bar{0}\lambda_2}$, and C' is a constant

Assuming that the ratio of extraterrestial radiation at the two wavelengths is constant and taking the natural log of both sides of (6) gives

$$\ln\left(\frac{V_1}{V_2}\right) = \ln C - (\tau_w m)^n \quad ,$$

where C is a constant.

The vertical optical depth of water vapor can be expressed as

$$\tau_w = K P_{\bar{0}} \quad ,$$

where K is an absorption coefficient and $P_{\bar{0}}$ is the vertical amount of water vapor expressed as equivalent liquid amount. The pressure and temperature dependency of K will be discussed later. The resulting expression for total water vapor is then

$$P_{\bar{0}} = \frac{1}{K m}\left[\ln\left(\frac{V_2}{V_1}\right) + \ln C\right]^{1/n} \quad . \tag{7}$$

Several options are now possible to determine the constants K, C, and n. The straightforward approach used and reported here was to calculate C from filter transmission curves, detector spectral response, different channel operations, a common extraterrestrial solar spectrum, theoretical Rayleigh extinction, and typical aerosol spectral extinction. The constant C is equal to the output voltage ratio in the absence of any water vapor. The constants n and K were then determined by a least-squares fit to a form of (7) using data on several ideal days when V_2/V_1 was measured at various values of m (air mass), and $P_{\bar{0}}$ was determined from the NWS radiosondes. The constants determined for two GMCC IR hygrometers are given in table 32.

This calibration procedure contains many uncertainties, and the resulting constants have a limited water vapor range of applicability. The range of applicability for the constants K and n is determined by the range of water vapor amounts encountered during the calibration process, because the shape of the water vapor extinction curve changes as more individual absorption lines

Table 32.--Values of constants in eq. (7) for two GMCC IR hygrometers

IR hygrometer	K	C	n
No. 4	1.04	0.71	0.50
No. 1	1.20	1.02	0.51

become saturated. The GMCC hygrometers were calibrated on very dry, stable days (Boulder, Colo., in January) and the calibration data indicate a constant absorption curve shape as long as the total slant-path water vapor (m P_0) does not exceed about 2.0 cm. For the intended field use of these instruments at MLO and SPO, this range restriction presents no major problem. The uncertainties accumulate from almost every step of the calibration process, but the total absolute uncertainty is believed to be less than ±10% including possible error in the water vapor determined from the radiosonde. In an informal intercomparision with the WPL microwave water vapor meter, spanning several weeks, the net difference between the two measurements was less than 2% although some individual comparisons differed by as much as 20%-30%. The large individual measurement differences probably resulted from line-of-sight differences since the vertical-looking microwave instrument was located in Denver while the GMCC instrument was in Boulder, 26 mi apart. However, the slant path of the IR hygrometer is in the general direction of Denver.

The long-term stability of the IR hygrometers is uncertain at this time and can best be monitored by repeating the calibration process, although the number of days suitable for the calibration are very limited and instruments sent to the field have little opportunity for recalibration.

An additional complication in the water vapor measurement is the pressure and temperature dependency of the effective absorption coefficient K. Since no vertical resolution is possible with the IR hygrometer, K is taken as a constant. The error involved in doing this will depend on the deviation of actual water vapor profiles from those used during the calibration of the hygrometer. Ideally the hygrometer would be used at a location the same as where it was calibrated; this was not the case for the GMCC hygrometer. To somewhat crudely account for the change in elevation between Boulder and the field sites and to some extent the difference between the vertical vapor profiles, a pressure and temperature correction expression for water vapor scale height was used. The expression used here was essentially that suggested by Lacis and Hansen (1974) and used in LOWTRAN 5.0 (Kneizys et al., 1980), with the scale heights determined from radiosonde data. SPO scale heights were estimated from an exponential decrease with height.

Correcting for scale heights between the calibration location and the field sites results in actual water vapor amounts whereas correcting between the field site and the sea level pressure and temperature yields equivalent sea level absorber amounts. All data reported here will be actual amounts.

Table 33 gives the monthly averages for 6 months of total vertical water vapor measurements at MLO and several measurements at SPO. The comparison with the 20-yr average record at Hilo is given only for general comparison and

Table 33.--Monthly averages for 6 months of total vertical water vapor measurements at MLO and several measurements at SPO

Date	GMCC IR hygrometer (cm)	Hilo radiosonde 20-yr average (cm)
MLO		
Sep 1981	0.47	0.40
Oct	0.34	0.42
Nov	0.42	0.42
Dec	0.32	0.37
Jan 1982	0.30	0.37
Feb	0.22	0.33
SPO		
15 Jan 1982	0.13	--
5-10 Jan 1982	0.12	--
23-25 Jan 1982	0.07	--

is not directly comparable because the 20-yr record is compiled for all days and the IR hygrometer operates only on clear days. Another possible bias in comparing the Hilo radiosonde with MLO IR hygrometer measurements results from the time-of-day differences; the radiosonde flights were at 0200 and 1400 LST, and most IR hygrometer data were obtained in the time interval 0800-1000 LST.

There is large variability on many time scales in the MLO amounts, with the extremes ranging from 0.08 to >1.2 cm during a 6-mo period. A tripling of water vapor in a few minutes has also been recorded. The observed variability in the record is believed to be real since the short-term measurement precision is better than 0.005 cm. Discrete measurements at SPO, as opposed to continuous monitoring at MLO (courtesy of NCAR/High Altitude Observatory), have shown relatively little variability day to day.

4.12 Sunphotometer Intercomparison

Several sunphotometers of modern design were intercompared by means of actual atmospheric observations in Boulder over a period of 2 months in the fall of 1981. Twelve instruments of five different designs and manufacture were compared. The results indicate that current modern sunphotometers are capable of measuring spectral atmospheric optical depth to within ±1.5% of the values obtained by a reference instrument with which the sunphotometers were initially compared. This translates to a measurement precision, between instruments, in terms of aerosol optical depth of 0.005 (base e) units at 500 nm and ≅0.01 units at 380 nm. Details of the intercomparison are given in Dutton and DeLuisi (1982).

The instruments participating in the intercomparison were calibrated in two different ways. One calibration technique was the commonly used Langley

plot method that results in an independent calibration of each instrument. The other calibration procedure was to define a reference optical depth measurement to which all instruments would be calibrated, resulting in a dependent calibration. The second calibration technique is most practical for calibrating large numbers of instruments since atmospheric conditions adequate for good Langley calibration can be rare. However, in application the dependent calibration procedure requires the establishment of a high-integrity reference instrument or instruments. Lacking such a reference instrument, the consensus of the intercomparison was chosen as an arbitrary reference for comparison only.

The principle conclusion of the intercomparison was that the establishment of a high-accuracy standard sunphotometer would permit sufficient quality network measurements to monitor aerosol optical depths of the magnitude typically encountered in clean remote locations.

4.13 The Photovoltaic Power System at SMO

Work began on preparation of the photovoltaic power system specifications at SMO after GMCC was notified that funds were awarded by the Federal Photovoltaic Utilization Program of DOE in April 1980. The system as defined in the request is to provide 1 kW of continuous electrical power to the SMO observatory. J. Jordan and G. Herbert prepared the specifications that subsequently became part of the request for proposal (RFP). A source evaluation board (SEB) was selected and approved in November 1980. The RFP was reviewed by the board and subsequently issued in May 1981 (NOAA no. 34-81). The responses to the RFP were reviewed by the SEB in July. All proposals were found to be nonresponsive because of technical difficiencies or excessive cost estimates. The three main reasons for the excessive cost estimates were (1) the request that the vendors supply all the technical and manual labor for the transportation and installation of the photovoltaic arrays; (2) problems with the purchase, transportation, and housing of the batteries; and (3) the absence of any specific limits on the physical size of the photovoltaic array.

Studies of the variables that determine the size of the photovoltaic array began with assembling SMO global insolation measurements into a data base of hourly average values from January 1976 through December 1979. All measurements were made with pyranometers operated on horizontal surfaces on the roof of the GMCC station at Cape Matatula. J. Osborn, NOAA Corps, edited the data, prepared tables of the daily available global solar energy, and published the tables with the RFP. The solar energy at Cape Matatula is typical of that found on the windward side of tropical islands: relatively clear mornings and cloudy afternoons. The measurements do show the occurrence of prolonged periods of excessive cloudiness; typically, periods of a week occur one or two times per year. In the 4 years of the data set the longest such period was 13 days. To build a system that would carry the load without use of island power for this period would not be feasible. The effect of tilting the photovoltaic arrays was also evaluated by installing a pair of pyranometers on tiltable stands (fig. 56) and recording the data. One stand is at a fixed tilt of 14°, the latitude of the station, the other is changed monthly from -10° to 35°. The ratio of daily insolation on the tilted surface to the daily insolation on a horizontal surface was averaged by month (table 34). For slightly more than a year the maximum increase resulting from tilting is about 10% at 14° and 22% at 35°. Theoretical results (Jordan and

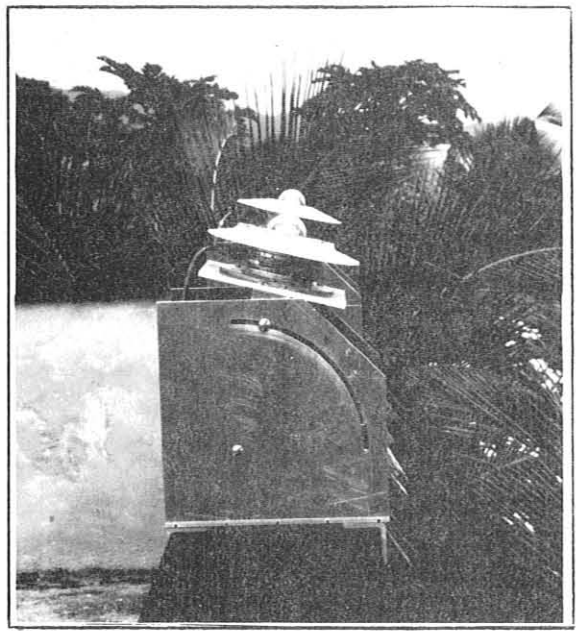

Figure 56.--Pyranometers on tilted stands on the roof of the SMO observatory.

Liu, 1977) tend to overpredict the enhancement. This is probably due to improper accounting for cloudiness.

The values provided in the response to the RFP were used in programming and operating a simple computer model to determine the overall performance of the system. Solar irradiance measurements were used as input to the model, a 1-kW load was assigned, and efficiency factors were used as specified in the proposals for individual components. The state of change of the batteries was computed and the charging cycle initiated at the specified level (usually 80% discharge). Battery life is directly related to the number of deep-discharge cycles. When the batteries reach the deep-discharge level they must be

Table 34.--Monthly averaged ratios of the daily insolation on a tilted surface to that on a horizontal surface

Month	14° tilt	14° tilt, Jordan and Liu*	Variable tilt
Jan	0.88	0.93	0.94
Feb	0.91	0.97	0.94
Mar	0.96	1.06	0.96
Apr	M	1.15	M
May	M	1.22	M
Jun	1.09	1.26	1.22
Jul	1.06	1.24	1.10
Aug	1.09	1.17	1.14
Sep	1.03	1.08	1.03
Oct	0.97	1.00	M
Nov	0.93	0.96	0.99
Dec	0.91	0.91	1.00

*Data extracted from Jordan and Liu (1977, fig. A-4).
Note: M = missing data.

recharged from island power or the system must be shut down to avoid damaging the batteries. The model, written by R. Clark of GMCC, also computes the number of hours the system is operated by solar power and the duration of fully charged periods. The results of such studies provided the limit guidelines needed for the second issue of the RFP.

The best information on photovoltaic batteries indicated that a reasonable life expectancy would be 8-10 years. The manufacturers specify the life in terms of 1,800 deep discharges but guarantee the unit for 800-1,000 deep discharges. Sizing criteria were selected that would yield approximately 100 deep discharges per year. Thus, the photovoltaic array was limited to a size that would produce 6,000 W of electrical energy at incident radiation of 1 kW m^{-2}. The capacity of the batteries was specified to carry the load of the system for not less than two consecutive sunless days. With such limits imposed in the second issue of the RFP (no. 54-81), issued in September 1981, the responses were, for the most part, technically acceptable and within the budget. The source evaluation board met in December 1981 and, after questioning the responders, agreed to make an award to Solarex Corp., Rockville, Md.

The photovoltaic array will be located on the southern end and along part of the eastern side of the observatory. The array will consist of 100 modules grouped in 5 subarrays, each approximately 15 m^2 in area. The total area of the array is therefore about 75 m^2. The subarrays will be positioned on tiltable stands (-10° to 35°) at a height of 3.7 m. The batteries will consist of 10 units to be wired in series and to be positioned along the south wall of the data room. The ventilation in this room will be increased to remove excessive hydrogen. The system controller, inverter, and battery charger will be located next to the batteries. GMCC staff will construct a monitoring system to measure the voltage on the direct current bus, the current at different points in the system, and the power delivered by the system. These measurements will be used in conjunction with the computer model to monitor the efficiency of the system as a function of time.

5. COOPERATIVE PROGRAMS

5.1 Ultraviolet Erythema Global Measuring Network

D. Berger
Skin and Cancer Hospital, Temple University
Philadelphia, PA 19140

A global network of meters recording the sunburning (erythema) effect of solar ultraviolet radiation has been providing data since 1973. The number of stations continues to increase; 30 stations now report regularly and 2 more stations are expected to start functioning next year.

The sunburning effect of ultraviolet radiation is proportional to a number of other effects that this most energetic part of the solar spectrum can produce in biota, such as DNA damage, human skin cancer, tobacco leaf spotting, reduced viability of shallow-laid fish eggs, and the induction of vitamin D formation.

A report based on results from 14 of the longest operating stations was published by Berger and Urbach (1982). A list of all stations appeared in the GMCC Summary Report for 1979 (Herbert, 1980, p. 100); two additional stations to be added to that list are La Jolla, Calif., online since April 1979, and Invercargill, New Zealand, in operation since July 1981. Data for this network are distributed by NOAA/ARL, 6010 Executive Blvd., Rockville, MD 20852.

5.2 NO_x Measurements at MLO

J. F. Noxon
Aeronomy Laboratory
NOAA/ERL, Boulder, CO 80303

Spectra of radiation emitted by the rising and setting sun have been measured at MLO to determine NO_x ($NO + NO_2$) in the free troposphere at ~3-km altitude (Noxon, 1981). Very low values were found for the mixing ratio (30 ± 10 pptv). Comparing these results with earlier measurements made by others at the sea surface in the mid-Pacific, one may infer that the source of the NO_x is almost certainly natural and must be located in the upper troposphere. However, some may also come from the stratosphere. Such low values for NO_x suggest that photochemical production of ozone is small in most of the remote marine lower troposphere.

NO_3 was also measured in both the troposphere and stratosphere at MLO using the moon as the light source (NO_3 is only present at night). The results show that stratospheric NO_3 behaves quite differently at low latitudes than at middle and high latitudes. At MLO the behavior is in agreement with the chemistry presently thought to govern nitrogen oxides in the stratosphere; at higher latitudes the behavior is not as expected, NO_3 being almost always far less than predicted.

The measurements of tropospheric NO_3 at MLO show that it is efficiently scavenged by a species as yet unknown. It appears that scavenging proceeds at about the same rate as it does in clean continental air. The significance of this scavenging to tropospheric chemistry remains unclear; it is not yet known whether or not the scavenging process corresponds to a sink for odd nitrogen. This program of measurements is expected to continue.

5.3 On the Relationship Between Surface Air Temperature and Concentration of Pollution-Derived Elements at BRW

W. E. Raatz
Geophysical Institute, University of Alaska
Fairbanks, AK 99708

Pronounced, repeatable seasonal variations of noncrustal vanadium, noncrustal manganese, and nonmarine sulfate as well as fluctuations on shorter time scales (days to weeks) have been observed (Rahn and McCaffrey, 1980; DeLuisi, 1981, p. 113). The research intention of this study is to explain these variations in terms of the meteorological conditions both at the sampling site and along the different transport pathways from the suspected source areas in midlatitudes. Here, we discuss the relationship between air temperature at BRW and noncrustal (pollution-derived) vanadium concentrations.

On the basis of data for four winters (October-April), the correlation coefficient of monthly averaged noncrustal vanadium concentrations and temperature was calculated to be $r = -0.8$. Cold temperatures are associated with high concentrations of noncrustal vanadium. Highest concentrations of noncrustal vanadium are usually found during March; a secondary maximum appears to be present during December (Rahn and McCaffrey, 1980). February is the coldest month at BRW, on the basis of a long-term average, but conditions can differ significantly during individual years. Wilson (1969) noted that temperature variations in the Arctic during winter conditions are mainly determined by fluctuations of the large-scale circulation patterns and associated storm tracks, and that changes from one persistent circulation pattern to another can be rapid. Thus, monthly mean values can be misleading, and it would be of interest to see how noncrustal vanadium concentrations and temperature correlate on time scales shorter than 1 month. In fact, correlation between daily noncrustal vanadium and daily mean temperature for December 1979-April 1980 provided a correlation coefficient of only $r = -0.1$. Thus, they correlate on long seasonal time scales, but the correlation disappears when the time series contains shorter frequencies.

To understand the breakdown of the correlation between noncrustal vanadium and temperature on short time scales, note that during March 1978 several injections of pollution aerosol had originated in Europe (based on the Mn/V ratio, Rahn, 1981), but arrived at BRW in air masses with differing temperatures as a result of modifications of the air masses associated with different paths and transport times. Thus, air masses arriving at BRW were similar according to their chemical characteristics but different according to their temperatures. Apparently, on short time scales, the variation of noncrustal vanadium is source related, whereas the variation in temperature is more dependent on transport pathways. Thus, an air mass can undergo considerable meteorological modification, yet still retain a memory of its earlier passage over pollution sources.

Spectral analysis of the daily temperature time series revealed a characteristic period of 18-20 days. The noncrustal vanadium also showed a period of 18-20 days, but in addition, there was a second period of 7 days, not seen in the temperature data. The characteristic period of 18-20 days is assumed to be associated with large-scale circulation patterns (McGuirk and Reiter, 1976). The causes for the 7-day period found in the noncrustal vanadium time series have not been confirmed. It is likely to be related to mesoscale synoptic systems traveling in the Arctic; if so, the chemical fingerprint of traveling air masses is preserved longer than the meteorological one.

5.4 Atmospheric ^{210}Pb at BRW and MLO

H. W. Feely and C. G. Sanderson
Environmental Measurements Laboratory
U.S. Department of Energy, New York, NY 10014

High-volume filter samplers are operated for EML at each of the four GMCC observatories. These are part of a network of about 20 samplers that are operated for EML, mainly in the Western Hemisphere. Monthly composites of the filter samples are analyzed routinely by gamma spectrometry for ^{7}Be, ^{95}ZR, ^{137}Cs, and ^{144}Ce. During mid-1974 to mid-1976 these filters were also routinely analyzed radiochemically for several radionuclides, including ^{210}Pb. It was noted that the concentration of ^{210}Pb in air appeared to reach a maximum in the winter at BRW and in the spring at MLO. Subsequently K. Rahn of URI pointed out that the high ^{210}Pb concentrations at BRW appeared to coincide with the influx of polluted air from midlatitudes, which produced the wintertime Arctic haze layer. He suggested that ^{222}Rn emitted from the deserts of Asia might be the source of this ^{210}Pb. Similarly, the ^{210}Pb maximum in air at MLO coincides with the arrival of dust from the Asian continent during the spring.

To verify the apparent seasonal variations in ^{210}Pb concentrations, samples collected during 1977, 1980, and 1981 at BRW and during 1980 and 1981 at MLO have now been analyzed for ^{210}Pb using gamma spectrometry. As shown in fig. 57 the new data confirm the seasonal variations shown by the older data. Beginning in December 1981 some quasi-weekly samples from BRW and MLO are

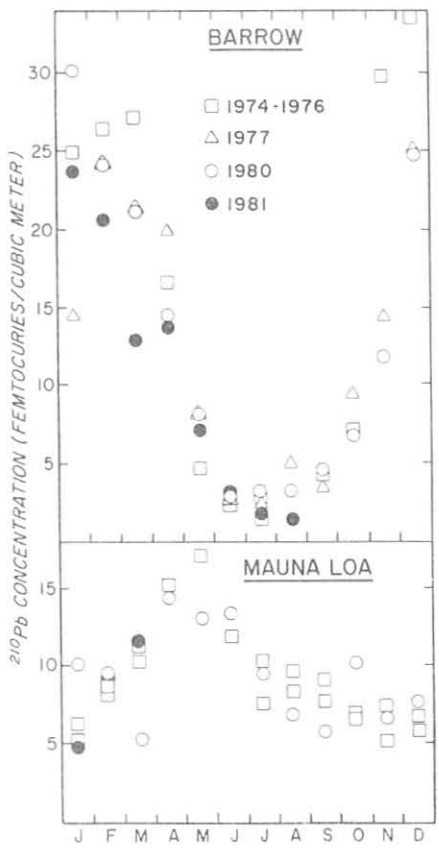

Figure 57.--Monthly concentrations of ^{210}Pb in surface air at BRW (top) and MLO (bottom).

being analyzed for ^{210}Pb by gamma spectrometry to provide finer resolution of the times of arrival of high concentrations of ^{210}Pb at these stations.

5.5 Air Chemistry Monitoring at Palmer Station

E. Robinson and W. L. Bamesberger
Air Pollution Research Section, College of Engineering
Washington State University, Pullman, WA 99164

The objectives of this research program are to measure continuously the trace chemical constituents of the atmosphere at Palmer Station, Antarctica, and to relate findings to meteorological conditions. The meteorological correlations will be sought on the basis of regional synoptic weather patterns and more general seasonal meteorological conditions. The air sampling facility was named the Anvers Island Air Chemistry Facility at the station dedication on 16 January 1982 by F. Williamson. The Palmer air chemistry station has been equipped to measure on a regular or continuous basis the trace atmospheric parameters listed in table 35. The frequency of measurement and the methods used are also listed.

The air sampling facility is a separate building with a 10- × 14-ft nominal floor space plus a 4- × 4-ft double-door entry vestibule for wind and weather protection. The station was prefabricated and then erected in a preliminary fashion at WSU at which time the sampling instruments were set up and checked. The air chemistry station is located east of the main Palmer Station

Table 35.--Trace atmospheric parameters and methods of measurement used at the Anvers Island Air Chemistry Facility*

Component	Frequency	Method
Ozone (O_3)	Continuous	UV photometer: Dasibi
Methane (CH_4)	1 h^{-1}	Automatic gas chromatograph: Carle Model 211
Carbon dioxide (CO_2)	1 h^{-1}	
Carbon monoxide (CO)	1 h^{-1}	
CCl_3F (CFC-11)	1 h^{-1}	Automatic dual-channel gas chromatograph: Hewlett-Packard Model 5880
CCl_2F_2 (CFC-12)	1 h^{-1}	
Carbon tetrachloride (CCl_4)	1 h^{-1}	
Methylchloroform (CH_3CCl_3)	1 h^{-1}	
Nitrous oxide (N_2O)	1 h^{-1}	
Aitken nuclei	Continuous	Expansion-type photometric system: Environment One

*The designation Anvers Island Air Chemistry Facility was given to the Palmer Station facility at its dedication 16 January 1982.

building complex, about 150 ft east of the old helicopter pad. Power for instrument operation and heat comes from the Palmer generating plant through a land line. A 5-cm-diameter stainless steel air inlet stack extending about 3 m above the building and leading to a connecting manifold inside is flushed by a small blower to provide a clean-air source for the sampling instruments.

The system including the computer-controlled data system was fully operational on 15 February 1982. All instrument outputs are recorded by a Hewlett-Packard 85 data system that also provides the cyclic control signals for the gas chromatographs. Strip charts provide backup for the HP 85 computer system. The instruments are standardized against gas mixtures that were calibrated against known standards prior to shipment to Palmer. Long-term standards are maintained at WSU. The CO_2 data will be standardized through cross-checks with the GMCC program. Weather data will be included in the data file by manually transcribing the observations from the Palmer station records. Recorded wind data and the response of the CNC will be used to identify periods when emanations from the Palmer activities may be affecting the sampling results. Available wind records indicate that flow from the west, which would result in contamination by effluents from the main station, is not a predominant wind direction.

The Anvers Island Chemistry Facility is expected to operate for a period of 4-5 years. Measurements made at the facility can be expanded as new instruments adaptable to the rugged Palmer environment and low background levels become available. The sampling results are expected to complement GMCC air sampling data collected at SPO and SMO, as well as data gathered at the Australian background station at Cape Grim, Tasmania. The particular interest of the WSU program is the interaction between air chemistry patterns and synoptic weather situations. Personnel at the air chemistry facility expose one pair of flasks each week for subsequent CO_2 analysis by GMCC. The facility can also provide support for other research investigators interested in air chemistry and related studies.

Acknowledgment

This research was supported by NSF under grant no. DDPP-8005797.

5.6 SEAREX Atmospheric Chemistry Studies at SMO

B. J. Ray and R. A. Duce
Graduate School of Oceanography, University of Rhode Island
Kingston, RI 02881

5.6.1 The SEAREX Program

SEAREX, supported by NSF, is a coordinated multi-institutional cooperative research program involving 11 laboratories investigating the atmospheric transport of both anthropogenic and natural trace substances to marine areas. The objectives of this program are (1) the quantitative measurement of the Pacific Ocean air-sea exchange of selected heavy metals and other trace elements, soil dust, ^{210}Pb and ^{210}Po, sulfate, nitrate, particulate organic carbon, and organic compounds, primarily PCB, DDT, aliphatic hydrocarbons, phthalate plasticizers, fatty acids, polycylic alcohols, and low-molecular-weight ketones and aldehydes; (2) the identification of the sources of these

substances in the marine atmosphere over the Pacific Ocean; and (3) the identification of mechanisms of exchange of these substances across the sea-air interface.

Since more than 90% of global atmospheric pollutants are injected into the Northern Hemisphere and since the tropospheric residence times of atmospheric particles are relatively short (days to 12 weeks) compared with relatively long (6 months to 2 years) tropospheric mixing times between the Northern and Southern Hemispheres (Junge, 1963; Duce et al., 1974; Newell et al., 1974), significant differences may be observed for anthropogenic substances present on atmospheric particles and certain trace gases at remote areas in the two hemispheres. Therefore, major differences in atmospheric concentration or deposition at these sites may be related to anthropogenic sources. Islands chosen as atmospheric sampling locations must necessarily be thousands of miles from continents and in strong trade wind or westerly regimes, thereby exhibiting nearly ideal atmospheric conditions. In addition they should be free of large sources of local anthropogenic inputs. SEAREX has chosen four regions of the Pacific that conform to these criteria. Experiments have or will be conducted on (1) Bokandretok Island, Enewetak Atoll, Marshall Islands (Northern Hemisphere trades, April-May and July-August 1979); (2) Cape Matatula, Tutuila Island, American Samoa (Southern Hemisphere trades, January-February and July-August 1981); (3) Ninety Mile Beach, North Island, New Zealand (Southern Hemisphere westerlies, June-August 1983); and (4) a cruise track north of the Hawaiian Islands at about 40°-50° latitude (Northern Hemisphere westerlies, July-August 1985). See DeLuisi (1981, pp. 116-117).

In April 1980 atmospheric tracer studies using sulfur hexafluoride (SF_6) were carried out at SMO to investigate the possibility of contamination due to eddying effects around the local topography and due to the small island of Aunu'u, as well as the passage of ships (Reible et al., 1982). Results of these studies were reported in DeLuisi (1981, pp. 118-121).

As a result of these preliminary studies, two aluminum-scaffold walk-up towers were erected on the eastward edge of the tip of Cape Matatula. An 18-m walk-up tower was used for the collection of all the atmospheric samples as well as for organic and nutrient rain collections. A 13-m walk-up tower was used for the collection of trace-element rain samples as well as for trace-element and organic dry-deposition samples. In addition to the towers, several buildings were erected at the site. The existing building erected at the base of the air tower in 1976 by URI was used for monitoring the meteorological and electronic status of the experiments. New buildings were constructed to house the organic and trace-element laboratories as well as to provide space for recreation, storage, and protection of the electrical transformers. An additional modular building was positioned at the top of the stairs to house a laboratory for analysis of pH, conductivity, and nutrients in rain. The construction phase was completed in August 1980.

SEAREX personnel returned in December 1980 to prepare for the experimental phase. Meteorological equipment for monitoring wind speed and direction, CN concentration, relative humidity, and rainfall were installed on the atmospheric sampling tower. Data from these sensors were fed into a control system that turned the air samplers on when the winds were from a preset oceanic sector (0°-145°) and CN counts were low, thus avoiding local island contamination effects. The site was manned 24 h day^{-1} during the experiment. The meteorological data were stored in a microcomputer that also monitored the

operational status of the various sampling systems. A Furuno weather radar was invaluable in predicting the onset of precipitation, especially at night, and the approach of vessels. Sampling on the tower was stopped when ships passed through the Clean Air Sector.

As many as 36 different sampling systems were operating on the tower for the collection of trace elements, sea salt, organic substances, and nutrients. At any time each research group could elect to sample in any or all of three different modes: (1) ISS (inside selected sector)--sampling occurring in the clean air sector; (2) OSS (outside selected sector)--sampling occurring from the island (local contamination) direction and/or conditions of high CN counts; and (3) manual--sampling occurring from all wind directions and irrespective of CN counts. Rain was sampled on an event basis. Frequently as many as six different precipitation samplers were in use simultaneously. To avoid contamination of the samples, great care was taken in the fabrication, preparation, and use of both the precipitation and atmospheric samplers and in the analytical procedures. Numerous sampling and handling blanks were collected and processed simultaneously with the samples as a further assessment of potential contamination. Samplers were also operated at ground level to investigate local vegetation and soil sources of contamination for organics and trace elements.

The sampling periods at SMO were January-February and July-August 1981, the local wet and dry seasons. During the first period rainfall was 36.8 cm, whereas during the second period it dropped to 11.2 cm. In addition to the Cape Matatula work, sea water samples were collected, about 4 mi offshore from a U.S. Coast Guard ship, for chemical analysis. Sixteen scientists participated in each of the SEAREX Samoa experiments.

5.6.2 Analytical Results

Although many analyses are still in progress, some preliminary data are available on the chemical composition of the aerosol, trace gas, and precipitation samples collected at SMO.

Rain pH and Major Ion Measurements

Precipitation measurements were made by the URI during both experiments to determine the major ion content and pH of Samoan rain. Collection of the samples was made in a carefully cleaned polyethylene rain sampler. As soon as possible after collection, pH was measured, and within ~72 hours of collection, Na^+, Cl^-, NO_3^-, $SO_4^=$, NH_4^+, NO_2^-, F^-, and $PO_4^\equiv$ were measured using a Dionex model 16 ion chromatograph. The rain was slightly acidic relative to an equilibrium solution of distilled water and atmospheric CO_2. For rain samples below $0.01^o/_{oo}$ salinity the mean pH was 5.52 (range: 5.33-5.98). For rain samples with salinity higher than $0.01^o/_{oo}$, the pH was slightly higher, with a mean of 5.80 (range: 5.53-6.57). The average NO_3^- concentration was 0.2 $\mu eq\ kg^{-1}$, and the non-seasalt (or excess) sulfate from

$$(SO_4^=)_{excess} = (SO_4^=)_{total} - (Na^+) \times (SO_4^=/Na^+)_{seawater}$$

was 1.5 $\mu eq\ kg^{-1}$. Model calculations indicated that this nitrate and sulfate, if present as the strong acids HNO_3 and H_2SO_4, could lower the pH to the values observed (Pszenny et al., 1982). The concentrations of other anions in

the rain were found to be $NH_4^+ \leq 20$ μg ℓ^{-1}; $NO_3^- \leq 5$ μg ℓ^{-1}; $F^- \leq 5$ μg ℓ^{-1}; and $PO_4^{\equiv} \leq 1$ μg ℓ^{-1} (Pszenny and Duce, 1981). Alkali and alkaline earth metal analyses are still in progress.

Chlorinated Hydrocarbons

Investigators from Texas A & M University have analyzed the SMO samples for heavy chlorinated hydrocarbons. They found concentrations to be 210 times lower at SMO than at the Northern Hemisphere sampling site at Enewetak. They found about 99% of the chlorinated hydrocarbons were present in the vapor phase with ≤1% in the particulate fraction. The mean concentrations observed were pentachlorobenzene, ~9 pg m^{-3}; hexachlorobenzene, 55 pg m^{-3}; hexachlorocyclohexane, 30 pg m^{-3}; lindane (dry season), 1.5 pg m^{-3}; PCB, 12 pg m^{-3}; ΣDDT (dry season), 1.5 pg m^{-3}; dieldrin (dry season), 2 pg m^{-3}; and chlordane (dry season), <1 pg m^{-3} (Giam and Atlas, 1982). These values are similar to values found by these investigators in the atmosphere over the upwelling waters off the coast of Peru. Rain concentrations of these substances at SMO were approximately an order of magnitude less than in Enewetak, but similar washout factors were observed. Concentrations of some of these substances in rain at SMO were hexachlorocyclohexane, 390 pg ℓ^{-1}; lindane, 33 pg ℓ^{-1}; PCB (1254), ≤200 pg ℓ^{-1}; ΣDDT, 17 pg ℓ^{-1}; dieldrin, <30 pg ℓ^{-1}; and chlordane, <30 pg ℓ^{-1} (Giam and Atlas, 1982).

During the wet season, oceanic air from the Clean Air Sector was found to have ~0.01 ng m^{-3} DDT whereas air that had passed over Samoa contained much higher DDT levels, ~1 ng m^{-3}, a concentration higher than that found at a sampling site in College Station, Tex. Similarly, the wet-season oceanic air was found to contain the (ΣC_{15}-C_{28}) n-alkanes at a mean total concentration of 3.9 ng m^{-3} while local island air averaged 28 ng m^{-3} (Giam and Atlas, 1981). These examples illustrate the potential problems of local contamination unless extreme care is taken during sample collection.

Particulate Trace Elements and Salt

Duce et al. (1982) have completed some analyses for trace elements in the aerosol samples from SMO. The concentrations for some elements are among the lowest ever reported near the Earth's surface. The preliminary concentrations are aluminum, 0.2-0.5 ng m^{-3}; iron, 0.15-0.22 ng m^{-3}; lead, 0.02-0.03 ng m^{-3}; selenium, 0.05-0.1 ng m^{-3}; dust, 2-7 ng m^{-3}; and sea salt, 6-12 μg m^{-3}.

On the basis of the analyses completed to date, the trace metals have similar concentrations during both sampling periods. Great care was taken to avoid contamination during the collection and analysis of these samples. Filters and filter holders as well as sample storage bags were all polyethylene and were acid-cleaned. A large number of handling and tower blanks were processed with all the samples, and all sample handling occurred in a clean room or clean bench. All personnel wore clean-room garb and gloves while handling the samples both on the tower and in the laboratory. The concentrations observed at SMO for many trace elements were 310 times lower than Northern Hemisphere concentrations observed by SEAREX at Enewetak.

Lead analysis of samples collected by personnel from URI and California Institute of Technology resulted in similar concentrations. The samples were

collected independently and utilized different collection and analytical procedures. For the January-February experiment, Patterson and Settle (1981, 1982) report rain concentrations for lead of 9-13 ng kg^{-1}, lead dry-deposition rates of 2.4 ng cm^{-2} yr^{-1}, aerosol concentrations of 0.04 ng m^{-3}, and surface seawater concentrations of 3.5 ng kg^{-1}. Dry-season measurements are still in progress.

A comparison of the atmospheric concentration of several trace elements was made between samples collected from the oceanic clean air sector (ISS) and those from OSS, i.e., susceptible to local island contamination (Duce et al., 1982). A comparison of two sample sets is shown in table 36.

Table 36.--Comparison of ISS vs. OSS trace element concentrations at SMO

Collection period (1981)	Trace Element Concentration				
	Al (ng m^{-3})	Fe (ng m^{-3})	Pb (ng m^{-3})	Se (ng m^{-3})	Na (μg m^{-3})
16 Jan-8 Feb					
ISS	0.25 ± 0.05	0.15 ± 0.04	0.020 ± 0.008	0.058 ± 0.008	1.7 ± 0.2
OSS*	1.3 ± 0.2	1.6 ± 0.3	0.100 ± 0.030	0.073 ± 0.009	5.0 ± 0.5
9 Feb-25 Feb					
ISS	<0.5	0.22 ± 0.13	0.025 ± 0.010	0.070 ± 0.010	2.4 ± 0.3
OSS*	4.9 ± 0.5	5.1 ± 0.6	0.110 ± 0.020	0.093 ± 0.010	6.0 ± 1.0

*Local contamination is clearly apparent for Al, Fe, Pb, and Na under OSS conditions.

Measurements by Yale University of ^{210}Pb in the aerosol indicate that oceanic (ISS) air contained 1.6-2.1 dpm $(10^3\ m^3)^{-1}$ while island air (OSS) contained 3.5 dpm $(10^3\ m^3)^{-1}$ for the January-February samples. Turekian et al. (1982) suggest that a local island source for that much ^{210}Pb is unlikely and postulate that the excess may come from the intrusion of high ^{210}Pb air from above the trade wind inversion.

Additional analyses are still in progress for the trace gas, aerosol, precipitation, dry-deposition, and sea water samples collected at SMO in 1981.

Upon completion of the SEAREX experiment at the end of August 1981, the SEAREX sampling towers were removed from the Cape Matatula site and forwarded to New Zealand for the next SEAREX experiment. Sampling gear and meteorological sensors were returned to the United States for refurbishing. One small wooden building was removed from the site, but other buildings, which were in good condition, were left at SMO. A 9-m tower for use by GMCC was erected on the site of the atmospheric sampling tower.

Acknowledgment

SEAREX personnel wish to express their appreciation to the GMCC staff for their support and assistance. In particular we wish to thank the personnel of the GMCC SMO station: R. Williams, E. Peau, and especially the Station Chief, D. Nelson, whose continued patience, cooperation, and assistance guaranteed the successful completion of the SEAREX experiments.

5.7 Atmospheric Trace Gases and Arctic Haze at BRW

R. A. Rasmussen and M. A. K. Khalil
Oregon Graduate Center
Beaverton, OR 97006

For several decades a winter haze has appeared in the Arctic, thousands of miles from the nearest area of dense human population or major industrial activity. Yet there is considerable evidence that this submicron-sized haze aerosol consisting of sulfate, soot, and organics results from human activities (Rahn and McCaffrey, 1980; Weschler, 1981; Rosen et al., 1981). The small ratios of primary to secondary components, the presence of combustion-derived soot and vanadium, and the presence of excessive amounts of anthropogenic gases all attest to the distant origins of Arctic haze (Rosen et al., 1981; Rahn and Heidam, 1981; Ottar, 1981; Husar and Patterson, 1979; Rahn and McCaffrey, 1980; Shaw, 1981; Khalil and Rasmussen, 1982). Although current knowledge favors Eurasia as the dominant source, significant contributions from other industrialized and populated areas, including the United States, cannot be ruled out (Rahn, 1981c; Barrie et al., 1981; Reiter, 1981). Except for a consensus that the presence of soot can heat the lower atmosphere of the Arctic, the possible environmental effects of continued or increased Arctic air pollution have yet to be worked out. See also Borys and Rahn (1981), Rahn (1981a), Rahn and Heidam (1981), and Rosen et al. (1981).

It is reasonable that many exotic trace gases that are produced at the same midlatitude regions of the Northern Hemisphere as the precursors of Arctic haze will also be transported to the Arctic. Such inert gaseous tracers can be used to identify the origins of Arctic haze in much the same way as the ratios of elemental tracers (Rahn, 1981b).

In this paper data are reported on eight potential anthropogenic gaseous tracers of Arctic haze, namely CFC-11 (CCl_3F), CFC-12 (CCl_2F_2), CFC-22 ($CHClF_2$), methyl chloroform (CH_3CCl_3), perchloroethylene (C_2Cl_4), trichloroethylene (C_2HCl_3), carbon monoxide (CO), and methyl chloride (CH_3Cl). The criteria for a gas to be a tracer of Arctic pollution are discussed, and finally conclusions that can be drawn from the trace gas studies are reviewed. Further details of most topics discussed here are presented in the paper of Khalil and Rasmussen (1982).

5.7.1 Data and Analysis

Since August 1980 samples of Arctic air have been collected by GMCC at BRW. Each week three samples are collected, one immediately after the other, in specially prepared, internally SUMMA-polished, stainless steel 0.8-ℓ flasks. An ultraclean Metal Bellows MB-158 pump is used to fill the flasks.

Table 37.--BRW monthly averaged concentrations of anthropogenic halocarbons, and CH_3Cl and CO

Month	$CHClF_2$	CCl_2F_2	CCl_3F	CH_3CCl_3	C_2Cl_4	C_2HCl_3	CH_3Cl	CO
1980								
8	65 (4)	321 (12)	192 (5)	155 (4)	--	--	545 (51)	96 (5)
9	66 (1)	327 (4)	192 (4)	155 (3)	--	--	542 (40)	107 (5)
10	66 (1)	331 (3)	194 (2)	159 (3)	--	--	542 (40)	96 (11)
11	68 (2)	332 (1)	195 (1)	162 (5)	--	--	561 (13)	113 (11)
12	71 (6)	336 (4)	195 (4)	171 (18)	--	--	581 (11)	153 (21)
1981								
1	81 (3)	334 (3)	193 (2)	185 (17)	--	--	627 (34)	149 (18)
2	69 (1)	337 (5)	147 (8)	166 (6)	145 (6)	51 (-)	608 (15)	174 (27)
3	67 (2)	333 (4)	198 (1)	167 (2)	106 (7)	15 (14)	623 (15)	157 (10)
4	69 (1)	331 (5)	199 (1)	166 (2)	104 (8)	12 (9)	623 (7)	160 (13)
5	69 (1)	336 (1)	200 (1)	167 (2)	74 (13)	9 (-)	639 (21)	146 (12)
6	69 (1)	335 (6)	200 (2)	165 (4)	74 (3)	6 (-)	621 (38)	106 (12)
7	69 (2)	337 (6)	200 (2)	162 (1)	62 (3)	4 (2)	565 (33)	78 (6)
8	70 (1)	340 (2)	199 (2)	162 (3)	62 (3)	8 (2)	541 (28)	70 (9)
9	71 (1)	338 (4)	198 (1)	168 (6)	56 (3)	6 (3)	506 (40)	83 (4)
10	71 (4)	345 (3)	197 (1)	166 (2)	75 (-)	11 (-)	536 (14)	107 (9)
11	73 (14)	348 (4)	200 (3)	189 (71)	--	--	587 (0)	123 (5)
12	79 (10)	349 (1)	204 (1)	182 (25)	106 (20)	34 (20)	587 (10)	116 (27)
1982								
1	75 (3)	350 (3)	205 (1)	181 (16)	111 (10)	31 (9)	583 (5)	146 (78)
2	77 (1)	354 (2)	208 (3)	176 (9)	120 (8)	37 (4)	646 (-)	183 (8)
3	77 (-)	354 (-)	205 (-)	177 (-)	--	--	--	--

Note: Concentrations are in pptv except CO, which are in ppbv. ( ) = 90% confidence limits based on the t-statistic.

This equipment was designed and supplied by OGC. The samples are sent by air to OGC where they are analyzed, usually within a week after being collected. Well-established gas chromatography techniques are used for the analyses as described in earlier papers (Rasmussen and Khalil, 1980; Rasmussen et al., 1982). Each flask is analyzed twice, thus providing six determinations of each trace gas every week. In related laboratory studies it has been established that the measured trace gases are inert in the sampling flasks for periods of many months. The precision of analysis of the halocarbons is <1% and for other gases, <5%. In all, the results of analyzing about 240 samples are reported here, constituting about 80 different sets of samples and spanning over 1½ years.

As discussed earlier, the concentrations of six anthropogenic halocarbons, of CO, and of CH_3Cl were higher during winter than in other seasons. Their monthly averaged concentrations are listed in table 37 along with 90% confidence limits of the means.

The data for CFC-11, -12, and -22, and for CH_3CCl_3 were analyzed by first subtracting the annual trends of atmospheric concentrations according to the following formula:

$$C_{ijk*} = C_{ijk} - bt_{ijk} ,$$

where C = concentration (pptv); ijk is a time index with i = week (1, 2, 3, 4), j = month (1, ... , 12), and k = year (1, 2, 3); b is the slope of the annual trend; and t is time. For example, t_{111} is August 1980, when data were first obtained. These monthly averages with the trend subtracted were used to construct fig. 58, which shows higher concentrations of these gases in winter than in other seasons. After the trend was subtracted, data for the same month but different years were pooled together by forming the average $C_{j*} = (1/N) \Sigma_{ik} C_{ijk*}$, where N is the number of data points for that month. These data were analyzed statistically, and the results were reported in detail by Khalil and Rasmussen (1982). The largest difference between such monthly means (δ^*) is given in table 38 along with other calculations based on the data.

The cases of CH_3Cl and CO are further complicated by natural seasonal cycles in their concentrations. Still, when the concentrations found at BRW were compared with extensive measurements made at Cape Meares, Ore. (45°N), it turned out that large excesses of these gases were present at the Arctic site only during winter. These tracers are important because they are released from specific combustion processes and could therefore aid in identifying the origins of Arctic air masses when the haze is present (Rasmussen et al., 1980; Crutzen et al., 1979; Rasmussen et al., 1982; Khalil and Rasmussen, 1981).

Table 38.--Comparison of the highest and lowest monthly concentrations of the Arctic haze tracers

Gas	Months of conc.		C_{max} ($\pm \delta C_{max}$)	C_{min} ($\pm \delta C_{min}$)	δ^* ($\pm \delta\delta^*$)	δ^* ($\pm \delta\delta^*$) (%)
	Max.	Min.				
$CHClF_2$ (pptv)	Jan	Jul	62.5 (± 3.9)	55.3 (± 0.9)	7.2 (± 3.9)	13.0 (± 7)
CH_3CCl_3 (pptv)	Jan	Jul	172.1 (± 11.2)	149.7 (± 1.0)	22.4 (± 11.2)	15.0 (± 7)
C_2Cl_4 (pptv)	Feb	Sep	128.0 (± 11)	56.0 (± 3)	72.0 (± 11)	129.0 (± 20)
C_2HCl_3 (pptv)	Mar	Jul	40.0 (± 7)	4.0 (± 2.5)	34.0 (± 7)	850.0 (± 480)
CCl_2F_2 (pptv)	Dec	Jun	326.7 (± 1.7)	318.7 (± 4.6)	8.0 (± 4.7)	2.5 (± 1)
CCl_3F (pptv)	Feb	Jul	202.6 (± 3.4)	192.3 (± 2.1)	10.3 (± 3.7)	5.4 (± 2)
CO (ppbv)	Feb	Jul	179.0 (± 11)	78.0 (± 7)	101.0 (± 11)	130.0 (± 18)
CH_3Cl (pptv)	Mar	Sep	623.0 (± 19)	523.0 (± 22)	100.0 (± 24)	19.0 (± 5)

Note: C_{max}, C_{min} are the average monthly highest and lowest concentrations during the year. δC are the 90% confidence limits of C. $\delta^* = (C_{max} - C_{min})$, and $\pm \delta\delta^*$ = 90% confidence limits of δ^*. $\delta^* > 0$ at $\alpha < 0.01$ (Welch test). $\delta^*\% = 100(C_{max} - C_{min})/C_{min}$: $\delta\delta^*\%$ are approximate 90% confidence limits.

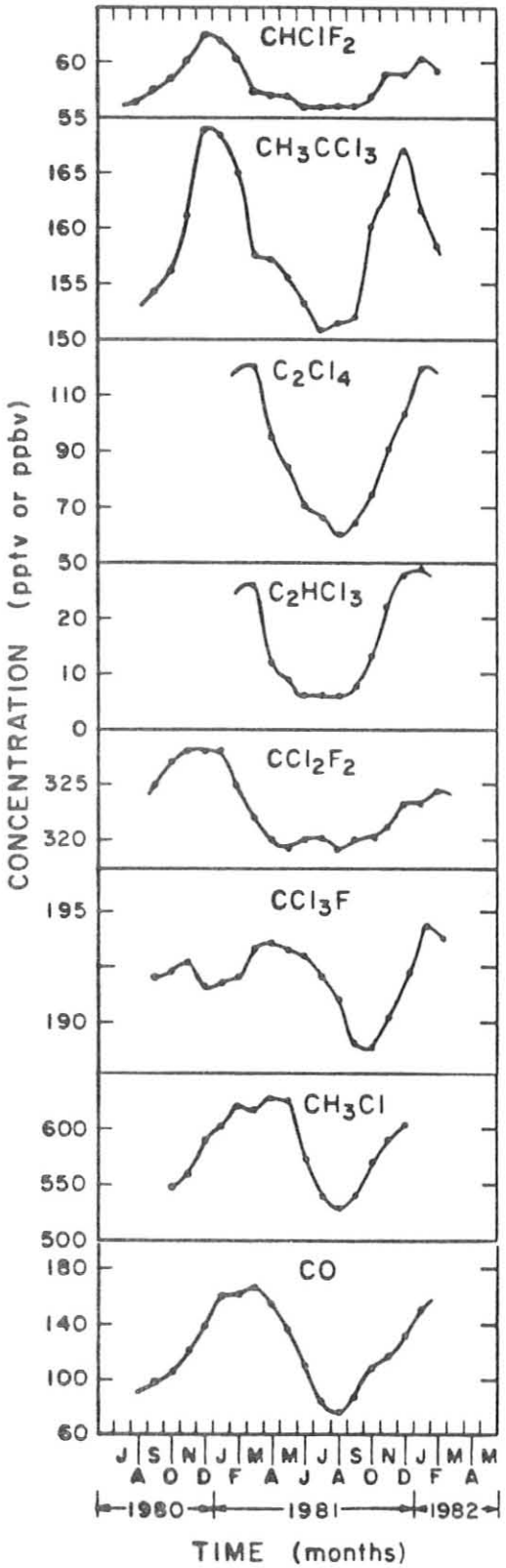

Figure 58.--Three-month running averages of the monthly average concentrations of eight gaseous tracers of Arctic haze at BRW. This provides evidence that the seasonal variations of these eight gases have repeated themselves over the two winters of observation (Khalil and Rasmussen, 1982).

5.7.2 Criteria for Gaseous Tracers

As table 38 shows, some tracers have more prominent winter maxima than others. Such tracers are desirable since their measurements can be used to estimate the contributions of various source regions more accurately than other tracers. The criteria for gases to be tracers of Arctic haze have been developed by Khalil and Rasmussen (1982) on the basis of data discussed earlier. In general the gases must (1) be entirely anthropogenic or must have large midlatitude anthropogenic sources, (2) have long enough lifetimes in winter to survive transport to the Arctic, and (3) have seasonal patterns that repeat year after year whenever Arctic haze is present. The seasonal pattern in condition (3) should mirror the seasonal pattern of Arctic haze aerosol; thus, maximum trace-gas concentrations must occur during the half year including Arctic winter (Rahn, 1981b; Rahn et al., 1977).

To satisfy the last condition the quantitative criteria

$$\bar{C}_{max} > \bar{C}_{min} \qquad (\alpha \leq 0.01)$$

$$\bar{C}_{max} > \bar{C}_{1} \qquad (\alpha \leq 0.01)$$

were chosen, where $\bar{C}_{max}$ is the average concentration of the trace gas in the Arctic during three successive winter months between December and May when maximum concentrations are observed, $\bar{C}_{min}$ is the average concentration during the 3 months of summer (June to August), $\bar{C}_1$ is the average concentration for the 9 months other than the three chosen to define $\bar{C}_{max}$, and α is the level of significance at which the hypotheses $\bar{C}_{max} = \bar{C}_{min}$ and $\bar{C}_{max} = \bar{C}_1$ can be rejected. It has been assumed that $\bar{C}_{max}$, $\bar{C}_{min}$, and $\bar{C}_1$ are calculated after any detectable long-term trends have been subtracted from the data. The criteria establish the high probability that concentrations of a trace gas during winter are significantly greater than during summer or the rest of the year.

The trace gases listed in tables 37 and 38 satisfy the criteria. Generally, the background concentrations of long-lived gases tend to be large compared with seasonal emissions, thus making it difficult to detect seasonal variations. Thus, gases found to be the most suitable tracers were those with global lifetimes of less than 5 years or with concentrations far less than those expected if current yearly emissions were in equilibrium.

5.7.3 Conclusions and Results Supported by Tracer Gases

The measurements of trace gases at BRW support several conclusions of previous studies of the Arctic haze aerosol. In particular, the following conclusions may be drawn.

(1) The six anthropogenic halocarbons ($CHClF_2$, CCl_3F, CCl_2F_2, C_2Cl_4, C_2HCl_3, CH_3CCl_3), and CO and CH_3Cl are produced at the same midlatitude regions as the precursors of Arctic haze. Their maximum concentrations in the Arctic occur during winter, closely following the occurrence of Arctic haze. These gases can therefore serve as quantitative tracers of the distant origins of Arctic haze.

(2) Since these gases are produced in industrialized and populated regions of the world, their increased concentrations during the Arctic winter

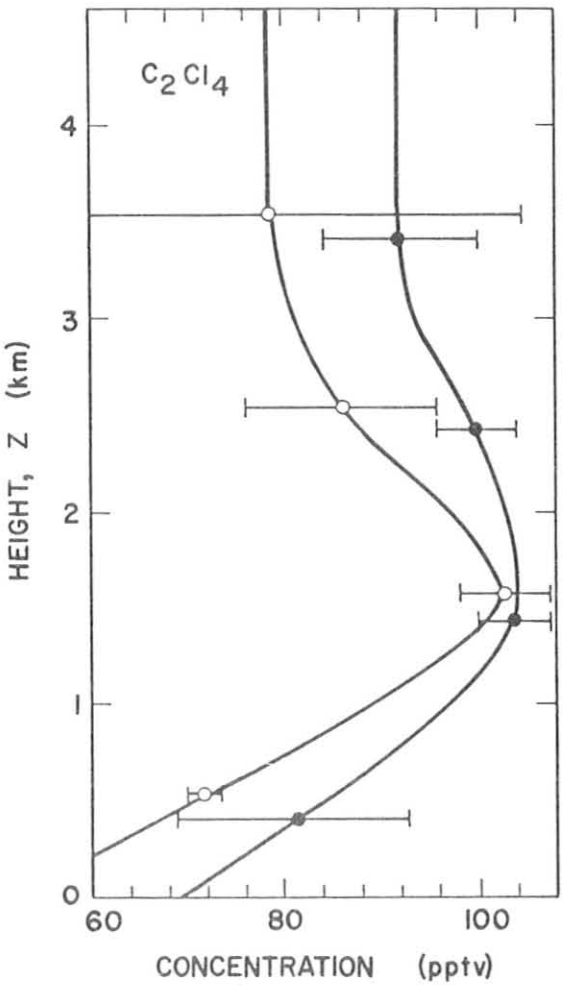

Figure 59.--The concentration of C_2Cl_4 as a function of height on 2 different days (filled circles, 7 May 1982; open circles, 13 May 1982). Polluted air occurs between 1 and 3 km.

can occur only because of long-distance transport. This result provides additional and independent support to previous studies indicating that the sources of Arctic haze aerosol are anthropogenic and located in the midlatitudes of the Northern Hemisphere (Rahn, 1981b).

(3) Several of the halocarbon tracers are released throughout the year and are so inert that their lifetimes do not vary significantly during the year. Their observed seasonal patterns are consistent with a faster transport during winter from polluted midlatitude locations to the Arctic. Such transport patterns may also contribute to the occurrence of Arctic haze.

(4) Differences in the seasonal patterns of CFC-11 and CFC-12 in the Arctic may indicate either the seasonal variations in the use patterns of these gases or the contributions of different sources to the Arctic atmosphere. Further studies may resolve whether there is a predominant location from which the Arctic haze aerosol originates or if pollution from a few separated locations combines to produce Arctic haze.

(5) More recent studies on the variation of tracer gas concentrations with height suggest that polluted air may be transported in a layer between 1 and 3 km and perhaps in higher layers as well. Figure 59 shows an example of a height profile of C_2Cl_4 (see also Rahn and Heidam, 1981).

(6) Currently, studies of the seasonal cycles of trace gases at BRW are continuing and are being supplemented with studies of the abundances of unique exotic gases in transit from specific industrialized areas of the world to the Arctic. It is hoped that this information will help reveal the origins of Arctic haze.

5.8 Time Series Analysis of Light-Scattering Data from MLO

M. Darzi and J. W. Winchester
Department of Oceanography, Florida State University
Tallahassee, FL 32306

5.8.1 Introduction

In previous reports (DeLuisi, 1981, pp.107-113; Darzi and Winchester, 1982a) results were presented of elemental analyses of a time series of aerosol samples collected each 3.7 hours at MLO (alt. 3.4 km) during a 13-day spring dust period, April-May 1979 (Shaw, 1980). Aerosol sulfur often exceeding 1 $\mu g\ m^{-3}$ was also present. Subsequently (Darzi and Winchester, 1982c) much higher dust loadings of continental composition were evident during spring than summer at the Hawaiian Volcano Observatory (alt. 1.2 km), which is consistent with interpretations based on light scattering (Bodhaine et al., 1981b). Time series analysis of springtime elemental concentrations at MLO showed strong coherency between sulfur and crustal dust elements and a strong periodicity near 21 hours, suggesting that large-scale processes, possibly related to Asian aerosol sources, affected concentration fluctuations at MLO during spring, rather than local meteorological effects from which a 24-h periodicity is expected. Moreover, crustal elemental concentrations were coherent with light-scattering data although not with CN counts, indicating that light scattering can be used as a quantitative indicator of aerosol constituents.

The record of hourly light-scattering data for four selected months during 1979 has since been examined (Darzi and Winchester, 1982b). Strong diurnality was found during summer, fall, and winter, but a shorter principal period, near 21 hours, was found for spring, which is consistent with the elemental concentration measurements. Therefore, it may be possible to calibrate light-scattering data with elemental composition determinations for short time resolution, thus permitting the interpretation of extensive records of MLO light-scattering data since 1974 in terms of dust, air pollution, and possibly other components of continental as well as local origin. In this report MLO 1979 and 1980 light-scattering records are examined by time series analysis using measurements of b_λ at 450-, 550-, 700-, and 850-nm wavelengths and the Angstrom exponent α, defined by $b_\lambda \sim \lambda^{-\alpha}$.

5.8.2 Results

Hourly light-scattering data for 1979 and 1980 from MLO at the four wavelengths were provided by GMCC. For every hour of January, April, July, and October of each year a regression fit to the relation $\log b_\lambda = -\alpha \log \lambda + \text{constant}$ was performed, and the correlation coefficient was generally >0.9. Hourly values of predicted $\log \hat{b}_{450}$ and $\log \hat{b}_{850}$ as well as α were computed from the regression line, thus making use of data at all four wavelengths.

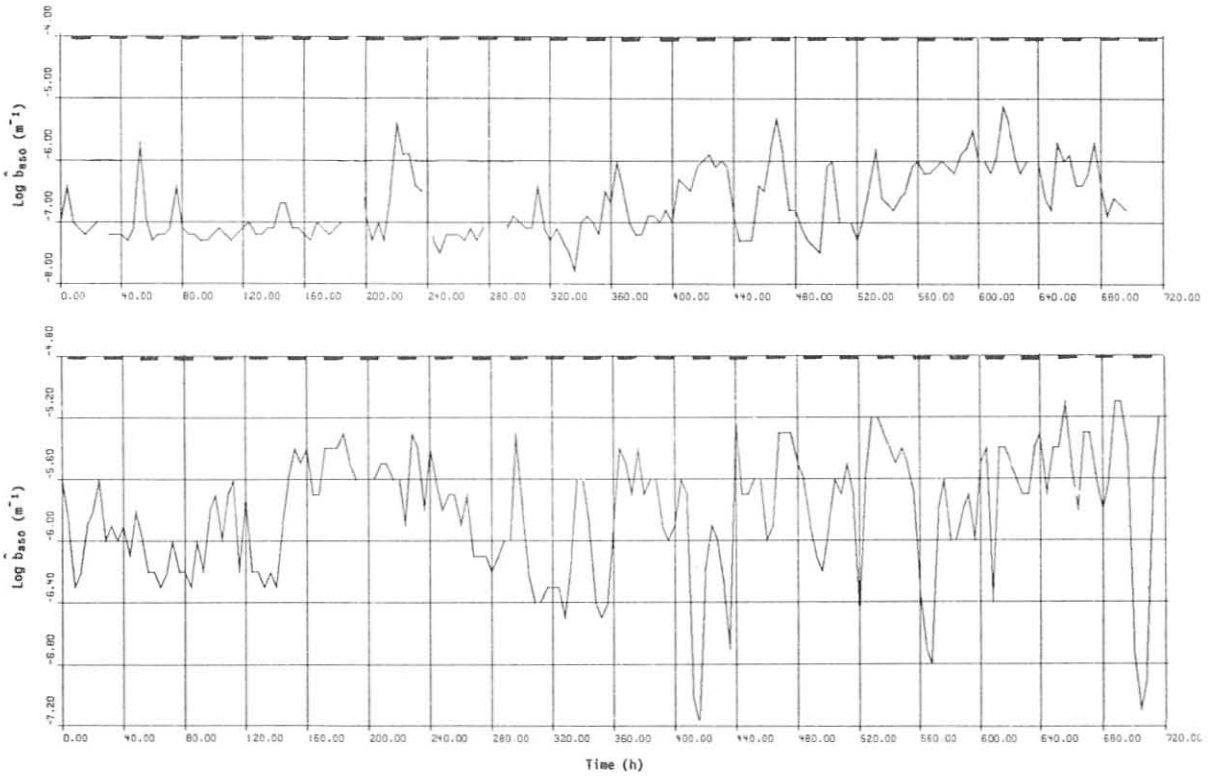

Figure 60.--MLO 4-h mean light scattering, log $\hat{b}_{850}$, at 850 nm for January (upper) and April (lower) 1979. Bars at top cover the 12-h night periods 2000-0800 HST. Note the January scale, -8.0 to -4.0, and April scale, -7.2 to -4.8, for log $\hat{b}_{850}$ (m^{-1}).

Four-hour means of these three parameters were calculated and used in subsequent time series analysis.

Light scattering, as well as elemental concentrations, often varies by several-fold over intervals of a few hours at MLO, indicating fluctuations in aerosol concentrations as air passes over the sampling site. The 4-h mean log $\hat{b}_{850}$ values for January and April 1979 are plotted in fig. 60. The January data show a general level of $\hat{b}_{850} \sim 10^{-7}$ m^{-1}. Additional peaks occurred at values at least several times greater but not preferentially at any particular time of day or night. Unlike January when nighttime peaks are seldom observed, in April peaks often occur at night. The high light scattering and its pattern of variability, apparently not related to diurnally varying local meteorological conditions, are characteristics that suggest aerosol transport from Asia during spring.

The eight monthly sets of 4-h mean values of log $\hat{b}_{850}$, log $\hat{b}_{450}$, and α have been subjected to time series analysis (Darzi, 1982, Appendix C). To examine the periodicities near 24 hours for the 8 months more closely, the variance densities at discrete Fourier periods from about 20 to 27 hours are listed in table 39. Except for April, high variance densities near 24 hours are generally found. In both April sets, however, higher variance densities at about 10% shorter periods, 21-22 hours, are found. This result, together with generally higher light-scattering intensities in April compared with the other 3 months each year, suggests unique aerosol characteristics during spring.

Table 39.--Variance densities at discrete Fourier periods*

Period (h)	1979†				1980†			
	Jan	Apr	Jul	Oct	Jan	Apr	Jul	Oct
b_{850}								
26.6	0.242	0.0619	0.0769	0.353	0.704	0.0283	0.0893	0.0732
25.7	0.201	0.0398	0.0978	0.419	1.08	0.0117	0.315	0.125
24.8	0.523	0.0251	0.156	0.622	1.22	0.0239	1.17	0.262
24.0	1.15	0.0335	0.206	0.459	1.23	0.0340	1.61	0.308
23.3	1.60	0.0277	0.170	0.290	1.12	0.0340	0.790	0.255
22.5	1.48	0.0428	0.0795	0.291	0.602	0.0272	0.396	0.297
21.9	1.18	0.118	0.0514	0.466	0.315	0.0432	0.802	0.264
21.3	0.956	0.159	0.0795	0.622	0.608	0.0569	1.02	0.0987
20.7	0.607	0.0963	0.0863	0.451	0.751	0.0291	0.881	0.0391
b_{450}								
26.6	0.229	0.0274	0.0450	0.260	0.485	0.0184	0.0783	0.0478
25.7	0.196	0.0219	0.0656	0.342	0.766	0.0060	0.259	0.101
24.8	0.435	0.0201	0.0803	0.474	0.885	0.0147	0.840	0.172
24.0	1.03	0.0191	0.106	0.322	0.934	0.0256	1.08	0.167
23.3	1.58	0.0217	0.120	0.233	0.814	0.0234	0.523	0.165
22.5	1.41	0.0339	0.0786	0.254	0.397	0.0172	0.322	0.255
21.9	0.945	0.0814	0.0467	0.409	0.207	0.0303	0.643	0.239
21.3	0.669	0.115	0.0530	0.567	0.418	0.0382	0.782	0.0967
20.7	0.407	0.0658	0.0636	0.374	0.507	0.0195	0.631	0.0538

*Hourly 4-λ data at MLO fit by $b \sim \lambda^{-\alpha}$. Resulting smoothed log $\hat{b}_{850}$ and log $\hat{b}_{450}$, as 4-h means, analyzed by time series.
†The two highest values in each set of nine are underlined.

Insight into whether the aerosol consists of a single population of particles distributed over a range of sizes, or two (or more) populations having different particle size distributions and varying somewhat independently with time, may be gained by examining coherency between light scattering at long and short wavelengths. Figure 61 shows coherency squared, plotted as a function of frequency obtained from the time series analysis. The right-hand scales give the equivalent confidence levels of coherencies. January and October 1979 have the highest coherencies, above the 99% confidence level for nearly all periods from 10 to 300 hours. April 1979 has the lowest coherency and July 1979 is intermediate. These results suggest that the January and October aerosols exhibit essentially parallel variations on concentrations of particles that scatter at long and short wavelengths; i.e., the particle size distribution exhibits little variability. In April the weaker coherency suggests the presence of fine and coarse aerosol components, as may be found in an external mixture of sulfate and crustal dust particles, and these exhibit somewhat independent variability in time. In July an intermediate result is found.

Further insight into the presence of fine and coarse aerosol components is gained from average values of α, listed in table 40 for the 8 months of 1979 and 1980. The lower values of α for both Aprils than for the other 6 months indicate a greater proportion of coarse particles compared with fine, during spring. This is consistent with the presence of continental dust. However, it should also be noted that light scattering at both short and long

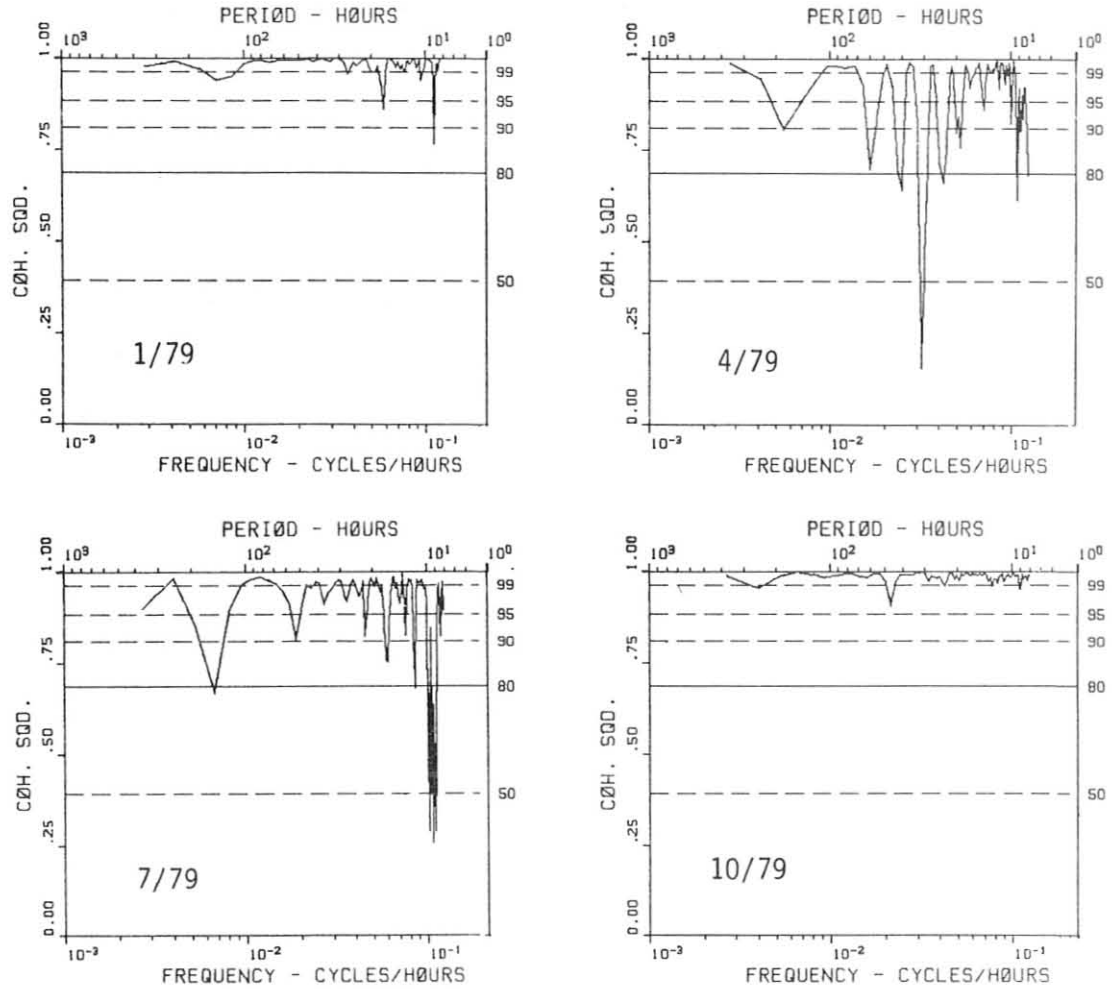

Figure 61.--Coherency squared of 4-h mean log $\hat{b}_{850}$ and log $\hat{b}_{450}$ for January, April, July, and October 1979. Percent confidence levels are indicated by scales on the right.

Table 40.--Seasonal variation of α*

Month 1979-80	α	SD/$n^{\frac{1}{2}}$
Jan	1.78	0.05
Apr	1.28	0.05
Jul	1.86	0.05
Oct	2.25	0.04
Jan	2.38	0.06
Apr	1.45	0.05
Jul	2.09	0.04
Oct	1.99	0.04

*Based on n ~ 180, 4-h means of 4-λ light-scattering observations monthly at MLO. α is defined by $b \sim \lambda^{-\alpha}$.

wavelengths is greater during April than in the other 3 months each year. This could be due to a dust component of broad particle size distribution so as to scatter short- as well as long-wavelength light, but it may also be consistent with enhanced concentrations during spring of both fine and coarse aerosol components, e.g., sulfate and terrestrial dust. Aerosol sulfur concentrations have been reported (Darzi and Winchester, 1982a) for 23 April-6 May 1979, averaging 0.3 $\mu g\ m^{-3}$, and often >1.0 $\mu g\ m^{-3}$, with similar time series characteristics for sulfur, iron, and the other crustal elements. These high concentrations and the time series results, together with air trajectories, suggested air pollution transport, along with dust, from Asian sources. Whether these high sulfur values represent spring enhancement or are part of a more persistently present fine component may be determined by suitable aerosol sulfur concentration measurements at other times of the year at MLO.

Further indication of the possibility of air pollution sulfur being transported from Asia during the spring dust season is given by 1980 measurements in Japan. In cooperation with investigators at Keio University, week-long sequential streaker samples were obtained of aerosol with 2-h time resolution from two kosa (yellow soil) dust events that occurred during the weeks of 19-25 April and 6-12 May 1980 (Hashimoto et al., unpublished results); the first dust storm was also sampled in Beijing, China, on 19 April (Wang et al., 1982). PIXE analyses indicate that the time of high dust concentrations (e.g., at Niigata for 2.5 days beginning 21 April) coincides with increased concentrations of aerosol sulfur at Niigata by 0.3-0.6 $\mu g\ m^{-3}$. These results suggest that Asian dust transported to Japan may contain an air pollution component.

5.8.3. Discussion

The location of MLO at a high altitude in the mid-Pacific makes it ideal for monitoring midtropospheric aerosol, especially for detecting long-range transport of continental dust and pollutants. This report points to the importance of comparing hourly light-scattering measurements with elemental concentrations that are also measured on a short time scale. Both sets of measurements are amenable to time series analysis and provide insights into dynamic properties as well as chemical composition as evidence of possible sources and transport pathways of aerosols to Hawaii.

5.9 Radiation Measurements at BRW

G. Wendler and F. Eaton
Geophysical Institute, University of Alaska
Fairbanks, AK 99701

The "radiation paradox", which was measured at BRW, was described last year. On clear sunny days on the North Slope the radiation balance at solar noon in May is less positive than on cloudy days, resulting in cooler ambient air temperatures. Although the net short-wave radiation increases, the increase is not substantial because of the high surface albedo. This small gain is overcompensated by the greater loss in the infrared under clear-sky conditions. Measurements of the short-wave and all-wave budget with a PD-4 Davos radiometer continue. Further, three more sensors were added to measure sky radiation, radiation received on a surface inclined to latitude, and radiation

received on a south wall. From the global and sky radiation, the direct beam can be calculated. These measurements together with the budget measurements are of scientific interest, but the measurements on inclined surfaces are of greater practical importance. They can be used for estimating the size of photovoltaic arrays, which are commercially used on the North Slope for microwave repeater stations. The data acquisiton system was changed to a Datel magnetic tape recorder.

5.10 Optical Measurements of Blowing Snow at SPO

F. Eaton and G. Wendler
Geophysical Institute, University of Alaska
Fairbanks, AK 99701

An optical system for measuring blowing snow was installed at SPO during austral summer of 1981-1982. The system is similar to that designed by R. Schmidt, but it was modified both electronically and mechanically by G. Mimkin in Fairbanks for use in extreme cold and corrosive (sea coast) sites. Low-temperature components were used, and the first year of testing low-temperature effects on the system will be carried out at SPO.

The system measures both concentration of blowing-snow particles and sizes of particles. The sensor is mounted on the same tower as the GMCC temperature and wind speed and direction probes; thus the ensemble of measurements at one point will be very useful in understanding blowing snow.

Interest in the effects of blowing snow caused by the katabatic wind stimulated the measurement program in Antarctica. Actual flux measurements of blowing snow are crucial to assess the importance of blowing snow due to density changes (by injection of particulate matter into the airstream, as well as by cooling of the air from sublimation of transported particles). Of particular interest for climatic studies are measurements of transported snow as it relates to the overall mass balance of the ice sheet in Antarctica. Blowing-snow measurements can also be used for understanding visibility and drifting snow.

5.11 Light Absorption Studies at MLO

A. D. Clarke and R. J. Charlson
Department of Civil Engineering, University of Washington
Seattle, WA 98195

The aerosol light absorption coefficient σ_{ap} was measured twice daily at MLO from late April through late May 1981. This time period was chosen because it was the most probable time for Asian dust episodes there (DeLuisi, 1981, pp. 107-113). The purpose of the measurement program was to determine values of σ_{ap} and its short-term variability at MLO, under conditions representative of the middle to upper troposphere, to identify the size fraction of the aerosol responsible and to try to determine sources.

A new technique, called the IS method (Clarke, 1982), was developed to measure the absorption rapidly under remote "clean" conditions. An 8-h sampling period at MLO was found sufficient for both day (upslope) and night

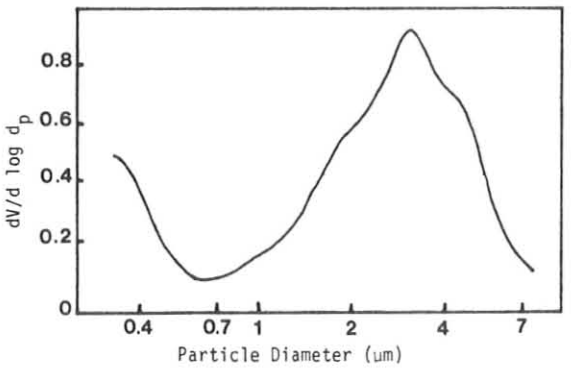

Figure 62.--A typical volume distribution of MLO aerosol as measured with a modified Royco OPC. Area under the curve is total volume measured (μm^3 cm^{-3}).

(downslope) measurements employing this method. Aerosol samples were collected daily for both regimes, and a cyclone sampler with a size cut at ~0.7-μm diameter was used to obtain fine-particle samples in addition to total-particle collections. Sample collections were made on both quartz fiber (Pallflex QAS 2500) and Nuclepore (0.4-μm) filters. A modified Royco 220 OPC, a three-wavelength nephelometer (Bodhaine, 1979), and a G.E. CNC were used to characterize the size distribution and the scattering coefficient σ_{sp} of the aerosol over the sampling periods. Meteorological variables including wind speed, wind direction, inversion height (from Hilo rawinsonde data), etc., were recorded to characterize the air mass and to assist in discrimination of incursions of aerosol from below the inversion layer. The OPC provided optical sizing data in the 0.35- to 9-μm range. Within this range the aerosol mass distribution typically revealed a well-defined bimodal character with a consistent minimum at approximately 0.7 μm (fig. 62). Mass peaks for the large-particle mode were centered near 3 μm, while the fine mode appeared to reach a maximum near the lower range of the OPC (<0.35 μm) such that only variations in the upper tail were measurable.

The short sampling period was unfortunate in that it coincided with relatively anomalous weather conditions and a variety of instrument failures at MLO. Consequently, clear and complete data sought to characterize the Asian dust episodes during this sampling period were not obtained. However, it is believed that features in the available data suggest significant characteristics of the aerosol at MLO, including Asian dust events. The primary variables of interest in this study are presented independently in fig. 63 as a function of day of year. Wind speed, wind direction, and inversion height are taken from the Hilo rawinsonde data. Data denoted by stars were taken at night (downslope flow); dots represent days (upslope flow). Vertical arrows point to data off scale and have the off-scale values printed above them. Relative inversion strength (as measured over Hilo) is suggested by the size of the data dot on the inversion height curve. Wind speed and direction (also measured over Hilo) are illustrated with wind direction (relative to North at the top of the page) pointing into the data point. The mass distribution plots were obtained from the OPC volume distribution by using an assumed density of 1.5 g cm^{-3} for the aerosol. For the case of fine-particle mass, the volume detected by the OPC in the range of 0.35-0.7 μm has been doubled to estimate the remaining part of the distribution below 0.35 μm and out of range for the OPC. Although this is an arbitrary choice, the fine mass as presented should be systematically uncertain by less than a factor of 3.

Comparisons of cycloned and uncycloned samples revealed that approximately 60%-85% of the absorption was due to the mass in the fine mode. Values

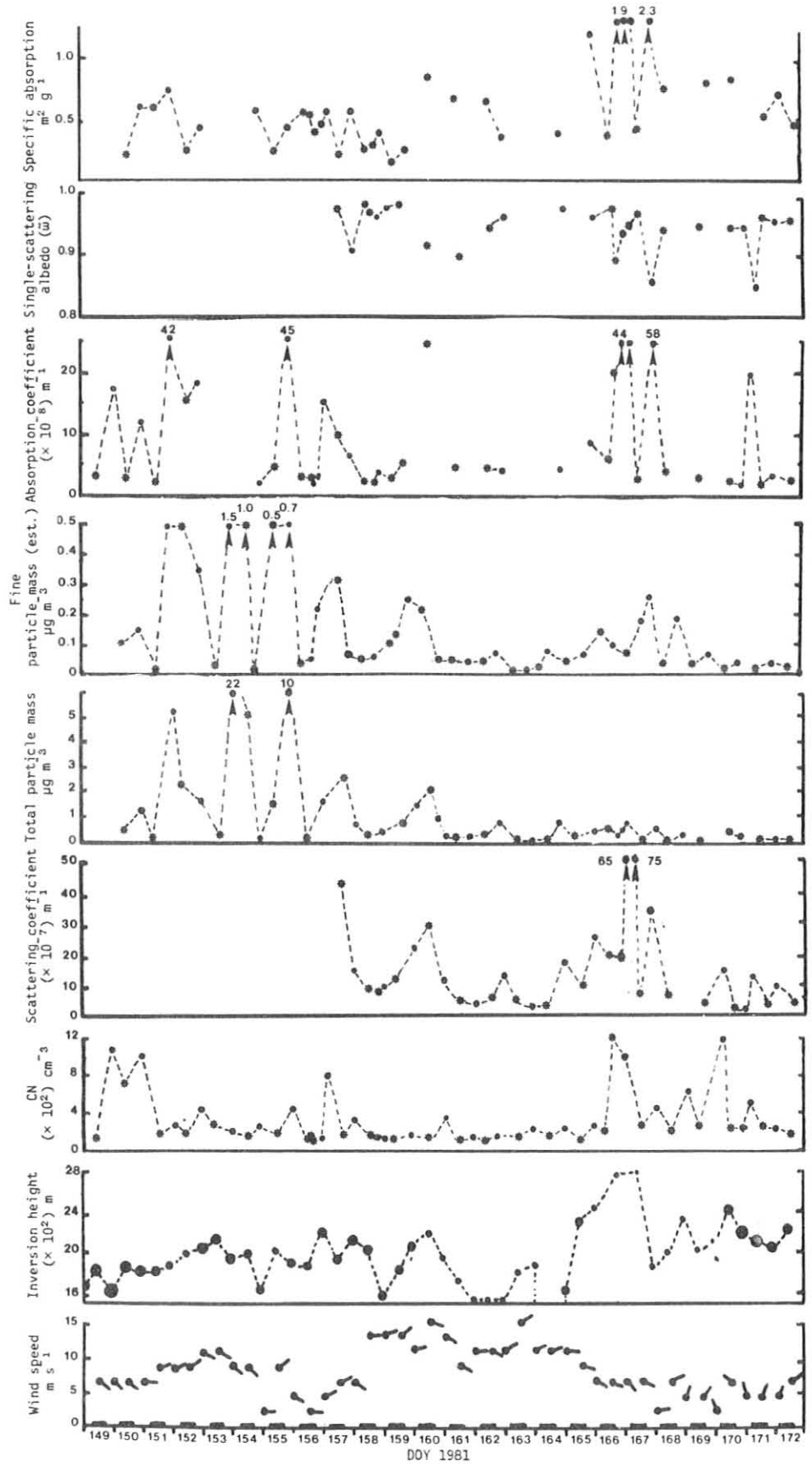

Figure 63.--Aerosol optical, physical, and aerometric data at MLO. See text for detailed explanation of symbols.

for specific absorption B_a presented in fig. 63 are calculated using the estimated fine-mode mass with the assumption of an average of 75% of the absorption attributable to that mode. In spite of these assumptions the magnitude and relative variation of B_a are valuable indications of the aerosols and air mass.

Hilo is located approximately 60 km northeast of MLO, and during the predominant trade wind flow the rawinsonde data taken there represent generally unperturbed characteristics of the air mass approaching the island. Orographic effects will modify wind speed, wind direction, and inversion height during its approach to MLO, and diurnal upslope and downslope flows will be superimposed on these characteristics in the vicinity of MLO (Mendonca, 1969). Consequently, separate sampling was performed during upslope (day) and downslope (night) conditions. Nighttime samples are indicated on the time axis with a darkened line segment and on the plotted values with a star symbol. Dashed lines connecting data points are illustrative and intended to indicate periods of consecutive sampling. No data for the light-scattering coefficient were available from the GMCC nephelometer because it was out of service. Figure 63 data commencing on DOY 157 were from a nephelometer obtained courtesy of A. Waggoner of the University of Washington.

Several events should be noted in conjunction with an interpretation of fig. 63 data. The first 3 days of sampling (148-150) were concurrent with a significant forest fire burning out of control in Volcanoes National Park approximately 50 km directly upwind of MLO. Both the mass and the absorption coefficient show large diurnal excursions with nighttime minima for these dates; these may be due to diurnal upslope winds bringing some soot and ash to MLO. High CN counts also suggest intrusions from the lower troposphere. Similar intrusions are more conspicuous for DOY 165-168. Though total OPC mass m_t remains relatively low in this period, the fine-particle mass m_f, σ_{sp}, σ_{ap}, B_a, and a weak high inversion all signal a prolonged invasion of the tropospheric aerosol. SEM photos during this event show numerous chains of particles similar to carbon, of combustion origin, which account for the high specific absorption for the fine-mass fraction in these samples.

Primary data for the period 151-164 reveal a more complex variation. With the exception of a few daytime values for this period, both the CN count and inversion height remain relatively low. At the same time, day and night values for σ_{sp}, σ_{ap}, m_f, and m_t are high and show similar variations over time. Unfortunately, σ_{sp} values prior to DOY 157 do not exist, so single-scattering albedo $\tilde{\omega}$ cannot be determined for those dates. However, when compared with the high-inversion period mentioned earlier, the specific absorption based on the estimated fine-particle mass maintains remarkably low values during the particularly high mass loading for DOY 153-157. In view of this, and SEM photos revealing irregular angular particles with a predominantly terrestrial mineral elemental composition, this period may represent long-distance transport of Asian dust.

The above considerations and other predominant features in this data set are summarized in table 41. Pending further analyses of these data and more extended data sets to be collected in 1982, this summary is presented as tentative. In spite of the anomalous meteorology during this study, some features of the data appear significant and warrant comment. Ignoring daytime samples and other periods of upslope flow or intrusions of high aerosol mass,

Table 41.--Summary of fig. 63 data features

DOY	Feature	Probable event
149-152	Strong day-night variability of σ_{ap}, m_f, m_t, CN	Strong upslope-downslope winds carrying some ashes from a forest fire 50 km downwind during day
152-155	(1) Large excursions in m_f and m_t with some high night values (2) Low CN variability (3) High winds (4) Average inversion	Possible Asian dust intrusion
155-161	(1) Coincident maxima in m_f, m_t, σ_{sp}, σ_{ap}, both during night and day (2) Low CN except DOY 156 (3) Low $\tilde{\omega}$ (4) Moderate B_a (5) SEM-EDXA shows strong crustal elements and S present (6) High winds associated with low pressure north of Hawaii	Asian dust suspected and/or lower tropospheric air
161-164	(1) Low m_f, m_t, CN, σ_{sp}, σ_{ap} (2) High $\tilde{\omega}$ (3) High winds (4) Low weak inversion	Possible example of background or typical aerosol at MLO
164-167	(1) Moderate to high m_f (2) Low m_t (3) High CN, σ_{sp}, σ_{ap}, B_a (4) High weak inversion (5) Average winds (6) SEM-EDXA shows crustal elements, NaCl, high Ci fibers, and carbon chains	Injection of boundary layer air with crustal, marine, and combustion components
167-172	(1) Low m_t (2) Diurnal variation in m_f, CN, σ_{sp}, σ_{ap}, $\tilde{\omega}$, and inversion height (3) Low variable winds with some upslope flow	Example of background MLO aerosol with some daytime incursions of upslope boundary layer air

Table 42.--Characteristics of MLO background aerosol

DOY	σ_{sp} ($\times 10^{-7}$ m^{-1})	σ_{ap} ($\times 10^{-7}$ m^{-1})	Fine mass* ($\mu g\ m^{-3}$)	Total mass ($\mu g\ m^{-3}$)	B_a† ($m^2\ gm^{-1}$)	$\tilde{\omega}$
158	8.0	0.22	0.051	0.291	0.32	0.973
167	5.2	0.16	0.030	0.085	0.42	0.968
170	3.5	0.19	0.017	0.042	0.83	0.948
171	3.6	0.12	0.018	0.032	0.50	0.970
172	4.5	0.18	0.024	0.067	0.56	0.962
Aver.	4.96	0.174	0.024	0.103	0.526	0.964

*Estimated fine mass based on OPC mass ($0.35 < d_p < 0.7$ μm) and assumed density of 1.5 (see text).
†Specific absorption of estimated fine-mode mass using typical 75% absorption due to fine mode (see text).

there is evidence of concurrent minimum values for several quantities. During the measurements, these minimum conditions occurred during approximately one-half of the evenings sampled. Although a more extensive set may alter or reduce these values, they are presented here as sample values for an upper troposphere background aerosol. Primary aerosol characteristics measured during five minimum nighttime periods when σ_{sp} values were available appear in table 42.

The two derived quantities in fig. 63, the single-scattering albedo ($\tilde{\omega} = \sigma_{sp}/[\sigma_{sp} + \sigma_{ap}]$) and the specific absorption ($B_a = \sigma_{ap}/m_f$), are of particular interest. The former quantity is a fundamental parameter for global climate models. If the above data, excluding pronounced events, are representative of the MLO aerosol and the upper troposphere, then a typical value of $\tilde{\omega}$ for the background aerosol appears to be approximately 0.97. This represents triple the absorption found in many models using an assumed value of 0.99. In spite of the assumptions used to estimate specific absorption in fig. 63, the daily variability and incursions from the troposphere stand out. The remaining values of B_a show remarkably little variation in comparison with those for m_f and are not far removed from values reported for remote continental areas (Weiss and Waggoner, 1980).

Since the size cut used here results in a fine-mode mass less than that typically analyzed by others, these values will be somewhat higher by comparison. However, they still indicate that substantial absorption is present on a fine-mass basis and are suggestive of a continental source. An extended sampling program is necessary to establish the generality of these observations and to identify the nature of the primary absorber. Should high specific absorption be a persistent trait of the background fine-mass aerosol, then graphitic carbon is a likely candidate. If this observation is typical for MLO, then long-distance transport may play an important role in both Asian dust episodes and in maintaining the character of the background aerosol.

5.12 Eight-Year Air Chemistry Measurement Program at SPO

D. Cronn and E. Robinson
Air Pollution Research Section, College of Engineering
Washington State University, Pullman, WA 99164

The objective of this program has been to measure the changes in the atmospheric burdens of the trace gases CFC-12 (CCl_2F_2), CFC-11 (CCl_3F), carbon tetrachloride (CCl_4), methyl chloroform (CH_3CCl_3), and nitrous oxide (N_2O) at a site (SPO) far removed from the anthropogenic sources (natural biogenic sources for N_2O) that are predominantly in the Northern Hemisphere. Samples have been collected on a nearly annual basis since January 1975 and analyzed by gas chromatography with electron capture detection based on a consistent set of long-term calibration standards. The measurement periods and the mixing ratios for each component are given in table 43. Gaps in the data record have been filled by data collected at McMurdo station (~78°S) or Mt. John, South Island, New Zealand (~43°S). The data set is complementary to (1) the GMCC air sampling data also collected at SPO, (2) annual latitudinal gradient studies made from 34°N to 78°S latitude of these same trace gas species since 1976, and (3) continuous ground-level monitoring by WSU since 1975 at a nonurban, midlatitude Northern Hemispheric site.

Each compound has had an increase with time as shown in table 44, although the slope for N_2O is only marginally significant. The percentage increases per year at the SPO based on a linear regression have been 6.8% ± 0.5% for CFC-11, 5.8% ± 0.3% for CFC-12, 2.1% ± 0.4% for CCl_4, 8.1% ± 0.7% for CH_3CCl_3, and 0.3% ± 0.1% for N_2O. These increases compare favorably with similar time trend data from the WSU monitoring station in the Northern Hemisphere (7.0% for CFC-11, 6.4% for CFC-12, 1.7% for CCl_4, 12% for CH_3CCl_3, and 0.4% for N_2O). An inspection of the data in table 43 also shows that the rate of increase for CFC-11 and CFC-12 has diminished through the course of the

Table 43.--Annual time trend of air sampling data

Time	Location	CFC-11 (pptv)	CFC-12 (pptv)	CCl_4 (pptv)	CH_3CCl_3 (pptv)	N_2O* (ppbv)
Jan 75	SPO	90	--	120	54	--
Jan 76	MCM†	113	195	121	57	--
Jan 77	SPO§	127	215	126	67	297
Nov 77	SPO	140	234	129	82	300
Dec 78	SPO	153	253	132	92	301
Sep 79	N.Z.**	160	270	138	106	298
Nov 80	SPO	171†	280	131	105	300
Nov 81	SPO	180	299	141	113†	303

*Based on present calibration (0.9038 × prior calibration).
†Ground samples from McMurdo area.
§Aircraft sampling in planetary boundary layer within 30 mi of SPO.
**From Mt. John near Christchurch, New Zealand.

Table 44.--Linear regression analysis of time trends

Trace gas compound	Slope	SEE*	Intercept	r^2†
CFC-11	12.7 pptv yr^{-1}	0.86	97.7	0.973
CFC-12	17.6 pptv yr^{-1}	0.87	179.7	0.988
CCl_4	2.9 pptv yr^{-1}	0.51	119.7	0.843
CH_3CCl_3	9.6 pptv yr^{-1}	0.85	51.3	0.954
N_2O	0.8 ppbv yr^{-1}	0.42	296.2	0.479

*Standard error about the regression line.
†Correlation coefficient squared.

measuring program. This is in keeping with the curtailment in the rate of growth of emissions following recognition that these compounds deplete stratospheric ozone. Rasmussen et al. (1981) have described the SPO time trends of these compounds with more statistical detail. They used the January 1975-January 1977 data shown here along with data gathered independently during the period 1978-1980.

Acknowledgment

This research has been supported by NSF under grant nos. OPP 76-00437, DPP 76-00437A01, DPP 77-22866, DPP 7921003, and DPP 8117488. The program was directed by R. Rasmussen from January 1975 to June 1977.

5.13 Trace-Element Sampling at BRW

K. A. Rahn
Center for Atmospheric Chemistry Studies, Graduate School of Oceanography
University of Rhode Island, Kingston, RI 02881

During the last year, trace-element data from URI's first 4 years of aerosol sampling at BRW (September 1976-September 1980) have been consolidated and finalized. Results are very reproducible from year to year with characteristic seasonal patterns of both natural and pollution-derived elements. Data for three pollution-derived constituents in individual samples are shown in figs. 64-66.

Noncrustal Mn (fig. 64) has two maxima, in December and March. The December maximum is normally roughly one-half as high as the March maximum, although it can be as high. The March maximum is considerably broader than the December maximum.

Noncrustal V (fig. 65) has the same two maxima plus a third in early February. The February maximum is quite variable in intensity, and is not always present. The March maximum is relatively stronger than it is for Mn.

Nonmarine sulfate (fig.66) has a weak maximum in December and a much stronger one in March-April. The latter lasts for nearly a month longer than

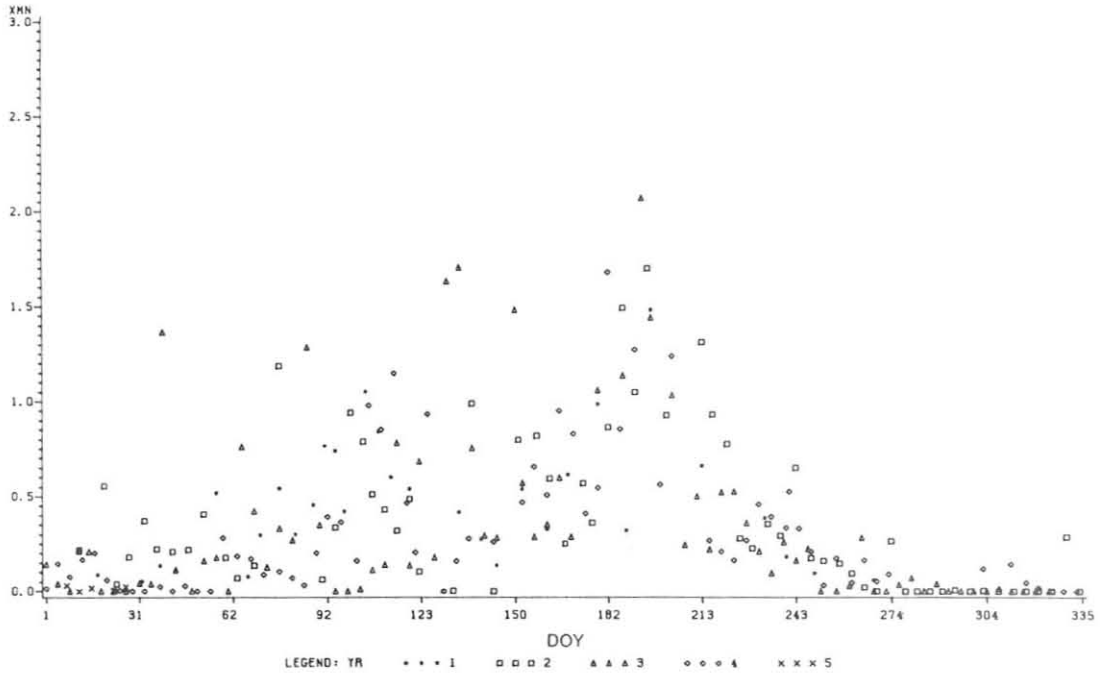

Figure 64.--Seasonal variations of noncrustal Mn (XMN--in ng m^{-3}) vs. DOY (1 Sep = DOY 1) for BRW, 1976-1981.

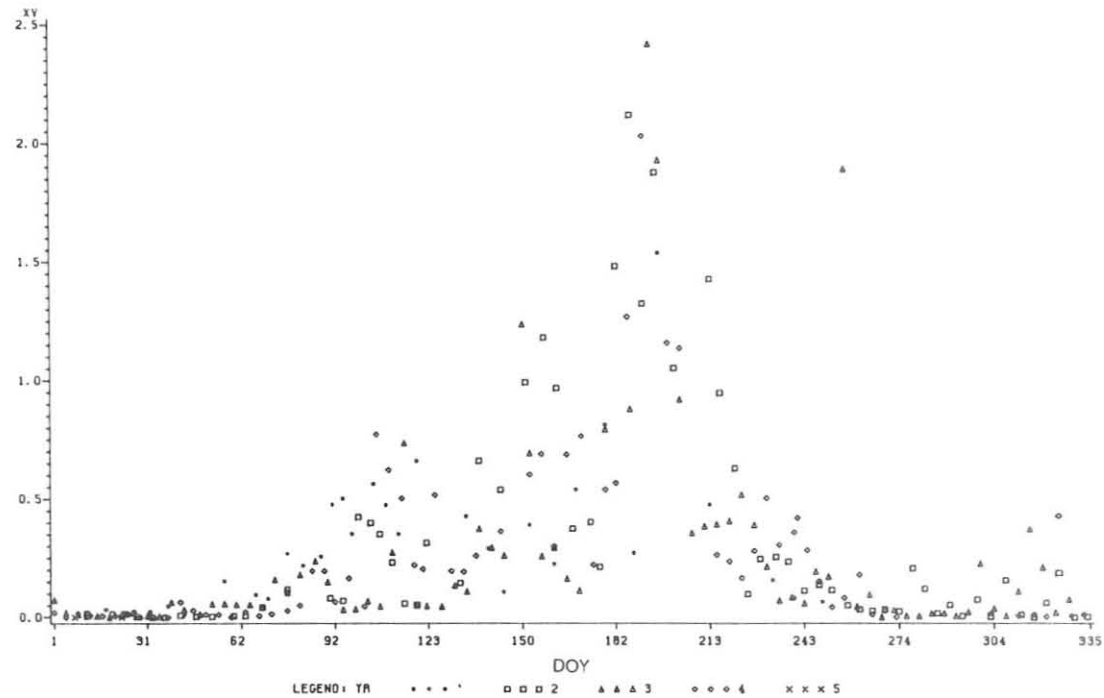

Figure 65.--Seasonal variations of noncrustal V (XV). See fig. 64 legend.

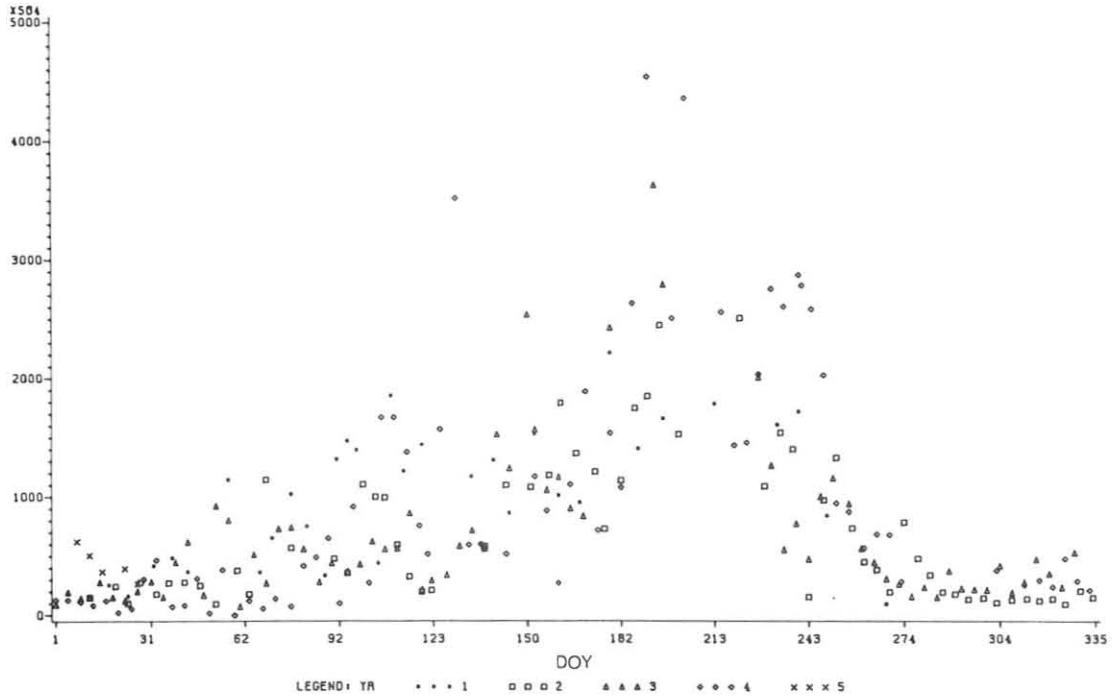

Figure 66.--Seasonal variations of nonmarine sulfate (XSO4). See fig. 64 legend.

it does for noncrustal Mn and V, and appears to be a photochemical effect, because the length of the day is increasing rapidly at this time.

The differences in composition between the various maxima suggest that the aerosol has had different source areas. The December maximum appears to be primarily Asian, whereas the March-April maximum shows a greater European influence.

5.14 Graphitic Carbon-to-Lead Ratio as a Tracer for Sources of the Arctic Aerosol

H. Rosen, A. D. A. Hansen, and T. Novakov
Lawrence Berkeley Laboratory
University of California, Berkeley, CA 94720

and

B. A. Bodhaine
Geophysical Monitoring for Climate Change
NOAA/ERL, Boulder, CO 80303

Recent studies at BRW indicate the presence of large aerosol concentrations that appear to be characteristic of the Arctic region as a whole (Rosen et al., 1981; Rahn and McCaffrey, 1980; Shaw, 1981; Bodhaine et al., 1981a). If the obvious natural aerosol components (e.g., sea salt and soil) are excluded, the predominant components of the Arctic aerosol are carbon- and

sulfur-containing particles. These particles occur at concentrations comparable with those found in urban areas in the continental United States (Rosen et al., 1981; Rahn and McCaffrey, 1980).

There is considerable indirect evidence that a major part of the Arctic aerosol is produced from combustion processes. However, the strongest and most direct substantiation of this is provided by the identification of large concentrations of graphitic carbon in the Arctic (Rosen et al., 1981). These graphitic species, which have a structure similar to carbon black, can only be produced by combustion processes. The concentration of these particles at BRW during the winter and spring approaches that found in urban areas (i.e., the concentrations are only a factor of 4 less than the average values found in Berkeley, Calif., and Gaithersburg, Md., and a factor of 10 less than those found in New York City).

Associated with these graphitic species are large optical absorption coefficients ($\cong 10\ m^2\ g^{-1}$), which could produce a significant perturbation of the heat balance over the Arctic. Preliminary model calculations indicate that present spring concentrations of graphitic particles could increase the atmospheric heating rate by an amount that is comparable with that expected from doubling the CO_2 concentration (Porch and MacCracken, 1982; Cess, 1982).

The sources of the Arctic aerosol are presently unknown. Part of the aerosol may be due to local Alaskan sources, but there is considerable evidence that a major fraction is due to long-range transport from other industrialized regions (Peterson et al., 1980; Barrie et al., 1981), with Eurasia suggested as a major source area (Rahn and McCaffrey, 1980). The use of the graphitic carbon-to-lead ratio as a tracer for the sources of the Arctic aerosol is reported in this paper.

An aerosol sampler has been operating at BRW since October 1979, collecting parallel filter samples on 47-mm quartz fiber and Millipore substrates at a flow rate of approximately 1.5 $ft^3\ min^{-1}$. Measurements of graphitic carbon and particulate lead concentrations from October 1979 through May 1980 are reported here. The graphitic carbon concentrations were obtained using the LBL laser transmission technique (Rosen et al., 1978) with an empirical calibration curve developed for urban particulates in the United States (Gundel et al., 1981). Independent measurements of the graphitic carbon concentration by an optico-thermal analysis technique are under way. Lead concentrations were determined using X-ray fluorescence analysis.

Natural concentrations of particulate lead are very low, and it is usually assumed that in polluted environments the major source is from the burning of leaded gasoline by automobiles. Typical ground-level lead concentrations in urban atmospheres in the United States are $\cong 2\ \mu g\ m^{-3}$. In the Arctic the concentrations are much smaller, as shown in fig. 67(a), but are probably also combustion generated since the enrichment factors relative to the Earth's average crustal abundance are large. For comparison the graphitic carbon concentration as a function of the time of year is shown in fig. 67(b). Although both aerosol components show their largest concentrations during the winter and spring, their seasonal variations are quite distinct. Whereas the graphitic carbon concentrations are roughly constant from December through April, the lead concentrations show a rather sharp peak in November and December and relatively low values for the rest of the year. As a result of these differences in behavior, the relative concentrations of graphitic carbon to lead

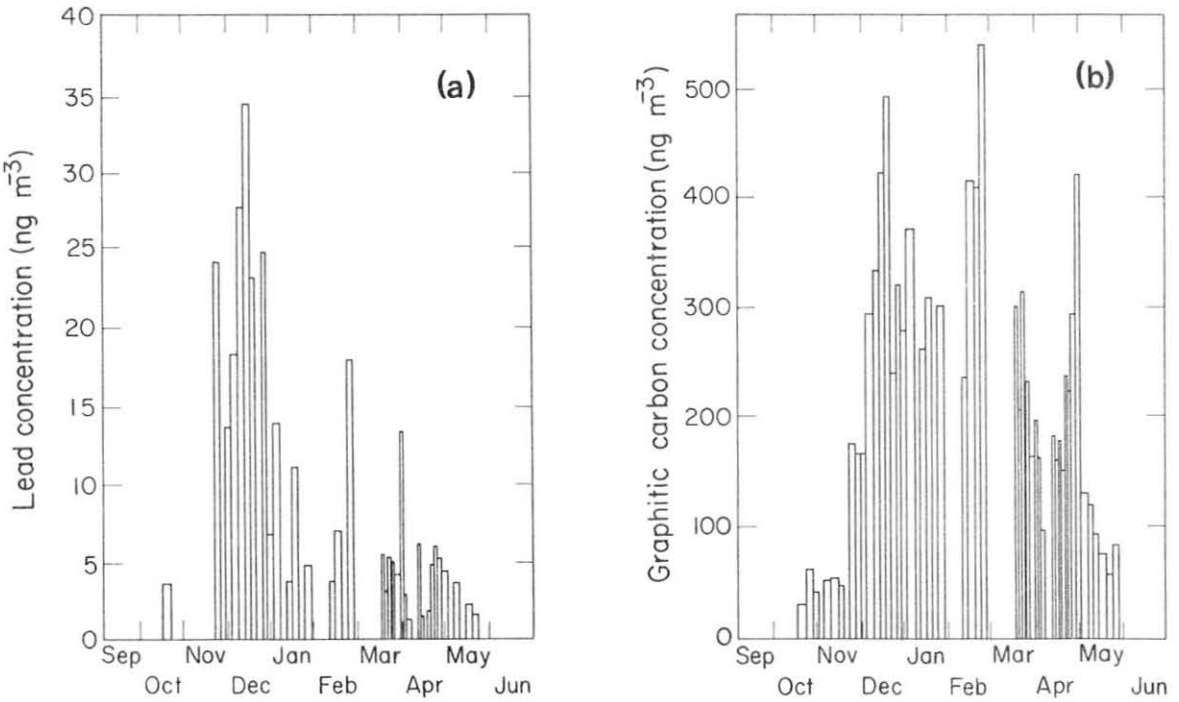

Figure 67.--(a) Particulate lead concentration and (b) graphitic carbon concentration, each as a function of the time of year for 1979-1980.

change substantially throughout the year, as shown in fig. 68. These variations could represent the contributions of different source regions during different times of year or represent a seasonal variation in the fuel mix of given source regions. It should be emphasized that the results reported here are only for 1 year, and interannual variation due to variability in the air trajectories that arrive at Barrow from year to year could be considerable.

Interpretations of these results are based on several crucial assumptions: (1) the graphitic carbon-to-lead ratio does not change significantly during transport because of different deposition rates for particulate lead and graphitic carbon, and (2) source regions may be characterized by ground-level graphitic carbon-to-lead ratios (i.e., these ratios do not change appreciably with altitude). These assumptions need further investigation.

It is interesting to compare the graphitic carbon-to-lead ratios in the Arctic with typical values in the Western and Eastern United States. As shown in fig. 68, the values in the Arctic are considerably larger than those found in the United States, especially during the March-April time period. During this time period, the average value is 10 times that found in the Eastern United States and 30 times that found in the Western United States. If the graphitic carbon-to-lead ratio in the Western United States is used to represent a source region dominated by automotive emissions, then these results could imply that source regions of the BRW aerosol during the March-April time frame do not have a large automotive component relative to other soot-generating combustion sources. For example, such a region could have a large diesel, wood-burning, or stationary-source component relative to automobiles. Furthermore, these results could imply that the United States or regions with similar fuel mixtures do not contribute significantly to the Arctic haze during these periods of high graphitic carbon-to-lead ratios.

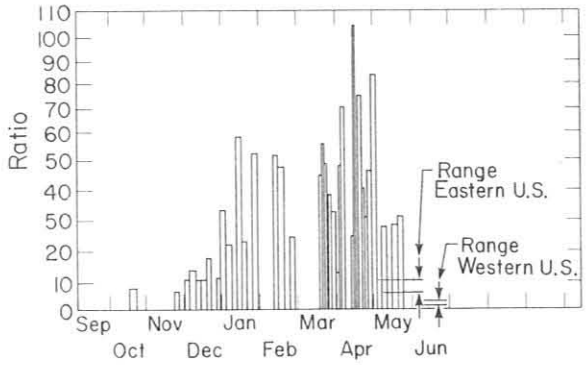

Figure 68.--Ratio of concentrations of graphitic carbon to particulate lead as a function of the time of year for 1979-1980. Also shown are the range of values for the Western United States (Anaheim, Berkeley, and Fremont, Calif.) and the Eastern United States (New York, N.Y.; Argonne, Ill.; and Gaithersburg, Md.). The range of values is defined as those values within one standard deviation of the average.

Acknowledgment

This research was supported by NOAA under contract no. NA31RAG00254, and by the Assistant Secretary for the Environment, Office of Energy Research, CO_2 Research Division of DOE under contract no. DE-AC03-76SF00098.

5.15 Effects of Sulfate and Non-Sulfate Particles on Light Scattering and Precipitation Chemistry at MLO

A. C. Dittenhoefer
Enviroplan, Inc., 59 Main St.
West Orange, NJ 07052

5.15.1 Introduction

Atmospheric transmission, CN concentration, and particle light scattering have been continuously monitored at MLO with the purpose of establishing long-term trends in global background turbidity for investigation of possible climatic effects. Precipitation chemistry at MLO and various other island locations has also been monitored in recent years. However, only a limited number of studies have been conducted to investigate the chemical and physical properties of the aerosol at MLO. During the period March 1980-April 1981, a field study was conducted to measure the size distributions and mass concentrations of sulfate and non-sulfate particles at MLO to evaluate their impact on light scattering and precipitation chemistry.

5.15.2 Experimental Method

A complete description of the experimental procedures used in the aerosol sampling and analysis is given in Dittenhoefer (1982). Particles were sampled on a raised platform approximately 5 m above the ground in a remote area of the observatory. Particles within the size range 0.1- to 2.0-μm diameter were collected with a cascade impactor onto Formvar-coated electron microscope screens. Sampling times were generally 1 hour at an impactor flow rate of 17.5 ℓ min^{-1}.

To obtain the size distribution of sulfate and non-sulfate particles, a $BaCl_2$ spot test was applied. After particle collection, a layer of $BaCl_2$ was vacuum evaporated onto two of the electron microscope screens. One screen was

then humidified at 75% to activate all chemical forms of sulfate, while the other screen received no humidification such that only sulfuric acid could react with the $BaCl_2$. A series of electron micrographs was taken across the line of impacted particles on each screen using the University of Hawaii-Hilo transmission electron microscope. The particles were then counted, sized, and categorized by type to estimate the size distributions of sulfate and non-sulfate particles, as well as the ratio of sulfuric acid to total sulfate.

5.15.3 Results

Of the approximately 75 samples collected during the nocturnal downslope flow at MLO over the 13-mo period, only 16 were classified as being completely devoid of contamination by local volcanic activity and high-humidity subinversion air. These 16 samples, believed representative of midtropospheric, natural-background aerosol particles, displayed wide variations in their chemistry and morphology.

Episodes of high concentrations of optically dense, non-sulfate particles occurred in the spring. There is considerable evidence that these were soil dust particles that originated from dust storms over the Gobi Desert in eastern Asia. Particle chemical analysis using a SEM X-ray microprobe (conducted by G. Shaw of the University of Alaska) revealed the predominance of the crustal elements Mg, Al, Si, K, Ca, and Fe in these samples. Particle light-scattering coefficients and mass concentrations measured during the springtime dust episodes were over 2 orders of magnitude larger than measurements typically observed under clean background conditions during other times of the year. These episodes were also characterized by a relatively flat particle size distribution in the optically active size range, favoring the large soil particles.

Sulfuric acid was the dominant aerosol component during very clean nocturnal downslope flow. The average $NH_4^+/SO_4^=$ aerosol mass ratio was estimated at approximately 0.07, indicating very little neutralization of the sulfuric acid by ammonia in the midtroposphere over Hawaii. This ratio agrees quite well with the $NH_4^+/SO_4^=$ ratios in MLO precipitation, suggesting that the wet removal of acidic sulfate aerosols could account for the relatively low pH of rainwater collected at MLO.

By use of the measured sulfate and non-sulfate particle volume distributions, together with the theoretical relationship between Mie scattering efficiency and optical particle size parameter (Friedlander, 1977), it was possible to compute light scattering as a function of particle diameter. The ratio of light scattering at 550 nm caused by sulfate particles to scattering caused by all particles is shown in fig. 69 as a function of diameter, categorized by the slope of the particle size distribution, β. Sulfates clearly dominated light scattering for sizes less than 0.4 μm. At larger particle sizes, the influence of non-sulfates became important, especially when the slope of the size distribution was small.

Figure 70 shows that the sulfate-to-total-particle scattering ratio and the slope of the particle size distribution were linearly related and highly correlated. Use of the regression line in fig. 70 represented a means for estimating the relative contribution of sulfate particles to observed light scattering at MLO using only the four-channel nephelometer data. This was

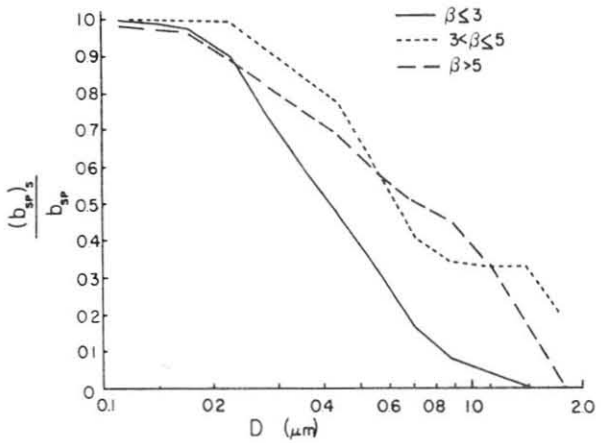

Figure 69.--The ratio of light scattering caused by sulfates to total scattering as a function of diameter, categorized by the slope of the particle size distribution, β.

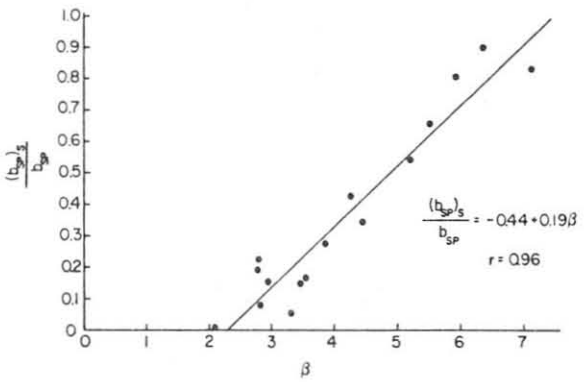

Figure 70.--The ratio of light scattering caused by sulfates to total scattering as a function of the slope of the particle size distribution, β.

applied to each component of a 5-yr MLO historical nephelometer data set, which consisted of hourly average scattering coefficients for the hour beginning at 1200 Z (i.e., 0200 LST), screened to exclude cases of contamination by local volcanic activity and moist subinversion air. The estimated annual variation of light scattering caused by sulfates and non-sulfates is shown in fig. 71. It is clearly evident that the springtime peak in light scattering at MLO is mainly due to non-sulfate particles, with scattering due to sulfate displaying comparatively little variation over the annual period. Sulfates and non-sulfates contribute about equally to light scattering during the latter half of the year.

The historical nephelometer data set was also analyzed with respect to 10-day air mass back-trajectories ending at 1200 Z at MLO. Transport winds were averaged within the vertical layer between 3,000 and 5,000 m using the ARL trajectory model. The back-trajectories were divided into five categories, corresponding to the NE, SE, SW, and NW quadrants and a special NW-E case (to account for 10-day back-trajectories originating from the northwest but arriving at MLO from the east), using the typing scheme of Miller (1981b).

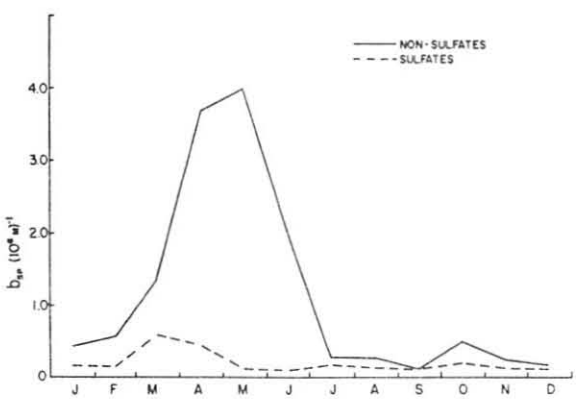

Figure 71.--The annual variation of particle light scattering caused by non-sulfate and sulfate particles.

Table 45.--Average light-scattering coefficient, Angstrom exponent, and estimated scattering coefficient due to sulfates, according to air mass trajectory type

Trajectory type	b_{sp} ($\times 10^{-6}$ m^{-1})	α	$(b_{sp})_s$ ($\times 10^{-6}$ m^{-1})
NW	1.56	1.80	0.30
NW-E	1.46	1.70	0.18
SW	0.85	2.24	0.13
NE	1.10	1.71	0.14
SE	0.72	2.45	0.17

Table 45 shows the average light-scattering coefficient at 550-nm wavelength, b_{sp}; the average Angstrom exponent computed from the four-channel nephelometer data, α (which describes the wavelength dependency of light scattering); and the estimated scattering coefficient at 550 nm caused by sulfate particles, $(b_{sp})_s$, for each trajectory type. Flow originating from the northwest is clearly associated with high light-scattering coefficients and low Angstrom exponents, indicating relatively high concentrations of large particles, and providing further evidence of the influence of Asian soil dust. Light scattering associated with large-scale flow from the SW and SE quadrants is roughly half that for NW flow and considerably less influenced by larger particles. Scattering due to sulfates is also highest for meteorological transport from the NW quadrant, implicating anthropogenic pollution sources in China and Japan as possible contributors (Darzi and Winchester, 1982a).

5.16 Stochastic Simulation Modeling of the Global Carbon Cycle

L. P. Steele
CSIRO Postdoctoral Studentship Program, Limestone Ave.
Ainslie, A.C.T., 2602, Australia

The objective of this study was to examine some existing mathematical models of the global carbon cycle using methods derived from control and system theory. The detailed results of this work will be available in a report currently being prepared for CSIRO.

The approach may be thought of as a generalized sensitivity analysis of the models of the carbon cycle. First, the model parameters are represented as statistical distributions that reflect the degree of certainty in the value of each parameter. Then one or more problem-defining behaviors of the system (such as the Suess effect or the increasing atmospheric concentrations of CO_2) are stipulated and a classification algorithm applied to the output of each model simulation. Monte Carlo simulations can then be performed, allowing the analysis to focus on the probabilities of various outcomes. Since each simulation run can be classified as producing the problem-defining behavior or not, the parameter vectors leading to each result may be analyzed to see if

the original parameter distributions separate under the behavioral mapping. The degree to which such separation occurs provides a clue to the importance of each parameter in determining the overall model behavior. Hypotheses about the modes of operation of the carbon cycle can also be easily parameterized and evaluated by use of this method. This approach has been previously used in other environmental modeling applications. For example, Hornberger and Spear (1980) used it to model the eutrophication of a large estuary.

Acknowledgment

This research was supported by a CSIRO Postdoctoral Studentship.

6. INTERNATIONAL ACTIVITIES

On 19-23 January 1981, J. DeLuisi traveled to the Institute of Geophysics, University of Mexico, under the auspices of WMO to meet with I. Galindo and two graduate students to establish a research project with the Dobson spectrophotometer owned and operated by the institute. The exceptional urban pollution conditions at Mexico City will affect Umkehr measurements, and significant amounts of CO_2 can affect measurements of total ozone. A research procedure was outlined to investigate both of these problems. While at the institute, DeLuisi gave an invited seminar entitled "Chemical, Physical, and Optical Characteristics of the Mt. St. Helens Dust Cloud."

Sponsored by the U.S.-U.S.S.R. Working Group VIII Committee on the Environment, a meeting was held between U.S.S.R. representatives V. Binenko and V. Zhulev and U.S. representatives J. DeLuisi, K. Hanson, B. Herman, V. Mohnen, G. D. Robinson, and V. Ramanathan to formulate the contents of the proposed U.S.-U.S.S.R. monograph on an assessment of aerosol research and climatic implications. The meeting was hosted by GMCC at Boulder on 11-13 February 1981. The U.S. chief editor designated for the task is G. D. Robinson. A provisional table of contents was written and recommendations were made for authors of the various sections. The table of contents and a meeting protocol were sent to all persons who were considered to have an interest in the project. This information is available upon request to either G. D. Robinson (Center for Environment and Man, Hartford, Conn.) or J. J. DeLuisi (GMCC, Boulder, Colo.)

Nine tanks of CO_2-in-air calibration, working, and zero gases were provided to the Main Geophysical Observatory in Leningrad, U.S.S.R., in March 1981 under the auspices of the U.S.-U.S.S.R. Working Group VIII Committee on the Environment. The gases will enable our Soviet colleagues to embark on atmospheric sampling and analysis programs that will yield results compatible with those obtained by GMCC. Previously, training in CO_2 sampling and analysis had been provided to A. Shashkov of the Main Geophysical Observatory.

A new CO_2 flask sampling station, Ocean Station M (66°N, 02°E) operated by the Norwegian Meteorological Institute, was incorporated during 1981 into the GMCC global CO_2 station network.

GMCC was designated by WMO in 1981 as the Central Laboratory for Dobson Ozone Spectrophotometers. Primary functions of this laboratory are to maintain the calibration of World Standard Dobson Instrument no. 83, and to repair and calibrate other domestic and foreign spectrophotometers. During 1981, two foreign spectrophotometers were reconditioned and calibrated, namely, instrument no. 64 from Potsdam, G.D.R., and instrument no. 41 from Bracknell, U.K.

J. Peterson and W. Komhyr traveled to Switzerland to attend two WMO-sponsored meetings on CO_2 research, 6-19 September 1981. The WMO/UNEP/ICSU Meeting on Instruments, Standardization, and Measurement Techniques for Atmospheric CO_2 was convened at WMO headquarters in Geneva on 8-11 September. In attendance was a small group of scientists from several countries directly involved in CO_2 measurement programs. The purpose was to develop recommendations for the international CO_2 measurement program, which is loosely organized through the WMO Background Air Pollution Monitoring Network (BAPMoN). On 14-18 September, the WMO/ICSU/UNEP Scientific Conference on Analysis and Interpretation of Atmospheric CO_2 Data convened at the University of Bern.

This was a conventional scientific conference, but with much discussion following most of the presentations. About 65 scientists from 19 countries attended. W. Komhyr talked on GMCC flask data, and J. Peterson gave a paper on data from BRW and Cold Bay, Alaska. D. Gillette, B. Halter, R. Schnell, and G. Herbert also had papers included in the proceedings.

From 6 November to 12 December, at the request of WMO, B. Mendonca visited Ecuador, Peru, Paraguay, and Brazil as a technical expert and advisor for WMO on BAPMoN observatories in those countries. The general tasks accomplished were to (1) assess the status of the BAPMoN observatories in each country; (2) offer technical expertise and advice when needed; (3) install, repair, and modify BAPMoN instrumentation when possible and as needed; (4) instruct on the proper operation of the instrumentation and on proper data collection procedures; and (5) report back to WMO and make recommendations when warranted.

7. PUBLICATIONS AND PRESENTATIONS BY GMCC STAFF, 1981

Bodhaine, B. A. Nuclei monitoring at baseline sites: Barrow, Alaska; Mauna Loa, Hawaii; American Samoa; and South Pole. Atmospheric Aerosols and Nuclei, Proceedings of the Ninth International Conference on Atmospheric Aerosols, Condensation, and Ice Nuclei, Galway, Ireland, 21-27 September 1977, Galway University Press, 244-248.

Bodhaine, B. A., and J. C. Bortniak. Four wavelength nephelometer measurements at South Pole. Geophys. Res. Lett. 8(5):539-542.

Bodhaine, B. A., J. M. Harris, and G. A. Herbert. Aerosol light scattering and condensation nuclei measurements at Barrow, Alaska. Atmos. Environ. 15(8):1375-1389.

Bodhaine, B. A., B. G. Mendonca, J. M. Harris, and J. M. Miller. Seasonal variations in aerosols and atmospheric transmission at Mauna Loa Observatory. J. Geophys. Res. 86(C8):7395-7398.

Bortniak, J. C. The wind climatology of American Samoa. NOAA Tech. Memo. ERL ARL-98, NOAA Environmental Research Laboratories, Boulder, Colo., 67 pp.

Coulson, K. L. Characteristics of skylight at the zenith during twilight as indicators of atmospheric turbidity: Part 2, Intensity and color ratio. Appl. Opt. 20:1516-1524.

Coulson, K. L. Radiation measurement techniques. In Radiation Manual, C. Frohlich (ed.), International Association of Meteorology and Atmospheric Physics, Boulder, Colo. (in press).

Coulson, K. L. Skylight measurements during periods of twilight at the Mauna Loa Observatory. Presented at Big Island Science Conference, Hilo, Hawaii, 2 May 1981.

Dave, J. V., C. L. Mateer, and J. J. DeLuisi. An examination of the effect of haze on the short Umkehr method for deducing the vertical distribution of ozone. Proceedings of the Quadrennial International Ozone Symposium, Boulder, Colo., 4-9 August 1980, International Association of Meteorology and Atmospheric Physics, Boulder, Colo., 222-229.

DeFoor, T. H. Lidar measurements of the Mt. St. Helens volcanic plume at the Mauna Loa Observatory. Presented at Big Island Science Conference, Hilo, Hawaii, 2 May 1981.

DeLuisi, J. J., and J. M. Harris. Characteristics of ultraviolet radiation in the human erythema band measured with a Robertson-Berger meter and a double monochromator. NOAA Tech. Memo. ERL ARL-99, NOAA Environmental Research Laboratories, Boulder, Colo., 43 pp.

DeLuisi, J. J., B. G. Mendonca, K. J. Hanson, M. Box, and B. M. Herman. Solar-band radiative characteristics of the Mt. St. Helens dust cloud, determined by remote sensing. Proceedings of the Fourth Conference on Atmospheric Radiation, Toronto, Canada, 16-18 June 1981, American Meteorological Society, Boston, Mass., 89-90.

Gillette, D. A., and K. J. Hanson. The effect of number of globally distributed sampling locations and sampling frequency on variance in estimates used in models of global annual CO_2 increase and global carbon cycle. Papers presented at the WMO/ICSU/UNEP Scientific Conference on Analysis and Interpretation of Atmospheric CO_2 Data, Bern, Switzerland, 14-18 September 1981, World Meteorological Organization, Geneva, Switzerland, 27-33.

Halter, B. C., and J. M. Harris. On the variability of atmospheric carbon dioxide concentration at Barrow, Alaska, during winter. Papers presented at the WMO/ICSU/UNEP Scientific Conference on Analysis and Interpretation of Atmospheric CO_2 Data, Bern, Switzerland, 14-18 September 1981, World Meteorological Organization, Geneva, Switzerland, 13-18.

Halter, B. C., and J. T. Peterson. On the variability of atmospheric carbon dioxide concentration at Barrow, Alaska, during summer. Atmos. Environ. 15(8):1391-1399.

Hanson, K. J., and J. J. DeLuisi. Forecasting solar energy on synoptic and longer time scales with mean values and persistence methods. Proceedings of the First Workshop on Terrestial Solar Resource Forecasting and on Use of Satellites for Terrestial Solar Resource Assessment, January 1981, International Solar Energy Society, Inc., Newark, Del., 17-21.

Hanson, K. J., J. T. Peterson, J. Namais, R. Born, and C. Wong. On the influence of Pacific ocean temperatures on atmospheric carbon dioxide concentration at Ocean Weather Station P. J. Phys. Oceanogr. 11(7):905-912.

Herbert, G. A., T. B. Harris, and J. S. F. Chin. Comparison of airborne CO_2 flask samples and measurements from the Mauna Loa Observatory during the HAMEC Project (June 1980). Papers presented at the WMO/ICSU/UNEP Scientific Conference on Analysis and Interpretation of Atmospheric CO_2 Data, Bern, Switzerland, 14-18 September 1981, World Meteorological Organization, Geneva, Switzerland, 79-85.

Herbert, G. A., J. M. Harris, M. S. Johnson, and J. R. Jordan. The acquisition and processing of continuous data from GMCC observatories. NOAA Tech. Memo. ERL ARL-93, NOAA Environmental Research Laboratories, Boulder, Colo., 79 pp.

Komhyr, W. D., R. D. Grass, and R. K. Leonard. WMO 1977 international comparison of Dobson ozone spectrophotometers. Proceedings of the Quadrennial International Ozone Sysmposium, Boulder, Colo., 4-9 August 1980, International Association of Meteorology and Atmospheric Physics, Boulder, Colo., 25-32.

Komhyr, W. D., R. D. Grass, E. G. Dutton, R. K. Leonard, and R. D. Evans. Trend determinations from provisional and corrected 1963-1979 Bismarck total ozone data. Proceedings of the Quadrennial International Ozone Symposium, Boulder, Colo., 4-9 August 1980, International Association of Meteorology and Atmospheric Physics, Boulder, Colo., 371-377.

Komhyr, W. D., R. D. Grass, R. D. Evans, and R. K. Leonard. Dobson spectrophotometer calibrations, possible errors in ozone absorption coefficients, and errors due to interfering pollutant gases. Proceedings of the Quadrennial International Ozone Symposium, Boulder, Colo., 4-9 August 1980, International Association of Meteorology and Atmospheric Physics, Boulder, Colo., 230-235.

Mateer, C. L., and J. J. DeLuisi. The estimation of the vertical distribution of ozone by the short Umkehr method. Proceedings of the Quadrennial International Ozone Symposium, Boulder, Colo., 4-9 August 1980, International Association of Meteorology and Atmospheric Physics, Boulder, Colo., 64-73.

Mendonca, B. G., J. J. DeLuisi, and J. A. Schroeder. Arctic haze and perturbations in the solar radiation fluxes at Barrow, Alaska. Proceedings of the Fourth Conference on Atmospheric Radiation, Toronto, Canada, 16-18 June 1981, American Meteorological Society, Boston, Mass., 95-96.

Miller, J. M., and A. M. Yoshinaga. The pH of Hawaiian precipitation: A preliminary report. Geophys. Res. Lett. 8(7):779-782.

Oltmans, S. J. Surface ozone measurements in clean air. J. Geophys. Res. 86(C2):1174-1179.

Oltmans, S. J., and J. London. The quasi-biennial oscillation (QBO) in atmospheric ozone. Proceedings of the Quadrennial International Ozone Symposium, Boulder, Colo., 4-9 August 1980, International Association of Meteorology and Atmospheric Physics, Boulder, Colo., 397-405.

Parungo, F., B. Bodhaine, and J. Bortniak. Seasonal variation in Antarctic aerosol. J. Aerosol Sci. 12(6):491-504.

Parungo, F., C. Nagamoto, R. C. Schnell, I. Nolt, E. Nickerson, and W. Caldwell. Hawaii Mesoscale Energy and Climate Project, III: Atmospheric aerosol and cloud microphysics measurements. Project Report, NOAA Environmental Research Laboratories, Office of Weather Research and Modification, Boulder, Colo., 75 pp.

Peterson, J. T. Analysis of CO_2 measurements from Cold Bay and Barrow, Alaska. Papers presented at the WMO/ICSU/UNEP Scientific Conference on Analysis and Interpretation of Atmospheric CO_2 Data, Bern, Switzerland, 14-18 September 1981, World Meteorological Organization, Geneva, Switzerland, 19-28.

Peterson, J. T. CO_2 measurements at Barrow, Alaska, and their relation to the global CO_2 budget. Proceedings of the Eighth Conference on Inadvertent and Planned Weather Modification, Reno, Nev., 5-7 October, 1981, American Meteological Society, Boston, Mass., 8-9.

Peterson, J. T., and C. J. Fee. Relationship between visibility and atmospheric turbidity at Raleigh, North Carolina. NOAA Tech. Memo. ERL ARL-92, NOAA Environmental Research Laboratories, Boulder, Colo., 12 pp.

Peterson, J. T., and C. J. Fee. Visibility--atmospheric turbidity dependence at Raleigh, North Carolina. Atmos. Environ. 15(12):2561-2563.

Peterson, J. T., E. C. Flowers, G. J. Berri, C. L. Reynolds, and J. H. Rudisill. Atmospheric turbidity over central North Canada. J. Appl. Meteorol. 20(3):229-241.

Rosen, H., T. Novakov, and B. A. Bodhaine. Soot in the Arctic. Atmos. Environ. 15(8):1371-1374.

Schnell, R. C. Atmospheric ice nucleus measurements around the Hawaiian Islands during the HAMEC Project--1980. Presented at IAMAP, Third International Assembly, Hamburg, Germany, August 1981,

Schnell, R. C. Biogenic ice nuclei: Intercomparison measurements using a thermal diffusion chamber, an NCAR counter, and a filter drop freezer technique. Presented at IAMAP, Third International Assembly, Hamburg, Germany, August 1981.

Schnell, R. C. Ice nucleus and cloud condensation nucleus characteristics of Mount Saint Helens effluents and their relationships to ash elemental composition. Presented at IAMAP, Third International Assembly, Hamburg, Germany, August 1981.

Schnell, R. C., and J. M. Harris. A possible drought-induced signal in the global atmospheric CO_2 record. Papers presented at the WMO/ICSU/UNEP Scientific Conference on Analysis and Interpretation of Atmospheric CO_2 Data, Bern, Switzerland, 14-18 September 1981, World Meteorological Organization, Geneva, Switzerland, 113-120.

Schnell, R. C., J. M. Harris, and J. A. Schroeder. A relationship between Pacific Ocean temperatures and atmospheric carbon dioxide concentrations at Barrow and Mauna Loa. Papers presented at the WMO/ICSU/UNEP Scientific Conference on Analysis and Interpretation of Atmospheric CO_2 Data, Bern, Switzerland, 14-18 September 1981, World Meteorological Organization, Geneva, Switzerland, 155-162.

Schnell, R. C., S. W. Miller, and P. A. Allee. Ice nucleation studies on a bacterial aerosol. Preprints, Fifth Conference on Biometeorology, Anaheim, Calif., 30 March-3 April 1981, American Meteorological Society, Boston, Mass., 22-24.

Schnell, R. C., S. A. Odh, and L. N. Njau. Carbon dioxide measurements in tropical East African biomes. J. Geophys. Res. 86:5362-5372.

Thompson, T. M. Pyrheliometer observations as an indicator of the climatological persistence of clouds. NOAA Tech. Memo. ERL ARL-97, NOAA Environmental Research Laboratories, Boulder, Colo., 78 pp.

8. REFERENCES

Bacastow, R. B., J. A. Adams, C. D. Keeling, D. J. Moss, and T. P. Whorf, 1980. Atmospheric carbon dioxide, the Southern Oscillation, and the weak 1975 El Niño. Science 210:66-68.

Barrett, E. W., F. P. Parungo, and R. F. Pueschel, 1979. Cloud modification by urban pollution: A physical demonstration. Meteorol. Resch. 32:136-149.

Barrie, L. A., R. M. Hoff, and S. M. Daggupaty, 1981. The influence of mid-latitudinal pollution sources on haze in the Canadian Arctic. Atmos. Environ. 15(8):1407-1419.

Berger, D., and F. Urbach, 1982. A climatology of sunburning ultraviolet radiation. Photochem. Photobiol. 35:187-192.

Bird, T. E., and R. L. Hulstrom, 1981. A simplified clear sky model for direct and diffuse insolation on horizontal surfaces. SERI Tech. Rep. SERI/TR-642-761, Solar Energy Research Institute, Golden, Colo., 38 pp.

Bodhaine, B. A., 1979. Measurement of the Rayleigh scattering properties of some gases with a nephelometer. Appl. Opt. 18:121-125.

Bodhaine, B. A., and M. E. Murphy, 1980. Calibration of an automatic condensation nuclei counter at the South Pole. J. Aerosol Sci. 11(3):305-312.

Bodhaine, B. A., J. M. Harris, and G. A. Herbert, 1981a. Aerosol light scattering and condensation nuclei measurements at Barrow, Alaska. Atmos. Environ. 15:1375-1389.

Bodhaine, B. A., B. G. Mendonca, J. M. Harris, and J. M. Miller, 1981b. Seasonal variations in aerosols and atmospheric transmission at Mauna Loa Observatory. J. Geophys. Res. 86(C8):7395-7398.

Borys, R. D., and K. A. Rahn, 1981. Long range atmospheric transport of cloud active aerosol to Iceland. Atmos. Environ. 15:1491-1501.

Box, E. O., 1978. Geographical dimensions of terrestrial net and gross primary productivity. Radiat. Environ. Biophys. 15:305-322.

Bradbury, N. W., and H. J. Meuron, 1938. The diurnal variation of atmospheric condensation-nuclei. Terr. Magn. Atmos. Electr. 43:231-240.

Cess, R. D., 1982. Arctic aerosols: Model estimates of interactive influences upon the surface-troposphere radiation budget. Atmos. Environ. (submitted).

Clarke, A. D., 1982. The integrating sandwich: A new method of measurement of the light absorption coefficient for atmospheric particles. Appl. Opt. (accepted).

Coyne, P. I., and J. J. Kelley, 1974. Variations in carbon dioxide across an Arctic snowpack during spring. J. Geophys. Res. 79:799-802.

Coyne, P. I., and J. J. Kelley, 1975. CO_2 exchange over the Alaskan Arctic tundra: Meteorological assessment by an aerodynamic method. J. Appl. Ecol. 12:587-611.

Crutzen, P. J., L. E. Heidt, J. P. Krasnec, W. H. Pollock, and W. Seiler, 1979. Biomass burning as a source of atmospheric gases CO, H_2, N_2O, NO, CH_3Cl, and COS. Nature 282:253-256.

Darzi, M., and J. W. Winchester, 1982a. Aerosol characteristics at Mauna Loa Observatory, Hawaii, after east Asian dust storm episodes. J. Geophys. Res. 87:1251-1258.

Darzi, M., and J. W. Winchester, 1982b. Dynamic properties of continental aerosol over Hawaii determined by time series analysis. Preprints, Second Symposium on the Composition of Nonurban Troposphere, Williamsburg, Va., 25-28 May 1982, American Meteorological Society, Boston, Mass., 150-153.

Darzi, M., and J. W. Winchester, 1982c. Resolution of basaltic and continental aerosol components during spring and summer within the boundary layer of Hawaii. J. Geophys. Res. 87 (in press).

Dave, J. V., J. J. DeLuisi, and C. L. Mateer, 1980. Results of a comprehensive theoretical examination of the optical effects of aerosols on the Umkehr measurement. Papers presented at the WMO Technical Conference on Regional and Global Observation of Atmospheric Pollution Relative to Climate, Boulder, Colo., 20-24 August 1979, WMO No. 549, Spec. Environ. Rep. No. 14, World Meteorological Organization, Geneva, Switzerland, 15-22.

DeLuisi, J. J. (ed.), 1981. Geophysical Monitoring for Climatic Change, No. 9: Summary Report 1980. NOAA Environmental Research Laboratories, Boulder, Colo., 163 pp.

Dittenhoefer, A. C., 1982. The effects of sulfate and non-sulfate particles on light scattering at the Mauna Loa Observatory. Water Air Soil Pollut. 18:105-121.

Duce, R. A., J. G. Quinn, and T. L. Wade, 1974. Residence time of nonmethane hydrocarbons in the atmosphere. Mar. Pollut. Bull. 5:59-61.

Duce, R., B. Ray, J. Williams, and A. Hewitt, 1982. Samoa trace element analysis proceeding well. SEAREX Newsl. 5(2):7-10.

Dutton, E., and J. DeLuisi, 1982: Results of a sunphotometer intercomparison held at Boulder, 19 October to 16 December 1981. NOAA Tech. Memo. ERL ARL-114, NOAA Environmental Research Laboratories, Boulder, Colo., 47 pp.

Ellis, H. T., 1978. The Observatory. Mauna Loa Observatory: A 20th anniversary report, J. M. Miller (ed.), NOAA Spec. Rep., NOAA Environmental Research Laboratories, Boulder, Colo., 24.

Ellis, H. T., and R. F. Pueschel, 1971. Solar radiation: Absence of air pollution trends at Mauna Loa. Science 172:845-846.

Fleig, A. J., K. F. Klenk, P. K. Bartia, K. D. Lee, C. G. Wellemeyer, and V. G. Kavashwar, 1981. Vertical ozone profile results from Nimbus-4 BUV data. Proceedings of the Fourth Conference on Atmospheric Radiation, Toronto, Canada, 16-18 June 1981, American Meteorological Society, Boston, Mass., 20-26.

Friedlander, S. K., 1977. Smoke, Dust, and Haze. John Wiley and Sons, New York, 317 pp.

Galloway, J. N., G. E. Likens, W. C. Keene, and J. M. Miller, 1982. The composition of precipitation in remote areas of the world. J. Geophys. Res. 87(C11):8771-8786.

Giam, C. S., and E. Atlas, 1981. Samoa experiment. SEAREX Newsl. 4(3):7-9.

Giam, C. S., and E. Atlas, 1982. Chlorinated hydrocarbons--Samoa and Peru. SEAREX Newsl. 5(2):17-19.

Gundel, L., R. Dod, and T. Novakov, 1981. Determination of black carbon by thermal analysis. Environmental Pollutant Studies, Report LBL-11986, Lawrence Berkeley Laboratory, Berkeley, Calif., 5.

Hanson, K. J. (ed.), 1977. Geophysical Monitoring for Climatic Change, No. 5: Summary Report 1976. NOAA Environmental Research Laboratories, Boulder, Colo., 110 pp.

Hanson, K. J., J. T. Peterson, J. Namais, R. Born, and C. S. Wong, 1981. On the influence of Pacific Ocean temperatures on atmospheric carbon dioxide concentration at Ocean Weather Station P. J. Phys. Oceanogr. 11:905-912.

Harris, J. M., and G. A. Herbert, 1980. Carbon dioxide, condensation nuclei, and wind climatology of the Barrow GMCC Observatory (1973-1979). NOAA Data Rep. ERL ARL-2, NOAA Environmental Research Laboratories, Boulder, Colo., 112 pp.

Harris, J. M., J. R. Jordan, and G. A. Herbert, 1980. Automation of GMCC's CO_2 laboratory operation using microprocessors. Papers presented at the WMO Technical Conference on Regional and Global Observation of Atmospheric Pollution Relative to Climate, Boulder, Colo., 20-24 August 1979, WMO No. 549, Spec. Environ. Rep. No. 14, Geneva, Switzerland, 103-108.

Heffter, J. L., and A. D. Taylor, 1975. Trajectory model: Part I, A regional-continental scale transport, diffusion, and deposition model. NOAA Tech. Memo. ERL ARL-50, NOAA Environmental Research Laboratories, Boulder, Colo., 28 pp.

Herbert, G. A. (ed.), 1980. Geophysical Monitoring for Climatic Change, No. 8: Summary Report 1979. NOAA Environmental Research Laboratories, Boulder, Colo., 120 pp.

Herzog, G., 1935. A large cloud chamber. J. Sci. Instr. 12:153-159.

Hornberger, G. M., and R. C. Spear, 1980. Eutrophication in Peel Inlet: 1, The problem defining behavior and a mathematical model for the phosphorous scenario. Water Res. 14:29-42.

Husar, R. B., and D. E. Patterson, 1979. Synoptic scale distribution of man-made aerosols. WMO Symposium on Long Range Transport of Pollutants, WMO No. 538, World Meteorological Organization, Geneva, Switzerland.

Jenne, R. L., 1975. Data sets for meteorological research. National Center for Atmospheric Research, Boulder, Colo., 194 pp.

Jordan, R. C., and B. Y. H. Liu, 1977. Availability of solar energy for flat-plate solar heat collectors. Applications of solar energy for heating and cooling of buildings, R. C. Jordan and B. Y. H. Liu (eds.), ASHRAE GRP 170, American Society of Heating, Refrigerating, and Air Conditioning Engineers, Inc., New York, V1-V16.

Junge, C. E., 1963. Air Chemistry and Radioactivity. Academic Press, New York, 382 pp.

Keeling, C. D., J. Adams, C. Ekdahl, and P. Guenther, 1976. Atmopsheric carbon dioxide variations at the South Pole. Tellus 28:552-564.

Kelley, J. J., and T. A. Gosink, 1979. Gases in sea ice: 1975-1979. Final Rep. to Office of Naval Research Contract No. N000 14-76C-0331, Institute of Marine Science, University of Alaska, Fairbanks, 104 pp.

Khalil, M. A. K., and R. A. Rasmussen, 1981. Atmospheric methyl chloride (CH_3Cl). Chemosphere 10:1019-1023.

Khalil, M. A. K., and R. A. Rasmussen, 1982. Gaseous tracers of Arctic haze. Environ. Sci. Technol. (submitted).

Kneizys, F. X., F. P. Shettle, W. O. Gallery, J. G. Chetwynd, Jr., L. W. Abreau, J. E. A. Selby, R. W. Fenn, R. A. McClatchey, 1980. Atmospheric transmission/radiance: Computer code LOWTRAN 5. AFGL-TR-80-0067, Air Force Geophysics Laboratory, Hanscomb AFB, Mass., 233 pp.

Knott, C. G. (ed.), 1923. Collected Scientific Papers of John Aitken. Cambridge University Press, London, 591 pp.

Komhyr, W. D., 1981. Pump piston-cylinder assembly with exterior ring seals. Patent No. 4, 285, 642, U.S. Patent Office, Washington, D.C., Aug. 25, 1981.

Komhyr, W. D., L. S. Waterman, and W. R. Taylor, 1982. Semi-automatic non-dispersive infrared analyzer apparatus for CO_2 air sample analyses. J. Geophys. Res. (accepted).

Kozo, T. L., 1979. Evidence for sea breezes on the Alaskan Beaufort Sea coast. Geophys. Res. Lett. 6(11):849-852.

Kozo, T. L., 1980. Mountain barrier baroclinity effects on surface winds along the Alaskan Arctic coast. Geophys. Res. Lett. 7(5):377-380.

Lacis, A. A., and J. E. Hansen, 1974. A parameterization for the absorption of solar radiation in the Earth's atmosphere. J. Atmos. Sci. 31:118-133.

Liu, B. Y. H., and D. Y. H. Pui, 1974. A submicron aerosol standard and the primary absolute calibration of the condensation nuclei counter. J. Colloid Inter. Sci. 47:155-171.

Liu, B. Y. H., D. Y. H. Pui, A. W. Hogan, and T. A. Rich, 1975. Calibration of the Pollak counter with monodisperse aerosols. J. Appl. Meteorol. 14:46-51.

Machta, L., 1974. Global scale atmospheric mixing. In Turbulent Diffusion in Environmental Pollution, F. Frenkiel and R. E. Munn (eds.), Academic Press, New York, 405 pp.

McGuirk, J. P., and E. R. Reiter, 1976. A vacillation in atmospheric energy parameters. J. Atmos. Sci. 33:2079-2093.

Mendonca, B. G., 1969. Local wind circulation on the slopes of Mauna Loa. J. Appl. Meteorol. 8(4):533-541.

Mendonca, B. G. (ed.), 1979. Geophysical Monitoring for Climatic Change, No. 7: Summary Report 1978. NOAA Environmental Research Laboratories, Boulder, Colo., 131 pp.

Mendonca, B. G., K. J. Hanson, and J. J. DeLuisi, 1978. Volcanically related secular trends in atmospheric transmission at Mauna Loa Observatory, Hawaii. Science 202:513-515.

Metnieks, A. L., and L. W. Pollak, 1959. Instructions for use of photo-electric condensation nucleus counters. Geophysical Bulletin No. 16, School of Cosmic Physics, Dublin Institute for Advanced Studies, Dublin, Ireland, 44 pp.

Miller, J. M., 1978. The complexity of the wind patterns at Mauna Loa Observatory. Mauna Loa Observatory: A 20th anniversary report, J. M. Miller (ed.), NOAA Spec. Rep., NOAA Environmental Research Laboratories, Boulder, Colo., 122-127.

Miller, J. M., 1981a. A five-year climatology of five-day back trajectories from Barrow, Alaska. Atmos. Environ. 15(8):1401-1405.

Miller, J. M., 1981b. A five-year climatology of year climatology of back trajectories from the Mauna Loa Observatory, Hawaii. Atmos. Environ. 15(9):1553-1558.

Miller, S. W., and B. A. Bodhaine, 1982a. Calibration of Pollak condensation nuclei counter using charged, monodisperse aeorsols. J. Aerosol Sci. (in press).

Miller, S. W., and B. A. Bodhaine, 1982b. Supersaturation and expansion ratios in condensation nuclei counters: An historical perspective. J. Aerosol Sci. (in press).

Murphy, M. E., and B. A. Bodhaine, 1980. The Barrow, Alaska, automatic condensation nuclei counter and four wavelength nephelometer: Instrument details and four years of observations. NOAA Tech. Memo. ERL ARL-90, NOAA Environmental Research Laboratories, Boulder, Colo., 101 pp.

Newell, R. E., G. J. Boer, and J. W. Kidson, 1974. An estimate of the interhemisphere transfer of carbon monoxide from tropical general circulation data. Tellus 26:103-107.

NMC (National Meteorological Center), 1979. Office Note 84: NMC 360/195 packed data fields. NOAA/NWS/NMC, Suitland, Md., 28 pp.

Nolan, P. J., and L. W. Pollak, 1946. The calibration of a photoelectric nucleus counter. Proc. Roy. Ir. Acad. 51A:9-31.

Noxon, J. F., 1981. NO_x in the mid-Pacific troposphere. Geophys. Res. Lett. 8:1223-1226.

Oltmans, S. J., 1981. Surface ozone measurements in clean air. J. Geophys. Res. 86:1174-1180.

Oltmans, S. J., and J. London, 1982. The quasibiennial oscillation in atmospheric ozone. J. Geophys. Res. (in press).

Ottar, R., 1981. The transfer of airborne pollutants to the Arctic region. Atmos. Environ. 15:1439-1446.

Patterson, C. C., and D. M. Settle, 1981. American Samoa: Small concentrations of lead in air verifies model. SEAREX Newsl. 4(2):13-17.

Patterson, C. C., and D. M. Settle, 1982. Magnitude of eolian lead inputs to the oceans control variations in vertical lead concentration profiles in the ocean. SEAREX Newsl. 5(2):21-26.

Peterson, J. T. (ed.), 1978. Geophysical Monitoring for Climatic Change, No. 6: Summary Report 1977. NOAA Environmental Research Laboratories, Boulder, Colo., 145 pp.

Peterson, J. T., K. J. Hanson, B. A. Bodhaine, and S. J. Oltmans, 1980. Dependence of CO_2, aerosol, and ozone concentrations on wind direction at Barrow, Alaska, during winter. Geophys. Res. Lett. 7:349-352.

Peterson, J. T., W. Komhyr, T. B. Harris, and L. S. Waterman, 1982. Atmospheric carbon dioxide measurements at Barrow, Alaska, 1973-1979. Tellus 34:166-175.

Pollak, L. W., and A. L. Metnieks, 1960. Intrinsic calibration of the photoelectric condensation nucleus counter model 1975 with convergent light-beam. Tech. Note No. 9, School of Cosmic Physics, Dublin Institute for Advanced Studies, Dublin, Ireland, 53 pp.

Porch, W. M., and M. C. MacCracken, 1982. Parametric study of the effects of Arctic soot on solar radiation. Atmos. Environ. (in press).

Pszenny, A. P., and R. Duce, 1981. Ionic composition of Samoan rain: Preliminary results. SEAREX Newl. 4(2):19-26.

Pszenny, A. P., F. MacIntyre, and R. Duce, 1982. Sea-salt acidity of marine rain on the windward cost of Samoa. Geophys. Res. Lett. (in press).

Rahn, K. A., 1981a. Atmospheric riverine and oceanic sources of seven trace constituents to the Arctic Ocean. Atmos. Environ. 15:1507-1516.

Rahn, K. A., 1981b. The Mn/V ratio as a tracer of large-scale sources of pollution aerosol for the Arctic. Atmos. Environ. 15:1457-1464.

Rahn, K. A., 1981c. Relative importances of North America and Eurasia as sources of Arctic aerosol. Atmos. Environ. 15:1447-1456.

Rahn, K. A., and N. Z. Heidam, 1981. Progress in Arctic air chemistry, 1977-1980: A comparison of the first and second symposia. Atmos. Environ. 15:1345-1348.

Rahn, K. A., and R. J. McCaffrey, 1980. On the origin and transport of winter Arctic aerosol. Ann. N.Y. Acad. Sci. 338:486-503.

Rahn, K. A., R. D. Borys, and G. E. Shaw, 1977. The Asian source of Arctic haze bands. Nature 268:713-715.

Rasmussen, R. A., and M. A. K. Khalil, 1980. Atmospheric halocarbons: Measurements and analyses of selected trace gases. Proceedings of the NATO Advanced Study Institute on Atmospheric Ozone: Its Variations and Human Influences, A. C. Aikin (ed.), Algarve, Portugal, 1-13 October 1979, Department of Transporation, Washington, D.C., 209-231.

Rasmussen, R. A., L. E. Rasmussen, M. A. K. Khalil, and R. W. Dalluge, 1980. Concentration distribution of methyl chloride in the atmosphere. J. Geophys. Res. 85:7350-7356.

Rasmussen, R. A., M. A. K. Khalil, and R. W. Dalluge, 1981. Atmospheric trace gases in Antarctica. Science 211:285-287.

Rasmussen, R. A., M. A. K. Khalil, and J. S. Chang, 1982. Atmospheric trace gases over China. Environ. Sci. Technol. 16:124-126.

Reible, D. D., F. H. Shair, R. J. Cayer, and D. W. Nelson, 1982. Atmospheric tracer studies associated with the evaluation of the SEAREX atmospheric sampling site at the NOAA/GMCC station in American Samoa. Boundary-Layer Meteorol. (in press).

Reiter, E. R., 1981. Planetary wave behavior and Arctic air pollution. Atmos. Environ. 15:1465-1471.

Rosen, H., A. D. A. Hansen, L. Gundel, and T. Novakov, 1978. Identification of the optically absorbing component in urban aerosols. Appl. Opt. 17:3859-3861.

Rosen, H., T. Novakov, and B. A. Bodhaine, 1981. Soot in the Arctic. Atmos. Environ. 15:1371-1374.

Rotty, R. M., 1982. Distribution of and changes in industrial carbon dioxide production. ORAU/IEA-82-2(M), Institute for Energy Analysis, Oak Ridge, Tenn., 23 pp.

SASC (Systems and Applied Sciences Corporation), 1981. Report presented to the SBUV NET Team, Goddard SFC, September 2, 1981. Riverdale, Md., 97 pp.

Schnell, R. C., and J. M. Harris, 1981. A possible drought-induced signal in the global atmospheric CO_2 record. Papers presented at the WMO/ICSU/UNEP Scientific Conference on Analysis and Interpretation of Atmospheric CO_2 Data, Bern, Switzerland, 14-18 September, World Meteorological Organization, Geneva, Switzerland, 113-120.

Schnell, R. C., J. M. Harris, and J. A. Schroeder, 1981. A relationship between Pacific Ocean temperatures and carbon dioxide concentrations at Barrow and Mauna Loa. Papers presented at the WMO/ICSU/UNEP Scientific Conference on Analysis and Interpretation of Atmospheric CO_2 Data, Bern, Switzerland, 14-18 September 1981, World Meteorological Organization, Geneva, Switzerland, 155-162.

Scholz, J., 1931. Ein neuer apparat zur bestimmung der zahl der geladenen und ungeladenen kerne. Z. Instrumentenk. 51:505-522.

Sehmel, G. A., and W. H. Hodgson, 1976. Predicted dry deposition velocities. Atmosphere-surface exchange of particulate and gaseous pollutants (1974), available as CONF-740921, National Technical Information Service, Springfield, Va., 988 pp.

Shaw, G. E., 1980. Transport of Asian desert aerosol to the Hawaiian Islands. J. Appl. Meteorol. 19:1254-1259.

Shaw, G. E., 1981. Eddy diffusion transport of Arctic pollution from the mid latitudes: A preliminary model. Atmos. Environ. 15:1483-1491.

Turekian, K., J. Cochran, and W. Graustein, 1982. The ^{210}Pb program at Yale University. SEAREX Newl. 5(2):26-28.

Verma, S. B., and N. J. Rosenberg, 1976. Carbon dioxide concentration and flux in a large agricultural region of the Great Plains of North America. J. Geophys. Res. 81:399-405.

Wang, M. X., J. W. Winchester, T. A. Cahill, and L. X. Ren, 1982. Chemical elemental composition of wind blown dust, Beijing, 19 April 1980. Kexue Tongbao Sci. Bull. (in press).

Weiss, R. E., and A. P. Waggoner, 1980. Optical measurements of airborne soot in urban, rural, and remote locations. In Particulate Carbon: Atmospheric Life Cycle, G. T. Wolfe and R. L. Klimisch (eds.), Plenum Press, New York, 317-325.

Weschler, C. J., 1981. Identification of selected organics in the Arctic aerosol. Atmos. Environ. 15:1365-1370.

White, W. B., and A. E. Walter, 1973. Meridional atmospheric teleconnections over the North Pacific from 1950 to 1972. Mon. Weather Rev. 101:817-822.

Wilson, C., 1969. Climatology of the cold regions: Part II. Cold Regions Science and Engineering Monograph I-A3b, Cold Regions Research and Engineering Laboratory, Hanover, N.H., 158 pp.

Wilson, C. T. R., 1897. Condensation of water vapour in the presence of dust-free air and other gases. Philos. Trans. Roy. Soc. London 189:265-307.

Winters, W., S. Barnard, and A. Hogan, 1977. A portable photo-recording Aitken counter. J. Appl. Meteorol. 16:992-996.

WMO (World Meteorological Organization), 1981. Environmental pollution monitoring programme. Report of the WMO/UNEP/ICSU Meeting on Instruments, Standardization, and Measurement Techniques for Atmospheric CO_2, Geneva, Switzerland, 8-11 September 1981, 27 pp.

9. GMCC STAFF, 1981

Director's Office

James Peterson, Director
Bernard Mendonca, Deputy Director
Jeanne Kelsey, Secretary
Carol Fee, CO-OP
Dale Gillette, CIRES
Edward Green, Electronic Engineer
Milton Johnson, Engineering Technician
Cynthia McFee, NOAA Corps
Judith Schroeder, Mathematician
Chandra Shastri, CIRES
Constance Shilvock, Jr. Fellow
Gregory Siedelberg, Electronic Technician
Paul Steele, Guest Scientist

Acquisition and Data Management Group

Gary Herbert, Chief
Jo-Ann Garner, Secretary
Richard Clark, Computer Programmer
Joyce Harris, Computer Specialist
Troy Higgins, Jr. Fellow
James Jordan, Electronic Engineer
Gloria Koenig, Computer Programmer
Kenneth Thaut, Electronic Technician

Monitoring Trace Gases Group

Walter Komhyr, Chief
Jo-Ann Garner, Secretary
Ruth Alvirez, CO-OP
Edguardo Blanco, CO-OP
Amar Chopra, CIRES
Thomas Conway, CIRES
Robert Evans, CIRES
Robert Grass, Physicist
Thomas Harris, Meteorological Technician
Kent Leonard, CIRES
Samuel Oltmans, Physicist
Frank Polacek, III, Meteorological Technician
Gerald Roybal, Contract
William Taylor, CIRES
Kirk Thoning, CIRES
Lee Waterman, Chemist

Aerosols and Radiation Monitoring Group

John DeLuisi, Chief
Bonnie Hill, Secretary
Barry Bodhaine, Meteorologist
Kenneth Cameron, CIRES
Ellsworth Dutton, Meteorologist
Daniel Endres, CIRES
John Osborn, NOAA Corps
Steven Zobrist, Jr. Fellow

Analysis and Interpretation Group

John DeLuisi, (Acting) Chief
Bonnie Hill, Secretary
Haesook Cho, Research Associate
Joanne Edwards, CIRES
Bradley Halter, CIRES
Russell Schnell, CIRES
Thayne Thompson, Physicist

Mauna Loa Observatory

Kinsell Coulson, Director
Judith Pereira, Secretary
John Bortniak, NOAA Corps
John Chin, Physicist
Thomas DeFoor, Electrical Engineer
Howard Ellis, Physicist
Steven Garcia, Contract
Mamoru Shibata, Electronic Technician
Alan Yoshinaga, Analytical Chemist

Barrow Observatory

David Smith, Station Chief
Kenneth Bauer, Electronic Technician
Randy Fox, Physical Scientist

Samoa Observatory

Donald Nelson, Station Chief
Roger Williams, Electronic Technician
Efaraima Peau, W. G. Laborer

South Pole Observatory

Cynthia McFee, NOAA Corps, Station Chief
Edward Green, Electronic Engineer
Robert Williscroft, NOAA Corps, Station Chief
Mark VandeRiet, Electronic Technician

☆ U.S. Government Printing Office 1982 - 676-001/1207 Reg. 8